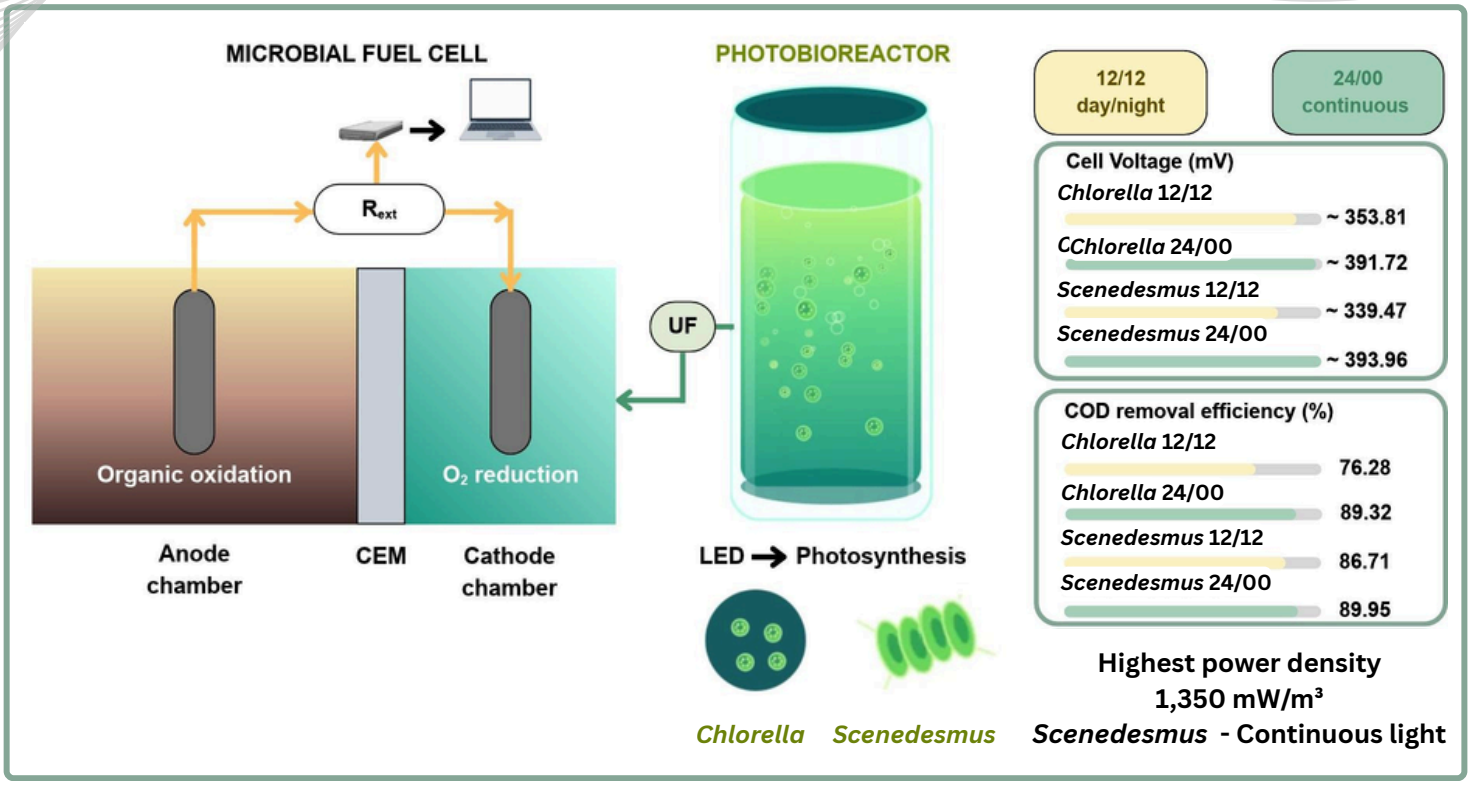
ISSN 2408-2384 (ONLINE)

Environment and Natural Resources Journal

Volume 24 Number 6 November - December 2026



Integrating double-chamber microbial fuel cells (MFCs) with a photobioreactor (PBR) using the microalgae *Chlorella vulgaris* and *Scenedesmus protuberans* achieved up to 89.95% removal of chemical oxygen demand (COD) and a power density of up to 1,350 mW/m³. This showcases a sustainable technology for wastewater treatment and bioenergy production from microalgae.

Source: Nguyen HPT, Vo NXQ, Dao TS, Nguyen HD. Performance of Microbial Fuel Cells Integrated with a Photo-Bioreactor: Effects of Light Regimes and Microalgae (*Chlorella* vs. *Scenedesmus*). Environ. Nat. Resour. J. 2026;24(6):751-763.

Scopus Clarivate Analytics EBSCO HOST DOAJ ASEAN CITATION INDEX TCI

Environment and Natural Resources Journal (EnNRJ)
Volume 24, Number 6, November - December 2026 ISSN: 2408-2384 (Online)

FOCUS AND SCOPE

Environment and Natural Resources Journal (EnNRJ) is a peer-reviewed journal which provides a platform for exchanging and distributing knowledge and cutting-edge research in environmental science and natural resource management to academicians, scientists, and researchers.

The scope of the journal covers the integration of multidisciplinary sciences for prevention, control, treatment, environmental clean-up, and restoration. The study of existing or emerging problems related to the environment and natural resources in Southeast Asia and the development of innovative knowledge and/or creative recommendations for mitigation measures and sustainable development are emphasized. The subject areas are diverse, but specific topics of interest include:

- Biodiversity
- Climate change
- Detection and monitoring of pollutants and their sources (e.g., agriculture, industry, mining, urban activities, accidents)
- Disaster (e.g., forest fires, flooding, earthquakes, tsunamis or tidal waves)
- Ecological/Environmental modelling
- Emerging contaminants/hazardous wastes investigations and remediation
- Environmental dynamics (e.g., coastal erosion, rising sea levels)
- Environmental assessment tools, policy, and management [e.g., GIS, remote sensing, and Environmental Management Systems (EMS)]
- Pollution control and innovative solutions for pollution reduction
- Remediation technology in contaminated environments
- Transboundary pollution
- Waste and wastewater treatments and disposal technology

Schedule
Environment and Natural Resources Journal (EnNRJ) is published 6 issues per year in January-February, March-April, May-June, July-August, September-October, and November-December.

Publication Fees
An article publication fee in the Environment and Natural Resources Journal is set at a rate of 250 USD per article, payable after the final acceptance of the manuscript.

Ethics in publishing
EnNRJ follows closely a set of guidelines and recommendations published by Committee on Publication Ethics (COPE).

Environment and Natural Resources Journal (EnNRJ)
Volume 24, Number 6, November - December 2026 ISSN: 2408-2384 (Online)

EXECUTIVE CONSULTANT TO EDITOR

Professor Dr. Benjaphorn Prapagdee
(Mahidol University, Thailand)
Associate Professor Dr. Kitikorn Charmondusit
(Mahidol University, Thailand)

EDITOR

Associate Professor Dr. Noppol Arunrat
(Mahidol University, Thailand)

ASSOCIATE EDITOR

Assistant Professor Dr. Piangjai Peerakiatkhajohn
(Mahidol University, Thailand)
Dr. Jakkapon Phanthuwongpakdee
(Mahidol University, Thailand)

EDITORIAL BOARD

Professor Dr. Aysegul Pala
(Dokuz Eylul University, Türkiye)
Professor Dr. Hermann Knoflacher
(Vienna University of Technology, Austria)
Professor Dr. Hideki Nakayama
(Nagasaki University, Japan)
Professor Dr. Jung-Ho Yun
(Kyung Hee University, South Korea)
Professor Dr. Sompon Wanwimolruk
(Mahidol University, Thailand)
Professor Dr. Uwe Strotmann
(University of Applied Sciences, Germany)
Associate Professor Dr. Chuleemas Boonthai IWAI
(Khon Kaen University, Thailand)
Associate Professor Dr. Devi N. Choesin
(School of Life Sciences and Technology, Indonesia)
Associate Professor Dr. Pasicha Chaikaew
(Chulalongkorn University, Thailand)
Associate Professor Dr. Pirom Noisumdaeng
(Thammasat University, Thailand)
Associate Professor Dr. Pongchai Dumrongrojwatthana
(Chulalongkorn University, Thailand)
Associate Professor Dr. Sate Sampattagul
(Chiang Mai University, Thailand)

Associate Professor Dr. Schradh Saenton
(Chiang Mai University, Thailand)
Associate Professor Dr. Takehiko Kenzaka
(Setsunan University, Japan)
Associate Professor Dr. Vimoltip Singtuen
(Khon Kaen University, Thailand)
Associate Professor Dr. Xu Tian
(Shanghai Jiao Tong University, China)
Assistant Professor Dr. Anish Ghimire
(Asian Institute of Technology, Thailand)
Assistant Professor Dr. Said Munir
(University of Leeds, United Kingdom)
Assistant Professor Dr. Toru Hamamoto
(Tohoku University, Japan)
Dr. Davide Poggio (Research Associate)
(University of Sheffield, United Kingdom)
Dr. Ho Ngo Anh Dao
(Ton Duc Thang University, Viet Nam)
Dr. Miaoqiang Lyu
(The University of Queensland, Australia
Dr. Mohamed F. Yassin
(Kuwait Institute for Scientific Research, Kuwait)

ASSISTANT TO EDITOR

Assistant Professor Dr. Thunyapat Sattraburut
Dr. Praewa Wongburi
Dr. Shreema Rana

MANAGING EDITOR

Isaree Apinya

JOURNAL EDITORIAL OFFICER

Nattakarn Ratchakun
Parynya Chowwiwattanaporn

Editorial Office Address
Research and Academic Service, Research Management Unit,
Faculty of Environment and Resource Studies, Mahidol University
999, Phutthamonthon Sai 4 Road, Salaya, Phutthamonthon, Nakhon Pathom, Thailand, 73170
Phone +662 441 5000 ext. 2108
Website: https://ph02.tci-thaijo.org/index.php/ennrj/index
E-mail: ennrjournal@gmail.com

Environment and Natural Resources Journal (EnNRJ)

Volume 24, Number 6, November - December 2026 ISSN: 2408-2384 (Online)

CONTENT

Mechanical Properties and Volatile Pollutants Absorbing Capacity of Mortar Composites with Addition of Coconut Shell Activated Carbon and Gamal Wood Chips Aggregates **642**
Baiq Mirawati, Muhammad Sadir, Albert Hendriko, I Gde Adi Suryawan Wangiyana, Ismail Budiman, Dede Hermawan, Gustan Pari, and Ariadne Lakshmidevi Juwono

Oxidative Stress Responses and Antioxidant Gene Regulation in Daphnia pulex Following Chronic Benzyl Alcohol Exposure **661**
Ghufran Saad Aljanabi and Adel Mashaan Rabee

Spatio-Temporal Assessment of Air Quality and AQI in Former Khanh Hoa Province, Vietnam (2021-2024) **673**
Le Viet Thang and Ho Minh Dung

Identifying Geospatial Priority Hotspots of Tourism Sustainability Risk using a Destination Sustainability Index (DSI) Devised from Online Tourist Dissatisfaction and Getis-Ord Gi* Statistics **689**
Tobthong Chancharoen, Asamaporn Sitthi, Parinya Nakpathom, and Narong Pleerux

Scenario-Based Assessment of Greenhouse Gas Mitigation in the Municipal Solid Waste: Cambodia Case Study and Regional Comparison in Asia **701**
Take Kyoko and Thai-Huyen Nguyen

Effects of Climate Change on Streamflow of Upper Lam Nam Chi and Lam Saphung Subwatershed Using SWAT Model **713**
Chawakon Sakkaew, Supattra Thueksathit, and Patchares Chacuttrikul

Changes in Carbon Stocks and the Economic Value of Forest Carbon in a Secondary Forest of Mt. Nacolod, Silago, Southern Leyte, Philippines **723**
Christian Albert L. Martinez, Renezita S. Come, Dennis P. Peque, Moises Neil V. Seriño, and Melvin Lippe

Integrating Phytoremediation and Socio-Economic Potential of Water Hyacinth for Sustainable Post-Mining Void Management **737**
Priyaji Agung Pambudi, Suyud Warno Utomo, and Roni Setyo Handoko

Performance of Microbial Fuel Cells Integrated with a Photo-Bioreactor: Effects of Light Regimes and Microalgae (*Chlorella vs. Scenedesmus*) **751**
Hoang Phuong Tuan Nguyen, Nguyen Xuan Que Vo, Thanh Son Dao, and Hoang Dung Nguyen

A Preliminary Physical Property Characterization of *Artocarpus blancoi* (Antipolo) from Maguindanao Province of Mindanao **764**
Ben G. Dres, Rafael T. Acob, Jayric F. Villareal, Cindy E. Poclis, Rowena C. Benavides, and Oliver S. Marasigan

Environment and Natural Resources Journal

Volume 24
Issue 6
2026

Mechanical Properties and Volatile Pollutants Absorbing Capacity of Mortar Composites with Addition of Coconut Shell Activated Carbon and Gamal Wood Chips Aggregates

Baiq Mirawati[1*], Muhammad Sadir[1], Albert Hendriko[2], I Gde Adi Suryawan Wangiyana[1], Ismail Budiman[3], Dede Hermawan[4], Gustan Pari[3], and Ariadne Lakshmidevi Juwono[2]

[1]*Department of Forestry, Faculty of Engineering and Applied Sciences, Universitas Pendidikan Mandalika, Mataram 83125, Indonesia*
[2]*Department of Physics, Faculty of Mathematics and Natural Sciences, Universitas Indonesia, Depok 16424, Indonesia*
[3]*Research Center for Biomass and Bioproducts, Badan Riset dan Inovasi Nasional, Cibinong 16911, Indonesia*
[4]*Department of Forest Products, Faculty of Forestry and Environment, IPB University, Bogor 16680, Indonesia*

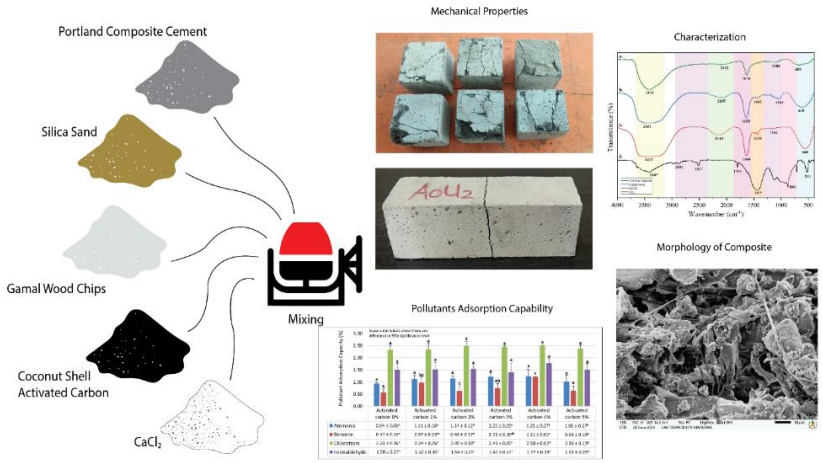
ARTICLE INFO

Received: 25 Nov 2025
Received in revised: 5 Apr 2026
Accepted: 17 Apr 2026
Published online: 12 Oct 2026
DOI: 10.32526/ennrj/24/20250337

Keywords:
Cement composites/ Biomass/ Activated carbon/ Volatile pollutant/ Mechanical properties

*** Corresponding author:**
E-mail:
baiqmirawati@undikma.ac.id

GRAPHICAL ABSTRACT



ABSTRACT

The use of biomass has the potential to improve the mechanical characteristics of cement-based composites. Activated carbon is considered competitive in absorbing hazardous pollutants in the air, is able to reduce cracking and increase the mechanical strength of cement-based composites. The addition of gamal wood chips also has the potential to increase flexibility in mortar composites. The purpose of this study was to analyze the characteristics of the mechanical properties and pollutant absorption capacity of mortar composites with the addition of activated carbon and gamal wood chips. In this study, activated carbon is used as a fine aggregate (filler) with an addition of 1-5% to the weight of cement. Gamal wood chips are used as much as 1.5% of the total weight. Composite brick testing includes density, compressive strength, modulus of elasticity (MOE), modulus of rupture (MOR), adsorption capacity for ammonia, benzene, chloroform, and formaldehyde and thermal analysis of Field Emission Electron Microscopes (FE-SEM) and Fourier-transform infrared spectroscopy (FTIR). The density of composite mortar with the addition of activated carbon and gamal wood chips ranges from 1950.36±19.54-2137.24±45.09 kg/m^3, compressive strength 8.48±0.76-9.71±1.68 MPa, MOE 421.74±69.59 -645.58±57.51 MPa, MOR 2.14±0.27-2.75±0.20 MPa. The composite mortar exhibited a total pollutant absorption rate of less than 3% for all tested parameters. The addition of activated carbon up to 4% can increase the mechanical strength and pollutant absorption capacity and can produce more $CaCO_3$ in composite bricks. Morphological observations as analyzed by FE-SEM, were found to correlate with FTIR analysis, namely the formation of $CaCO_3$. The following method produces an environmentally friendly mortar composite that performs exceptionally well and has a lot of potential for use in sustainable building.

HIGHLIGHTS

- Activated carbon and gamal wood chips enhanced mortar composite performance.
- A 4 wt% activated carbon addition produced the optimum mechanical properties.
- Composite mortar showed measurable adsorption of ammonia, benzene, chloroform, and formaldehyde.
- FE-SEM and FTIR analyses confirmed enhanced $CaCO_3$ formation in the composites.
- The developed mortar offers a sustainable and environmentally friendly building material.

Citation: Mirawati B, Sadir M, Hendriko A, Wangiyana IGAS, Budiman I, Hermawan D, Pari G, Juwono AL. Mechanical properties and volatile pollutants absorbing capacity of mortar composites with addition of coconut shell activated carbon and gamal wood chips aggregates. Environ. Nat. Resour. J. 2026;24(6):642-660. (https://doi.org/10.32526/ennrj/24/20250337)

1. INTRODUCTION

Along with the development of a civilization, especially after the industrial revolution, human intervention often causes air pollution to become an unavoidable problem, where the consequences of this air contamination can specifically affect health and mortality rates in various nations, especially those that are left behind and still developing (Meda et al., 2022). One of the major emissions that is a pollutant is ammonia (NH_3) emissions, which amount to ~80% comes from the agricultural sector, where ammonia is actually a precursor to fine particulate matter (PM 2.5) which is more dominant than nitrogen oxide (NO_x) and sulfur dioxide (SO_2); and contributes to respiratory health problems (Wyer et al., 2022). Chloroform ($CHCl_3$) is also one of the largest contributors to atmospheric chlorine emissions that can have an impact on ozone damage, where chloroform often appears due to various organic matter found in the soil naturally or deposited due to human intervention such as its use in various refrigerants (Enyoh et al., 2020; Zhang et al., 2021).

In a study conducted by Van Tran et al., (2020) it was explained that indoor air pollution also has a significant impact on human health (mortality of ~3.8 million people per year), where humans spend 90% of their time indoors. Formaldehyde (HCHO) compounds are volatile compounds that produce emissions from indoor furniture produced from the use of resin, paint, and varnish in the manufacturing process, where this compound contributes to soft tissue irritation in the respiratory tract, nose, eyes, and has the potential to be carcinogenic (Mannan and Al-Ghamdi 2021; Salthammer, 2019). Benzene is a volatile compound that is unknowingly present as an indoor pollutant caused by heating and combustion processes such as smoking and cooking with fossil fuels, where benzene has the potential to be carcinogenic (Sekar et al., 2019: Zhang et al., 2020).

Activated carbon is a widely used adsorbent that can be produced from biomass waste such as coconut shells. Coconut shells are widely utilized as biomass waste owing to their hardness, high carbon density, and renewability. While coconut shells offer a renewable feedstock for activated carbon production, the conventional manufacturing route, which relies on high-temperature pyrolysis under inert conditions, is energy-intensive. This results in a substantial embodied energy within the product and a considerable carbon footprint, posing a significant challenge to the overall life-cycle sustainability of the material. The use of coconut (*Cocos nucifera*) shells as activated carbon (Figure 1(d)) has succeeded in becoming a highly useful commodity and is easily obtained commercially, in addition to having high availability and competitive prices, this material has stable and environmentally friendly physicochemical characteristics (Wang et al., 2019; Sujiono et al., 2022). The use of activated carbon from biomass as an option for absorbing pollutants has begun to be widely developed to overcome environmental pollution problems, in addition to being more sustainable and easily regenerated, this biomass activated carbon has resistance to high temperatures, resistance to strong acids and bases, and good chemical stability (Gayathiri et al., 2022). Research conducted by Sadir et al. (2022) used activated carbon from kenaf stems (*Hibiscus cannabinus* L.) to absorb hazardous volatile compounds such as ammonia, benzene, chloroform and formaldehyde.

Gliricidia sepium (Figure 1(a)-(b)) is a type of leguminous plant that is widely found in tropical and subtropical areas starting from Southeast Asia, Sub-Saharan Africa, to Central America, which has many uses especially in terms of reforestation, soil preservation, and organic fertilizer (Barberi, 2019; Aulanni'am et al., 2021; Alamu et al., 2023). Coulibaly et al. (2017) explained that *G. sepium* is a plant that has the potential to contribute nutrients to the soil in the form of organic compounds and nitrogen; and its wood waste is widely used as firewood. In Indonesia, *G. sepium* is known as gamal wood, which is widely used for shade plants in various plantations because it has good morphology and grows quickly in non-ideal soil conditions, such as in soil with high calcium content (Khusnul et al., 2020). Barberi (2019) explained that biomass production from coppicing fallow legume species such as *G. sepium*, *Leucaena trichandra*, and *Calliandra calothyrsus*; is 8 times higher than from non-coppicing fallow legume species such as *Sesbania sesban*, *Mucuna pruniens*, and *Tephrosia vogelii*.

As a composite material, concrete has mechanical advantages such as high compressive strength, good heat insulation, sound absorption capacity, fire resistance, and seismic damping (Aslam et al., 2016). Despite its superior performance, concrete composites have weaknesses that affect their performance, such as low tensile strength and ductility, so that concrete is susceptible to cracking because the tensile strength value is lower than the compressive strength value (Hermawan et al., 2022). In the process

of making cement as the main raw material for concrete, it is one of the contributors to carbon emissions in the world (~7-8% CO_2), so the development of sustainable concrete is very relevant to answer this problem (Nilimaa, 2023). Onyelowe et al. (2022) explains that one of the efforts to develop sustainable concrete is to use various renewable materials to reduce or replace concrete materials that have an environmental impact, with the hope of maintaining or improving the mechanical properties of the concrete.



Figure 1. Picture of: a. Gamal wood plant; b. Cross section of gamal wood; c. Gamal wood chips; d. Coconut shell activated carbon

The development of natural materials and other lignocellulosic cement-based materials will be able to bond well into composites if the chemical components of hemicellulose and wood extractives are first removed or reduced; one of which is done by hydrothermal carbonization which is more environmentally friendly and effective in reducing the content of hemicellulose and wood extractives at low temperatures (Majzoobi et al., 2016). Increasing concern for environmental issues, urging more versatile environmentally friendly materials, has led to increasing attention to polymer composites, namely fillers or reinforcing materials derived from renewable and biodegradable sources (Alzard et al., 2022). The use of activated carbon as an additional aggregate to improve the quality of cement composites has gained high traction in this decade, such as in the study of Zheng et al. (2017) explained that there was an improvement in the mechanical properties (compressive and flexural strength) of cement mortar with the addition of powdered activated carbon aggregate up to 2.0%. One of the advantages of using activated carbon as an aggregate is that it can increase the adsorption capacity of volatile organic compounds as in the study of Krou et al. (2015) where the addition of activated carbon to cement paste can increase the adsorption capacity of actaldehyde and toluene.

Prior research has explored the enhancement of mechanical and functional properties of concrete through various additives. For instance, a composite incorporating 4% NaOH-modified wood powder combined with 3% silane coupling agent demonstrated improvements in flexural and compressive strength. Specifically, flexural strength increased by 31.6% compared to mortar without wood powder, and by 27.1% compared to mortar containing unmodified wood powder. Meanwhile, compressive strength showed a 28.7% increase relative to the unmodified wood powder composite, although it remained slightly lower than the control mortar without wood powder (35.4 MPa vs. control) (Li et al., 2025). Regarding pollutant adsorption, high-silica fly ash (SDS-FA) modified with sodium dodecyl sulfate achieved a maximum methylene blue adsorption capacity of 84.46 mg/g, while mesoporous silica material (MSM) reached 115.34 mg/g, underscoring the enhanced efficiency achieved through material modification (Guo et al., 2024).

However, existing approaches often focus on improving a single performance aspect either mechanical or functional potentially at the expense of other properties. Consequently, a knowledge gap exists in the development of mortar composite materials that achieve synergy between enhanced mechanical properties particularly tensile and flexural strength and significant pollutant adsorption capacity. Technically, this study does not merely evaluate partial aggregate substitution but aims to create an integrated composite system wherein the two materials complement each other gamal wood chips serve as a lightweight filler, while activated carbon particles function as an adsorbent agent. This combination has the potential to equip the mortar with the ability to adsorb air pollutants, regulate humidity, and enhance bonding within the

cement matrix through the microscopic porous structure of the activated carbon. Based on this explanation, the purpose of this study was to analyze the characteristics of the adsorption capacity of hazardous pollutants of composite mortar with the addition of commercial activated carbon from coconut shells and to analyze the characteristics of the mechanical properties of composite mortar with the addition of activated carbon from coconut shells and gamal wood chips (*G. sepium*).

2. METHODOLOGY

2.1 Materials

The main materials that used in this research are the form of portland composite cement (PCC) (Bosowa); silica sand taken from local miners in East Lombok, Indonesia; gamal wood (*G. sepium*) taken from local plantations in Sedau, Central Lombok, Indonesia; and commercial coconut shell activated carbon (AF Carb). For additives, calcium chloride ($CaCl_2$) was used with the aim of creating a more stable mixture and controlling the hydration rate so that it can potentially become an accelerator that accelerates the formation of silica sand strength (Salain, 2019; Almajed et al., 2023). The solutions used as a reflection of pollutants were 25% ammonia solution, benzene solution, chloroform solution, and 37% formaldehyde solution.

2.2 Research methods

The research process is divided into three stages. In the first stage, gamal wood chips were made and the raw materials were characterized before the composite mortar was made. In the second stage, cubes and blocks of composite mortar were made, followed by various mechanical tests such as compression tests, density measurements, modulus of elasticity tests, modulus of rupture tests, and pollutant absorption analysis. In the third stage, the selected mortar composition was characterized using FTIR and microstructural analysis using an electron microscope. Figure 2 shows a more comprehensive and thorough research flow.

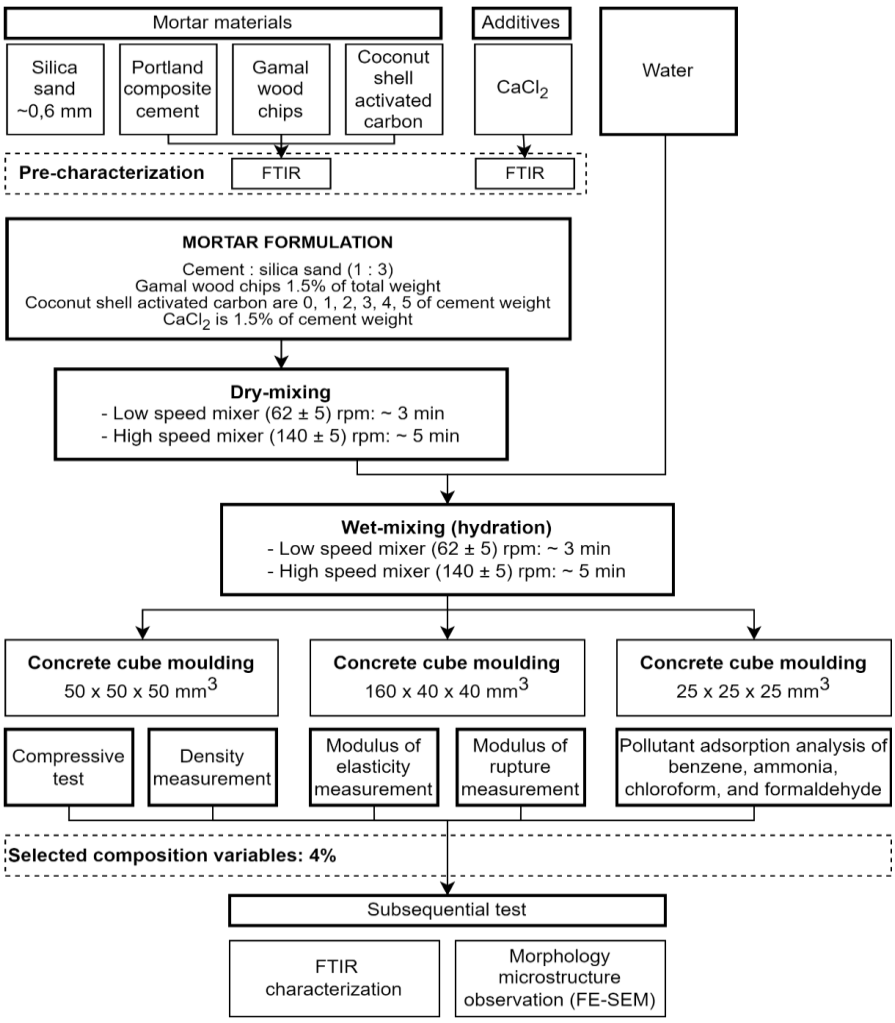


Figure 2. Research flowchart

2.2.1 Manufacturing process of gamal wood chips

Gamal wood is dried in the sun to reduce its water content to <10% which is measured by sampling using a moisture meter. After being separated from its skin, the gamal wood is cut into 1-2 cm sizes. Furthermore, the gamal wood chips are boiled using boiling water for 2 h. This aims to clean the dirt that is still attached, then the gamal wood chips are dried again until they reach a water content of <10%. Gamal wood chips can be seen in Figure 1(c).

2.2.2 Preliminary characterization of mortar composition using Fourier-Transform Infrared Spectroscopy (FTIR)

Characterization using FTIR (Perkin Elmer) was used to determine the chemical bonds contained in the mortar raw materials in this study, namely coconut shell activated carbon, gamal wood chips, $CaCl_2$, and portland cement. This material characterization was used in the initial stage as confirmation that the material used was in accordance with its characteristics and uses, where 2 mg of each finely ground sample was analyzed with a resolution of 32 cm^{-1} at a wave number of 450-4,000 cm^{-1} (Emmanuel et al., 2015; Tighsazzadeh et al., 2019; Jesus et al., 2024). This FTIR characterization was also carried out on selected mortar composition specimens that had the best mechanical properties.

2.2.3 Manufacturing of mortar composite

Composite mortar in the form of mortar is made with a mixture of sand, cement, water, gamal wood chips, additives ($CaCl_2$), and coconut shell activated carbon. The manufacture of composite mortar is carried out by adopting SNI 8837-1:2019 (BSN, 2019). The ratio of cement and sand is 1:3, with the percentage of water addition of 50% of the weight of the cement (w/c ratio 0.5). Furthermore, activated carbon is added with a percentage of 1, 2, 3, 4, and 5% of the weight of the cement, and $CaCl_2$ of 1.5% of the weight of the cement. Gamal wood chips are used as much as 1.5% of the total weight of the mortar formulation mixture. Wood swells when it absorbs water; hence, adding wood chips to the mortar is expected to affect the fresh and hardened properties of the mixture, particularly its workability, density, and dimensional stability under varying moisture conditions. The formulation for making composite mortar can be seen in Table 1.

Table 1. Mortar formulation

Sample code	Materials				Additives	Total weight (kg)	Water (L)
	PCC	Silica sand 0.6	Gamal wood chips	Activated carbon	$CaCl_2$		
	kg	kg	kg	kg	kg		
Activated carbon 0%	3	9	0.18	-	0.045	12.225	1.5
Activated carbon 1%	3	9	0.18	0.03	0.045	12.255	1.5
Activated carbon 2%	3	9	0.18	0.06	0.045	12.285	1.5
Activated carbon 3%	3	9	0.18	0.09	0.045	12.315	1.5
Activated carbon 4%	3	9	0.18	0.12	0.045	12.345	1.5
Activated carbon 5%	3	9	0.18	0.15	0.045	12.375	1.5

In this experimental investigation, silica sand was selected for its high SiO_2 content to promote pozzolanic reactions and enhance mortar properties, with its technical benefits justifying the higher cost. A fixed 1.5% dosage of Gamal wood chips was employed across all mixtures as a controlled secondary variable, enabling isolated evaluation of activated carbon content (0-5%) as the primary variable; this dosage was chosen based on preliminary studies or literature to minimize adverse effects such as increased porosity or weak interfacial zones. The manufacture of composite mortar mixture begins with mixing dry ingredients according to the composition used using a mixer (3 min, 60 rpm and 5 min, 140 rpm). Hydration is carried out by adding water mixed with a mixer at the same time and speed as dry mixing. The mixture is poured into a mold with dimensions of 50×50×50 mm^3 and left for 24 h to set, then cured in water for 28 days. The manufacture of mortar cubes in more detail will be explained in point 2.2.4 regarding the compression test by adopting the method from SNI 03-6825-2002 (BSN, 2002b). The results of the manufacture of mortar cubes can be seen in Figure 3(a).

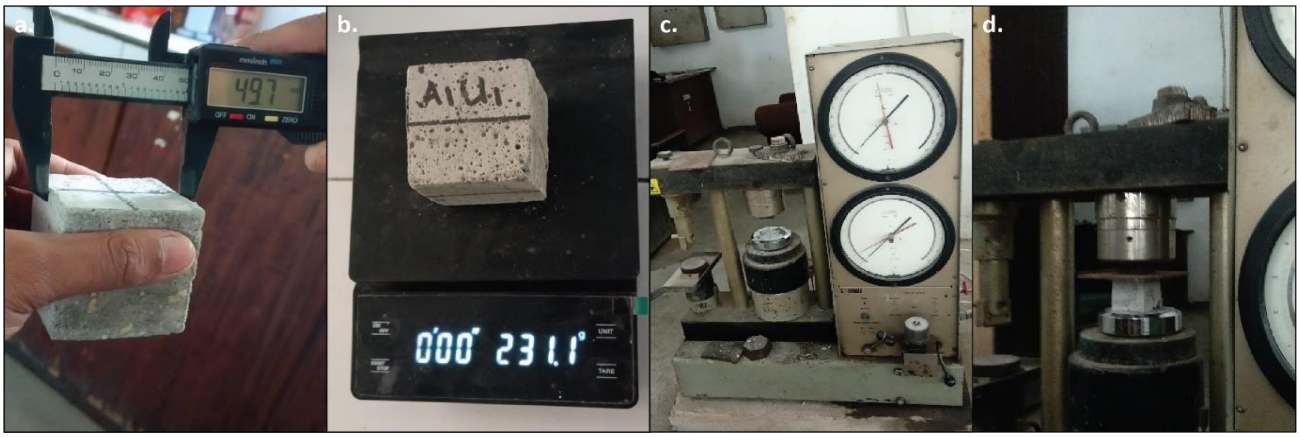


Figure 3. Test specimen; a. mortar cube; b. sample weight; c. and compressive test; d.

2.2.4 Compressive strength test

Compression testing was carried out based on SNI 03-6825-2002 (BSN, 2002b). In line with the mortar making process, the homogeneous mortar mixture was molded into a steel mold with dimensions of 5×5×5 cm^3. The molding was done in 2 layers to avoid too much air being trapped. Each layer must be compacted 32 times with 4 rotations and must be started no later than 2.5 min after mixing.

The upper surface of the test cube mold was leveled and allowed to set overnight (24 h) and then released from the mold and cured in a tub filled with clean water. The curing time was determined periodically until the 28th day. Samples for the compression test in this study were taken in triplicate at the curing time on the 28th day. The compression test was carried out with a 1000 KN universal testing machine (Controls) and is shown in Figure 3(c)-(d). The results of the compression test can be calculated using Equation 1, where f'_m is the compressive strength (MPa), P_{max} is the maximum compressive force (N), and A is the test cross-sectional area (cm^2).

$$f'_m = \frac{P_{max}}{A} \quad (1)$$

2.2.5 Measurement of density

Density measurements were carried out based on SNI 03-6825-2002 (BSN, 2002b) using sample specimens with dimensions similar to the sample specimens used for the compressive strength test, namely 5×5×5 cm^3. The sample specimens tested for density were sample specimens in a condition that had been set and had been air-dried in room conditions (not in wet conditions after soaking). Density measurements can be seen in Figure 3(b) and are calculated using Equation 2 where ρ is the mortar density (kg/m^3), m is the mass of the sample (kg), and v is the volume of the sample (m^3).

$$\rho = \frac{m}{v} \quad (2)$$

2.2.6 Modulus of elasticity (MOE) and Modulus of rupture test (MOR)

Measurement of modulus of elasticity and modulus of rupture were carried out simultaneously by adopting the method of EN 1015-11-2000 (CEN, 2000), where in the elastic modulus the test specimen can still return to its original shape, while in the modulus of rupture the test specimen is pressed to its breaking point. Figure 4 shows the process of testing the modulus of elasticity and modulus of rupture.

The test specimen was molded in the form of a block with a size of 160×40×40 mm^3. The modulus of elasticity is calculated by Equation 3 where MOE is the modulus of elasticity (MPa), P is the load before the proportion limit (N), ΔY is the bending distance at the load P (mm), L is the height of the support (mm), b is the length of the test specimen (mm), and h is the thickness of the test specimen (mm). The modulus of rupture is calculated by Equation 4 where MOR is the modulus of rupture (MPa), P is the load before the proportion limit (N), L is the height of the support (mm), b is the length of the test specimen (mm), and h is the thickness of the test specimen (mm).

$$MOE = \frac{\Delta PL^3}{4\Delta Ybh^3} \quad (3)$$

$$MOR = \frac{3PL}{2bh^2} \quad (4)$$

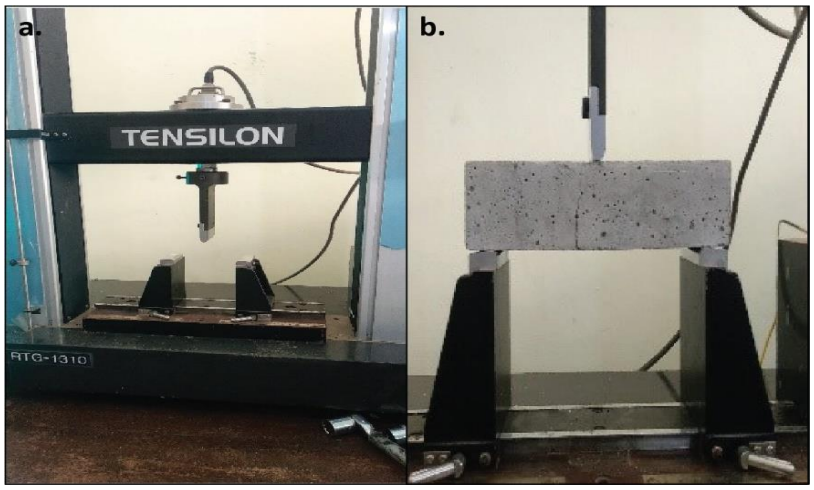


Figure 4. Flexural test specimen: a. instrument for bending test; b. testing procedure

2.2.7 Pollutant adsorption analysis

Pollutant adsorption testing was carried out by adopting the method from SNI 06-3730-1995 (BSN, 1995), where in principle pollutant absorption is seen from the difference in weight of the test specimen. Pollutants are reflected with technical solutions in the form of ammonia, benzene, chloroform, and formaldehyde. The test specimen was printed in a size of 2.5×2.5×2.5 cm^3 and weighed its initial weight and then stored in a desiccator for 24 h with the bottom (where the silica gel is) replaced with 100 mL of pollutant solution. The volatile nature of this pollutant solution will cause it to be absorbed into the mortar specimen. Pollutant adsorption testing is seen in Figure 5 and calculated using Equation 5, where N is the percentage of pollutant adsorption (%), W_1 is the initial weight of the test specimen (g), and W_2 is the final weight of the test specimen (g).

$$N = \frac{W_2 - W_1}{W_1} \times 100\% \quad (5)$$

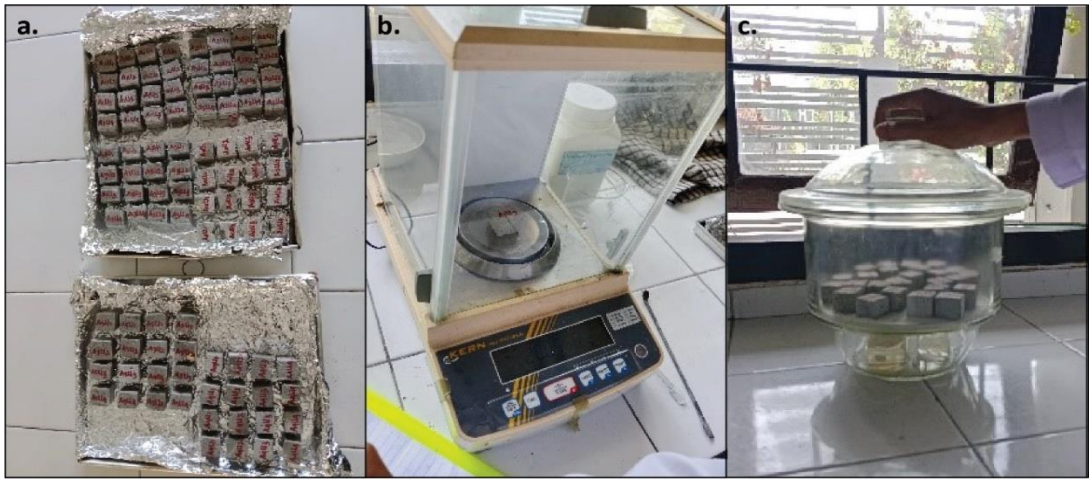


Figure 5. Pollutant adsorption test: a. Mortar cube; b. Sample weight; c. Pollutant induction in desiccator

2.2.8 Microstructure analysis on selected composition using field emission - scanning electron microscope (FE-SEM)

Morphological observation of mortar samples was carried out using Field Emission - Scanning Electron Microscope (JEOL) imaging using back-scattered electrons with an intensity of 10 keV Choi et al. (2005) with a magnification of 300× and 1000×. The preparation of test specimens was carried out by adopting the method in Nemati (1997), where the samples were cut with dimensions of 25×25 mm^2 and a thickness of 5 mm which were fixed with a 25mm diameter glass slide.

2.3 Data analysis

Statistical analysis was conducted on the results of compression, density, modulus of elasticity, modulus of rupture, and percentage of pollutant adsorption capacity tests. Statistical tests were conducted using the one-factor completely randomized design (CRD) method and Duncan's test with a significance level of 95%.

3. RESULTS AND DISCUSSION

3.1 FTIR analysis of raw materials

The characterization of materials in this study includes coconut shell activated carbon, gamal wood chips, calcium chloride ($CaCl_2$), and portland cement using FTIR which is shown in the collection of spectra in Figure 6. The FTIR spectrum of activated carbon in Figure 6(a) shows absorption bands related to hydroxyl groups, carboxyl groups, phenolic hydroxyl groups, and carbonyl groups. The hydroxyl group (O-H) is shown at a wave number of 3,433 cm^{-1}. The wave number of 2,062 cm^{-1} indicates the presence of a C≡N bond, where bonds with nitrogen elements are common in plant-based materials (Xie et al., 2020; Nedjai et al., 2021). The wave number of 1,636 cm^{-1} indicates the C=C group in the aromatic ring as a result of changes in the C-O group, and the activity of the carboxyl-oxygen atom (Ahmad et al., 2015; Lazim et al., 2015). The wave number of 1,086 cm^{-1} is the C-O group, which is a stretch in the lactonic group, alcohol and carboxylic group (Kumar et al., 2013; Deng et al., 2009). The wave number of 688 cm^{-1} indicates the presence of aromatic C-H groups (Koseoglu and Akmil-Basar, 2015). Functional groups like C-O stretches in cellulose/lignin, aromaticity peaks, and oxygenated groups to assess stability, surface chemistry, and activation effects (McCall et al., 2025; Marangon et al., 2025).

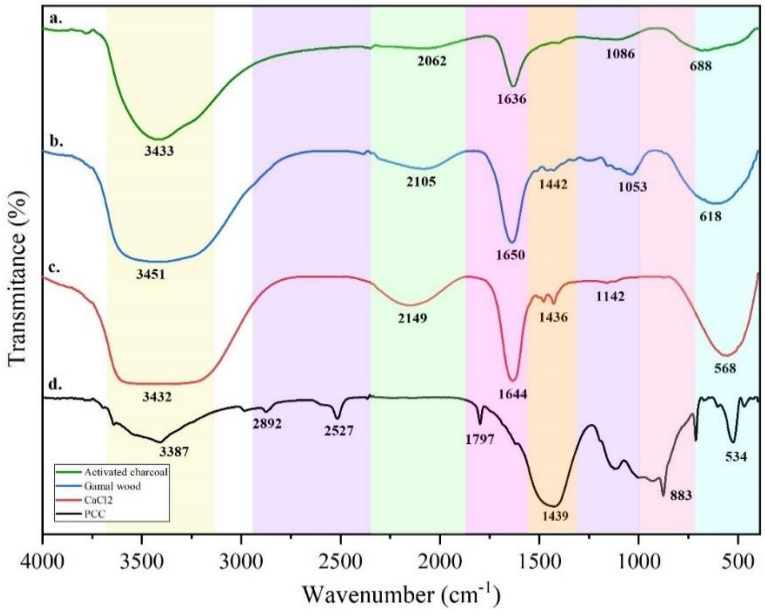


Figure 6. FTIR Spectra: a. activated carbon; b. gamal wood; c. $CaCl_2$; d. PCC

The FTIR spectrum of gamal wood chips in Figure 6(b) shows absorption bands related to alcohol, aldehyde, alkane, amine, aliphatic and aromatic groups. At a wave number of 3,451 cm^{-1} shows the O-H group caused by phenolic and alcohol compounds (Oladunmoye et al., 2018). The O-H group in gamal wood affects the curing process of cement. The wave number of 2,105 cm^{-1} shows C-H stretching, the identified compound is carbonyl. This absorption area is caused by alkanes and alkenes (Valdivielso et al., 2023). The same results were obtained in the study Oyelere and Oluwadare (2019). Wave number 1,650 cm^{-1} indicates C=C stretching, Wave number 1,442 cm^{-1} indicates C-H group, chemical compounds in both absorptions are alkanes. Absorption band 1,053 cm^{-1} indicates C-N stretching, chemical compounds identified are aromatic amines. Absorption band 618 cm^{-1} indicates C-Br group, chemical compounds identified are aliphatic bromo compounds. This FTIR data provides a scientific basis for understanding how chemical modification of the surface of gamal wood can increase interfacial adhesion between wood

particles and cement matrix, reduce water absorption by wood and improve the mechanical performance and durability of the resulting composite mortar.

FTIR spectrum of calcium carbonate ($CaCl_2$) in Figure 6(c) shows absorption bands related to hydroxyl, ether, and carboxylate groups. The $CaCl_2$ spectrum shows a peak at wave number 3,432 cm^{-1} with asymmetric O-H stretching (Pongjanyakul and Rongthong, 2010). The H-O-H group at wave number 1,644 cm^{-1} is caused by the presence of water in $CaCl_2$ (Cho et al., 2014). The use of $CaCl_2$ in cement can increase the initial binding time with cement paste (De Weerdt, 2021). The addition of additives ($CaCl_2$) to cement can increase workability, and reduce water bleeding during hydration (Dobiszewska et al., 2023). These spectral features are useful for identifying $CaCl_2$ phases and assessing hydration and dehydration processes via FTIR. The presence of water and Ca-Cl bonds can be clearly distinguished, providing insights into chemical structure and physical state changes of $CaCl_2$ (Mustapha et al., 2024; Zhao et al., 2024; Kudzin et al., 2025).

The FTIR spectrum of PCC (Cement Portland Composite) in Figure 6(d) shows the hydroxyl group (O-H) spectrum at 3,387 cm^{-1} absorption, C-H groups at 2,892 cm^{-1} and 2,527 cm^{-1} absorption, C-O groups at 1,797 cm^{-1} and 534 cm^{-1} absorption, and deformed C-H groups at 1,439 cm^{-1} and 883 cm^{-1}. The results of this study are in line with the research of Horgnies et al. (2013). The peak at wave number 3,387 cm^{-1} corresponds to $Ca(OH)_2$, which is formed as a silicate phase in cement, and the absorption at 1,500 cm^{-1} to 1,700 cm^{-1} is indicative of the formation of calcium silicate hydrate (CSH) (Ylmen et al., 2009). Key hydration products detected by FTIR include calcium silicate hydrate (C-S-H), portlandite (calcium hydroxide), and calcium carbonate formed during carbonation. FTIR spectra can reveal changes in functional groups and phases, such as the decalcification-polymerization of C-S-H and carbonation effects that influence the mechanical and chemical properties of cementitious materials (Adem et al., 2025; Li et al., 2025).

3.2 Density measurement of mortar composite

The density of composite mortar with the addition of activated carbon and gamal wood chips ranges from 1,950.36±19.54 - 2,137.24±45.09 kg/m^3 (Figure 7).

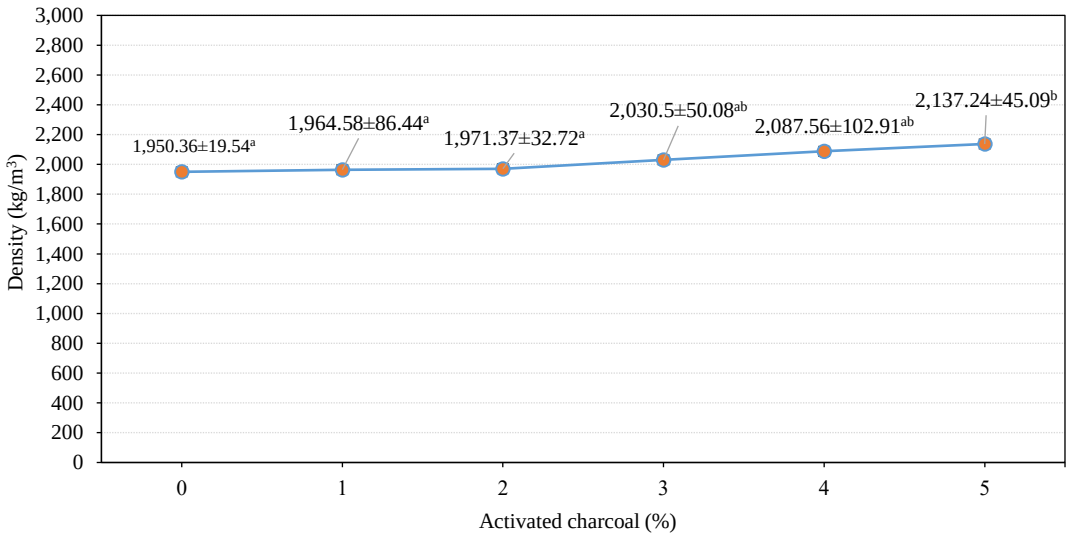


Figure 7. Density measurement of mortar composite

The results of the study showed that the density of the composite mortar increased with the increase in the content of activated carbon. The results of statistical analysis showed that there was a significant difference in the addition of activated carbon to the density of composite mortar. The addition of activated carbon to the cement matrix will make the mortar denser, improving the microstructure of the cement matrix (Nagrockiene et al., 2017). Research conducted by Mahoutian et al. (2015) explained that the number of air cavities in the mortar will decrease with the addition of 10% activated carbon from the weight of cement. Moon et al. (2017) explained that the hydration process of activated carbon and hydration products that fill the pores of the cement paste, affect the slightly greater density, as seen in this study. Chin

et al. (2020) explained that there was a significant weight reduction in the range of 14% to 27%, with the addition of activated carbon, compared to the density of conventional concrete of ~2,400 kg/cm^3. Wood and rice husk biochars (5%) increased compressive strength by 29% via filler effects and internal curing, implying density stabilization; manure biochar reduced strength and likely density due to coarse particles (Kang et al., 2025). Activated carbon or biochar additions to mortar, often as cement replacements (0.1-24%), noting effects on density, strength, and durability through pozzolanic reactions, filler effects, and internal curing (Wu et al., 2025). The reduction of density in mortars also being affected by the usage of gamal wood chips, where in nature the density of gamal wood chips it self are pretty much lower than common aggregates such as sand.

3.3 Compressive strength of mortar composite

The compressive strength test results of the composite mortar ranged from 8.48±0.76 - 9.71±1.68 MPa (Figure 8). Overall, there was an increase in the compressive strength value with the addition of activated carbon, but with the addition of 5% activated carbon, the compressive strength value decreased. There was an increase in the compressive strength value of 14.57% with the percentage of activated carbon addition of 4%. This phenomenon is attributed to the porous structure of activated charcoal and its capillary adsorption effect, which effectively absorbs free water within the cement mortar, thereby reducing the effective water-to-cement ratio and promoting the formation of a dense cementitious matrix that significantly enhances mechanical strength (Li et al., 2025). The incorporation of activated carbon at a dosage of up to 4% improves compressive strength through a micro-filler mechanism that densifies the matrix and provides nucleation sites for calcium silicate hydrate (C-S-H) growth; however, at a 5% addition level, strength reduction occurs due to the material's high specific surface area, which absorbs excessive water, thereby inhibiting hydration and increasing porosity.

The inclusion of 1.5% Gliricidia wood chips tends to marginally reduce compressive strength, attributed to the formation of a weak interfacial transition zone between the organic wood particles and the cement paste, as well as the hygroscopic nature of the wood chips that disrupts local hydration, although this adverse effect remains relatively minimal at such a low dosage. The interaction between these materials indicates that the combination of 4% activated carbon with 1.5% wood chips represents the optimal scenario, as the densification benefits of the carbon effectively compensate for the weaknesses introduced by the wood chips, whereas the combination of 5% activated carbon with 1.5% wood chips yields the most pronounced reduction in strength, as the high porosity caused by excess carbon is exacerbated by the weak zones introduced by the wood chips.

The compressive strength value is much greater than without the addition of activated carbon. This shows that increasing the content of activated carbon has an effect on increasing the compressive strength value (Zheng et al., 2017; Swaroop and Raj, 2019). The results of the statistical analysis showed a significant difference in the addition of activated carbon (especially in the addition of 4% of activated carbon) to the compressive strength value of the composite mortar (Figure 8).

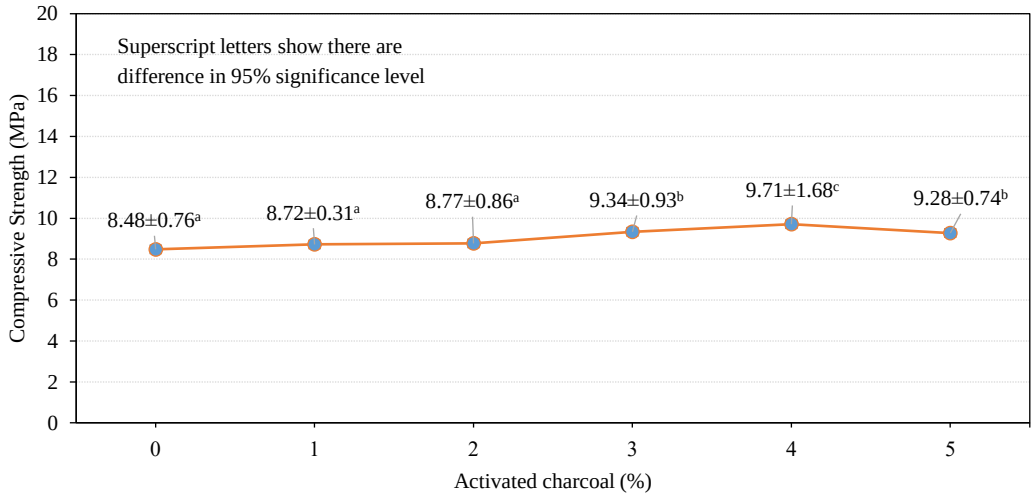


Figure 8. Compressive strength of mortar composite on 28th day curing time

Excessive activated carbon content results in a significant decrease in strength (Na et al., 2021). The compressive strength value of the results of this study decreased by around 4.49% with the addition of 5% activated carbon. The higher compressive strength value in this study can be attributed to the hydration process of activated carbon that fills the pores of the cement paste (Moon et al., 2017). A smaller concentration of activated carbon can accelerate the curing process (Justo-Reinoso et al., 2018). The compressive strength value of the results of this study is in line with previous studies (Chin et al., 2020; Na et al., 2021; Shafigh et al., 2011). Overall, the compressive strength value of the composite mortar from this study is classified as K100 concrete quality which is intended for non-structural concrete (quality fc>8.3 MPa) according to the standard of SNI 03-2847-2002 (BSN, 2002a).

3.4 Modulus of elasticity and modulus of rupture of mortar composite

The results of the modulus of elasticity (MOE) test of composite mortar ranged from 421.74±69.59 - 645.58±57.51 MPa (Figure 9(a)). With the addition of 4% activated carbon, the MOE was higher than mortar composite without activated carbon, and decreased with increasing activated carbon content. The MOE value tends to be linear with the resulting compressive strength value. This statement is supported by research by Nazari and Riahi, (2011) that there is linearity between the compressive and flexural strength values in mortar or concrete. Based on Figure 10a, it shows that there is an increase in the MOE value of 53.08% with the percentage of activated carbon addition of 4%, and a decrease of around 32.04% with the addition of 5% activated carbon. The most effective activated carbon content is 4% in practical use and performance (Youn et al., 2009; Khushnood et al., 2015). The results of statistical analysis showed significant difference in the addition of activated carbon to the MOE value. Research conducted by Hermawan et al. (2022) also explains that the MOE value increases with the addition of activated carbon up to 3% of the cement weight.

The results of the modulus of rupture (MOR) test of composite mortar ranged from 2.14±0.27 - 2.75±0.20 MPa (Figure 9(b)), where there was an increase in the MOR value of 28.50% with the addition of 4% activated carbon, and decreased by around 20.73% with the addition of 5% activated carbon. This decrease is due to the proportion of mortar that is not reactive in the cement hydration process. This is in line with the findings in the addition of carbon nanotubes to mortar (Chin et al., 2020). These results show that MOR can increase with the inclusion of activated carbon as a filler in the composite. The results of the statistical analysis showed no significant difference in the addition of activated carbon to the MOR value (Figure 9(b)). The same increasing trend occurred in the compression and MOE tests, meaning that the optimal strength obtained in this study was found in the addition of 4% activated carbon.

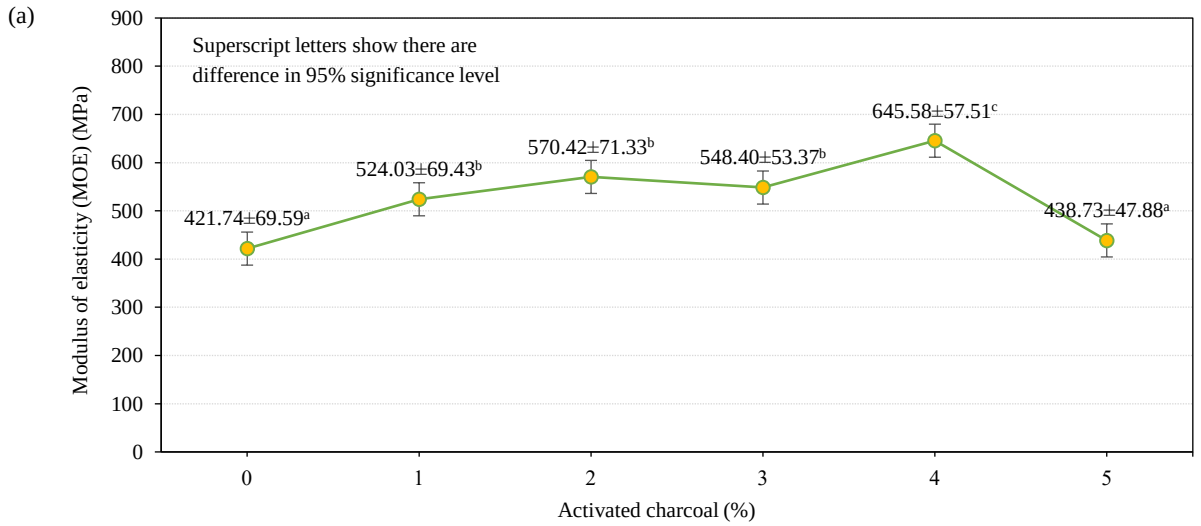


Figure 9. Flexural properties: (a) modulus of elasticity; (b) modulus of rupture

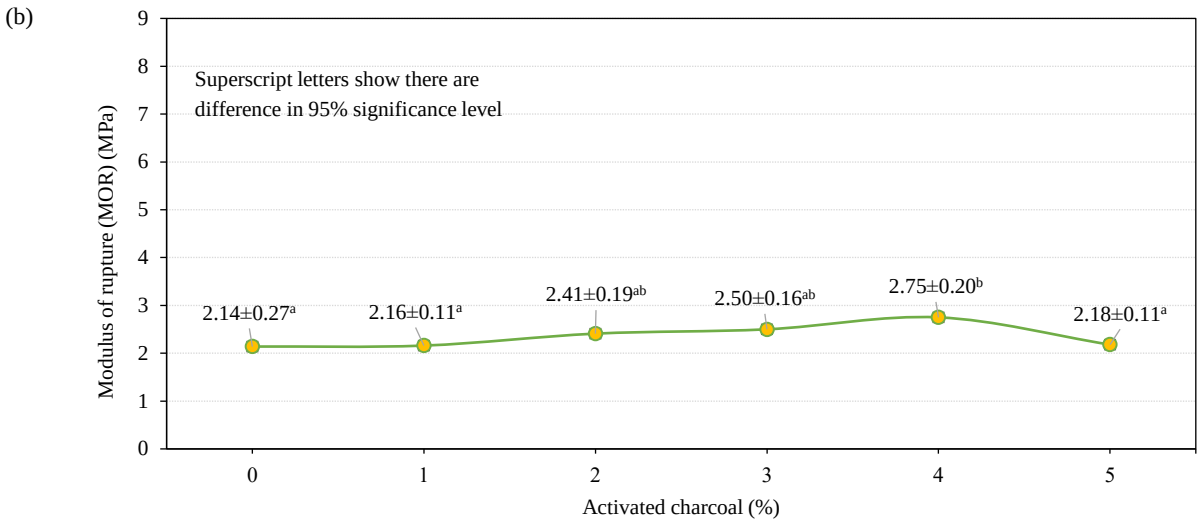


Figure 9. Flexural properties: (a) Modulus of elasticity; (b) Modulus of rupture (cont.)

The addition of 4% activated charcoal by cement weight in the mortar mixture can significantly enhance the Modulus of Elasticity (MOE) and the Modulus of Rupture (MOR) due to the pozzolanic properties of activated charcoal, which is rich in silica and alumina and effectively fills the micro-pores in the mortar's microstructure, thereby strengthening the cement-sand matrix bond (Dias et al., 2025). This improvement is also supported by increased density and durability of the composite mortar, where an optimal composition of 3-4% activated charcoal improves mechanical properties without disrupting the cement hydration process. MOR increases with the amount of activated carbon used, this is related to the hygroscopic nature of activated carbon. The use of more activated carbon will produce more $CaCO_3$ crystals. The chemicals in these crystals provide mechanical strength to the mortar (Hermawan et al., 2022). The addition of additives that act as fillers in high-quality concrete affects the MOR value (Salami et al., 2024). The use of activated carbon with a smaller size and smaller proportion will produce stronger mechanical properties.

3.5 Pollutant adsorption percentage of mortar composite

Pollutant adsorption test on composite mortar shows the level of activated carbon's ability to adsorb hazardous pollutant materials based on the SNI 06-3730-1995 (BSN, 1995) standard, on standard test methods for adsorption of benzene, chloroform, and iodine. Pollutant adsorption test of composite mortar includes adsorption of ammonia, benzene, chloroform, and formaldehyde. The results of the pollutant adsorption test can be seen in Figure 10.

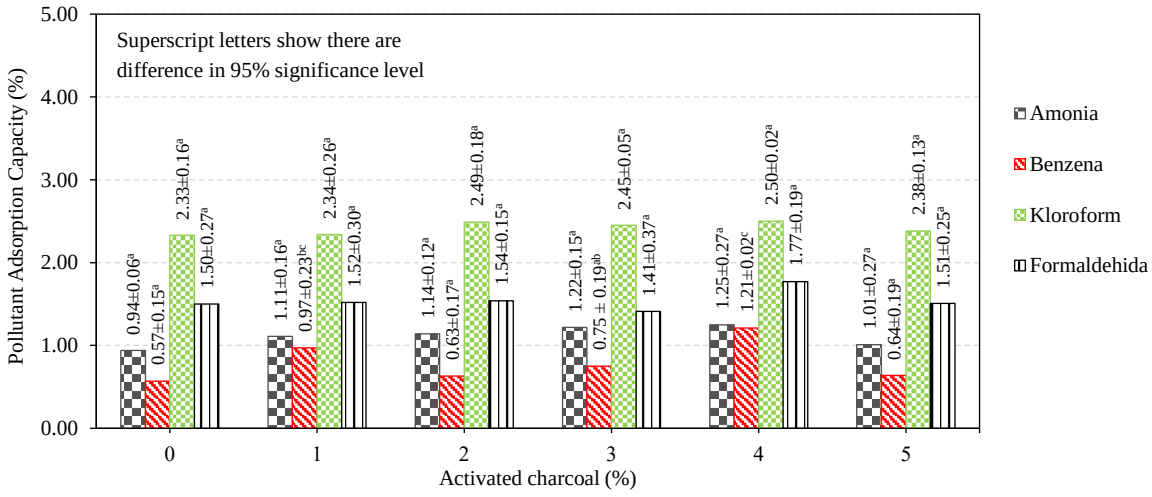


Figure 10. Percentage of pollution adsorption capacity of mortar composite

The pollutant adsorption of composite mortar to ammonia ranges from 0.94±0.06 - 1.25±0.27%. With the addition of 4% activated carbon, the ammonia adsorption is higher compared to mortar composite without activated carbon, and decreases with increasing activated carbon content. The percentage of pollutant adsorption to ammonia is much higher than after being applied to composite mortar. Previous studies reported that the adsorption capacity of activated carbon on ammonia from kenaf stems ranged from 11.21 to 29.78% (Sadir et al., 2022). The results of statistical analysis showed no significant difference in the addition of activated carbon on the ammonia adsorption capacity value. The modification process can result in blockage of the composite mortar's ability to drastically reduce the adsorption capacity (Guo et al., 2005). The ability of composite mortar to adsorb ammonia tends to increase with the amount of activated carbon used. The surface area and pore volume of activated carbon have an impact on the material's capacity to adsorb various contaminants (Budiman et al., 2019).

The adsorption capacity of composite mortar pollutants on benzene ranged from 0.57±0.15 - 1.21±0.02%. With the addition of 4% activated carbon, the adsorption capacity of benzene was higher compared to mortar composite without activated carbon, and decreased with increasing activated carbon content. The percentage of pollutant adsorption capacity for benzene is much higher than after being applied to composite mortar. According to previous studies, the adsorption capacity of benzene by activated carbon from kenaf stems ranges from 10.59 to 13.95% (Sadir et al., 2022). The results of statistical analysis show that there is a significant difference in the addition of activated carbon to the benzene adsorption capacity value (Figure 10). The pores or surface area of activated carbon are directly related to the adsorption value obtained, therefore the larger the surface area of activated carbon, the greater the adsorption capacity (Malini et al., 2023). In addition to reducing the load, activated carbon also functions as an adsorbent when added to mortar, but the low adsorption capacity of mortar is due to the reaction of activated carbon with other components such as cement (Hermawan et al., 2022).

The pollutant adsorption capacity of composite mortar for chloroform ranges from 2.33±0.16 - 2.50±0.02 %. With the addition of 4% activated carbon, the chloroform adsorption capacity was higher compared to mortr composite without activated carbon, and decreased with increasing activated carbon content. The effect of activated carbon formulation on chloroform adsorption capacity is illustrated in Figure 10. The percentage of pollutant adsorption capacity for chloroform was significantly higher than when applied to composite mortar. Previous studies have shown that activated carbon from kenaf stems can adsorb chloroform at a level of 20.5% to 26.72% (Sadir et al., 2022). The results of statistical analysis showed no significant difference in the addition of activated carbon to the chloroform adsorption value (Figure 10). The surface area and pore volume of activated carbon determine its ability to adsorb contaminants (Budiman et al., 2019). The adsorption capacity of activated carbon to chloroform shows that its surface is polar therefore, the higher the adsorption capacity, the more polar molecules remain on the surface of the activated carbon (Jia et al., 2024).

The pollutant adsorption capacity of composite mortar for formaldehyde ranges from 1.50±0.27 - 1.77±0.19%. With the addition of 4% activated carbon, the formaldehyde adsorption capacity is higher than that of mortar composite without activated carbon, and decreases with increasing activated carbon content. The effect of activated carbon formulation on the formaldehyde adsorption capacity is illustrated in Figure 10. The percentage of pollutant adsorption capacity for formaldehyde is much higher than after being applied to composite mortar. Previous studies have reported that the adsorption capacity of activated carbon on formaldehyde from kenaf stems ranges from 15.01-28.26% (Sadir et al., 2022). The results of statistical analysis showed no significant difference in the addition of activated carbon to the formaldehyde adsorption value (Figure 10). The adsorption capacity of formaldehyde is influenced by the chemical properties of the adsorbent surface (Boonamnuayvitaya et al., 2005). The adsorption capacity of formaldehyde in mortar will be greater with the content of activated carbon used (Hermawan et al., 2022). The Adsorption capacity can be strengthened by the addition of activated carbon (Krou et al., 2015). The addition of 0.5% activated carbon in the cement mixture will increase and extend its ability to absorb harmful gases such as NO_x, CO_2 and volatile organic compounds (Horgnies et al., 2015).

Composite mortar incorporating activated carbon demonstrates significant potential for adsorbing benzene pollutants, owing to the porous nature of activated carbon that effectively captures non-polar volatile compounds through physical-

chemical adsorption mechanisms, although specific research remains limited compared to standalone activated carbon studies.

3.6 FTIR characterization of selected mortar composition

The FTIR spectrum of selected composite mortar compositions is presented in Figure 11.

The spectrum of composite mortar with the addition of 4% activated carbon shows a peak at 3,404 cm^{-1} absorption with O-H stretching vibrations (Raki et al., 2004). The CO stretching vibration of carbonate molecules contributes to the other two bands at 1,428 cm^{-1} and 973 cm^{-1} absorption bands. Carbon dioxide and calcium hydroxide in the air combine to produce carbonate molecules (Yilmaz and Olgun, 2008; Choudhary et al., 2020; Bhat and Debnath, 2011). This condition is consistent with one of the progressive transitions of mortar constituents, where moisture and atmospheric carbon dioxide cause portlandite to change to calcite during the setting process (Chang and Chen, 2006). With increasing nano-silica content, these bands were observed to move towards the lower wavenumber side of 1,428 cm^{-1}. $CaCO_3$ formation in carbonated cement mortar, revealing portlandite consumption and C-S-H decalcification-polymerization effects from additives (Mohanraja and Sharma, 2025). FTIR indications of $CaCO_3$ production were observed in line with the morphological data identified by FE-SEM.

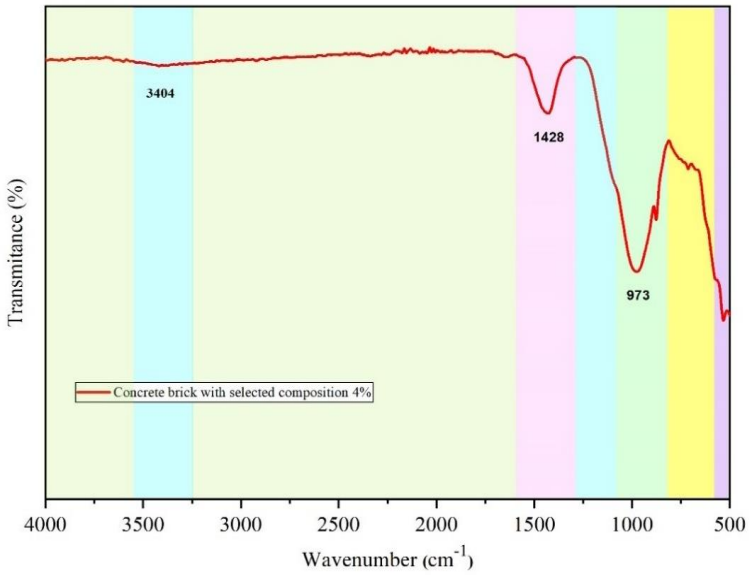


Figure 11. FTIR Spectra of selected mortar composite reinforced with 4% of activated carbon and 1.5% gamal wood chips

3.7 Morphological analysis of selected mortar composite using FE-SEM

Exploring the diversity of morphology, growth mechanisms, and crystal forms of $CaCO_3$ in cement can be done through scanning electron microscopy (FE-SEM). FE-SEM is another important step in the process of microscopic characterization of mortar. Figure 12 shows the results of observations using FE-SEM with selected compositions and different magnifications.

Figure 12(a) shows that the hydration process of cement with wood occurs optimally by the appearance of CSH bonds. This is indicated by the formation of calcium carbonate ($CaCO_3$) crystallization (Figure 12(b)). On the other hand, there are irregularly shaped pores (Figure 12(b)), which can affect the bonding of cement with particles. The degree of crystallinity of the binder (cement) increases, forming well-identified crystals, namely $CaCO_3$ (white crystal aggregate). The same findings on the compressive strength, MOE, MOR and FTIR analysis show that the addition of activated carbon can increase the optimal strength of the mortar (Hermawan et al., 2022).

The morphology of $CaCO_3$ crystals can vary under different conditions, such as cubes, prisms, spherical aggregates, and other irregular calcite shapes (Falini et al., 2009). The observed $CaCO_3$ crystals are mostly granular and aggregated together (Li et al., 2021; Liu et al., 2021). Overall, the formation of $CaCO_3$ can affect cement-based materials, such as increasing compressive and flexural strength and reducing atmospheric carbonation of the hydrated cement matrix (Savija and Lukovic, 2016).

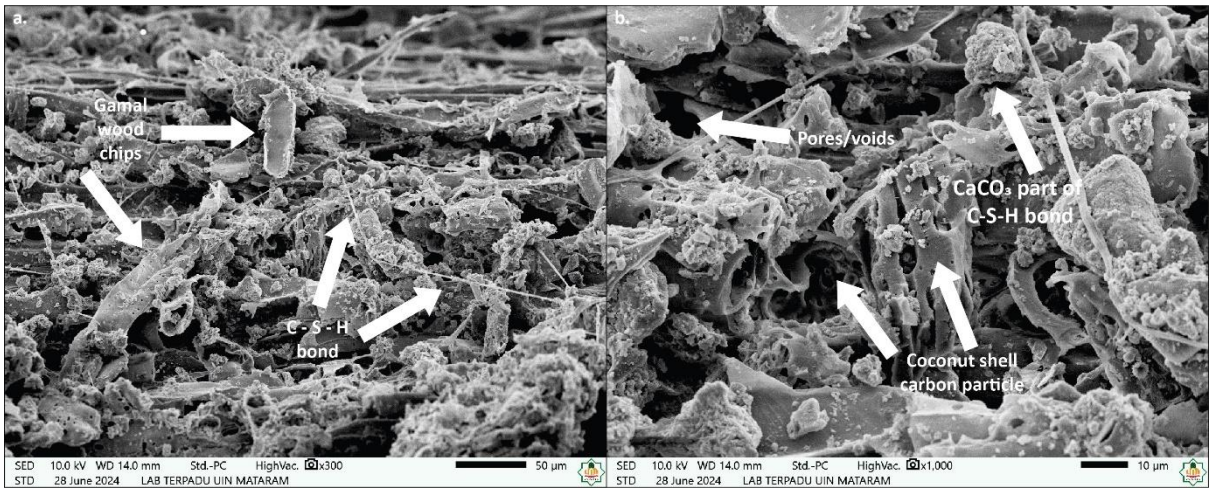
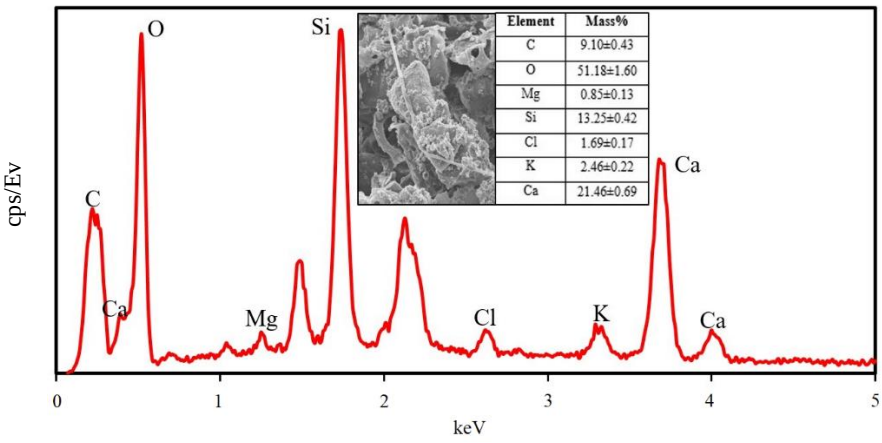


Figure 12. Morphological image of mortar composite reinforced with 4% activated carbon and 1.5% gamal wood chips

In addition, the compatibility of raw materials has a significant impact on crystal morphology and microstructure (Lu et al., 2022). The presence of magnesium and potassium in cement raw materials can affect crystallization. The presence of K ions functions to control the morphology of $CaCO_3$ crystals and stabilize the surface (Falini et al., 2009). The EDX data showed that $CaCO_3$ crystals were granular and evenly gathered throughout the identified area (Figure 13).

These results also indicate that variations in the concentration and type of oxygen functional groups play an important role in the reaction. Reactions containing calcium, calcium hydrate, and calcium silicate hydrate function to form $CaCO_3$ crystals (Yaseen et al., 2019). With elemental mapping (Al, Ca, Si) visualized $CaCO_3$ precipitation in carbonated mortar, showing refined microstructures (Li et al., 2024; Chylinski et al., 2025).



Element	Mass%
C	9.10±0.43
O	51.18±1.60
Mg	0.85±0.13
Si	13.25±0.42
Cl	1.69±0.17
K	2.46±0.22
Ca	21.46±0.69

Figure 13. EDX data of mortar composite reinforced with 4% activated carbon and 1.5% gamal wood chips

4. CONCLUSION

The addition of activated carbon to composite mortar did not significantly affect mechanical strength, including compressive strength, MOE, and MOR. The compressive strength value of composite mortar from this study was classified as K100 concrete quality which is intended for non-structural concrete (quality fc> 8.3 MPa). The percentage of 4% activated carbon addition can increase mechanical strength ranging from 14.57-53.08%, and decreased by around 4.49-32.04% with the addition of 5% activated carbon. This decrease is due to the proportion of mortar that is not reactive in the cement hydration process. Overall, the addition of 4% activated carbon to composite mortar can increase mechanical strength.

The addition of activated carbon to composite mortar did not significantly affect the adsorption capacity of ammonia, chloroform and formaldehyde, but significantly affected the adsorption capacity of benzene. Overall, the pollutant adsorption capacity of

composite mortar ranged from 0.57-2.50% or below 3%. The percentage of pollutant adsorption capacity is much higher than after being applied to composite mortar. The low pollutant adsorption capacity of composite mortar is caused by the reaction of activated carbon with other components such as cement, which results in the closure of the activated carbon pores.

The spectrum of composite mortar with the addition of 4% activated carbon shows a peak at 3,404 cm^{-1} absorption with O-H stretching vibrations. The CO stretching vibration of carbonate molecules plays a role in the other two bands at 1,428 cm^{-1} and 973 cm^{-1} absorption bands. Carbon dioxide and calcium hydroxide in the air combine to produce carbonate molecules. Morphological observations as analyzed by FE-SEM, were found to correlate with FTIR analysis, namely the formation of $CaCO_3$. The addition of activated carbon can produce more $CaCO_3$.

ACKNOWLEDGEMENTS

This study was conducted by the support dan research facility of Directorate General of Higher Education, Ministry of Education, Culture, Research and Technology of Indonesia; Forestry Laboratory and Chemistry Laboratory, Universitas Pendidikan Mandalika; Mathematics and Natural Sciences Laboratory and Civil Engineering Laboratory, Univeritas Mataram; and Integrated Laboratory of Universitas Islam Negeri Mataram. All researchers would also like to thank all research assistants and laboratory instrument operators who have supported the success of this research.

RESEARCH FUNDING

This research received grant from Directorate General of Higher Education, Ministry of Education, Culture, Research and Technology of Indonesia (grant number: 110/E5/PG.02.00.PL/2024).

AUTHOR CONTRIBUTIONS

All authors were involved as main contributors of this research. Baiq Mirawati and Muhammad Sadir conducted the experiments, and prepared the research manuscript. Albert Hendriko assisted in research instrumentation, processed research data, and prepare the research manuscript. I Gde Adi Suryawan Wangiyana, Ismail Budiman, Dede Hermawan, Gustan Pari, and Ariadne Lakshmidevi Juwono supervised the research, designed the experimental design, research methodology.

DECLARATION OF CONFLICT OF INTEREST

No potential conflict of interest was reported by the authors.

DATA AVAILABILITY STATEMENT

The data that support the findings of this study are available from the authors but restrictions apply to the availability of these data, which were used under license from the Department of Forestry, Faculty of Engineering and Applied Sciences, Universitas Pendidikan Mandalika; Department of Physics, Faculty of Mathematics and Natural Sciences, Universitas Indonesia; and Research Center for Biomasses and Bioproducts, Badan Riset dan Inovasi Nasional for the current study, and so are not publicly available. Data are, however, available from the authors upon reasonable request.

REFERENCES

Adem JK, Shimelis E, Oumer A, Park S, Gwon S, Yang B, et al. Application of FTIR, Raman, and TGA in carbonation of cementitious materials: A review. Journal of Building Engineering 2025;114:Article No. 114228.

Ahmad S, Khushnood RA, Jagdale P, Tulliani JM, Ferro GA. High performance self-consolidating cementitious composites by using micro carbonized bamboo particles. Materials and Design 2015;76:223-9.

Alamu EO, Adesokan M, Fawole S, Maziya-Dixon B, Mehreteab T, Chikoye D. *Gliricidia sepium* (Jacq.) Walp applications for enhancing soil fertility and crop nutritional qualities: A review. Forests 2023;14(3):1-13.

Almajed A, Dafalla M, Shaker AA. The combined effect of calcium chloride and cement on expansive soil materials. Applied Sciences 2023;13(8):Article No. 4811.

Alzard MH, El-Hassan H, El-Maaddawy T, Alsalami M, Abdulrahman F, Hassan AAA. Bibliometric analysis of the studies on self-healing concrete published between 1974 and 2021. Sustainability 2022;14(18):Article No. 11646.

Aslam M, Shafigh P, Jumaat MZ. Oil-palm by-products as lightweight aggregate in concrete mixture: A review. Journal of Cleaner Production 2016;126:56-73.

Aulanni'am A, Ora KM, Ariandini NA, Wuragil DK, Permata FS, Riawan W, et al. Wound healing properties of Gliricidia sepium leaves from Indonesia and the Philippines in rats (*Rattus norvegicus*). Veterinary World 2021;14(3):820-4.

Barberi P. Ecological weed management in Sub-Saharan Africa: Prospects and implications on other agroecosystem services. Advances in Agronomy 2019;156:219-64.

Bhat PA, Debnath NC. Theoretical and experimental study of structures and properties of cement paste: The nanostructural aspects of CSH. Journal of Physics and Chemistry of Solids 2011;72(8):920-33.

Boonamnuayvitaya V, Sae-Ung S, Tanthapanichakoon W. Preparation of activated carbons from coffee residue for the adsorption of formaldehyde. Separation and Purification Technology 2005;42(2):159-68.

Budiman I, Hermawan D, Febrianto F, Pari G. Optimization of activated carbon from oil palm shell hydrochar using response surface methodology. Journal of Tropical Wood Science and Technology 2019;17(1):8-21.

Chang CF, Chen JW. The experimental investigation of concrete carbonation depth. Cement and Concrete Research 2006; 36(9):1760-7.

Chin CO, Yang X, Kong SY, Paul SC, Wong LS. Mechanical and thermal properties of lightweight concrete incorporated with

activated carbon as coarse aggregate. Journal of Building Engineering 2020;31:Article No. 101347.

Cho AR, Chun YG, Kim BK, Park DJ. Preparation of alginate-$CaCl_2$ microspheres as resveratrol carriers. Journal of Materials Science 2014;49(13):4612-9.

Choi YW, Moon DJ, Chung JS, Cho SK. Effects of waste PET bottles aggregate on the properties of concrete. Cement and Concrete Research 2005;35(4):776-81.

Choudhary R, Gupta R, Nagar R. Impact on fresh, mechanical, and microstructural properties of high strength self-compacting concrete by marble cutting slurry waste, fly ash, and silica fume. Construction and Building Materials 2020;239:Article No. 117888.

Chylinski F, Kupisz P, Wiech P, Brunarski L. Determination of composition of masonry mortars for conservation of historical constructions using artificial neural networks. Materials 2025;18(16):Article No. 3851.

Coulibaly JY, Chiputwa B, Nakelse T, Kundhlande G. Adoption of agroforestry and the impact on household food security among farmers in Malawi. Agricultural Systems 2017;155:52-69.

De Weerdt K. Chloride binding in concrete: Recent investigations and recognised knowledge gaps: RILEM Robert L'Hermite Medal Paper 2021. Materials and Structures 2021;54(214):1-16.

Deng H, Yang L, Tao G, Dai J. Preparation and characterization of activated carbon from cotton stalk by microwave assisted chemical activation-application in methylene blue adsorption from aqueous solution. Journal of Hazardous Materials 2009;166(2-3):1514-21.

Dias JO, Siqueira RD, Coelho BF, Conceicao AO. Analysis of the mechanical properties of polymer composites reinforced withcharcoal particulate. Materials 2025;18(12):Article No. 2746.

Dobiszewska M, Bagcal O, Beycioglu A, Goulias D, Koksal F, Płominski B, et al. Utilization of rock dust as cement replacement in cement composites: An alternative approach to sustainable mortar and concrete productions. Journal of Building Engineering 2023;69:Article No. 106180.

Emmanuel V, Odile B, Celine R. FTIR spectroscopy of woods: A new approach to study the weathering of the carving face of a sculpture. Spectrochimica Acta Part A: Molecular and Biomolecular Spectroscopy 2015;136(PC):1255-9.

Enyoh CE, Verla AW, Qingyue W, Ohiagu FO, Chowdhury AH, Enyoh EC, et al. An overview of emerging pollutants in air: Method of analysis and potential public health concern from human environmental exposure. Trends in Environmental Analytical Chemistry 2020;28:e00107.

European Committee for Standardization (CEN). EN 1015-11:2000 Methods of Test for Mortar for Masonry-Part 11: Determination of Flexural and Compressive Strength of Hardened Mortar. Brussels, Belgium: European Committee for Standardization; 2000.

Falini G, Fermani S, Goisis M, Manganelli G. Calcite morphology and aggregation in the presence of comb-like polymers adsorbed on cement particles. Crystal Growth and Design 2009;9(5):2240-7.

Gayathiri M, Pulingam T, Lee KT, Sudesh K. Activated carbon from biomass waste precursors: Factors affecting production and adsorption mechanism. Chemosphere 2022;294:Article No. 133764.

Guo J, Xu WS, Chen YL, Lua AC. Adsorption of NH_3 onto activated carbon prepared from palm shells impregnated with H_2SO_4. Journal of Colloid and Interface Science 2005;281(2):285-90.

Guo X, Zhao Z, Gao X, Dong Y, Fu H, Zhang X. Study on the adsorption performance of modified high silica fly ash for methylene blue. RSC Advances 2024;14(30):21342-54.

Hermawan D, Budiman I, Febrianto F, Subyakto S, Pari G, Ghozali M, et al. Enhancement of the mechanical, self-healing and pollutant adsorption properties of mortar reinforced with empty fruit bunches and shell chars of oil palm. Polymers 2022;14(3):Article No. 410.

Horgnies M, Chen JJ, Bouillon C. Overview about the use of FTIR spectroscopy to study cementitious materials. WIT Transactions on Engineering Sciences 2013;77:251-62.

Horgnies M, Dubois-Brugger I, Krou NJ, Batonneau-Gener I, Belin T, Mignard S. Reactivity of NO_2 and CO_2 with hardened cement paste containing activated carbon. The European Physical Journal Special Topics 2015;224(9):1985-94.

Jesus E, Franca T, Calvani C, Lacerda M, Gonçalves D, Oliveira SL, et al. Making wood inspection easier: FTIR spectroscopy and machine learning for Brazilian native commercial wood species identification. RSC Advances 2024;14(11):7283-9.

Jia Y, Chen D, Li Y, Li E, Zhao L, Guo L. Study on the adsorption mechanism of polar and non-polar VOCs by the activated carbon with surface oxygen. Chemical Engineering Journal 2024;490:Article No. 151907.

Justo-Reinoso I, Srubar WV, Caicedo-Ramirez A, Hernandez MT. Fine aggregate substitution by granular activated carbon can improve properties of cement mortars. Construction and Building Materials 2018;164:750-9.

Kang SB, Yun HD, Choi W. Feasibility on diverse biochars as supplementary cementitious materials. Scientific Reports 2025;15:Article No. 40732.

Khushnood RA, Ahmad S, Ferro GA, Restuccia L, Tulliani JM, Jagdale P. Modified fracture properties of cement composites with nano/micro carbonized bagasse fibers. Fracture and Structural Integrity 2015;9(34):534-42.

Khusnul K, Suratno, Prihatin J, Sudarti. An analysis of the utilization of Gamal plant (*Gliricidia sepium*) as a shade for coffee plants. Journal of Physics: Conference Series 2020;1563:Article No. 012014.

Koseoglu E, Akmil-Basar C. Preparation, structural evaluation and adsorptive properties of activated carbon from agricultural waste biomass. Advanced Powder Technology 2015; 26(3):811-8.

Krou NJ, Batonneau-Gener I, Belin T, Mignard S, Javierre I, Dubois-Brugger I, et al. Reactivity of volatile organic compounds with hydrated cement paste containing activated carbon. Building and Environment 2015;87:102-7.

Kudzin MH, Kaczmarek A, Mrozinska Z, Hernandez C, Piekarska K, Wozniak K, et al. Hybrid alginate graphene composites: Biochemical features and biomedical potential. Marine Drugs 2025;23(8):Article No. 323.

Kumar A, Gupta A, Sharma KV, Nasir M, Khan TA. Influence of activated carbon as filler on properties of wood composites. International Journal of Adhesion and Adhesives 2013; 46:34-9.

Lazim ZM, Hadibarata T, Puteh MH, Yusop Z. Adsorption characteristics of bisphenol A onto low-cost modified phyto-waste material in aqueous solution. Water, Air, and Soil Pollution 2015;226:Article No. 34.

Li G, Yan D, Liu J, Yang P, Zhang J. Study on the mechanical properties of crack mortar repaired by enzyme-induced calcium carbonate precipitation (EICP). Materials (Basel) 2024;17(12):Article No. 2978.

Li M, Wang Q, Yang J, Guo X, Zhou W. Strength and mechanism of carbonated solidified clay with steel slag curing agent. KSCE Journal of Civil Engineering 2021;25(3):805-21.

Li Z, Wang X, Wang S, Feng X. Comparative study on the effect of agricultural waste biochar on the properties of cement mortar. Industrial Crops and Products 2025;227:Article No. 120854.

Liu Y, Zhuge Y, Chow CWK, Keegan A, Li D, Pham PN, et al. Compressive behaviour and environmental evaluation of sludge-derived masonry walls. Case Studies in Construction Materials 2021;15:e00736.

Lu J, Ruan S, Liu Y, Wang T, Zeng Q, Yan D. Morphological characteristics of calcium carbonate crystallization in CO_2 pre-cured aerated concrete. RSC Advances 2022;12(23):14610-20.

Mahoutian M, Lubell AS, Bindiganavile VS. Effect of powdered activated carbon on air void characteristics of concrete containing fly ash. Construction and Building Materials 2015;80(1):84-91.

Majzoobi M, Pesaran Y, Mesbahi G, Farahnaky A. Evaluation of the effects of hydrothermal treatment on rice flour and its related starch. International Journal of Food Properties 2016;19(9):2135-45.

Malini K, Selvakumar D, Kumar NS. Activated carbon from biomass: Preparation, factors improving basicity and surface properties for enhanced CO_2 capture capacity - A review. Journal of CO_2 Utilization 2023;67:Article No. 102318.

Mannan M, Al-Ghamdi SG. Indoor air quality in buildings: A comprehensive review on the factors influencing air pollution in residential and commercial structures. International Journal of Environmental Research and Public Health 2021; 18(6):Article No. 3276.

Marangon A, Orlando G, Cala E, Croce A, Avattaneo E, Cara E, et al. Comparison of different activation methods for activated carbon produced using various methods from *Phyllostachys edulis* (bamboo moso) biomass. Carbon Trends 2025;21:Article No. 100590.

McCall MA, Watson JS, Tan JSW, Septhon MA. Biochar stability revealed by FTIR and machine learning. ACS Sustainable Resource Management 2025;2:842-52.

Meda US, Vora K, Athreya Y, Mandi UA. Titanium dioxide based heterogeneous and heterojunction photocatalysts for pollution control applications in the construction industry. Process Safety and Environmental Protection 2022;161,771-87.

Mohanraj R, Sharma N. Characterization of concrete with Nano-TiO_2 particles using compression and FTIR methods. Procedia Structural Integrity 2025;70:358-64

Moon GD, Oh S, Jung SH, Choi YC. Effects of fineness of limestone powder and cement on hydration and strength development of PLC concrete. Construction and Building Materials 2017;135:129-36.

Mustapha LS, Obayomi OV, Diekola Yahya MD, Lau SY, Obayomi KS. Exploring the synergistic effects of calcium chloride modification on stem bark eucalyptus biochar for Cr (VI) and Pb(II) ions removal: Kinetics, isotherm, thermodynamic and optimization studies. Bioresource Technology Reports 2024;25:Article No. 101699.

Na S, Lee S, Youn S. Experiment on activated carbon manufactured from waste coffee grounds on the compressive strength of cement mortars. Symmetry 2021;13(4):Article No. 619.

Nagrockiene D, Girskas G, Skripkiunas G. Properties of concrete modified with mineral additives. Construction and Building Materials 2017;135: 37-42.

Nazari A, Riahi S. The effects of ZnO_2 nanoparticles on strength assessments and water permeability of concrete in different curing media. Materials Research 2011;14(2):178-88.

Nedjai R, Kabbashi NA, Alam MZ, Al-Khatib MFR. Production and characterization of activated carbon from baobab fruit shells by chemical activation. Journal of Physics: Conference Series 2021;2129:Article No. 012009.

Nemati KM. Fracture analysis of concrete using scanning electron microscopy. The Journal of Scanning Microscopies 1997;19(6):426-30.

Nilimaa J. Smart materials and technologies for sustainable concrete construction. Developments in the Built Environment 2023;15:Artcle No. 100177.

Oladunmoye M, Ayantola K, Agboola A, Olowe B, Adefemi O. Antibacterial and FTIR spectral analysis of methanolic extract of *Gliricidia sepium* leaves. Journal of Advances in Microbiology 2018;9(4):1-10.

Onyelowe KC, Ebid AM, Riofrio A, Baykara H, Soleymani A, Mahdi HA, et al. Multi-objective prediction of the mechanical properties and environmental impact appraisals of self-healing concrete for sustainable structures. Sustainability 2022;14(15):Article No. 9573.

Oyelere AT, Oluwadare AO. Studies on physical, thermal and chemical properties of wood *Gliricidia sepium* for potential bioenergy production. International journal of biomass and renewables 2019;8(2):28-38.

Pongjanyakul T, Rongthong T. Enhanced entrapment efficiency and modulated drug release of alginate beads loaded with drug-clay intercalated complexes as microreservoirs. Carbohydrate Polymers 2010;81(2):409-19.

Raki L, Beaudoin JJ, Mitchell L. Layered double hydroxide-like materials: Nanocomposites for use in concrete. Cement and Concrete Research 2004;34(9):1717-24.

Sadir M, Hermawan D, Budiman I, Pari G, Sutiawan J. Characteristics and pollutan absorbtion capacity of activated charcoal made from kenaf (*Hibiscus cannabinus* L.). Forest Products Research Journal 2022;40(1):7-18.

Salain IMAK. Using calcium chloride as an accelerator for Portland pozzolan cement concrete compressive strength development. IOP Conference Series: Materials Science and Engineering 2019;615:Aticle No. 012016.

Salami BA, Bahraq AA, Haq MM. Ul, Ojelade OA, Taiwo R, Wahab S, et al. Polymer-enhanced concrete: A comprehensive review of innovations and pathways for resilient and sustainable materials. Next Materials 2024;4:Article No. 100225.

Salthammer T. Formaldehyde sources, formaldehyde concentrations and air exchange rates in European housings. Building and Environment 2019;150:219-32.

Savija B, Lukovic M. Carbonation of cement paste: Understanding, challenges, and opportunities. Construction and Building Materials 2016;117:285-301.

Sekar A, Varghese GK, Varma, RMK. Analysis of benzene air quality standards, monitoring methods and concentrations in indoor and outdoor environment. Heliyon 20195(11):e02918.

Shafigh P, Jumaat MZ, Mahmud H. Oil palm shell as a lightweight aggregate for production of high strength lightweight concrete. Construction and Building Materials 2011;25(4):1848-53.

National Standardization Agency of Indonesia (BSN). SNI 03-2847-2002. Code for the Structural Design of Concrete for Buildings. Jakarta, Indonesia: National Standardization Agency of Indonesia; 2002a.

National Standardization Agency of Indonesia (BSN). SNI 03-6825-2002. Standard Test Method for Compressive Strength of Portland Cement. Mortar. Jakarta, Indonesia: National Standardization Agency of Indonesia; 2002b.

National Standardization Agency of Indonesia (BSN). SNI 06-3730-1995. Technical Activated Carbon. Jakarta, Indonesia: National Standardization Agency of Indonesia; 1995.

National Standardization Agency of Indonesia (BSN). SNI 8837-1-2019. Ready-Mixed Mortar-Part 1: Adhesive for Ceramic Tiles and Natural Stone. Jakarta, Indonesia: National Standardization Agency of Indonesia; 2019.

Sujiono EH, Zabrian D, Zurnansyah, Mulyati, Zharvan V, Samnur, et al. Fabrication and characterization of coconut shell activated carbon using variation chemical activation for wastewater treatment application. Results in Chemistry 2022;4:Article No. 100291.

Swaroop MSD, Raj GPA. Experiment on concrete containing with activated carbon and nano-fly ash, nano metakaolin. International Journal of Innovative Technology and Exploring Engineering 2019;86(4):1030-3.

Tighsazzadeh M, Mitchell JC, Boateng JS. Development and evaluation of performance characteristics of timolol-loaded composite ocular films as potential delivery platforms for treatment of glaucoma. International Journal of Pharmaceutics 2019;566(5):111-25.

Valdivielso DY, Kerpal C, Schollkopf W, Meijer G, Fielicke A. IR spectra and structures of saturated ruthenium cluster carbonyl cations. Dalton Transactions 2023;52(29):9929-39.

Van Tran V, Park D, Lee, YC. Indoor air pollution, related human diseases, and recent trends in the control and improvement of indoor air quality. International Journal of Environmental Research and Public Health 2020;17(8):Article No. 2927.

Wang X, Zhou X, Chen W, Chen M, Liu C. Enhancement of the electrochemical properties of commercial coconut shell-based activated carbon by H_2O dielectric barrier discharge plasma. Royal Society Open Science: Chemistry 2019;6(2):Article No. 180872.

Wu F, Zhang Q, Dong S, Cai Y, Yang S, Xu F, et al. Biochar modification enhances mechanical and durability properties of cement-based materials. Scientific Reports 2025;15:Article No. 22174.

Wyer KE, Kelleghan DB, Blanes-Vidal V, Schauberger G, Curran TP. Ammonia emissions from agriculture and their contribution to fine particulate matter: A review of implications for human health. Journal of Environmental Management 2022;323:Article No. 116285.

Xie M, Zhao Z, Holder AL, Hays MD, Chen X, Shen G, et al. Chemical composition, structures, and light absorption of N-containing compounds from burning wood and charcoal. Atmospheric Chemistry and Physics 2020;20(22):14077-90.

Yaseen SA, Yiseen GA, Li Z. Elucidation of calcite structure of calcium carbonate formation based on hydrated cement mixed with graphene oxide and reduced graphene oxide. ACS Omega 2019;4(6):10160-70.

Yilmaz B, Olgun A. Studies on cement and mortar containing low-calcium fly ash, limestone, and dolomitic limestone. Cement and Concrete Composites 2008;30(3):194-201.

Ylmen R, Jaglid U, Steenari BM, Panas I. Early hydration and setting of Portland cement monitored by IR, SEM and Vicat techniques. Cement and Concrete Research 2009;39(5):433-9.

Youn JN, Sung CY, Kim YI. Physical and mechanical properties of porous concrete using waste activated carbon. Journal of The Korean Society of Agricultural Engineers 2009;51(4): 21-7.

Zhang D, Liu J, Liu M, Liu L, Do DD. On the capture of ultralow-level benzene in indoor environments: Experiments, modeling and molecular simulation. Separation and Purification Technology 2020;251:Article No. 117306.

Zhang W, Jiao Y, Zhu R, Rhew RC, Sun B, Dai H. Chloroform ($CHCl_3$) emissions from coastal Antarctic tundra. Geophysical Research Letters 2021;48(18):1-10.

Zhao S, Liu Y, Yang L, Zhao Y, Zhu M, Wang H, et al. Low-frequency alternating magnetic field and $CaCl_2$ influence the physicochemical, conformational and gel characteristics of low-salt myofibrillar protein. Food Chemistry 2024;22:Article No. 101341.

Zheng C, Liu Z, Xu J, Li X, Yao Y. Compressive strength and microstructure of activated carbon-fly ash cement composites. Chemical Engineering Transactions 2017;59:475-80.

Environment and Natural Resources Journal

Volume 24
Issue 6
2026

Oxidative Stress Responses and Antioxidant Gene Regulation in *Daphnia pulex* Following Chronic Benzyl Alcohol Exposure

Ghufran Saad Aljanabi*and Adel Mashaan Rabee

Department of Biology, College of Science, University of Baghdad, Baghdad, Iraq

ARTICLE INFO

Received: 8 Feb 2026
Received in revised: 18 May 2026
Accepted: 1 Jun 2026
Published online: 25 Aug 2026
DOI: 10.32526/ennrj/24/20260053

Keywords:
Aquatic toxicology/ Antioxidant biomarkers/ Benzyl alcohol/ *D. pulex*/ Gene expression/ Oxidative stress

*** Corresponding author:**
E-mail:
ghufran.s@sc.uobaghdad.edu.iq

ABSTRACT

Benzyl alcohol was evaluated for its short-term and long-term toxicity in Daphnia pulex, with an emphasis on oxidative stress biomarkers and antioxidant-related gene expression. Acute toxicity was evaluated over 48 h to estimate the LC50, and two sublethal concentrations (11.5 and 23 mg/L) were subsequently selected for a 21-day exposure. Activities of catalase (CAT), superoxide dismutase (SOD), and glutathione S-transferase (GST), and the expression profiles of cat and sod were measured, and associations between biochemical and molecular responses were examined. Mortality increased with concentration, yielding a 48 h LC_{50} of 229.68 mg/L. Prolonged exposure produced contrasting responses moderate stress stimulated antioxidant enzymes and gene expression, whereas higher exposure suppressed enzymatic activity, depleted glutathione reserves, and reduced transcriptional responses. Enzyme activities were positively correlated with gene expression, indicating coordinated regulation of the antioxidant defense system. These patterns indicate that oxidative imbalance develops at concentrations well below lethal thresholds and precedes overt mortality, supporting the use of biochemical and molecular biomarkers as sensitive indicators of chronic toxic stress in freshwater invertebrates.

HIGHLIGHTS

- Benzyl alcohol caused moderate acute toxicity in *Daphnia pulex*.
- Chronic exposure triggered biphasic antioxidant enzyme response.
- Glutathione depletion indicated a progressive oxidative imbalance.
- Cat and sod genes showed dose-dependent transcriptional regulation.
- Biomarkers were more sensitive indicators than mortality endpoints.

1. INTRODUCTION

Organic contaminants and other environmental stressors have become increasingly recognised for their potential to influence ecologically significant changes in aquatic ecosystems, where aquatic life is always under a combination of natural and anthropogenic pressures (Al-Jaff, 2021). For instance, research conducted on water fleas, *Daphnia pulex* demonstrated their biological responses to a combination of environmental stressors, including temperature, salinity, and nutrient levels, and cues for waterborne contaminants, even when there was a lack of acutely toxic substances. The pervasiveness and ecological relevance of emerging contaminants and other environmental stressors in aquatic ecosystems have also been emphasized by the fact that aquatic life is more likely to respond to long-term, low-level exposures rather than to acutely toxic substances. Aquatic life is likely to respond with physiological, morphological, and life-history alterations through long-term, low-level exposure to environmental stressors. As a result, the response to sublethal toxicity is considered to have ecological relevance for aquatic life (McKnight et al., 2023).

Benzyl alcohol is an aromatic alcohol widely used as a solvent and preservative in pharmaceutical, cosmetic, household, and sanitizer-related formulations. Owing to these widespread applications, its release into wastewater streams and subsequent entry into receiving freshwater systems are environmentally plausible (Manjunatha et al., 2021; Musee et al., 2023; Api et al., 2025). Environmental

Citation: Aljanabi GS, Rabee AM. Oxidative stress responses and antioxidant gene regulation in *Daphnia pulex* following chronic benzyl alcohol exposure. Environ. Nat. Resour. J. 2026;24(6):661-672. (https://doi.org/10.32526/ennrj/24/20260053)

monitoring studies have reported the presence of benzyl alcohol in wastewater treatment plants at concentrations of 500-11,000 ng/L in influents and 150-400 ng/L in effluents, and it has also been detected in groundwater with a median concentration of 582 ng/L (Kong et al., 2016; Musee et al., 2023). Aquatic toxicity data further support its ecological relevance, with reported 24 h and 48 h EC50 values of 55 mg/L and 230 mg/L, respectively, for *Daphnia magna* (Musee et al., 2023). Previous studies in aquatic models, including zebrafish embryos, have also shown that benzyl alcohol can induce mortality, developmental abnormalities, and organ-level toxicity (Manjunatha et al., 2021). However, information remains limited regarding its long-term sublethal effects on oxidative stress biomarkers and antioxidant-related gene expression in freshwater invertebrates such as *Daphnia pulex*.

Daphnia species are widely recognized as important model organisms in ecology and freshwater ecotoxicology because of their ecological role in pelagic food webs, sensitivity to dissolved contaminants, short generation time, and suitability for mechanistic toxicity studies. In addition, their usefulness in linking molecular and biochemical responses to organism- and population-level effects has made them valuable models for evaluating contaminant-induced stress in aquatic systems (Ebert, 2022; Reilly et al., 2023). Therefore, *Daphnia pulex* was selected in the present study as a suitable freshwater model for assessing chronic sublethal oxidative stress responses to benzyl alcohol exposure.

Oxidative stress is commonly defined as an imbalance between the production of reactive oxygen species (ROS) and the antioxidant defense system's capacity to detoxify them, leading to cellular oxidative damage. In aquatic invertebrates, environmental stressors have been shown to disrupt antioxidant defenses through altered ROS production and impaired redox homeostasis, thereby supporting oxidative stress as a central mechanism of toxicity (Atli and Sevgiler, 2024; Esterhuizen et al., 2024).The antioxidant defense system also includes antioxidant enzymes such as superoxide dismutase (SOD), catalase (CAT), and glutathione-S-transferase (GST) which have also been reported to be highly sensitive to changes due to the presence of toxicants as well as changes in the homeostasis of the cells. Other non-enzymatic antioxidants, such as reduced glutathione have also been widely measured in combination with antioxidant enzymes to evaluate antioxidant status. The difference in antioxidant defense systems has also been widely used to measure the early changes of stress in the field of ecotoxicology, where changes due to the presence of toxicants can be clearly detected before any toxicity and/or cell death are evident (Atli and Sevgiler, 2024; Mahaye and Musee, 2022). Although antioxidant enzymes such as CAT and SOD are widely recognized as sensitive biomarkers of chemical stress in Daphnia, studies specifically addressing long-term benzyl alcohol-induced enzymatic responses in freshwater cladocerans remain very limited. Recent experimental studies on *Daphnia pulex* provide quantitative evidence of the sensitivity of CAT and SOD to chemical stressors. Under chronic nanoplastic exposure (0.1-1.0 mg/L for 21 days) SOD expression was significantly upregulated at 0.5 and 1.0 mg/L whereas CAT expression was significantly downregulated at 0.5-2.0 mg/L compared to controls ($p<0.05$) (Liu et al., 2018). Field investigations in cyanobacteria-impacted freshwater systems reported catalase activities of 25.21 U/mg protein in contaminated reservoirs compared to 14.13 U/mg protein in reference lakes, with seasonal maxima reaching 40.94 U/mg protein (Wojtal-Frankiewicz et al., 2013). Acute exposure to cyanotoxin mixtures resulted in an approximately 28% reduction in CAT activity within 24 h at 100 µg/L (Esterhuizen-Londt et al., 2016). Similarly, combined copper (40 µg/L) and cadmium (20 µg/L) exposure reduced SOD activity from approximately 6 U/min/mg protein in controls to about 2 U/min/mg protein after 24 h and to 2.5-3.0 U/min/mg protein after 48 h (Sadeq, 2018).

The gene expression response was found to be an essential mechanism in the adaptation of *Daphnia* spp. to oxidative stress, where oxidative stress is often the result of environmental contaminants, Antioxidant-related gene categories in *Daphnia* spp., including the gene categories of cat and sod, were found to be responsive to oxidative stress, as these gene categories play an essential role in the regulation of the antioxidant defense system in aquatic animals (Kim et al., 2011; Wang et al., 2019). Such changes in the expression levels are often accompanied by similar changes in the corresponding enzymatic activities, underscoring the significance of the transcriptional control process (Sonmez et al., 2025). Combining molecular biomarkers, including gene expression profiles, with the measurement of the parameters of the antioxidant defense system would enable a wider approach to the assessment of oxidative stress in *Daphnia* spp., as gene expression changes can occur

either prior to or in conjunction with enzymatic changes, which would greatly strengthen the ecotoxicological assessment results (Wang et al., 2019; Guevara et al., 2024). Nevertheless, comparable long-term transcriptional evidence for benzyl alcohol exposure in *Daphnia pulex* remains scarce, which further supports the need for the present investigation. The above trends have been observed in Iraqi freshwater species exposed to organic/petroleum pollutants. According to the literature, the activity of antioxidant enzymes in invertebrates exposed to organophosphate pollutants is considerably affected by the rise in oxidative stress levels, which negatively influences the activity of the aforementioned enzymes (Al-Fanharawi et al., 2019). Fish species in polluted aquatic cultures experience remarkable changes in the activity of antioxidant enzymes due to long-term stress caused by pollutants (Alkatrani et al., 2024). Oxidative stress biomarkers respond intensively to hydrocarbon pollutants, which makes them applicable for the early detection of oil pollution using the sublethal method (Abdulameer and Hussein, 2023). Chronic pollutant exposure may alter antioxidant enzyme activity in a concentration and duration-dependent manner. Antioxidant enzymes may initially increase as an adaptive response to elevated ROS production, whereas prolonged or stronger stress can reduce enzyme activity as a result of impaired antioxidant regulation, reduced protective capacity, or partial homeostatic adjustment (Mustafa et al., 2024).

Although benzyl alcohol has been investigated in aquatic models and acute toxicity data are available for *Daphnia magna* (Manjunatha et al., 2021; Musee et al., 2023), evidence specifically addressing its long-term sublethal effects on oxidative stress biomarkers and antioxidant-related gene expression in *Daphnia pulex* is still scarce. Therefore, the present study aimed to evaluate the acute toxicity of benzyl alcohol and to investigate its long-term sublethal effects on oxidative stress biomarkers and antioxidant-related gene expression in *Daphnia pulex*.

2. METHODOLOGY

2.1 Chemical test

Benzyl alcohol (>99% purity; C_7H_8O; molecular weight: 108.14 g/mol; CAS No. 100-51-6) was obtained from Loba Chemie, India, and used without further purification. A stock solution was freshly prepared in distilled water and stored at 4°C until use. Working exposure solutions were prepared by diluting the stock solution with the exposure medium to the required concentrations. Fresh exposure media were renewed every 48 h during the chronic exposure period. Concentrations are expressed as mg/L. The exposure concentrations of benzyl alcohol were derived from the 48 h LC_{50} value obtained in the present acute toxicity test using *Daphnia pulex*. For the 21-day chronic experiment, 5% and 10% of the LC_{50} were selected as sublethal exposure levels, corresponding to 11.5 and 23 mg/L, respectively. These LC_{50}-derived fractions were selected to represent low and higher sublethal exposure levels for evaluating biochemical and molecular biomarker responses, consistent with previous *Daphnia* studies using LC_{50} based fractions in chronic and molecular toxicity assessments (Bang et al., 2015; Poynton et al., 2011).

2.2 Test organism and culture conditions

The test organism used was *D. pulex*, a freshwater cladoceran. The test cultures were maintained under laboratory-controlled conditions and were exposed to aerated water prepared as reconstituted ASTM hard water (ASTM International, 2014) at a constant temperature of 20±1°C, a lighting period of 16 hours and a dark period of 8 hours, and with an aqueous solution of the green algae *Scenedesmus* sp. at approximately 1×10^5 cells/mL to ensure that the test animals were never food limited. The exposure medium was renewed every 48 h to maintain water quality throughout the experiment. All acute and chronic exposure experiments were conducted using *Daphnia pulex* neonates less than 24 h old. Before starting the test, the test organisms were subjected to acclimatization under laboratory conditions.

2.3 Acute toxicity and selection of sublethal concentrations

A 48 h acute toxicity test was conducted following OECD Test Guideline 202 (OECD, 2004) to determine the LC_{50} of benzyl alcohol and to select sublethal concentrations for the chronic exposure experiment. The assay was performed using *Daphnia pulex* neonates less than 24 h old. Benzyl alcohol was tested at concentrations of 150, 180, 210, 240, and 270 mg/L, in addition to a control group without benzyl alcohol. Each concentration consisted of three replicates with 10 individuals per replicate (n=30). In the acute test carried out to determine the LC_{50} values of benzyl alcohol, individuals showing no movement after gentle agitation were considered dead. LC_{50}

values were estimated by probit analysis using log-transformed concentrations, following the statistical method described by Finney (1971). The calculated 48 h LC_{50} was 230 mg/L. Two sublethal concentrations were then selected for the chronic test at 5% and 10% of the calculated LC_{50}, corresponding to 11.5 and 23 mg/L, respectively.

2.4 Chronic exposure setup and sampling strategy

Replicate beakers were prepared to correspond to each treatment group: control (0 mg/L), treatment group of 11.5 mg/L, and treatment group of 23 mg/L. Each replicate initially contained 20 neonates (<24 h old), which were maintained for 21 days under chronic exposure conditions, with three independent biological replicates per treatment (n=60 per group). Organism density did not exceed one individual per 10 mL. The exposure medium was renewed every 48 h under semi-static conditions using freshly prepared nominal concentrations to help maintain benzyl alcohol exposure levels and water quality throughout the chronic exposure period. Exposure vessels were kept partially covered to reduce possible evaporative loss and concentration fluctuation. At the end of the exposure period, *D. pulex* individuals were collected separately for biochemical and gene expression analyses (RT-qPCR).

2.5 Antioxidant enzyme and oxidative stress biomarkers

After 21 days of exposure to benzyl alcohol, *Daphnia pulex* samples were collected and homogenized in ice-cold phosphate buffer (100 mM, pH 7.4) at a ratio of 1:4 (w/v). The homogenates were centrifuged at 10,000 × g for 10 min at 4°C, and the resulting supernatants were used for subsequent biochemical analyses (Peppos et al., 2011). To evaluate oxidative stress responses in the exposed *Daphnia* populations, CAT, SOD, and GST activities were determined spectrophotometrically using the methods of Aebi (1984), Beauchamp and Fridovich (1971), and Habig et al. (1974), respectively. Reduced glutathione (GSH) content was measured colorimetrically according to Ellman (1959). Total protein concentration was determined using the Bradford method (Bradford, 1976), with bovine serum albumin as the standard. Enzyme activities and GSH content were normalized to total protein content and expressed per mg protein.

2.6 Gene expression analysis by RT-qPCR

For the purpose of gene expression analysis, approximately 10 adult *D. pulex* individuals were pooled per biological replicate, with three independent replicates (n=3) to prepare the samples. These were snap-frozen in liquid nitrogen and stored at -80°C. Total RNA was extracted from the samples using the TRIzol reagent according to the manufacturer's protocol. RNA integrity and quality were verified prior to cDNA synthesis. Reverse transcription was conducted using commercial reverse transcription kits according to the manufacturer's protocol, using a reaction volume of 20 µL. RT-qPCR was conducted on the extracted cDNA samples using the CFX96 Real-Time PCR System (Bio-Rad, USA) to quantify the expression of the cat and sod genes in the samples. The primers were specific to the cat and sod genes of *D. pulex* samples, and the primer sequences and annealing temperatures are presented in Table 1.

Table 1. Primer sequences and annealing temperatures used for RT-qPCR analysis in *D. pulex*

Gene	Primer	Sequence (5′-3′)	Annealing temperature (°C)
cat	Forward	TCCATTTGAACTTTTCTGCTTC	57.6
	Reverse	CCGACCAAGGGATTCGTAAT	57.6
sod	Forward	ATTGCTTTGTTGGTCTTGATGG	58.0
	Reverse	CCTTGCGGGGGTTGTAGTG	58.0
tbp	Forward	GCTGGCCATAGTGATCTTGG	59.0
	Reverse	CAGGAGTGATGCTGCTGTTG	59.0

The reference gene tbp was selected a priori for RT-qPCR normalization based on previous reference-gene evaluation studies in *Daphnia* species (Heckmann et al., 2006; Schwarzenberger et al., 2009; Spanier et al., 2010). This selection was further supported by the relatively consistent Cq values observed across control and treated samples under the present experimental conditions. Primer specificity was assessed using melt-curve analysis, and relative

expression levels of cat and sod were calculated using the $2^{-}\Delta\Delta Ct$ method with tbp as the reference gene.

2.7 Statistical analysis

Data were presented as mean±standard deviation (SD) of three biological replicates (n=3). For RT-qPCR data, technical replicates were averaged within each biological replicate, and statistical analysis was performed using ΔCt values, while $2^{-}\Delta\Delta Ct$ fold-change values were used for graphical presentation. Normality and homogeneity of variances were assessed using the Shapiro-Wilk and Levene's tests, respectively. One-way analysis of variance (ANOVA) followed by Tukey's HSD post hoc test, was applied to compare differences among treatment groups. Different letters in the figures indicate statistically significant differences among treatments. All analyses were performed using IBM SPSS Statistics.

3. RESULTS

3.1 Acute toxicity (LC_{50})

The acute toxicity of benzyl alcohol was determined, and mortality of *D. pulex* increased with increasing exposure concentrations after 48 h. No mortality was observed in the control group maintained in ASTM-reconstituted water (0 mg/L). Exposure to 150 mg/L resulted in 8 deaths out of 30 individuals (26.7%). Mortality increased to 33.3% and 43.3% at 180 and 210 mg/L, respectively, and further increased to 50.0% and 63.3% at 240 and 270 mg/L. Probit analysis of the mortality data estimated a 48 h LC_{50} of 229.68 mg/L, which was used to select sublethal concentrations for the chronic exposure experiments, as summarized in Table 2.

The selected chronic concentrations (11.5 and 23 mg/L) correspond to approximately 5% and 10% of the calculated LC_{50}, respectively.

3.2 Antioxidant biomarkers

Chronic exposure of *D. pulex* to benzyl alcohol for 21 days resulted in significant concentration-related alterations in antioxidant and oxidative stress biomarkers, as shown in Figure 1.

Table 2. Acute toxicity of benzyl alcohol to *D. pulex* after 48 h of exposure, showing the number of exposed and dead organisms at each concentration and corresponding mortality percentages.

Concentration (mg/L)	Exposed (N)	Dead (48 h)	Mortality (%)
0 (Control)	30	0	0.0
150	30	8	26.7
180	30	10	33.3
210	30	13	43.3
240	30	15	50.0
270	30	19	63.3

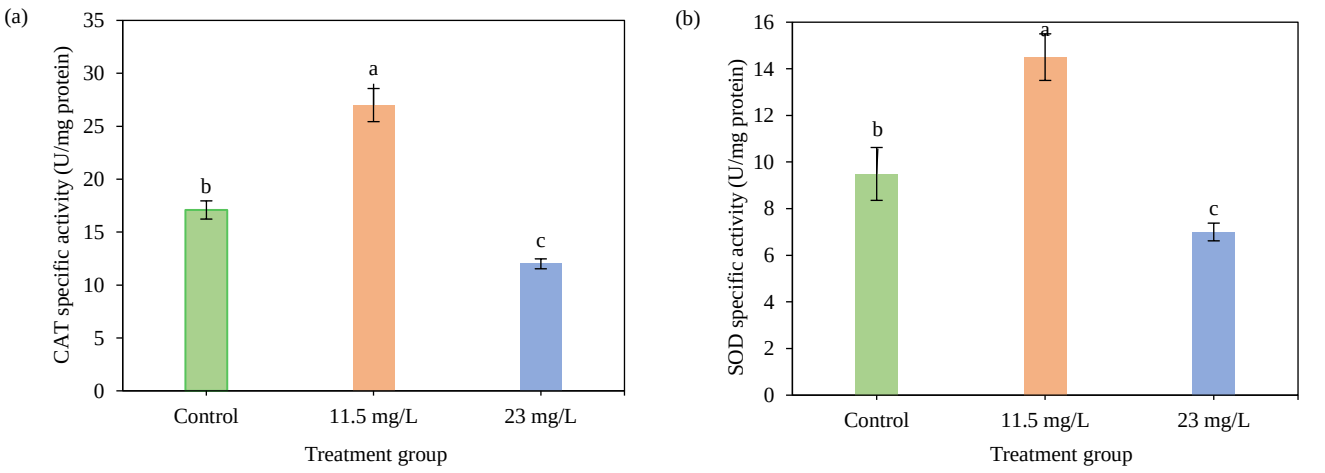


Figure 1. Effects of 21-day benzyl alcohol exposure on antioxidant biomarkers in *D. pulex*: (a) catalase (CAT), (b) superoxide dismutase (SOD), (c) glutathione S-transferase (GST), and (d) reduced glutathione (GSH). Data are presented as mean±SD (n=3). Different letters indicate significant differences among treatments (one-way ANOVA followed by Tukey's HSD test, $p<0.05$).

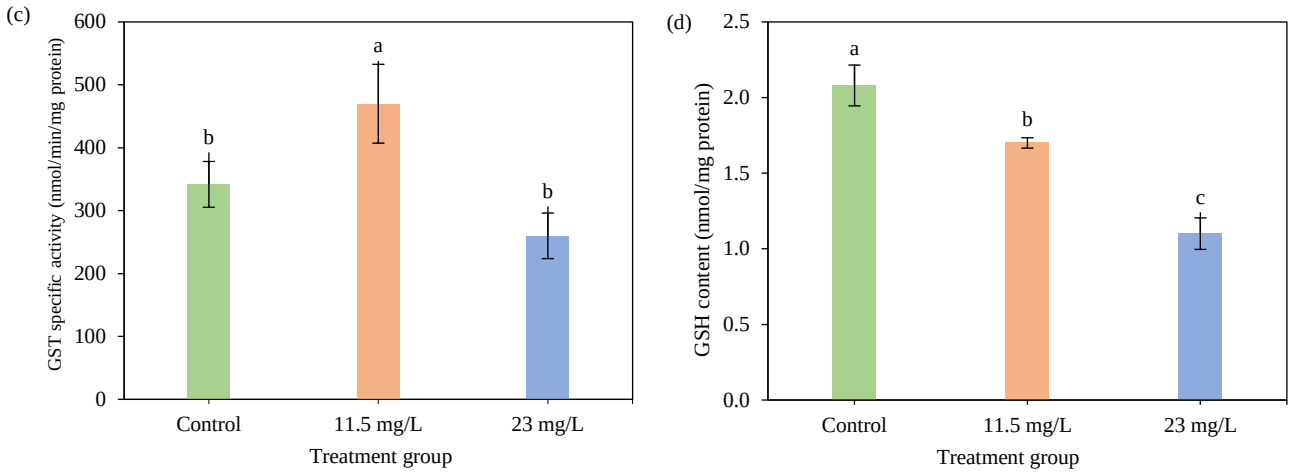


Figure 1. Effects of 21-day benzyl alcohol exposure on antioxidant biomarkers in *D. pulex*: (a) catalase (CAT), (b) superoxide dismutase (SOD), (c) glutathione S-transferase (GST), and (d) reduced glutathione (GSH). Data are presented as mean±SD (n=3). Different letters indicate significant differences among treatments (one-way ANOVA followed by Tukey's HSD test, $p<0.05$) (cont.).

Catalase (CAT) activity increased significantly from 17.09±0.86 U/mg protein in the control group to 27.00±1.57 U/mg protein at 11.5 mg/L, followed by a marked decrease to 12.00±0.47 U/mg/protein at 23 mg/L. Reduced glutathione (GSH) content showed a progressive decline from 2.08±0.14 nmol/ mg protein in the control to 1.70±0.03 nmol/ mg protein at 11.5 mg/L and further to 1.10±0.10 nmol mg/ protein at 23 mg/L. Glutathione S-transferase (GST) activity increased significantly at the lower concentration (470.00±62.63 nmol/min/mg protein) compared with the control (341.77±36.40 nmol/min/mg protein), but declined at 23 mg/L to 260.00±36.27 nmol/min/mg protein. Similarly, superoxide dismutase (SOD) activity rose from 9.49±1.13 U/mg protein in the control to 14.50±1.00 U/mg protein at 11.5 mg/L, then decreased significantly to 7.00±0.38 U/mg protein at 23 mg/L. Different superscript letters indicate statistically significant differences among treatments ($p<0.05$), demonstrating a biphasic antioxidant response characterized by enzymatic activation at moderate exposure and antioxidant impairment at higher benzyl alcohol concentrations.

3.3. Transcriptional responses of cat and sod genes

Chronic exposure of *D. pulex* to benzyl alcohol for 21 days induced significant, concentration-dependent regulation of antioxidant gene expression, as shown in Figure 2.

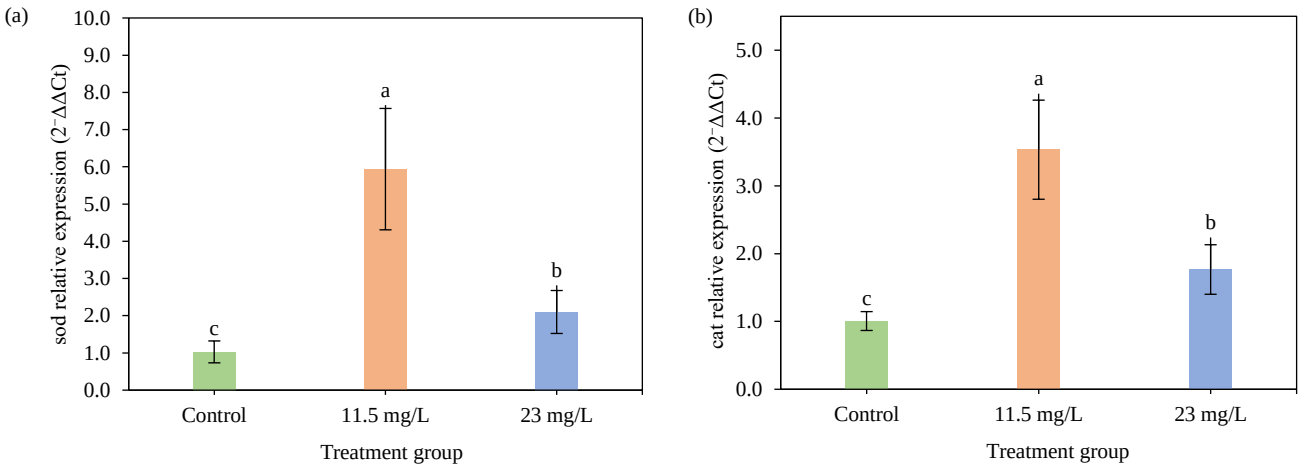


Figure 2. Relative expression of antioxidant-related genes: (a) sod and (b) cat in *D. pulex* after 21-day exposure to nominal benzyl alcohol concentrations.

Data are mean±SD (n=3 biological replicates). Different letters indicate significant differences among treatments (one-way ANOVA/Tukey's HSD, $p<0.05$); statistical analysis was performed using ΔCt values. Relative to the control group, cat expression increased significantly to 3.53±0.73-fold at 11.5 mg/L, followed by a decrease to 1.77±0.37-fold at 23 mg/L. However, cat expression at 23 mg/L remained significantly higher than the control and significantly lower than the 11.5 mg/L group. Similarly, sod expression increased significantly to 5.94±1.63-fold at 11.5 mg/L, then declined to 2.10±0.58-fold at 23 mg/L, remaining significantly above the control level but below the lower exposure group.

3.4 Correlation analysis

Results of Spearman correlation analysis showed that there were significant correlations between levels of antioxidant enzyme activity and expression response for antioxidant pathway genes in exposed populations of *D. pulex* in the benzyl alcohol exposure experiment (Figure 3).

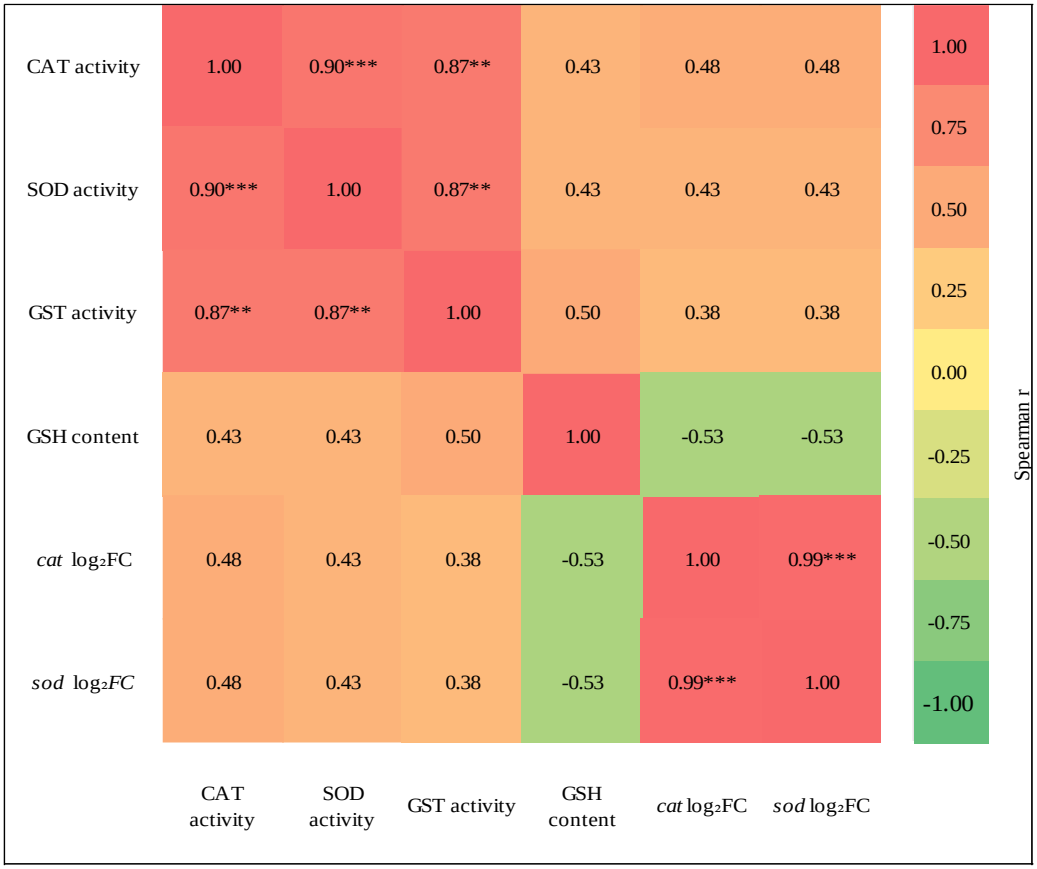


Figure 3. Spearman correlation heatmap showing the relationships between antioxidant enzyme activities (CAT, SOD, GST, and GSH) and the relative expression of cat and sod genes (log_2 fold change) in *D. pulex* after 21-day exposure to benzyl alcohol. Values represent Spearman correlation coefficients (r). Asterisks indicate statistically significant correlations (*p<0.05, **p<0.01, ***p<0.001).

Spearman correlation analysis showed strong positive relationships among antioxidant enzyme activities. CAT activity was strongly correlated with SOD activity ($r=0.90$, $p<0.001$), and both CAT and SOD activities were strongly correlated with GST activity ($r=0.87$, $p<0.01$). Regarding transcriptional responses, cat expression showed a near-perfect positive correlation with sod expression ($r=0.99$, $p<0.001$), suggesting coordinated regulation of antioxidant-related genes. Moderate positive associations were observed between antioxidant gene expression and enzyme activities, including associations between cat expression and CAT activity ($r=0.48$) and SOD activity ($r=0.43$). Similarly, sod expression showed moderate positive associations with CAT activity ($r=0.43$) and SOD activity ($r=0.48$). GSH content showed negative associations with cat and sod expression levels ($r=-0.53$), while its associations with CAT and SOD activities were weak.

4. DISCUSSION

4.1 Acute toxicity (LC_{50})

Although benzyl alcohol exhibited only moderate acute lethality (48 h LC_{50}=229.68 mg/L), chronic exposure produced pronounced enzymatic and transcriptional disturbances at concentrations nearly an order of magnitude lower than the lethal threshold. This discrepancy demonstrates that survival and mortality endpoints alone underestimate toxicological risk, as sublethal biochemical and physiological biomarkers in *Daphnia* frequently respond at concentrations far below those causing acute mortality (Mahaye and Musee, 2022). The acute mortality pattern was therefore less sensitive than chronic biomarker responses, indicating that oxidative stress-mediated physiological dysfunction precedes death and that biochemical endpoints provide earlier and more sensitive indicators of toxicity than lethality alone (Mahaye and Musee, 2022).Collectively, these findings highlight oxidative stress as the primary mechanistic pathway underlying both acute and chronic toxicity in *D. pulex*, consistent with broader evidence that chronic and multigenerational stress responses provide a more realistic estimate of ecological hazard (Livingstone, 2001; Regoli and Giuliani, 2014).

4.2 Antioxidant enzyme responses

After 21 days of exposure, clear changes were observed in the antioxidant defense system of *D. pulex*, and these changes depended strongly on benzyl alcohol concentration. At the intermediate level (11.5 mg/L), CAT, SOD, and GST activities increased compared with the control, suggesting that the animals activated their antioxidant defenses to cope with increased reactive oxygen species. Similar increases in enzyme activity have been reported in *Daphnia* exposed to sublethal contaminants (Esterhuizen et al., 2024; Queiroz and Torresi, 2025). This reaction may be linked to mitochondrial disruption and membrane damage, which can increase electron leakage and ROS production, thereby activating transcriptional and enzymatic defense mechanisms (Liu et al., 2021; Liu et al., 2022). At moderate concentrations, this pattern most likely reflects an early compensatory antioxidant response in which the defense system remained sufficiently functional to limit ROS-mediated damage and maintain redox balance. The situation changed, though, at the higher concentration (23 mg/L). Activities of CAT, SOD, and GST significantly decreased, and GSH levels steadily dropped. GSH depletion suggests that antioxidant reserves were being used up more quickly than they could be replenished because it is a significant non-enzymatic antioxidant and a necessary substrate for GST. Rather than indicating a simple loss of defense, this shift suggests that antioxidant regulation was altered under prolonged or stronger stress, with evidence of reduced protective capacity at the higher exposure level (De Felice et al., 2022; Mahaye and Musee, 2022). When combined, these findings reveal a common biphasic pattern, characterized by enzyme stimulation at the lower concentration and inhibition at the higher concentration, indicating a shift from an adaptive response to physiological impairment under long-term chemical stress. Antioxidant enzymes in *Daphnia* respond dynamically to oxidative stress. Ukhueduan et al. (2022) reported that higher SOD and CAT activities in *D. pulex* were associated with increased oxidative pressure, suggesting that enzyme elevation reflects a compensatory response to rising ROS levels. A similar trend was also described by Shen et al. (2019), where antioxidant enzymes were initially stimulated and later suppressed as contaminant stress intensified. However, unlike De Felice et al. (2022), who observed minimal changes in oxidative biomarkers under chronic nanoplastic exposure, the present findings indicate a clear redox disturbance induced by benzyl alcohol. Direct evidence on benzyl alcohol-induced antioxidant responses in aquatic organisms is still limited. However, its release through household and commercial waste streams, together with its detection in groundwater, supports its environmental relevance (Corcoran and Ray, 2014; Kong et al., 2016). In zebrafish embryos, benzyl alcohol has been reported to cause mortality, delayed hatching, cardiac defects, apoptosis, liver inhibition, and neuronal disruption, indicating potential toxicity to aquatic organisms (Manjunatha et al., 2021). Therefore, the antioxidant changes observed in the present study may represent early sublethal responses that could affect the physiological condition of freshwater organisms before mortality occurs (Musee et al., 2023).

4.3 Gene expression responses

Our understanding of the biochemical alterations caused by long-term exposure to benzyl alcohol has improved thanks to gene expression analysis. In general, the expression patterns of sod and cat mirrored the trend seen in enzyme activity. In comparison to the control group, sod expression rose

by nearly six times at 11.5 mg/L, and both genes were clearly upregulated. In response to increasing oxidative stress, this increase implies that antioxidant defenses were transcriptionally activated at an early stage. This transcriptional upregulation at the moderate concentration likely represents an early adaptive regulatory response, indicating that the organisms were still capable of activating stress-responsive pathways under sublethal oxidative challenge. Other *Daphnia* species exposed to low or sublethal contaminant levels have shown comparable increases in antioxidant-related genes, where gene expression alterations take place as part of an early stress response (Poynton and Vulpe, 2009; Liu et al., 2022; Hu et al., 2023). However, both cat and sod expression decreased at the higher concentration (23 mg/L), which was in line with the decrease in enzyme activity. The decline in both transcripts and enzyme activity suggests that under more severe stress, regulatory efficiency was disrupted, possibly reflecting both stress-induced impairment and reduced protective capacity under prolonged exposure. Similar transcriptional suppression has also been reported in *Daphnia* (Lampert, 2011; Lee et al., 2024). The findings collectively imply that alterations in the expression of antioxidant genes may function as sensitive and early markers of oxidative stress caused by benzyl alcohol. In comparison with recent chronic exposure studies, both similarities and differences can be observed. De Felice et al. (2022) reported modulation of antioxidant-related genes, including sod and cat, during 21-day exposure of *Daphnia magna* to polystyrene nanoplastics. However, in their study, transcriptional changes were mainly influenced by exposure time, and treatment effects were generally limited. In contrast, the present results demonstrate a clearer concentration-dependent response, with marked upregulation at moderate exposure followed by suppression at higher stress levels. A comparable stress intensity-dependent regulation has also been described in *Daphnia pulex* exposed to chemical stressors (Liu et al., 2018), where disruption of antioxidant pathways occurred under intensified conditions. Together, these comparisons indicate that while antioxidant genes consistently respond to chronic stress, the magnitude and direction of regulation depend strongly on the nature and intensity of the contaminant.

4.4 Integrated mechanistic interpretation

When combining the results of the acute, enzymatic, and gene expression analyses, a distinct pattern of toxicity in *D. pulex* is revealed. The animals increased gene expression and enzyme activity, demonstrating that they could still activate their antioxidant defenses at moderate concentrations. This points to a transient adaptive reaction to oxidative stress. Yet, this protective ability decreased at greater concentrations. Gene expression, glutathione levels, and antioxidant enzymes all declined. This suggests that the antioxidant defense system was altered under prolonged stress, possibly reflecting an adaptive regulatory response at first, but with evidence of reduced protective capacity at higher exposure levels. Notably, these molecular and biochemical alterations occurred at concentrations significantly lower than the acute LC_{50}, demonstrating that physiological disruption starts long before mortality is apparent. Additionally, prior research has linked extended oxidative stress to decreased *Daphnia* growth, reproduction, and overall fitness, which could eventually affect population stability (Liess et al., 2016). Because of this, biochemical and molecular biomarkers are thought to be helpful in identifying sublethal toxicity before mortality-based endpoints are reached (Jemec Kokalj et al., 2023). The ecological relevance of the present findings is supported by the documented occurrence of benzyl alcohol in wastewater-related environments, indicating that aquatic organisms may encounter this compound under real-world exposure scenarios. Benzyl alcohol has been reported in wastewater treatment plant influents at ng/L levels, which confirms environmental occurrence even though these concentrations are lower than the experimental levels used here. Taken together with its demonstrated toxicity in aquatic models, these observations suggest that chronic low-level exposure may contribute to sublethal physiological disturbance in freshwater biota, with possible consequences for organismal fitness and ecosystem function (Musee et al., 2023; Manjunatha et al., 2021). Similar integrated biomarker-based approaches may therefore be useful for hazard assessment in *Daphnia* species. Overall, the findings of the present study indicate that oxidative stress is a major contributor to the long-term toxicity of benzyl alcohol.

5. CONCLUSION

In conclusion, benzyl alcohol caused measurable toxic effects in *D. pulex* under the tested exposure conditions. Although acute exposure resulted in only moderate mortality (48 h LC_{50}=229.68 mg/L), chronic exposure to much lower levels (11.5-23 mg/L; 5-10% of LC_{50}) produced significant biochemical and transcriptional disruptions. Together with glutathione depletion, the observed biphasic response of antioxidant enzymes and the marked induction of cat and sod expression (approximately 3-6-fold) suggest that oxidative stress is a major factor in this compound's toxicity. The significance of these sublethal biomarkers as early indicators of environmental stress is highlighted by the fact that they responded more quickly and sensitively than mortality. Overall, the enzymatic and molecular biomarkers supported their value as early-warning indicators of physiological stress because only two LC_{50}-derived sublethal concentrations were used, these responses should be interpreted as exposure-level-related patterns rather than a complete dose-response relationship. However, the molecular and biochemical biomarkers measured in this study should be interpreted as early mechanistic indicators of sublethal stress and potential precursors of higher-level biological effects, rather than as direct evidence of population-level impairment. Therefore, future studies should integrate these biomarkers with ecologically relevant apical endpoints, such as reproduction, growth, brood production, survival, and time to first brood, to better link benzyl alcohol-induced redox disruption with ecological outcomes. From an environmental perspective, the present findings suggest that benzyl alcohol may pose a risk to freshwater organisms even at nonlethal concentrations, supporting the value of sublethal biomarker responses as early-warning tools in aquatic environmental monitoring and risk assessment.

AUTHOR CONTRIBUTIONS

Ghufran Saad Aljanabi: Conceptualization, study design, experimental execution, sample collection, biochemical assays, molecular analysis (RT-qPCR), data curation, statistical analysis, visualization, and original draft preparation. Adel Mashaan Rabee: Methodological supervision, validation of experimental procedures, interpretation of results, critical revision of the manuscript for important intellectual content, and overall scientific guidance. All authors have read and approved the final version of the manuscript.

DECLARATION OF CONFLICT OF INTEREST

The authors declare that they have no conflict of interest.

REFERENCES

Abdulameer AH, Hussein SZ. Assessment of oxidative stress parameters for some of Baghdad City fuel stations workers. Iraqi Journal of Science 2023;64(6):2669-80.

Aebi H. Catalase in vitro. Methods in Enzymology 1984;105: 121-6.

Al-Fanharawi AA, Rabee AM, Al-Mamoori AMJ. Multi-biomarker responses after exposure to organophosphates chlorpyrifos in the freshwater mussels *Unio tigridis* and snails *Viviparous benglensis*. Human and Ecological Risk Assessment: An International Journal 2019;25(5):1137-56.

Al-Jaff DK, Jaweir HJ. Aquatic Oligochaeta (Annalida:Clitellata) as bio indication for sediment quality assessment in Tigris River within Baghdad City/Iraq. Baghdad Science Journal 2021;18(1):665-9.

Alkatrani LMAA, Obaid ZH, Salman JM. Identification of some biochemical indicators to indicate the contamination of some fish farms in Hilla City/Iraq. Baghdad Science Journal 2024;21(12):3785-96.

Api AM, Bartlett A, Belsito D, Botelho D, Bruze M, Bryant-Friedrich A, et al. Update to RIFM fragrance ingredient safety assessment, benzyl alcohol, CAS Registry Number 100-51-6. Food and Chemical Toxicology 2025;204(Supplement 1):Article No. 115644.

American Society for Testing and Materials (ASTM). Standard Guide for Conducting Acute Toxicity Tests on Test Materials with Fishes, Macroinvertebrates, and Amphibians: ASTM E729-96(2014). West Conshohocken, PA: ASTM International; 2014.

Atli G, Sevgiler Y. Binary effects of fluoxetine and zinc on the biomarker responses of the non-target model organism *Daphnia magna*. Environmental Science and Pollution Research 2024;31:27988-8006.

Bang SH, Ahn JY, Hong NH, Sekhon SS, Kim YH, Min J. Acute and chronic toxicity assessment and the gene expression of Dhb, Vtg, Arnt, CYP4, and CYP314 in *Daphnia magna* exposed to pharmaceuticals. Molecular and Cellular Toxicology 2015;11(2):153-60.

Beauchamp C, Fridovich I. Superoxide dismutase: Improved assays and an assay applicable to acrylamide gels. Analytical Biochemistry 1971;44(1):276-87.

Bradford MM. A rapid and sensitive method for the quantitation of microgram quantities of protein utilizing the principle of protein-dye binding. Analytical Biochemistry 1976;72:248-54.

Corcoran GB, Ray SD. Benzyl alcohol. In: Wexler P, editor. Encyclopedia of Toxicology. 3rd ed. Oxford: Academic Press; 2014. p. 429-32.

De Felice B, Sugni M, Casati L, Parolini M. Molecular, biochemical and behavioral responses of *Daphnia magna* under long-term exposure to polystyrene nanoplastics. Environment International 2022;164:Article No. 107264.

Ebert D. *Daphnia* as a versatile model system in ecology and evolution. Developmental Biology Advances 2022;13:Article No.16.

Ellman GL. Tissue sulfhydryl groups. Archives of Biochemistry and Biophysics 1959;82(1):70-7.

Esterhuizen M, Monticelli M, Lee SA, Kim Y, Pflugmacher S, Kim YJ. Oxidative stress status and antioxidative responses in neonate versus adult *Daphnia magna* exposed to polystyrene leachate. Toxicology and Environmental Health Sciences 2024;16:171-9.

Esterhuizen-Londt M, von Schnehen M, Kühn S, Pflugmacher S. Oxidative stress responses in the animal model, *Daphnia pulex* exposed to a natural bloom extract versus artificial cyanotoxin mixtures. Aquatic Toxicology 2016;179:151-7.

Finney DJ. Probit Analysis. 3rd ed. Cambridge, UK: Cambridge University Press; 1971

Guevara RD, Pastor JJ, López-Vergé S, Manteca X, Tedo G, Llonch P. Physiology, gene expression, and behavior as potential indicators of oxidative stress in piglets. BMC Veterinary Research 2024;20:Article No. 471.

Habig WH, Pabst MJ, Jakoby WB. Glutathione S-transferases: The first enzymatic step in mercapturic acid formation. Journal of Biological Chemistry 1974;249(22):7130-9.

Heckmann LH, Connon R, Hutchinson TH, Maund SJ, Sibly RM, Callaghan A. Expression of target and reference genes in *Daphnia magna* exposed to ibuprofen. BMC Genomics 2006;7:Article No. 175.

Hu C, Zhang N, Hu L, Tang T, Yang Y, Ning X. Assessment of ecotoxicity effects of aspirin on non-target organism (*Daphnia magna*) via analysis of the responses of oxidative stress, DNA methylation and life traits. Ecotoxicology 2023;32(2):137-49.

Jemec Kokalj A, Heinlaan M, Novak S, Drobne D, Kühnel D. Defining quality criteria for nanoplastic hazard evaluation: The case of polystyrene nanoplastics and aquatic invertebrate *Daphnia* spp. Nanomaterials 2023;13(3):Article No. 536.

Kim BM, Rhee JS, Park GS, Lee J, Lee YM, Lee JS. Cu/Zn- and Mn-superoxide dismutase (SOD) from the copepod *Tigriopus japonicus*: Molecular cloning and expression in response to environmental pollutants. Chemosphere 2011;84(10):1467-75.

Kong L, Kadokami K, Duong HT, Chau HTC. Screening of 1300 organic micro-pollutants in groundwater from Beijing and Tianjin, North China. Chemosphere 2016;165:221-30.

Lampert W. *Daphnia*: Development of a Model Organism in Ecology and Evolution. Oldendorf/Luhe, Germany: International Ecology Institute; 2011.

Lee JS, Kim JR, Byeon E, Kim DH, Kim HS, Lee JS. Molecular events in response to triclosan-induced oxidative stress in CRISPR/Cas9-mediated p53-targeted mutants in *Daphnia magna*. Environmental Science and Technology 2024; 58(38):16738-49.

Liess M, Foit K, Knillmann S, Schäfer RB, Liess HD. Predicting the synergy of multiple stress effects. Scientific Reports 2016;6:Article No. 32965.

Liu S, Lin J, Ding R, Nie X. Simvastatin as an emerging pollutant on non-target aquatic invertebrates: Effects on antioxidant-related genes in *Daphnia magna*. Environmental Science and Pollution Research 2022;29(34):52248-62.

Liu Z, Cai M, Yu P, Chen M, Wu D, Zhang M, et al. Age-dependent survival, stress defense, and AMPK in Daphnia pulex after short-term exposure to a polystyrene nanoplastic. Aquatic Toxicology 2018;204:1-8.

Liu Z, Li Y, Pérez E, Jiang Q, Chen Q, Jiao Y, et al. Polystyrene nanoplastic induces oxidative stress, immune defense, and glycometabolism change in *Daphnia pulex*: Application of transcriptome profiling in risk assessment of nanoplastics. Journal of Hazardous Materials 2021;402:Article No. 123778.

Livingstone DR. Contaminant-stimulated reactive oxygen species production and oxidative damage in aquatic organisms. Marine Pollution Bulletin 2001;42(8):656-66.

Mahaye N, Musee N. Effects of two antiretroviral drugs on the crustacean *Daphnia magna* in river water. Toxics 2022;10(8):Article No. 423.

Manjunatha B, Sreevidya B, Lee SJ. Developmental toxicity triggered by benzyl alcohol in the early stage of zebrafish embryos: Cardiovascular defects with inhibited liver formation and degenerated neurogenesis. Science of the Total Environment 2021;752:Article No. 141631.

McKnight EGW, Jones CLC, Pearce NJT, Frost PC. Environmental stress and the morphology of *Daphnia pulex*. Physiological and Biochemical Zoology 2023;96(6):438-49.

Musee N, Ngwenya P, Motaung LK, Moshuhla K, Nomngongo P. Occurrence, effects, and ecological risks of chemicals in sanitizers and disinfectants: A review. Environmental Chemistry and Ecotoxicology 2023;5:62-78.

Mustafa SA, Al-Rudainy AJ, Salman NM. Effect of environmental pollutants on fish health: An overview. Egyptian Journal of Aquatic Research 2024;50(2):225-33.

Organisation for Economic Co-operation and Development (OECD). OECD Guidelines for the Testing of Chemicals, Section 2: Test No. 202: *Daphnia* sp. Acute Immobilisation Test. OECD Publishing, Paris; 2004.

Peppos P, Salifoglou A, Hadjispyrou S. Superoxide dismutase activity in the freshwater crustacean *Daphnia magna* exposed to Pb(II). Journal of Agroalimentary Processes and Technologies 2011;17(2):116-8.

Poynton HC, Taylor NS, Hicks J, Colson K, Chan S, Clark C, et al. Metabolomics of microliter hemolymph samples enables an improved understanding of the combined metabolic and transcriptional responses of *Daphnia magna* to cadmium. Environmental Science and Technology 2011;45(8):3710-7.

Poynton HC, Vulpe CD. Ecotoxicogenomics: Emerging technologies for emerging contaminants. Journal of the American Water Resources Association 2009;45(1):83-96.

Queiroz LG, Torresi SIC. Metal and metal-oxide nanoparticles inducing changes in reactive oxygen species levels and enzymes of oxidative stress: A review focused on daphnids. Ecotoxicology 2025;34(7):1334-49.

Regoli F, Giuliani ME. Oxidative pathways of chemical toxicity and oxidative stress biomarkers in marine organisms. Marine Environmental Research 2014;93:106-17.

Reilly K, Ellis LJA, Davoudi HH, Supian S, Maia MT, Silva GH, et al. *Daphnia* as a model organism to probe biological responses to nanomaterials—from individual to population effects via adverse outcome pathways. Frontiers in Toxicology 2023;5:Article No. 1178482.

Sadeq SAR. The Response of *Daphnia pulex* to Multiple Environmental Stressors [dissertation]. Sheffield (UK): The University of Sheffield; 2018.

Schwarzenberger A, Courts C, von Elert E. Target gene approaches: Gene expression in *Daphnia magna* exposed to predator-borne kairomones or to microcystin-producing and microcystin-free *Microcystis aeruginosa*. BMC Genomics 2009;10:Article No. 527.

Shen C, Wei J, Wang T, Wang Y. Acute toxicity and responses of antioxidant systems to dibutyl phthalate in neonate and adult *Daphnia magna*. PeerJ 2019;7:e6584.

Sonmez G, Temizkan MC, Culha MH. SOD1 and CAT gene expressions in stray and owned animals. Veterinarni Medicina 2025;70(8):273-8.

Spanier KI, Leese F, Mayer C, Colbourne JK, Gilbert D, Pfrender ME, et al. Predator-induced defences in *Daphnia pulex*: Selection and evaluation of internal reference genes for gene expression studies with real-time PCR. BMC Molecular Biology 2010;11:Article No. 50.

Ukhueduan B, Schumpert C, Kim E, Dudycha JL, Patel RC. Relationship between oxidative stress and lifespan in *Daphnia pulex*. Scientific Reports 2022;12:Article No. 2354.

Wang T, Wei J, Wang L, Lu Y, Zhang Q, Wang Y. Effect of dibutyl phthalate on antioxidant parameters and related gene expression in *Daphnia magna*. IOP Conference Series: Earth and Environmental Science 2019;227(5):Article No. 052052.

Wojtal-Frankiewicz A, Bernasińska J, Jurczak T, Gwoździński K, Frankiewicz P, Wielanek M. Microcystin assimilation and detoxification by *Daphnia* spp. in two ecosystems of different cyanotoxin concentrations. Journal of Limnology 2013; 72(1):e13.

Environment and Natural Resources Journal

Volume 24
Issue 6
2026

Spatio-Temporal Assessment of Air Quality and AQI in Former Khanh Hoa Province, Vietnam (2021-2024)

Le Viet Thang[1] and Ho Minh Dung[2*]

[1]Industrial University of Ho Chi Minh City, 12 Nguyen Van Bao Street, Hanh Thong Ward, Ho Chi Minh City, Vietnam
[2]Institute for Environment and Resources, VNU-HCM, 142 To Hien Thanh Street, Dien Hong Ward, Ho Chi Minh City, Vietnam

ARTICLE INFO

Received: 5 Mar 2026
Received in revised: 22 May 2026
Accepted: 9 Jun 2026
Published online: 7 Sep 2026
DOI: 10.32526/ennrj/24/20260091

Keywords:
Air quality/ AQI/ TSP/ Khanh Hoa Province/ Spatio-temporal variation

*** Corresponding author:**
E-mail:
minhdung@hcmier.edu.vn

ABSTRACT

Air pollution has become an increasingly important environmental and public health concern, particularly in rapidly urbanizing coastal provinces. This study aimed to evaluate the spatio-temporal variation characteristics of key air quality parameters (TSP, SO_2, NO_2, and CO) and the Air Quality Index (AQI) in former Khanh Hoa Province during the period 2021-2024. Periodic monitoring data collected from 28 monitoring sites across four functional zones (North, South, West, and Central) were analyzed using descriptive statistics, seasonal comparison, Pearson correlation analysis, AQI calculation, and GIS-based spatial interpolation (IDW). The results showed that SO_2 and CO concentrations significantly decreased by 62% and 22%, respectively ($p<0.05$), while NO_2 remained relatively stable and TSP showed signs of increasing, particularly in 2024. TSP was identified as the dominant pollutant, accounting for more than 95% of AQI deterioration and frequently exceeding the annual average standard in the Central region. Overall air quality was generally classified as "Good" and "Moderate"; however, localized pollution hotspots and short-term unhealthy AQI events were observed, especially during the dry season in urbanized areas with high traffic density and intensive construction activities. Pearson correlation analysis revealed that humidity and wind speed played important roles in pollutant dispersion and washout effects, while noise levels showed significant positive correlations with TSP, NO_2, and CO, indicating the strong influence of transportation-related emissions. These findings suggest that air quality management should prioritize TSP source control, particularly in the Central region, and strengthen seasonal monitoring strategies to support sustainable environmental management in rapidly developing coastal provinces of Vietnam.

HIGHLIGHTS

- GIS-AQI analysis across four zones in Khanh Hoa (2021-2024)
- TSP dominates pollution, contributing more than 95% of AQI deterioration
- SO_2 and CO decreased significantly; NO_2 remained stable
- Hotspots occur in urban areas during the dry season
- Traffic emissions strongly influence TSP, NO_2, and CO levels

1. INTRODUCTION

Air quality is currently one of the most serious environmental and public health challenges on a global scale, causing negative impacts on human health, ecosystems, and sustainable economic development (Li et al., 2014; Rakholia et al., 2023). Urban air pollution is not only occurring in megacities but is also rapidly increasing in medium and small-sized cities due to the development of industrial activities and regional economic growth (Dadhich et al., 2018). According to the World Health Organization (WHO), approximately 99% of the world's population is exposed to air quality levels that exceed recommended limits, causing millions of premature deaths and significant economic losses worldwide (Alsowaidan et al., 2024; Rad et al., 2022; WHO, 2024). However, the severity and spatial distribution of air pollution vary considerably among regions depending on urbanization intensity, industrial activities, and local meteorological conditions. Studies have confirmed a strong link between major air

Citation: Thang LV, Dung HM. Spatio-temporal assessment of air quality and AQI in Former Khanh Hoa Province, Vietnam (2021-2024). Environ. Nat. Resour. J. 2026;24(6):673-688. (https://doi.org/10.32526/ennrj/24/20260091)

pollutants such as total suspended particles (TSP), sulfur dioxide (SO_2), and nitrogen dioxide (NO_2) and adverse human health effects. High concentrations of TSP can penetrate the respiratory system, causing respiratory irritation, reduced lung function, chronic bronchitis, asthma aggravation, and increased risks of cardiovascular and pulmonary diseases, particularly among children, the elderly, and sensitive groups (Lang et al., 2025; Makinde et al., 2023). SO_2 exposure is associated with airway inflammation, bronchoconstriction, and worsening of asthma symptoms, while prolonged exposure to NO_2 may damage lung tissue, reduce immune defenses of the respiratory system, and increase the risk of cardiovascular and neurological disorders such as Alzheimer's or Parkinson's disease (Makinde et al., 2023; Rad et al., 2022). Although CO concentrations are often lower than regulatory limits, prolonged exposure can reduce oxygen transport in the blood through hemoglobin binding, leading to headaches, dizziness, cardiovascular stress, and serious health risks under high exposure conditions (Rad et al., 2022; WHO, 2024).

In Vietnam, rapid industrialization and urbanization have led to a serious decline in air quality in major cities like Hanoi and Ho Chi Minh City, frequently exceeding national and international permissible levels (Ho et al., 2025; Nguyen et al., 2022; Rakholia et al., 2023). Not only in major economic centers, but also in key economic regions like Dong Nai and coastal provinces like Bac Lieu, are experiencing pollution pressure from traffic, production, and waste management (Lang et al., 2025; Nguyen et al., 2025). In particular, transportation is identified as the main source of emissions, accounting for over 70-80% of emissions in developing cities, due to the enormous volume of motorcycles and underdeveloped infrastructure (Nguyen et al., 2022; Nguyen et al., 2025).

The former Khanh Hoa Province, with its position as a center for coastal tourism and a strategic economic corridor, is undergoing a strong recovery of socio-economic activities after the Covid-19 pandemic. Extreme temperature changes and extreme weather events in the locality over the past decades have shown clear signs of climate change (Pham et al., 2023), this can further complicate the dispersion and accumulation of air pollutants. Studies in tropical monsoon regions show that air pollutant concentrations vary dramatically seasonally, often peaking during the dry season due to calm atmospheric conditions and temperature inversions (Ho et al., 2025; Nguyen et al., 2025; Xu et al., 2019). Although former Khanh Hoa Province generally maintains relatively good air quality compared to major metropolitan areas in Vietnam, localized pollution hotspots still occur, particularly in densely urbanized and traffic-concentrated areas such as the Central region. Short-term increases in TSP concentrations during the dry season and periods of intensive construction activity may lead to temporary deterioration of AQI (Air Quality Index), especially for sensitive groups. Therefore, understanding the spatial and temporal variability of pollution is more important than evaluating only the overall annual air quality status (Dang and Vu, 2024; Watcharavitoon et al., 2013; Xu et al., 2019). Urban noise has also been shown to have a very strong positive correlation with CO and NO_2 concentrations, which serve as important representative indicators of traffic intensity (Nguyen et al., 2025).

In modern air quality research, the application of Geographic Information Systems (GIS) has become a powerful and flexible tool for spatially estimating and analyzing pollution levels (Dadhich et al., 2018; Nguyen et al., 2025). GIS provides a digital environment that integrates data from various sources, enabling the visualization of pollution trends (Dadhich et al., 2018). Through spatial interpolation techniques such as Inverse Distance Weighting (IDW) or Kriging, GIS allows for the forecasting of particulate and air pollutant concentrations in areas without monitoring stations based on sample data from known locations (Dadhich et al., 2018; Nguyen et al., 2025; Zaib et al., 2022). This GIS-based approach effectively supports the identification of pollution "hotspots" and the assessment of air quality differences between various functional areas such as residential areas, industrial zones, or major transportation routes (Dadhich et al., 2018; Nguyen et al., 2025). The use of high-resolution map layers helps managers accurately identify critical zones that require priority emission control to protect public health (Nguyen et al., 2022; Sharma and Mauzerall, 2022).

Although several studies have assessed climatic characteristics and general environmental conditions in Khanh Hoa province (Nguyen, 2003; Pham et al., 2023), however, comprehensive spatio-temporal assessments of air quality during the post-Covid-19 economic recovery period (2021-2024), particularly those integrating pollutant trends, AQI spatial distribution, and their relationships with

meteorological and noise factors across different functional zones, remain limited. Previous studies have mainly focused on climate patterns or isolated environmental indicators, while updated assessments of key air pollutants and their relationships with meteorological and anthropogenic factors are still lacking (Dang and Vu, 2024; Watcharavitoon et al., 2013; Xu et al., 2019). In particular, no previous study has systematically integrated annual, monthly, and seasonal variations of major pollutants (TSP, SO_2, NO_2, CO), dominant pollutant identification, GIS-based AQI spatial distribution, and correlation analysis between air pollutants, meteorological parameters, and noise levels across different functional zones of the province. This gap limits the understanding of local pollution dynamics and hinders the development of effective and sustainable air quality management policies for this rapidly urbanizing coastal province. Therefore, this study aims to provide the first comprehensive spatio-temporal assessment of air quality in former Khanh Hoa Province during 2021-2024. The main objectives are to: (i) assess the trends of key air quality parameters (TSP, SO_2, NO_2, CO) across annual, monthly, and seasonal cycles; (ii) identify dominant pollutants and analyze AQI evolution across different functional zones using GIS-based interpolation; and (iii) examine the correlations between meteorological factors (temperature, humidity, pressure, wind speed), noise levels, and air quality parameters. The findings are expected to provide a scientific basis for targeted air pollution control strategies and sustainable environmental management at the local level.

2. METHODOLOGY

2.1 Research and data collection area

The study area is the mainland region of Khanh Hoa Province (former), a coastal province in South Central Vietnam, notable for its developing tourism, service, and industrial activities (Khanh Hoa PPC, 2023). The topography of Khanh Hoa Province slopes gradually from west to east, with over 67% of its area being hills and mountains, forming an arc that blocks winds from the north to the west, surrounded by narrow coastal plains in the districts of Van Ninh, Ninh Hoa, Dien Khanh, and Cam Ranh (Nguyen et al., 2013). The province's climate is characterized by a typical tropical monsoon climate. It is divided into two seasons, the dry season from January to August, and the rainy season from September to December. The prevailing wind direction during the dry season is southeast, and during the rainy season it is north and northeast (Khanh Hoa PPC, 2023; Nguyen, 2003).

To reflect the diverse characteristics of emission sources and population density, the study area is divided into four main sub-regions based on natural geography, population characteristics, development conditions, and projected development potential according to the Khanh Hoa Province development plan for the period 2021-2030, with a vision to 2050 (Figure 1): The North (NR) comprises Van Ninh District and the Ninh Hoa Town area within the Van Phong Economic Zone, a dynamic economic center developing new, high-level industries, focusing on high-tech industries and high-end integrated tourism; the South (SR) comprises Cam Ranh city and Cam Lam urban area, a logistics and trade center with Cam Ranh International Airport and seaport playing a crucial role in the province's development; the West (WR) comprises Khanh Vinh District, Khanh Son District, and the western area of Ninh Hoa Town, an inland mountainous area with the least developed economy in the province; and the Central (CR) area comprises Nha Trang City and the southern part of Ninh Hoa, Dien Khanh District, serving as the province's administrative, political, tourism, and commercial center (Khanh Hoa PPC, 2023). This zoning allows for a more detailed assessment of air quality variability across space, similar to studies conducted in other coastal cities (Yan et al., 2025; Zhang et al., 2022).

The data used in this study are periodic monitoring data of meteorological parameters and air quality over a four-year period, from 2021 to 2024, and 12 months (12 periods), two seasons of the year (dry season: 8 periods corresponding from January to August; and rainy season: 4 periods corresponding from September to December) at 28 monitoring points, divided into Northern (5 points), Southern (9 points), Western (2 points), and Central (12 points) areas (Figure 1). Meteorological parameters included temperature (°C), humidity (%), pressure (hPa), and wind speed (m/s). Air quality parameters of interest were TSP, SO_2, NO_2, and CO. In addition, noise levels were also collected. All data were provided by the local environmental management agency, ensuring accuracy and representativeness of the current air quality status in Khanh Hoa Province (DONRE Khanh Hoa, 2025).

2.2 Data analysis methods

Descriptive statistical methods (mean, standard deviation, minimum, maximum) were applied to

provide an overview of the characteristics of each air quality and meteorological parameter. Trends in pollutant concentrations over the year, month, and season were analyzed to identify patterns and cycles. Percentage changes between years were calculated to quantify the increase/decrease in pollutant concentrations. The independent sample t-test was applied to evaluate the statistical significance of interannual differences in mean concentrations of air pollutants (TSP, SO_2, NO_2, and CO) during the monitoring period from 2021 to 2024. The primary objective of this analysis was to compare annual variations and determine whether changes between monitoring years were statistically significant, rather than to detect monotonic long-term temporal trends. Given that the dataset was based on periodic monthly monitoring observations over a relatively short period (four years), the t-test was considered appropriate for assessing year-to-year differences and supporting practical interpretation of short-term air quality changes, similar to studies on air quality variability over time (Lu et al., 2023; Pham and Nguyen, 2024). In contrast, methods such as the Mann-Kendall test and Sen's slope estimator are generally more suitable for longer continuous time-series data aimed at robust monotonic trend detection.

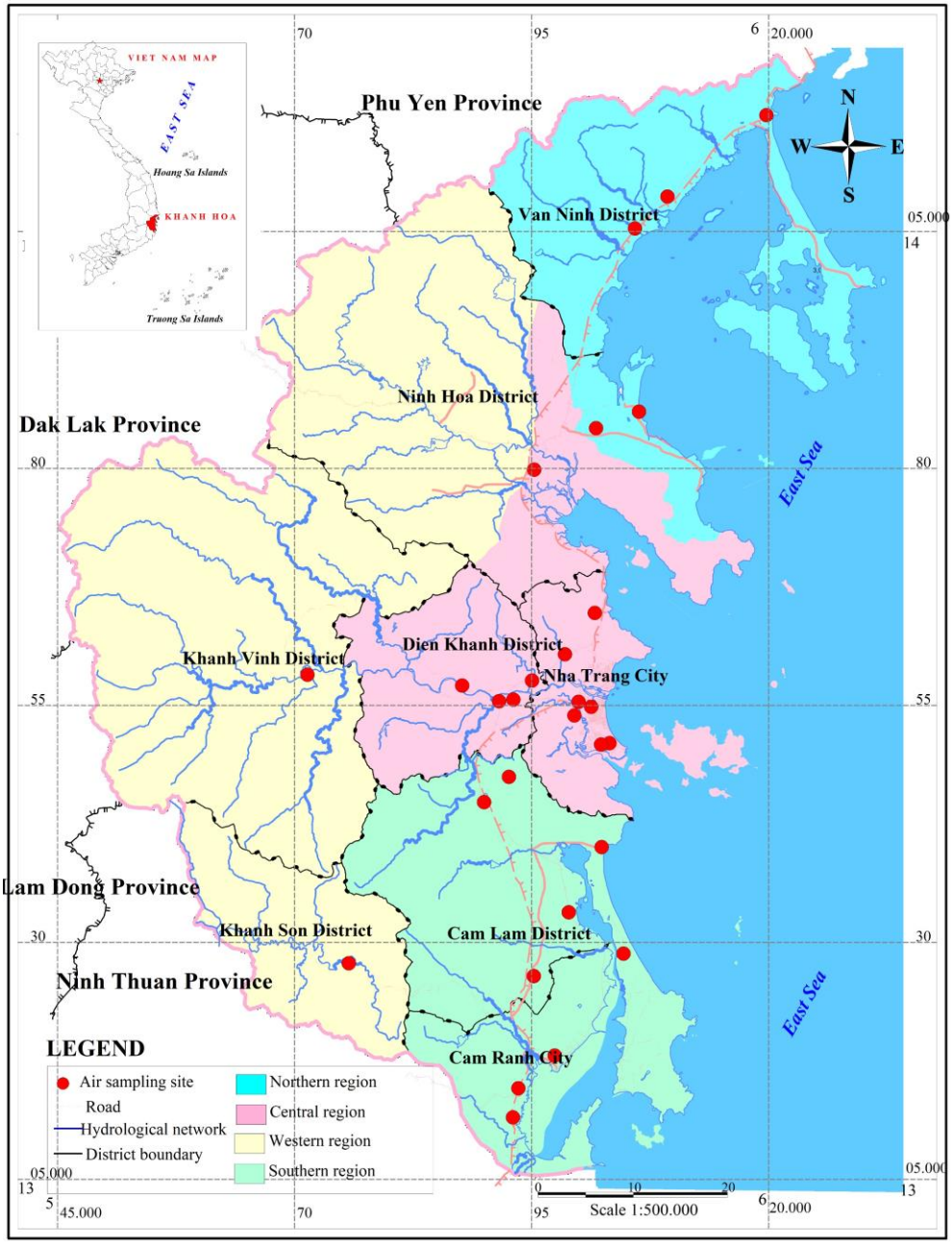


Figure 1. Map of the study area and locations for air quality monitoring sampling

Pearson correlation analysis was used to assess the linear relationship between meteorological parameters (temperature, humidity, pressure, wind speed), noise levels, and concentrations of air pollutants (TSP, SO_2, NO_2, CO), as well as the AQI (Lu et al., 2017; Shrestha and Kazama, 2007). The correlation coefficient (r) and p-value ($p<0.05$; $p<0.01$; $p<0.001$) were used to determine the magnitude and statistical significance of the relationship. Understanding this correlation is crucial for identifying factors influencing air quality and proposing effective control solutions (Tian et al., 2024; Xia et al., 2025). Data processing and charting were done using Rstudio 2023.06.0 Build 421 statistical software and Excel 2016.

The Air Quality Index (AQI) is calculated according to the guidelines of Decision No. 1459/QD-TCMT of the Vietnam General Department of Environment (VEA, 2019), based on parameters such as TSP, SO_2, NO_2, and CO, the AQI is a composite index reflecting the level of air pollution and its impact on human health. It is classified into six levels where, Green (0-50, Good); Yellow (51-100, Moderate); Orange (101-150, Unhealthy for sensitive groups); Red (151-200, Unhealthy); Purple (201-300, Very Unhealthy); and Maroon (301-500, Hazardous). Analyzing the AQI across space and time helps to assess the overall air quality situation and identify areas and times with a high risk of pollution (Ali et al., 2026).

Spatial interpolation for the AQI was performed using the IDW algorithm in ArcGIS 10.8. According to Vorapracha et al. (2015), IDW demonstrates significant advantages over kriging methods in forecasting air pollution trends. In this study, IDW utilized data collected from 28 monitoring points to predict AQI in areas lacking direct data. The IDW interpolated maps were then visualized using a color scale, clearly illustrating the spatial distribution of AQI.

3. RESULTS AND DISCUSSION

3.1 Trends in the concentration of air quality parameters over time and space

3.1.1. Trends in the concentration of air quality parameters over the year

Table 1 shows that the average air pollutants values for SO_2, CO, and NO_2 during the period 2021-2024 were all lower than the limits of QCVN 05:2023/BTNMT: Vietnam National Technical Standard on Air Quality (MONRE, 2023) calculated based on annual and hourly averages. However, although TSP levels reached the hourly average (300 µg/Nm^3), there were signs of exceeding the annual average (100 µg/Nm^3) in 2021, 2022, and 2024. The average noise level still met QCVN 26:2010/BTNMT: National Technical Standard on Noise (MONRE, 2010). During the study period, SO_2 decreased significantly (by 62%), CO decreased by 22%, while TSP increased slightly by 2.83% and NO_2 decreased slightly by 7.10%. The sharp decrease in SO_2 and CO concentrations demonstrates the effectiveness of controlling emissions from industrial zones and improving vehicle engine technology (Dang and Trinh, 2022; Nguyen et al., 2025). However, TSP is trending slightly upward in 2024, reflecting a strong recovery in infrastructure construction and transportation activities after the pandemic (Xu et al., 2019; Zhang et al., 2022).

Simultaneously, meteorological factors also showed notable fluctuations during this period. Average temperature tended to increase slightly by 1.8% ($p<0.05$), while humidity increased by 5.1% ($p<0.05$). Notably, wind speed decreased significantly by -26.0% ($p<0.05$). This decrease in wind speed may reduce the dispersion of pollutants, contributing to the maintenance or increase of local pollutant concentrations, especially dust (Tian et al., 2024). Noise levels also increased slightly by 2.9% ($p<0.05$), indicating a strong correlation between increased economic activity, traffic, and physical environmental noise pollution (Goldberg et al., 2001; Pope III et al., 2002). These changes in meteorological factors need to be carefully considered when assessing air quality trends in Khanh Hoa. The standard deviation of TSP is relatively large compared to the annual average, implying the existence of short-term increases due to events (construction, increased traffic density during the tourist season, unfavorable dispersal conditions, or regional dust sources).

The statistical comparison of annual mean concentrations using the t-test showed that SO_2 and CO significantly decreased during the study period ($p<0.05$), while NO_2 remained relatively stable and TSP showed an increasing tendency in 2024.

3.1.2. Variation in the concentration of air quality parameters between months of the year

Figure 2 illustrates the monthly fluctuations of air quality parameters in four sub-regions within the study area from 2021 to 2024. CO and NO_2 exhibit an inverted "U-shaped" curve pattern, with the peak (high

concentration) in May and June each year, and gradually sloping towards the lowest points in January and December. This fluctuation is consistent across all four sub-regions, suggesting that this trend may be related to overall climatic conditions in the province rather than emission intensity or sub-regional climatic differences. Research by Pham et al. (2023) shows that the monthly temperature variation in Khanh Hoa Province observed from 1981 to 2020 follows a similar trend of an inverted "U-shaped" curve (temperature peaks in June and gradually decreases in both directions). This is in contrast to the U-shaped trend of wind speed observed at the Nha Trang station over the 30 years from 1986 to 2016 (Tu and Tran, 2018): Wind speeds are lowest in June and gradually increase towards January and December. As wind speeds increase, the dilution and dispersion of pollutants occur more quickly, helping to reduce local concentrations (Watcharavitoon et al., 2013). Conversely, low wind speeds result in stagnant atmospheric conditions, leading to pollution to accumulate, especially in urban areas with high traffic density (Dadhich et al., 2018; Watcharavitoon et al., 2013).

Table 1. Descriptive statistics (mean±standard deviation) of periodic observation data on meteorological parameters, noise levels, and air quality in Khanh Hoa Province (former) from 2021 to 2024

Parameters	Year				Change level [(a)]	QCVN 05:2023 (1h avg/annual avg)
	2021	2022	2023	2024		
Temp. (°C)	30.2±3.1	29.9±2.6	30.9±2.6	30.8±2.4	1.8%*	-
Humidity (%)	66.4±11.0	72.9±8.9	72.6±8.4	69.8±6.1	5.1%*	-
Pressure (hPa)	1,006.6±8.2	1007.5±7.7	1,007.9±8.2	1,007.8±9.1	0.12%	-
Wind speed (m/s)	1.1±0.93	1±0.68	0.83±0.54	0.81±0.58	-26.0%*	-
Noise level (dBA)	61.6±5.7	60.3±7.2	62.9±6.5	63.4±5.21	2.9%*	70 / - [(b)]
TSP (µg/Nm^3)	110.6±130.1	105.6±124.1	92.1±130.6	113.8±153.0	2.8%	300 / 100
SO_2 (µg/Nm^3)	18.8±2.1	18.5±2	16.1±5.4	7.1±2.4	-62.4%*	350 / 50
NO_2 (µg/Nm^3)	10.2±5.8	8.62±3.3	9.2±2.6	9.4±5.6	-7.1%	200 / 40
CO (µg/Nm^3)	2,704±1,222	2,069±724	1,714±321	2,092±350	-22.7%*	30,000 / -

Note: [(a)] Change level %: Indicates the relative rate of change between 2021 and 2024; *: The change between the two years tested was statistically significant ($p<0.05$). [(b)] QCVN 26:2010/BTNMT: National technical standard on noise (in normal areas, from 6-21 hours). QCVN 05:2023 is an abbreviation of QCVN 05:2023/BTNMT: Vietnam National technical standard on air quality.

Regarding SO_2 concentrations, significant changes were observed between the dry season (January-August) and the rainy season (September-December) in all four sub-regions. During the dry season, the average SO_2 concentration ranged from 15.65 to 16.49 µg/Nm^3, which was statistically significantly higher than during the rainy season (values ranging from 12.92 to 13.38 µg/Nm^3). The four rainy months in Khanh Hoa account for 75-80% of the province's total annual rainfall (Nguyen, 2003). Rain helps dissolve and remove dust particles as well as water-soluble air pollutants in water such as SO_2 (Nghiem et al., 2021), therefore, this process reduces the concentration of these pollutants compared to the dry season .

The monthly fluctuations of TSP concentration (Figure 2(d)) during the study period show a "U" shaped curve with the highest peak values in January (124.5 µg/Nm^3) at the beginning of the year and October (129.8 µg/Nm^3) near the end of the year. Interestingly, the lowest TSP values (the two troughs of the U) occurred in February (88.3 µg/Nm^3) and September (72.5 µg/Nm^3) - the months adjacent to the two peaks. This variation may be the result of a complex interaction between meteorological factors: rainfall, wind patterns, temperature, humidity, and continuous dust emissions from socio-economic activities. Increased rainfall during the rainy season likely helps remove suspended particles from the atmosphere, resulting in lower TSP concentrations. Higher humidity and frequent rainfall may also contribute to this decrease. However, this interpretation is based on monthly monitoring data and general seasonal trends, since detailed rainfall data such as intensity and duration were not available. Therefore, the effect of individual rainfall events on TSP concentrations could not be quantitatively evaluated. Although rain helps clean the air, high humidity after rain can cause small dust particles to clump together, forming larger particles that are more difficult to disperse in low wind conditions (Ali et al., 2026). October had the lowest average wind speed at the monitoring points in this

study, at 0.72 m/s, further reinforcing the above conclusion. In January, the low temperature (27.7°C - the lowest in 12 months) may contribute to temperature inversion conditions, creating a barrier that prevented pollutants from dispersing upwards, leading to a surge in concentration (Ho et al., 2025; Xu et al., 2019), at the same time, low wind speeds this month (reaching 0.87 m/s - the second lowest in the 12 months) can stagnant atmospheric conditions, causing pollution to accumulate, especially in urban areas with high traffic density (Dadhich et al., 2018; Watcharavitoon et al., 2013). To gain a more accurate picture, more continuous and detailed data are needed regarding rainfall intensity, duration, and other meteorological factors, as well as the activity of emission sources in the area.

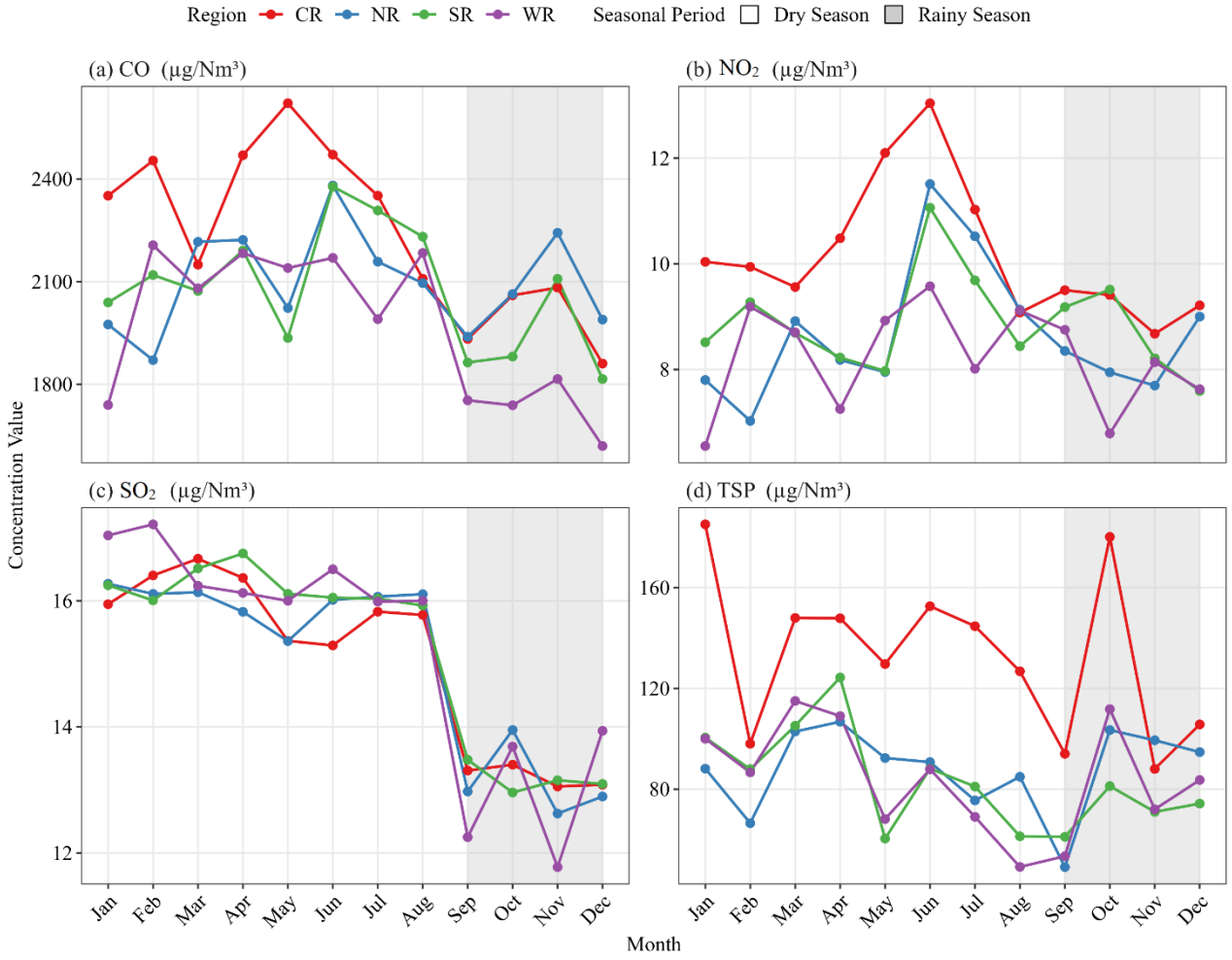


Figure 2. Monthly variations of the four key air quality parameters (TSP, SO_2, NO_2, CO) in the four sub-regions (NR, SR, WR, CR) of Khanh Hoa Province (former) from 2021-2024.

In terms of monthly spatial distribution, the Central (CR) zone generally had higher concentrations of TSP, CO, and NO_2 than the other areas at many times, especially for TSP: The Central zone consistently recorded the highest TSP concentrations, with an average TSP value of 129 µg/Nm^3 (exceeding the average annual TSP limit of 100 µg/Nm^3 according to the Vietnamese National Standard), while all three other sub-regions had values below 100 µg/Nm^3 (ranging from 83-88 µg/Nm^3) (Figure 2). This can be explained by the significantly higher population density and traffic volume in the central urban area compared to the surrounding areas (Lu et al., 2017; Lu et al., 2023). Conversely, the Northern (NR), Southern (SR), and Western (WR) regions have more stable air quality due to lower building density and larger open spaces. For SO_2, concentrations across these areas are relatively uniform and significantly lower than the standard, suggesting that SO_2 emissions may not be heavily related to urban emission sources.

3.1.3. Characteristics of seasonal variations in the concentration of air quality parameters throughout the year

The differences between the dry and rainy seasons (Figure 3) play a key role in understanding the local pollution dispersion mechanisms. The results show that the concentrations of most air pollutants are significantly higher in the dry season than in the rainy season ($p<0.05$). For example, in the CR, the TSP concentration in the dry season was 141.6 µg/Nm^3 compared to 116.9 µg/Nm^3 in the rainy season. Studies in Vietnam and the tropical regions also note that TSP concentrations are generally higher in the dry season and lower in the rainy season (Hien et al., 2002; Nguyen et al., 2024).

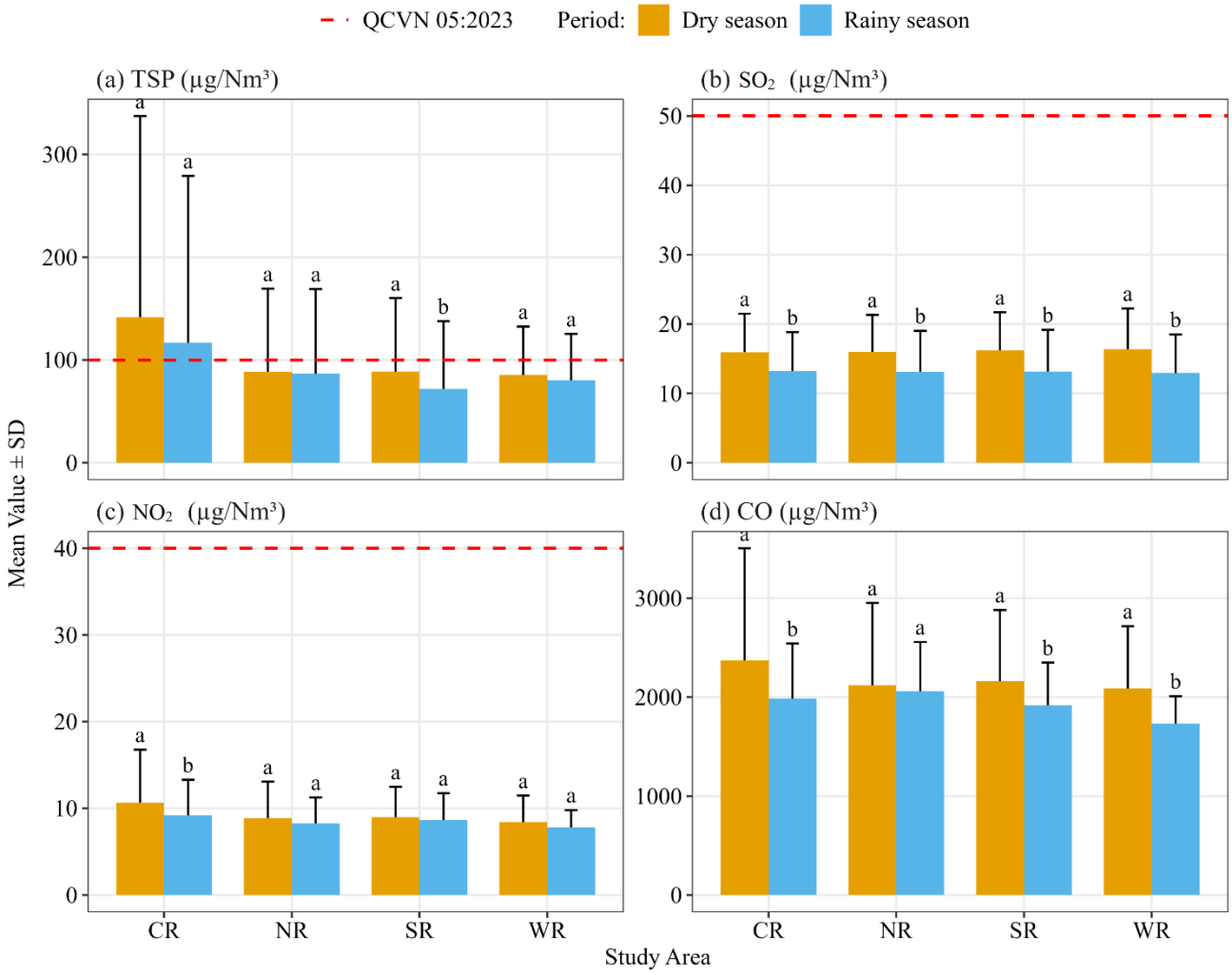


Figure 3. Seasonal changes of the four key air quality parameters (TSP, SO_2, NO_2, CO) in the four areas (NR, SR, WR, CR) of Khanh Hoa Province (former) from 2021-2024. (Note: error bars represent the standard deviation of the mean. Statistically significant differences ($p<0.05$) are indicated by the letters a, b)

This is consistent with the climate characteristics of Khanh Hoa, where the rainy season is concentrated in the last months of the year (usually from September to December) and the dry season is longer, with an average annual rainfall of about 2,000 mm in the North and gradually decreasing towards the South (Nguyen, 2003; Tu and Tran, 2018). Rainwater runoff is a crucial natural mechanism for cleaning the atmosphere, removing dust particles and dissolving air pollutants (Ali et al., 2026; Tian et al., 2024). Conversely, during the dry season, high temperatures, low humidity, and reduced wind speed create favorable conditions for the accumulation of suspended particulate matter and for chemical reactions leading to secondary pollutant formation. Heavy and very heavy rainfall, often concentrated in October and November, plays a crucial role in cleaning the air, significantly improving air quality during these periods (Nguyen et al., 2013). It is noteworthy that TSP is a pollutant with concentrations

exceeding the average annual standard in both the rainy and dry seasons. However, this excess is only observed in the central area**,** due to high traffic and construction density combined with rapid urbanization. Although the dry season values are higher than the rainy season, there is no statistically significant difference ($p>0.05$), indicating that the mechanism of pollutant accumulation from TSP emission sources is quite high in the Central area, leading to a relatively weak influence of meteorological factors on concentration reduction. Therefore, pollution control solutions at the source for TSP are needed in the central urban areas of the study region.

3.2 Major air pollutants

Analysis of the dominant pollutant (Figure 4) shows that TSP is the primary pollutant in most cases. Across the province, TSP accounted for 96% of samples throughout the year; seasonally, TSP remained dominant (93% in the rainy season and 97% in the dry season), reaching as high as 98% in the central area during the dry season. CO was the second most dominant pollutant, but with a small percentage (4.2% of the province), while SO_2 and NO_2 were almost non-dominant, with values of 0.15% and 0.00% respectively. The monthly distribution of pollutant variations (Figure 5) also shows this, with TSP being the dominant pollutant in all months from 2021-2024, except for September 2021, when CO was the dominant pollutant. Among particulate pollutants, TSP was the only parameter consistently monitored across all monitoring sites during the study period, allowing for a spatially and temporally comparable analysis. However, $PM_{2.5}$ and PM_{10} were not included due to data limitations, although these finer particles are more closely associated with adverse health effects, far surpassing gaseous pollutants such as SO_2 or NO_2 (Xu et al., 2019; Zhang et al., 2022). This result implies that dust control measures (traffic, construction, secondary dust-emitting activities) play a crucial role in improving AQI.

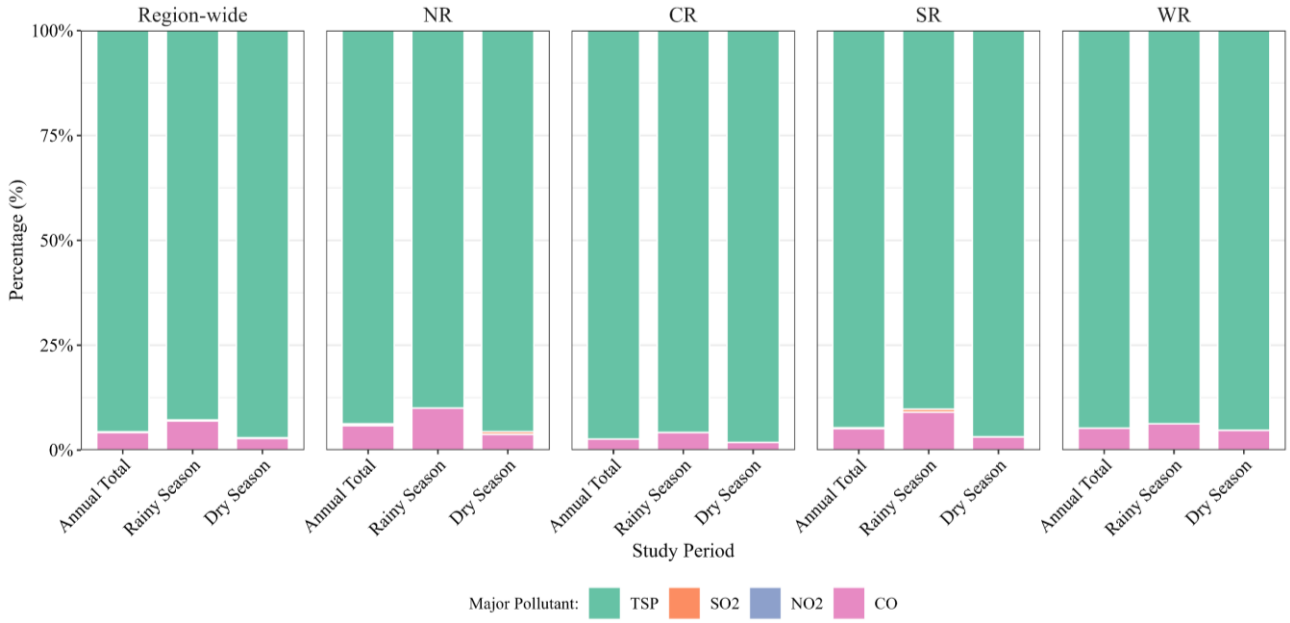


Figure 4. Percentage of major pollutants by season and year in different zones and across the entire Khanh Hoa Province (Note: The percentage of dominant pollutants was determined based on the AQI value of the representative pollutant for each observation. Specifically, for each sample, the AQI was defined by the highest sub-index among the four pollutants (TSP, SO_2, NO_2, and CO), and the pollutant with the highest AQI was considered the dominant pollutant. A total of 1,344 observations were analyzed (28 monitoring sites × 12 months × 4 years). The percentage of each pollutant was calculated as the frequency at which it was identified as the dominant pollutant divided by the total number of observations.)

3.3 The spatial and temporal variations of the AQI

The AQI provides an overview of air safety levels for public health (Figure 6, Figure 7). Analysis of the IDW interpolation map of AQI values (Figure 6) shows a clear spatial and temporal variation in air quality in Khanh Hoa. Overall, most of Khanh Hoa Province maintained “Good” air quality (Green, AQI 0-50) throughout the 2021-2024 study period, particularly in the NR, SR, and part of the WR areas. This reflects the relatively clean natural environment and low density of polluting activities in these regions.



Figure 5. Monthly fluctuations of major pollutants across sub-regions from 2021-2024

However, the Central (C) and parts of the Western areas (the central part of the Western area may be affected by high concentrations of pollutants, especially total particulate matter in the Central area, which can be dispersed by the Southeast monsoon in summer) frequently show areas with "Moderate" (AQI: 51-100) and sometimes "Unhealthy for Sensitive Groups" (AQI: 101-150) air quality. This is particularly evident in the annual maps (Figure 6(a-d)) and the dry season maps (Figure 6(e-h)). The Central area, with its high population density and traffic and construction activity, is a hotspot for air pollution. The appearance of yellow/orange spots here indicates that the concentrations of pollutants, especially TSP, frequently exceed safe levels for sensitive groups (Lu et al., 2017; Lu et al., 2023).

The differences between the dry and rainy seasons are also clearly shown in Figure 6. During the dry season (Figure 6(e-h)), the area of yellow and orange zones tends to expand, especially in the central area and some points in the west. This is consistent with the previous analysis of dry season meteorological conditions (weak winds, little rain) creating conditions for pollutant accumulation. Conversely, during the rainy season (Figure 6(i-l)), the maps are mostly green, indicating that the washout effect of rain has significantly improved air quality throughout the province. Nevertheless, there are still localized areas and times (such as the central region) that appear yellow even during the rainy season, indicating that emission sources remain active and need to be controlled. Particularly during the 2024 rainy season, the percentage of "Moderate" AQI increased to 40% and "Good" decreased to 57%, suggesting that the AQI was more adversely affected during this period compared to previous years, possibly related to the economic recovery process after the Covid-19 pandemic.

Overall, although air quality was mostly "Good" (57%-85% according to Figure 7), the occurrence of "Unhealthy", "Very Unhealthy", and even "Hazardous" samples (especially during the dry seasons of 2022, 2023, and 2024) is a warning sign. These extreme AQI values were mainly due to local spikes in TSP concentrations. This indicates that although the province's baseline air quality is quite good, short-term pollution events still occur and may pose health risks to sensitive groups (Goldberg et al., 2001; WHO, 2018). AQI maps provide a visual overview of areas requiring priority monitoring and air

quality management. Additionally, for a more accurate picture, it's necessary to analyze topographic and meteorological factors in air pollution dispersion models to more accurately assess the spread of pollutants between areas.

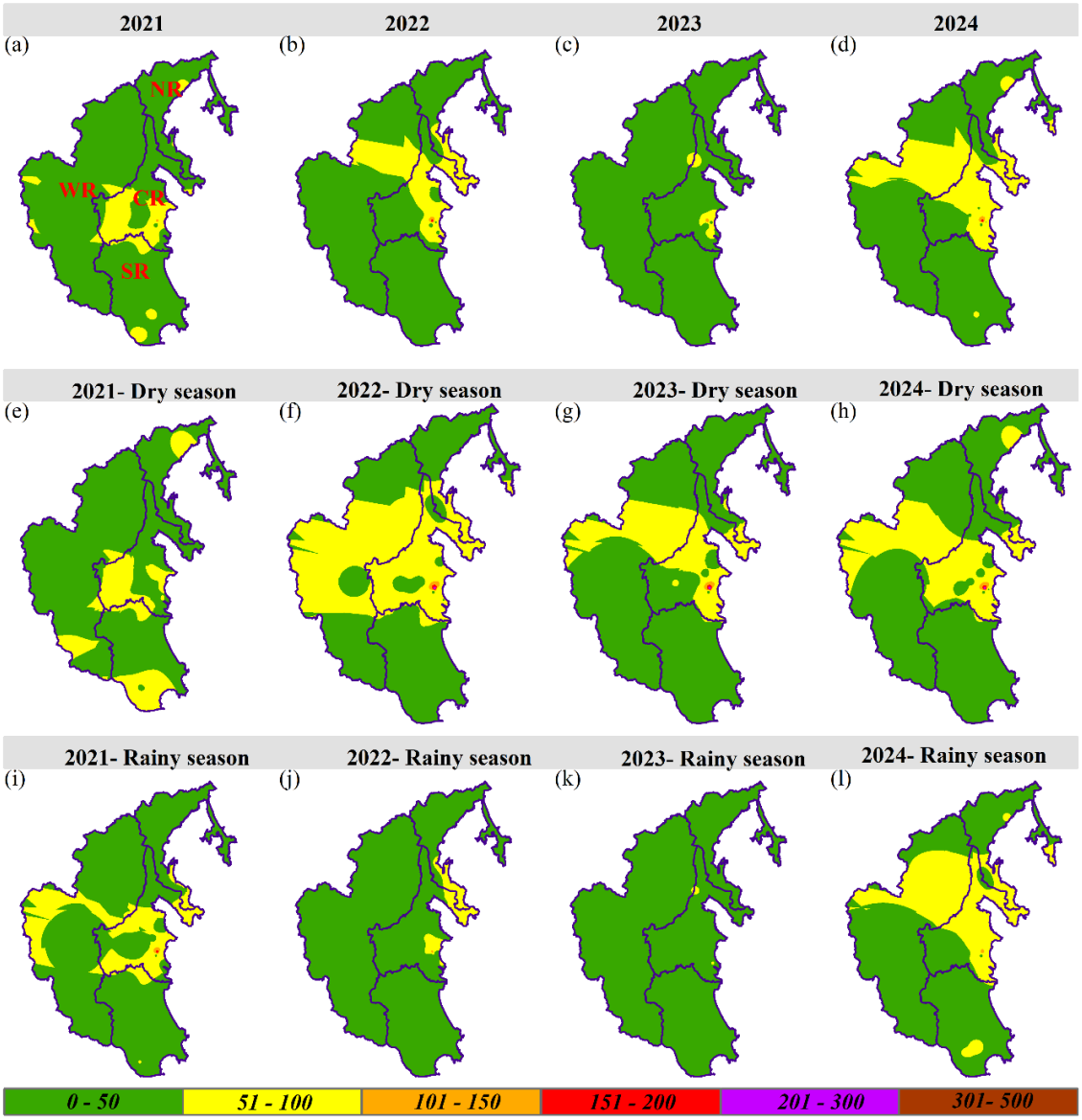


Figure 6. Spatial distribution by year and season of the AQI for the period 2021-2024 in 4 sub-regions of Khanh Hoa Province (former)

3.4. The correlation between meteorological factors, noise levels, air pollutants and AQI

Pearson correlation analysis (Table 2) was performed to quantify the linear relationship between meteorological factors, noise levels, and air quality parameters, and to provide a complex and multi-dimensional picture of air pollution dynamics in Khanh Hoa.

One of the key findings is the clear role of humidity in improving air quality. In most sub-regions, particularly in the SR during the dry season, humidity showed a statistically significant inverse correlation with TSP ($r=-0.202$; $p<0.001$), NO_2 ($r=-0.230$; $p<0.001$), and especially with CO (moderately inverse correlation, $r=-0.311$; $p<0.001$). This confirms the "washout" and wet deposition mechanism, where airborne water vapor particles help remove particulate matter and dissolve air pollutants, a mechanism widely documented in air pollution studies (Ali et al., 2026; Tian et al., 2024). The inverse correlation between wind speed and AQI in the NR ($r=-0.164$; $p<0.05$) during the dry season also indicates the positive role of wind in dispersing and diluting pollutants, improving overall air quality.

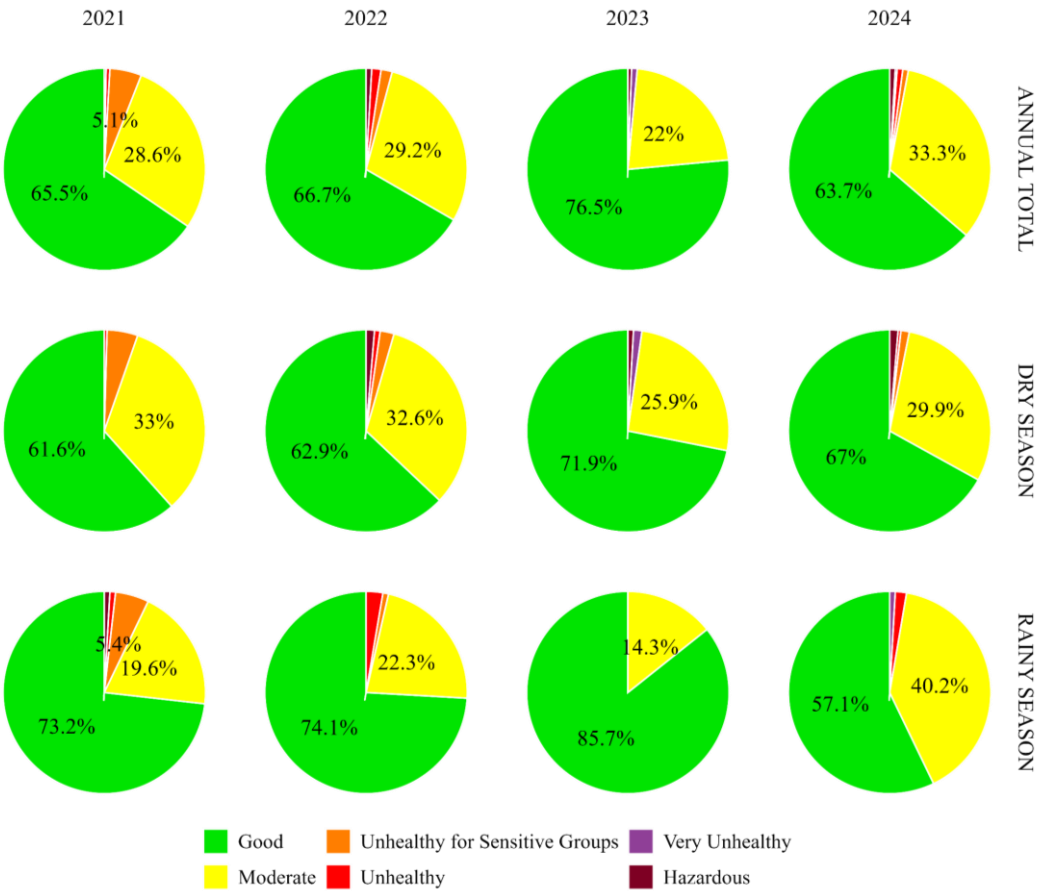


Figure 7. Percentage rates by year and season for AQI classifications in Khanh Hoa Province (former) during the period 2021-2024

In the Central area, where urban activities are concentrated, a positive correlation with high statistical significance was found between noise levels and traffic-specific pollutants such as TSP ($r=0.193$; $p<0.001$), NO_2 ($r=0.276$; $p<0.001$), and CO ($r=0.111$; $p<0.05$) during the dry season. The higher TSP concentrations and noise levels observed in the Central region are likely associated with intensive traffic activities, urban construction, and high population density. This interpretation is supported by the strong positive correlations among noise, TSP, NO_2, and CO, as well as the region's urban characteristics. However, no quantitative emission inventory (e.g., vehicle counts, traffic flow, or construction activity data) was available. Therefore, source attribution was based on spatial patterns and correlation analysis, and the relative contributions of emission sources could not be precisely determined (Goldberg et al., 2001; Pope III et al., 2002). This finding underscores that solutions aimed at reducing traffic congestion not only improve air quality but also positively affect the urban acoustic environment.

The study found several "unusual" correlations that can be explained by scientific mechanisms. Most notably, there was a weak positive correlation between wind speed and AQI in the southern region during the dry season ($r=0.129$; $p<0.05$). This contrasts with the weak negative correlation between wind speed and AQI in the northern region ($r=-0.164$; $p<0.05$), as mentioned above. This may be related to the specific wind patterns of the two study areas: In the northern part of the province during the dry season, there is a distinctive topographic wind pattern called the Tu Bong wind, which blows strongly and continuously from the west towards the Van Phong Bay Area (Nguyen, 2003). This wind pattern may enhance the dispersion and dilution of pollutants, especially the concentration of TSP (an indicator characterizing the AQI value in the study area). Meanwhile, the southern region is strongly influenced by the southeast monsoon during the dry season (Nguyen, 2003). Instead of dispersing, strong winds in dry conditions can increase pollution. This is explained by the phenomenon of "dust entrainment", where wind carries dust particles from dry land surfaces, roads, and construction sites into the air-a mechanism that has been observed in studies in other arid regions (Zhang et al., 2022).

Table 2. Correlation analysis between meteorological factors, noise levels, and air quality parameters in different zones within Khanh Hoa Province (former)

Parameters	Dry season					Rainy season				
	TSP	SO_2	NO_2	CO	AQI	TSP	SO_2	NO_2	CO	AQI
Northern										
Temp.	-0.068	-0.046	0.290***	0.224**	-0.078	-0.038	0.054	-0.044	-0.023	-0.074
Humidity	0.034	-0.196*	-0.137	-0.251**	0.038	0.143	0.021	0.189	0.019	0.161
Pressure	0.059	-0.142	-0.136	-0.124	0.079	-0.089	-0.077	0.008	-0.088	-0.088
Wind speed	-0.134	0.114	0.023	0.093	-0.164*	-0.072	0.313**	0.081	0.208	-0.054
Noise level	0.093	-0.204**	0.144	-0.007	0.122	0.084	-0.086	0.063	-0.063	0.093
Southern										
Temp.	-0.089	-0.100	0.185**	0.065	-0.09	0.104	-0.124	0.184*	-0.163	0.142
Humidity	-0.202***	-0.049	-0.230***	-0.311***	-0.189**	-0.131	0.204*	-0.150	0.072	-0.189*
Pressure	0.025	-0.21***	-0.153**	-0.153**	0.015	-0.034	-0.061	0.011	0.004	-0.02
Wind speed	0.112	0.112	0.027	-0.022	0.129*	-0.007	0.310***	-0.178*	0.004	0.009
Noise level	0.098	-0.148*	0.103	-0.013	0.112	-0.083	-0.169*	0.047	-0.178*	-0.019
Western										
Temp.	-0.155	-0.058	0.198	0.173	-0.171	-0.084	-0.159	0.100	0.087	-0.051
Humidity	-0.198	0.011	0.063	-0.185	-0.2	-0.193	-0.001	-0.081	-0.254	-0.188
Pressure	0.026	0.044	0.085	0.224	0.108	0.069	-0.024	0.024	-0.127	0.071
Wind speed	0.076	0.13	0.157	0.164	0.069	0.193	0.148	-0.269	0.210	0.234
Noise level	0.083	0.073	0.064	0.103	0.113	-0.042	-0.073	-0.046	-0.063	0.026
Central										
Temp.	-0.008	-0.030	-0.011	-0.106*	-0.004	0.133	-0.206**	0.032	0.011	0.135
Humidity	0.041	-0.180***	0.027	-0.104*	0.043	-0.069	0.295***	-0.028	0.049	-0.080
Pressure	-0.003	-0.109*	-0.047	-0.003	-0.003	-0.109	0.051	-0.024	-0.034	-0.110
Wind speed	0.059	0.001	-0.081	-0.034	0.056	-0.062	0.105	-0.042	0.069	-0.065
Noise level	0.193***	-0.155**	0.276***	0.111*	0.199***	0.145*	0.010	0.275***	0.151*	0.156*

Note: *, **, *** indicate statistically significant correlations at the 0.05, 0.01, and 0.001 levels (two-tailed test), respectively. Pearson correlation analysis was conducted using monthly monitoring observations. For each monitoring site, dry season data included 32 observations (8 months × 4 years), while rainy season data included 16 observations (4 months × 4 years). The total sample size (n) varied by sub-region according to the number of monitoring points.

Another noteworthy phenomenon is the average positive correlation between wind speed and SO_2 in the Northern ($r=0.313$; $p<0.01$) and Southern ($r=0.310$; $p<0.001$) regions during the rainy season. This contradicts the usual dispersing role of wind. Elevated SO_2 concentrations observed in coastal areas near Van Phong Bay and Cam Ranh Bay may be associated with maritime transportation activities and port operations, as well as the potential transport of ship-related emissions under the influence of the Northeast monsoon during the rainy season. This interpretation is supported by the proximity of monitoring sites to major port areas and the prevailing seasonal wind direction, which may facilitate the transport of coastal air masses toward inland areas. However, the present study did not include atmospheric dispersion modeling, ship emission inventories, or source apportionment techniques to directly verify transport pathways or quantify the contribution of maritime emissions (Jang et al., 2017).

A notable finding is the absence of statistically significant correlations in the Western (WR) area in both seasons. This is not a data defect but rather a significant finding: it suggests that this area has clean, stable air quality and is less affected by major emission sources and meteorological fluctuations. This can be considered an important "background area" for comparing and evaluating pollution levels in other areas of Khanh Hoa Province (Lu et al., 2017). This interpretation is consistent with the actual conditions in the Western area, which is the most mountainous and underdeveloped area of the province (Khanh Hoa PPC, 2023).

4. CONCLUSION

In-depth research on the spatiotemporal characteristics of air quality in Khanh Hoa Province during the period 2021-2024 has yielded important conclusions. Although the concentrations of air pollutants such as SO_2, NO_2, and CO showed significant improvement, reflecting the effectiveness of emission control measures, TSP pollution remains a considerable challenge, especially with the increase in concentrations observed in 2024 after the Covid-19 pandemic. The dominance of TSP in the study area indicates not only an environmental concern but also a significant public health risk, particularly for urban residents frequently exposed to traffic emissions and construction dust. The spatial and temporal differentiation of pollution is evident, with the central area (Nha Trang and surrounding areas) emerging as a TSP hotspot. Seasonal analysis also indicates that the dry season is more sensitive to pollution due to stagnant atmospheric conditions and dust entrainment, while the rainy season plays a crucial role in improving air quality through wet deposition mechanisms. Meteorological factors such as humidity and wind speed were identified as key elements in the dilution and removal of pollutants. In particular, the strong correlation between noise pollution and dust/emission concentrations in urban areas confirms the dominant role of traffic and construction activities as major emission sources. From a policy perspective, air quality management in former Khanh Hoa Province should prioritize TSP control, especially in the Central region. Key actions include dust suppression, stricter emission control, and cleaner transport. Enhanced monitoring in the dry season and GIS-based AQI mapping can support targeted interventions, while the Western region can serve as a background reference area. These findings support sustainable air quality management in rapidly urbanizing coastal areas. The study has several limitations. It only analyzed four pollutants (TSP, SO_2, NO_2, and CO), excluding finer particles like $PM_{2.5}$ and PM_{10}. The use of monthly data limits the ability to capture short-term pollution events. The IDW method for AQI mapping does not fully reflect complex dispersion processes. Additionally, key factors such as traffic intensity, emission inventories, and detailed rainfall data were not included. A limitation of the present trend analysis is that the study focused on interannual mean comparison using the t-test rather than formal monotonic trend detection methods such as the Mann-Kendall test and Sen's slope estimator. Due to the relatively short monitoring period (2021-2024) and periodic monthly observations, the current approach was considered suitable for evaluating short-term annual differences. Future studies with longer continuous datasets should apply more robust non-parametric trend analysis methods to strengthen long-term air quality assessment. Based on these findings, the study recommends prioritizing dust control solutions at the source in construction and traffic activities in the Central region. Furthermore, subsequent research should focus on analyzing fine particulate matter ($PM_{2.5,}$ PM_{10}) together with health risk assessment and applying advanced dispersion models to predict air quality trends more accurately in the context of climate change. Future studies should also apply back-trajectory models such as HYSPLIT, together with ship emission inventories and source apportionment approaches, to better quantify the contribution of maritime emissions to coastal air quality. In addition, incorporating emission inventories and source apportionment techniques would improve the accuracy of pollution source identification and support more targeted air quality management.

ACKNOWLEDGEMENTS

The authors would like to express sincere gratitude to the Department of Natural Resources and Environment of Khanh Hoa Province (former) for providing data and support that contributed to the completion of this study.

AUTHOR CONTRIBUTIONS

Conceptualization, LV.T., H.M.D.; Methodology, LV.T., H.M.D.; Data curation, LV.T.; Writing-review draft preparation, LV.T.; Writing-original and editing, H.M.D.; All authors have read and agreed to the published version of the manuscript.

DECLARATION OF CONFLICT OF INTEREST

The authors declare that this article is the author's own research work, has not been published anywhere else, is not copied from previous research, and is not subject to any conflict of interest.

REFERENCES

Ali D, Singh M, Khan AA, Vidyarthi AK, Ahmed S. Impact of meteorological drivers on air quality index: A case study from Delhi. Environmental Pollution 2026;388:Article No. 127324.

Alsowaidan S, Al-Hurban A, Alsaber A, Anbar A. Assessment of seasonal variations in the air quality index (2019-2022) in Al-Jahra city, Kuwait. Kuwait Journal of Science 2024; 51(4):Article No. 100280.

Dadhich AP, Goyal R, Dadhich PN. Assessment of spatio-temporal variations in air quality of Jaipur city, Rajasthan,

India. The Egyptian Journal of Remote Sensing Space Science 2018;21(2):173-81.

Dang HAH, Trinh TA. The beneficial impacts of COVID-19 lockdowns on air pollution: evidence from Vietnam. The Journal of Development Studies 2022;58(10):1917-33.

Dang LKT, Vu HV. Air quality prediction in Hanoi using a deep learning approach. Science on Natural Resources and Environment 2024;54:172-9.

Department of Natural Resources and Environment of Khanh Hoa Province (DONRE Khanh Hoa). Report of Environmental Quality Monitoring Results in Khanh Hoa Province Monitoring Area for the Years 2021, 2022, 2023, and 2024. DONRE Khanh Hoa; 2025.

Goldberg MS, Burnett RT, Bailar JC, Tamblyn R, Ernst P, Flegel K, et al. Identification of persons with cardiorespiratory conditions who are at risk of dying from the acute effects of ambient air particles. Environmental Health Perspectives 2001;109(Suppl 4):487-94.

Hien P, Bac V, Tham H, Nhan D, Vinh L. Influence of meteorological conditions on $PM_{2.5}$ and $PM_{2.5-10}$ concentrations during the monsoon season in Hanoi, Vietnam. Atmospheric Environment 2002;36(21):3473-84.

Ho QB, Vu K, Nguyen HD, Nguyen T, Nguyen H, Do L, et al. Assessment of air quality and health impact in Hanoi (Vietnam) due to traffic emission—Seasonal analysis and traffic emission reduction scenarios. Atmosphere 2025;16(11):Article No. 1301.

Jang E, Do W, Park G, Kim M, Yoo E. Spatial and temporal variation of urban air pollutants and their concentrations in relation to meteorological conditions at four sites in Busan, South Korea. Atmospheric Pollution Research 2017;8(1): 89-100.

Khanh Hoa Provincial People's Committee (Khanh Hoa PPC). Report on the Khanh Hoa Provincial Planning for the Period 2021-2030, with a Vision to 2050. Khanh Hoa PPC; 2023.

Lang TT, Thao TQ, Hien NT, Van Trinh TT, Huy NN. Environmental challenges and air pollution in Bac Lieu, Vietnam: assessing sources and impacts. Journal of Umm Al-Qura University for Applied Sciences 2025;11:169-84.

Li L, Qian J, Ou CQ, Zhou YX, Guo C, Guo Y. Spatial and temporal analysis of Air Pollution Index and its timescale-dependent relationship with meteorological factors in Guangzhou, China, 2001-2011. Environmental Pollution 2014;190:75-81.

Lu D, Xu J, Yang D, Zhao J. Spatio-temporal variation and influence factors of $PM_{2.5}$ concentrations in China from 1998 to 2014. Atmospheric Pollution Research 2017;8(6):1151-9.

Lu F, Yuan Y, Hong F, Hao L. Spatiotemporal variations and trends of air quality in major cities in Guizhou. Frontiers in Environmental Science 2023;11:Article No. 1254390.

Makinde P, Idowu A, Pokauh E, Priscilla A. Urban air pollution: Sources, impacts, and sustainable mitigation strategies for a cleaner future. World Journal of Advanced Research and Reviews 2023;20(01):1298-313.

Ministry of Natural Resources and Environment (MONRE). QCVN 05:2023/BTNMT - National Technical Regulation on Air Quality. Ha Noi: MONRE; 2023.

Ministry of Natural Resources and Environment (MONRE). QCVN 26:2010/BTNMT - National Technical Regulation on Noise. Ha Noi: MONRE; 2010.

Nghiem T-D, Mac D-H, Nguyen A-D, Le NC. An integrated approach for analyzing air quality monitoring data: A case study in Hanoi, Vietnam. Air Quality, Atmosphere Health 2021;14(1):7-18.

Nguyen CD. Climate assessment of Khanh Hoa Province. Journal of Hydro-Meteorology 2003;512:1-7.

Nguyen GTH, La LT, Hoang-Cong H, Le AH. An exploration of meteorological effects on $PM_{2.5}$ air quality in several provinces and cities in Vietnam. Journal of Environmental Sciences 2024;145:139-51.

Nguyen TH, Hung NT, Nagashima T, Lam YF, Doan Q-V, Kurokawa J, et al. Development of current and future high-resolution gridded emission inventory of anthropogenic air pollutants for urban air quality studies in Hanoi, Vietnam. Urban Climate 2022;46:Article No. 101334.

Nguyen VK, Tong TP, Do TL, Tran DA. Heavy rainfall in Khanh Hoa province - causes and frequency. Journal of Hydro-Meteorology 2013;635:1-8.

Nguyen XT, Le TT, Nguyen KH, Nguyen TTT, Luu TPK. Assessing air pollution and seasonal variations in Dong Nai Province, Vietnam: A geospatial analysis of key air quality parameters (2022-2023). Urban Climate 2025;61:Article No. 102475.

Pham MT, Le MLT, Nguyen HT, Tran HTT. Research to assess the trend and degree of extreme temperature change in Khanh Hoa province in the period 1981-2020. Journal of Hydrometeorology 2023;750(1):53-66.

Pham NQ, Nguyen GT. Assessing air quality using multivariate statistical approaches. Civil Engineering Journal 2024; 10(2):521-33.

Pope III CA, Burnett RT, Thun MJ, Calle EE, Krewski D, Ito K, et al. Lung cancer, cardiopulmonary mortality, and long-term exposure to fine particulate air pollution. Jama 2002;287(9):1132-41.

Rad AK, Shamshiri RR, Naghipour A, Razmi S-O, Shariati M, Golkar F, et al. Machine learning for determining interactions between air pollutants and environmental parameters in three cities of Iran. Sustainability 2022;14(13):Article No. 8027.

Rakholia R, Le Q, Ho BQ, Vu K, Carbajo RS. Multi-output machine learning model for regional air pollution forecasting in Ho Chi Minh City, Vietnam. Environment International 2023;173:Article No. 107848.

Sharma D, Mauzerall D. Analysis of air pollution data in India between 2015 and 2019. Aerosol Air Quality Research 2022;22(2):Article No. 210204.

Shrestha S, Kazama F. Assessment of surface water quality using multivariate statistical techniques: A case study of the Fuji river basin, Japan. Environmental Modelling Software 2007;22(4):464-75.

Tian X, Zhang C, Liu H, Zhang B, Lu C, Jiao P, et al. Research on air quality in response to meteorological factors based on the informer model. Sustainability 2024;16(16):Article No. 6794.

Tu TN, Tran VS. Study on the wind characteristics in the southern central region. Journal of Hydro-Meteorology 2018(691): 50-9.

Vietnam Environment Administration (VEA). Decision No. 1459/QD-TCMT on the Issuance of Technical Guidelines for Calculating and Publishing the Vietnam Air Quality Index (VN_AQI). Ha Noi: VEA; 2019.

Vorapracha P, Phonprasert P, Khanaruksombat S, Pijarn N. A comparison of spatial interpolation methods for predicting concentrations of particle pollution (PM_{10}). International Journal of Chemical, Environmental Biological Sciences 2015;3(4):302-6.

Watcharavitoon P, Chio CP, Chan CC. Temporal and spatial variations in ambient air quality during 1996-2009 in Bangkok, Thailand. Aerosol Air Quality Research 2013;13(6):1741-54.

World Health Organization (WHO). Air pollution [Internet]. 2024 [cited 2026 Feb 10]. Available from: https://www.who.int/health-topics/air-pollution#tab=tab_1.

World Health Organization (WHO). Air Pollution and Child Health: Prescribing Clean Air Summary. Geneva, Switzerland; 2018.

Xia X, Du Z, Liu T, Xu K, Yuan C. The influence of meteorological factors and air pollution on acute cardiovascular and cerebrovascular events in Western Guizhou. Scientific Reports 2025;15(1):Article No. 22676.

Xu W, Tian Y, Liu Y, Zhao B, Liu Y, Zhang X. Understanding the spatial-temporal patterns and influential factors on air quality index: The case of North China. International Journal of Environmental Research Public Health 2019;16(16):Article No. 2820.

Yan X, Wang J, Wu F, Bai J, Zhang X, Li G, et al. Spatial and temporal variation characteristics of air pollutants in coastal areas of China: From satellite perspective. Remote Sensing 2025;17(11):Article No. 1861.

Zaib S, Lu J, Bilal M. Spatio-temporal characteristics of air quality index (AQI) over Northwest China. Atmosphere 2022;13(3):Article No. 375.

Zhang J-B, Rong Y-M, Yin Q-F, Zhang P, Zhao L-R, Chen C-L. Spatiotemporal variation and influencing factors of TSP and anions in coastal atmosphere of Zhanjiang City, China. International Journal of Environmental Research and Public Health 2022;19(4):Article No. 2030.

Environment and Natural Resources Journal

Volume 24
Issue 6
2026

Identifying Geospatial Priority Hotspots of Tourism Sustainability Risk using a Destination Sustainability Index (DSI) Devised from Online Tourist Dissatisfaction and Getis-Ord G_i^* Statistics

Tobthong Chancharoen[1], Asamaporn Sitthi[2], Parinya Nakpathom[3], and Narong Pleerux[1*]

[1]*Faculty of Humanities and Social Sciences, Burapha University, Thailand*
[2]*Faculty of Social Sciences, Srinakharinwirot University, Thailand*
[3]*International College, Burapha University, Thailand*

ARTICLE INFO

Received: 27 Nov 2025
Received in revised: 26 Jun 2026
Accepted: 30 Jun 2026
Published online: 3 Sep 2026
DOI: 10.32526/ennrj/24/20250343

Keywords:
Destination Sustainability Index (DSI)/ Hotspot analysis (G_i^*)/ Sentiment analysis/ Spatial clustering/ Tourist dissatisfaction data

*** Corresponding author:**
E-mail: narong_p@go.buu.ac.th

ABSTRACT

Managing tourism sustainability effectively requires identifying specific localized risks, which remains a significant challenge for many destinations. This research aims to identify priority hotspots of unsustainability in marine and beach tourism destinations in Eastern Thailand by employing geospatial analysis and tourist-perceived data to support targeted policy decisions. Drawing from 11,047 geotagged Tripadvisor reviews as a primary data source, the methodology commenced with processing these reviews using a high-precision transformer-based (BERT) sentiment analysis model, achieving 87% precision in the negative class. This was followed by N-gram analysis to extract specific problem phrases, which were used to construct the Destination Sustainability Index (DSI) across three main dimensions: Environmental (DSIEnv), Congestion/Access (DSIAcc), and Service/Value (DSISrv). The DSI was then subjected to hotspot analysis (Getis-Ord Gi*) to confirm the statistical significance of spatial clustering. Results confirm that Environmental problems (rubbish/dirty) and Congestion/Access issues (crowded, boat) are the most frequent concerns. The analysis clearly demonstrated that tourism dissatisfaction is not randomly distributed but localized in statistically significant spatial locations. Priority hotspots showing overlapping risks in Chonburi Province require immediate intervention, while the successful management of the Koh Kood cluster offers a blueprint for sustainable development.

HIGHLIGHTS

This study develops the Destination Sustainability Index (DSI) using tourist dissatisfaction data from 11, 047negative online reviews. Hotspot analysis (G_i^*) was then employed to map spatial risks. Key findings confirm that the highest risk hotspots overlap in Congestion/Access and Service/Value dimensions within the Chonburi cluster (Koh Larn, Si Racha). These areas require urgent structural investment and the implementation of Carrying Capacity limits. Conversely, the Koh Kood cluster (Trat) is the most robust coldspot across multiple dimensions and should be established as the best practice model. The research demonstrates the effectiveness of using tourist dissatisfaction data for DSI and G_i^* in precise policy prioritization.

1. INTRODUCTION

As a cornerstone of Thailand's economy, tourism contributes approximately 17% to the national GDP (MOTS, 2023), with marine and beach attractions in the Eastern region remaining primary destinations (TAT, 2024). However, this tourism-driven economic growth has triggered rapid environmental deterioration, including increased waste generation, pollution, and congestion (MOTS, 2023), issues now exacerbated by global climate change (TAT, 2024). Implementing sustainable resource management is thus an urgent necessity aligned with Thailand's National Strategy (MOTS, 2023), requiring empirical evidence for targeted policy decisions.

In the digital era (Cui and He, 2019), TripAdvisor reviews (Jeacle and Carter, 2011) serve as high-volume Big Data reflecting authentic tourist perspectives (Li et al., 2017; Alfred et al., 2023). Integrating sentiment analysis of these reviews

Citation: Chancharoen T, Sitthi A, Nakpathom P, Pleerux N. Identifying geospatial priority hotspots of tourism sustainability risk using a Destination Sustainability Index (DSI) devised from online tourist dissatisfaction and Getis-Ord G_i^* statistics. Environ. Nat. Resour. J. 2026;24(6):689-700. (https://doi.org/10.32526/ennrj/24/20250343)

(Valdivia et al., 2017) with geospatial techniques (Jabalameli et al., 2022) enables a deeper understanding of destination dynamics. While most previous studies have focused primarily on positive indicators, (Singgalen et al., 2024; Charfaoui and Mussard, 2024) this approach often overlooks the granular, spatial manifestations of systemic failure (Gadekar, 2024). Therefore, a significant research gap exists in utilizing negative sentiments to map spatial problem density through advance language models like BERT (Yuan, 2024; Xi et al., 2024).

Consequently, this research employs N-gram analysis (Ojo et al., 2021) and a novel Destination Sustainability Index (DSI) derived from geo-locatable negative feedback to identify and map "Priority Hotspots." This methodology aims to categorize problems into Environmental, Congestion/Access, and Service/Value dimensions, providing empirical geospatial evidence for government agencies to prioritize resource restoration and management interventions.

2. METHODOLOGY

2.1 Study area

Focusing on the coastal and marine attractions of Eastern Thailand, this study encompasses the strategic provinces of Chonburi, Rayong, Chanthaburi, and Trat (Figure 1). This region serves as a pivotal economic engine for the national tourism sector, primarily driven by intensive maritime and beach-based activities (MOTS, 2023). However, the high volume of tourism has exerted substantial pressure on fragile ecosystems (Baltranaite et al., 2025), evidenced by resource degradation from uncontrolled tourism expansion (ONEP, 2024), critical marine waste challenges (Abirami, 2024), and arrivals that frequently exceed carrying capacity limits (Yusoh et al., 2021). Consequently, this area provides a representative case study for applying geospatial analysis to identify spatial problem density and assess marine resource degradation under high-intensity tourism pressure.

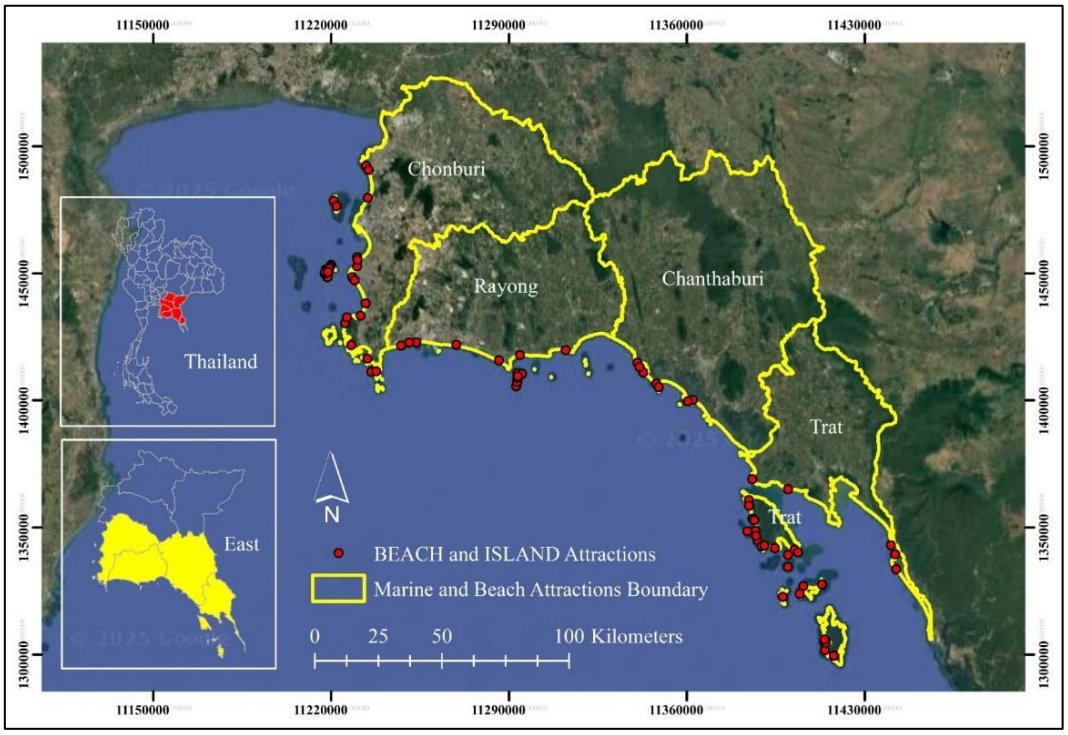


Figure 1. Study area and distribution of marine and beach attractions in Eastern Thailand

2.2 Data collection and preprocessing

2.2.1 Data source and scope

International tourist reviews of marine and beach attractions in Eastern Thailand were retrieved from TripAdvisor (Valdivia et al., 2017) spanning a ten-year period from 2014 to 2023. The dataset includes 11,047 reviews categorized as BEACH and ISLAND attractions (DOT, 2018). Data acquisition was performed through web scraping using Python, specifically leveraging the BeautifulSoup, Pandas, and Selenium libraries (Muthukadan, 2024).

2.2.2 Text cleaning and normalization

The raw review data underwent a systematic multi-step cleaning process to isolate essential features for sentiment analysis (Ramadhani et al., 2021). This included converting text to lowercase and removing punctuation, URLs, numbers, and special characters. Stop words were eliminated; however, negation terms such as "no" and "not" were retained to maintain the contextual integrity of negative sentiments. Finally, lemmatization was applied to reduce words to their lexical base forms before tokenizing the text into individual lexical unit (Chakriswaran et al., 2019).

2.3 Deep learning-based sentiment analysis and feature extraction

2.3.1 Deep learning model for sentiment classification

This study utilized the Pysentimiento framework (Pérez et al., 2024), which is built upon the BERT (Bidirectional Encoder Representations from Transformers) architecture (Devlin et al., 2019). BERT was selected for its bidirectional contextual learning architecture (Yuan, 2024), which allows the model to capture nuances in tourist language—such as sarcasm or complex negations—more effectively than traditional lexicon-based approaches VADER.

2.3.2 Model evaluation and validation

Performance was validated through hyperparameter fine-tuning and systematic error checks to mitigate classification bias (Devlin et al., 2019). Evaluation metrics derived from the confusion matrix (Table 1) included precision (P), recall (R), F1-score, and overall accuracy (A) (Pleerux et al., 2023). Specific focus was placed on the precision of the negative class to ensure the reliability of the dataset for subsequent geospatial analysis (Equation 1-4).

Table 1. Confusion matrix for sentiment model validation

Actual/prediction	Positive	Neutral	Negative
Positive	a	b	c
Neutral	d	e	f
Negative	g	h	i

$$P(neg) = \frac{i}{(c+f+i)} \quad (1)$$

$$N(neg) = \frac{i}{(g+h+i)} \quad (2)$$

$$F1(neg) = \frac{2P(neg) \times R(neg)}{P(neg) + R(neg)} \quad (3)$$

$$A = \frac{a+e+i}{a+b+c+d+e+f+g+h+i} \quad (4)$$

2.3.3 N-gram for specific problem identification

To identify the precise nature of tourist dissatisfaction, word frequency analysis was conducted using the NLTK library (Bird et al., 2009). This study employed N-gram techniques (ranging from unigram to four-gram models) to determine the frequency of adjacent word sequences, specifically targeting phrases that reflect environmental and service-related impacts on marine and beach resources (Singgalen et al., 2024). The extracted N-grams were systematically categorized into three principal dimensions: Environmental (P_{Env}), Congestion/Access (P_{Acc}), and Service/Value (P_{Srv}), providing a structured dataset for geospatial planning and intervention.

2.4 Destination Sustainability Index (DSI) and hotspot analysis

2.4.1 Destination Sustainability Index (DSI)

The Destination Sustainability Index (DSI) is a composite index developed specifically for this study as a novel diagnostic tool, extending the core concept of the Tourist Satisfaction Index (TSI) (Gadekar, 2024). The DSI serves as a quantitative measure of geospatial sustainability risk based on the analysis of tourist dissatisfaction factors (Sari and Lestari, 2021) linked to physical and spatial management failures. It is constructed using the negative N-gram phrases extracted from reviews as input data (Ojo et al., 2021). The DSI calculation involves three steps:

(1) Creating the Binary Flag ($BF_{p,i}$): The process begins by calculating the Problem Density Ratio ($R_{p,i}$) for each dimension (p), which is the proportion of negative reviews mentioning problem p ($N_{p,i}$) relative to the total number of reviews (T_i).

$$R_{P,i} = \frac{N_{p,i}}{T_i} \quad (5)$$

(2) Defining the structural issue threshold: A problem density threshold of 5% was established based on the frequency distribution analysis of negative sentiments in large-scale social media datasets (Yuan, 2024). This operational decision is crucial to identify structural issues that require urgent policy intervention, ensuring that only recurring problems—rather than isolated incidents—are captured. The $R_{p,i}$ must exceed this level (corresponding to 5 out of every 100 reviews) for a problem dimension to be deemed structural. The

Binary Flag ($BF_{p,i}$) thus measures the appearance or non-appearance of the structural problem at destination i, assigned a value of 1 if $R_{p,i}$ >5% and 0 otherwise.

$$BF_{p,i} = \begin{cases} 1 \text{ if } R_{p,i} < 5\% \\ 0 \text{ if } R_{p,i} \leq 5\% \end{cases} \quad (6)$$

(3) DSI Calculation: The DSI_i value is calculated from the summation of the $BF_{p,i}$ across the three main problem dimensions (M=3: DSI_{Env}, DSI_{Acc}, and DSI_{Srv}). The index is structured as a normalization scale where a value close to 1.00 indicates high sustainability (low problem occurrence), and a value close to 0.00 indicates low sustainability (high problem occurrence) (adapted from Gadekar, 2024).

$$DSI_i = 1 - \frac{\sum_{p=1}^{M} BF_{p,i}}{M} \quad (7)$$

Where; DSI_i is the Destination Sustainability Index for destination i; $\sum_{p=1}^{M} BF_{p,1}$ is the summation of the Binary Flag (with values 0 or 1) across the three dimensions; and M represents the total number of problem dimensions, which is a constant value equal to 3.

2.4.2 Geospatial Hotspot mapping

To ensure the accurate and statistically significant identification of problem clusters, this research employs the hotspot analysis technique utilizing the G_i^* statistic (Getis and Ord, 1992). The DSI_i values derived from Equation (7) serve as the input variable (x_j), representing the attribute intensity analyzed at each location j. The spatial relationship is defined through a spatial weight matrix ($w_{i,j}$), and the G_i^* statistic assesses spatial clustering patterns as follow:

$$G_i^* = \frac{\sum_{j=1}^{n} w_{ij}x_j - \bar{X}\sum_{j=1}^{n} w_{ij}}{S\sqrt{\frac{n\sum_{j=1}^{n} w_{ij}^2 - \left(\sum_{j=1}^{n} w_{ij}\right)^2}{n-1}}} \quad (8)$$

Where; G_i^* is the G_i^* statistic value for destination i; x_j is the DSI_j value (input variable); $w_{i,j}$ is the spatial weight matrix value; n is the total number of destinations; $\bar{X}$ is the mean of all DSI values; and S is the standard deviation of all DSI values.

The G_i^* statistic generates a Z-Score and p-value to determine the significance of spatial associations. In this framework, a statistically significant negative Z-score (Z<-1.65 for 90% confidence level) indicates a spatial clustering of low DSI values (approaching 0.00), signifying a high sustainability risk (hotspot) characterized by high problem density. Conversely, a significant positive Z-score denotes a clustering of high DSI values (approaching 1.00), indicating high sustainability (coldspot). The resulting hotspot maps provide empirical geospatial evidence (Zhu and Newsam, 2024) for identifying critical zones within the Environmental, Congestion/Access, and Service/ Value dimensions. By differentiating significant hotspots by attraction type (BEACH and ISLAND), this approach maintains robust statistical power while offering precise evidence for targeted policy interventions and resource management (Singgalen et al., 2024).

2.5 Research framework and implementation

The research framework is designed as a sequential integration of deep learning and geospatial analysis to address tourism sustainability (Figure 2). The implementation commences with the collection and systematic pre-processing of geotagged reviews, followed by deep sentiment classification using the Pysentimiento model. Building upon the identified negative sentiments, N-gram analysis is employed for specific problem extraction, which serves as the fundamental input for calculating the Destination Sustainability Index (DSI) via the Binary Flag method. These indices are subsequently processed through geospatial Hotspot analysis using the Getis-Ord G_i^* statistic within a GIS environment (e.g., ArcGIS Pro or QGIS) to generate statistically significant problem maps. Finally, these spatial results are synthesized to formulate actionable sustainable tourism policies tailored for marine and beach attractions in Eastern Thailand. This integrated workflow ensures that complex textual data is effectively transformed into precise geospatial evidence for sustainability management.

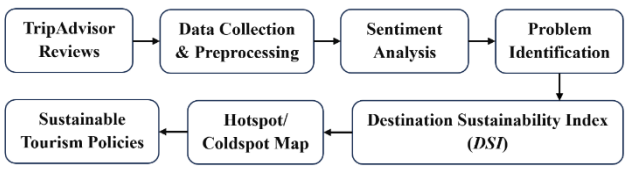


Figure 2. Integrated framework combining deep learning and geospatial analysis

3. RESULTS AND DISCUSSION

3.1 Sentiment analysis and model validation

3.1.1 Model performance and classification

The evaluation of the Pysentimiento model (BERT architecture) demonstrates robust classification performance, particularly within the negative class, which is central to this study. The model achieved a high precision value of 87%, confirming its reliability in accurately identifying reviews that contain specific dissatisfaction and management issues in the present study. While the overall classification accuracy was recorded at 0.76 due to the linguistic complexity of neutral sentiments, the high precision for the negative class (0.87) ensures that the subsequent geospatial analysis is based on highly reliable dissatisfaction data, minimizing false-positive errors in risk identification (Table 2).

From the total dataset of 11,047 reviews, the model classified 64.92% (7,172 reviews) as Positive, 16.52% (1,825 reviews) as Neutral, and 18.56% (2,050 reviews) as Negative. This distribution indicates that while the majority of tourists expressed satisfaction, nearly one-fifth of the digital feedback reflected structural or environmental concerns. Consequently, these 2,050 negative reviews were isolated to serve as the primary dataset for the subsequent N-gram feature extraction and Destination Sustainability Index (DSI) calculation. By focusing exclusively on this high-precision negative subset, the analysis ensures that the identified sustainability hotspots are derived from validated tourist dissatisfaction data, thereby enhancing the sensitivity of the DSI in detecting localized management failures.

Table 2. Performance metrics of deep learning sentiment model

Actual/prediction	Positive	Neutral	Negative	Recall	F1-score	Total
Positive	235	27	3	0.89	0.86	265
Neutral	29	33	8	0.47	0.42	70
Negative	15	26	75	0.66	0.74	116
Precision	0.84	0.38	0.87			
Accuracy					0.76	451

3.1.2 Spatial distribution of negative reviews

The visual concentration of negative feedback is illustrated in Figure 3, revealing a distinct clustering around high-density tourist hubs. Dissatisfaction is most prominent in the urbanized coastal zones near Pattaya City in Chonburi Province, as well as major marine destinations in Rayong and Trat Provinces. This initial spatial screening serves as the baseline for identifying potential risk locations. By providing a broad overview of dissatisfaction density, this distribution justifies the transition to the Destination Sustainability Index (DSI) calculation and subsequent hotspot analysis to confirm the statistical significance of these emerging patterns. Specifically, this visual density provides the necessary context for the Getis-Ord G_i^* analysis, ensuring that identified hotspots reflect true spatial dependencies rather than isolated incidents of negative feedback.

3.2 Specific problem identification and Destination Sustainability Index (DSI)

3.2.1 N-gram analysis and problem categorization

The N-gram analysis successfully isolated specific dissatisfaction clusters, confirming that while complaints are diverse, Environmental (P_{Env}) and Congestion/Access (P_{Acc}) issues are the most prominent concerns (Table 3). Environmental concerns are the most frequent, with 50% of the top 10 terms directly related to waste and hygiene (e.g., plastic, rubbish, dirty). This highlights waste management failures as a primary disruptor of the tourist experience. Similarly, Congestion/Access issues—consistently reflected through terms like "boat" and "crowded"—emerge as major dissatisfaction drivers. Although Service/Value (P_{Srv}) issues (e.g., "restaurant", "expensive") appear less frequently, they indicate underlying concerns regarding service quality and pricing. All extracted phrases were systematically categorized (Table 3) to serve as the functional foundation for calculating the Binary Flag ($BF_{p,i}$) and the subsequent DSI.

3.2.2 Destination Sustainability Index (DSI) overview

The Destination Sustainability Index (*DSI*) provides a quantitative synthesis of sustainability risks across 45 beaches and 12 islands (Table 4). Calculated via the Binary Flag ($BF_{p,i}$) method Equation (7), the results indicate that ISLAND attractions possess a

higher average sustainability level (0.47) compared to BEACH attractions (0.40). Despite this relative difference, both categories remain significantly below the ideal threshold, confirming that nearly all investigated sites face at least one structural problem dimension exceeding the 5% density threshold.

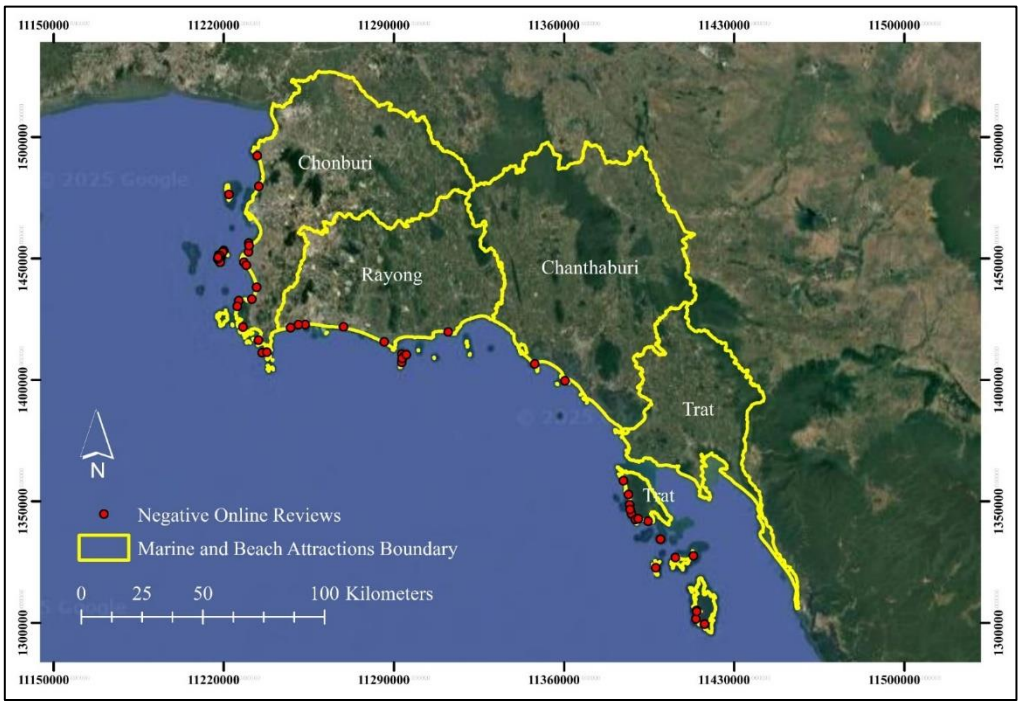


Figure 3. Spatial distribution of negative reviews

Table 3. Categorization of problem related N-grams and definition problem types (P)

Problem categories (P)	Description	High-frequency N-gram example
Environmental (P_{Env})	Physical quality and sustainability (waste, pollution, cleanliness)	plastic, rubbish, dirty, garbage, trash, bottle, filthy, litter, smell, polluted
Congestion/access (P_{Acc})	Space management, transport capacity, traffic	tourist, boat, crowded, road, noisy, street, busy, jetski, taxi, bike
Service/value (P_{Srv})	Service quality, price, feeling unsafe/unfair	restaurant, resort, hotel, vendor, shop, charge, expensive, staff, dog, police

Table 4. Average DSI values by problem dimension and attraction type

Type of attractions	$DSI_{Overall}$ (%)	DSI_{Env} (%)	DSI_{Acc} (%)	DSI_{Srv} (%)
BEACH	0.40	0.40	0.38	0.42
ISLAND	0.47	0.58	0.42	0.42

Dimension-specific analysis reveals critical structural profiles: Environmental quality (DSI_{Env}) serves as a comparative strength for the ISLAND group (0.58), suggesting that over half of these destinations remain free from structural environmental crises. Conversely, the BEACH group exhibits severe structural weakness in this dimension (0.40), reflecting widespread ecological degradation. The most acute risk identified is Congestion/Access (DSI_{Acc}) for the BEACH group (0.38), the lowest value in the dataset, which underscores the extreme vulnerability of easily accessible coastal mainland sites. Meanwhile, service/value (DSI_{Srv}) risks appear uniform across both groups (0.42), indicating a systemic challenge in service quality management that transcends attraction types.

3.3 Geospatial Hotspot mapping and policy implication

The application of Getis-Ord G_i^* statistics transforms numerical $DSI_{Overall}$ results into empirical geospatial evidence, pinpointing locations where sustainability risks are significantly clustered (Figure 4). The analysis confirms that these risks are not randomly distributed but exhibit a distinct spatial spectrum, ranging from high-sustainability clusters (coldspots) at 95%-99% confidence to emerging risk areas (hotspots) at 90% confidence (Table 5).

The strongest coldspot (99% confidence, $p<0.01$) was identified at Ao Phrao (Island, Trat), where a perfect $DSI_{Overall}$ of 1.00 was recorded. This cluster serves as a statistically significant "best practice management model," demonstrating effective problem control across all dimensions. Primary coldspots at 95% confidence were also observed across the beach group in Trat Province (average DSI 0.67), suggesting a regional trend of higher sustainability in the easternmost coastal zone. Conversely, a significant emerging hotspot (90% confidence) was detected near the Chonburi coastline, specifically encompassing Koh Si Chang and Koh Loi. These areas exhibit low DSI scores (0.00 to 0.67), indicating pervasive and dense sustainability challenges. From a policy perspective, this 90% confidence cluster requires immediate intervention and monitoring to prevent its escalation into a high-confidence sustainability crisis.

Notably, the majority of investigated destinations (e.g., Koh Kham, Chao Lao Beach, Wong Amat Beach) were categorized as not significant (Gi_Bin=0). Although some sites within this group reported low $DSI_{Overall}$ values (e.g., Koh Larn, Ao Wai), their dissatisfaction is not statistically clustered in a holistic sense. This suggests that while Koh Larn faces significant local challenges—particularly in service quality as detailed later—these issues do not yet constitute a regional-scale spatial contagion in the overall sustainability index. These "localized problems" suggest site-specific issues resolvable through internal management, rather than requiring broader regional-scale policy interventions.

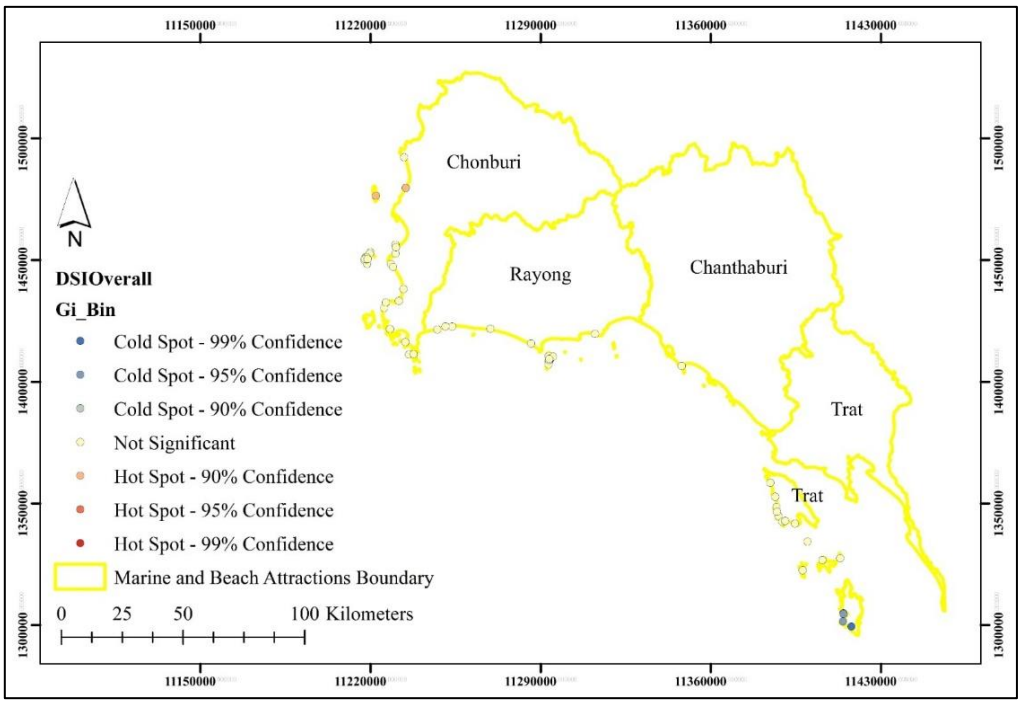


Figure 4. Geospatial hotspot analysis of overall sustainability ($DSI_{Overall}$)

3.4 Dimension-specific geospatial risk assessment

To provide granular insights for policy formulation, hotspot analysis was disaggregated into three core sustainability dimensions: Environment (P_{Env}), (P_{Acc}), and Service (P_{Srv}).

3.4.1. Environmental sustainability (DSI_{Env})

Results for P_{Env} reveal a unique spatial pattern where no statistically significant clusters were detected (Gi_Bin=0 for all locations). While sites like Pattaya and Koh Samed reported low local DSI_{Env} (0.00), these remained localized issues without

systematic spatial contagion. However, an "emerging risk" was identified in the Koh Samed cluster (Gi_Zscore ≈ -1.599, p ≈ 0.10), categorized as the highest watchlist area. This finding highlights the DSI's capability as an early warning tool, identifying forming clusters of degradation before they reach critical statistical significance (Figure 5, Table 6).

Table 5. Overall hotspot/coldspot summery ($DSI_{Overall}$)

Cluster type	Confidence (Gi_Bin)	Cluster area	Strategic policy implication
Strongest coldspot	99% (Gi_Bin=+3)	Ao Phrao Beach (Trat)	Management model: Replicate this "best practice" for high-value sustainability.
Primary coldspot	95% (Gi_Bin=+2)	Trat Beaches group (Avg. DSI: 0.67)	Standard support: Maintain high sustainability in coastal beach zones.
Emerging hotspot	90% (Gi_Bin=-1)	Koh Si Chang, Koh Loi (Chonburi)	Urgent watchlist: Immediate intervention required to prevent risk escalation.
Not significant	p>0.10 (0) (Gi_Bin=0)	Most destinations	Localized management: Address site-specific issues via internal measures.

Table 6. Summary of dimension-specific hotspot/coldspot analysis and management strategies

Problem dimension (P)	Cluster type	Confidence level	Primary locations	Strategic policy implication
Environmental (P_{Env})	Emerging risk	Approaching 90% (Z ≈ -1.60)	Koh Samed group (Rayong)	Highest watchlist: Implement early-warning waste management and proactive pollution control.
	Not significant	p>0.10	Most destinations	Maintain localized environmental standards; no regional contagion detected.
Congestion/access (P_{Acc})	Strongest coldspot	99% (Gi_Bin=+3)	Ao Phrao (Trat)	Management model: High-quality infrastructure; replicate this "low-density" model elsewhere.
	Primary hotspot	95% (Gi_Bin=-2)	Koh Si Chang, Koh Loi (Chonburi); White Sand Beach (Trat)	High crisis: Severe utility/transport deficits. Requires urgent structural investment and capacity limits.
	Significant coldspot	90% (Gi_Bin=+1)	Chao Lao Beach (Chanthaburi)	Sustainable access: Promote effective traffic and facility management as a secondary model.
Service/value (P_{Srv})	Primary hotspot	95% (Gi_Bin=-2)	Wonnapha and Wong Amat Beach (Chonburi)	Systemic failure: Critical service quality/safety risks. Enforce strict operator regulations and quality audits.
	Primary coldspot	95% (Gi_Bin=+2)	Ao Phrao (Trat)	Premium zone: Exceptional service standards. Designate as a benchmark for high-value tourism.
	Significant hotspot	90% (Gi_Bin=-1)	Koh Larn and Koh Si Chang clusters	Risk area: Rapid growth outpaces quality control. Urgent need for operator certification and service upgrades.

3.4.2 Congestion/access sustainability (DSI_{ACC})

Spatial clustering for P_{Acc} exhibits a sharp contrast between high-sustainability coldspots in Trat and high-risk hotspots in Chonburi (Figure 6, Table 6). The strongest coldspot (99% confidence) at Ao Phrao (Koh Kood) confirms that its infrastructure management serves as an ultimate best-practice model. Conversely, the upper Chonburi cluster (Koh Si Chang and Koh Loi) and the White Sand Beach (Trat) were identified as significant hotspots (95% confidence). These areas suffer from structural congestion where tourist volumes far exceed existing utility and transport capacities, requiring urgent infrastructure reinvestment.

3.4.3 Service/value sustainability (DSI_{Srv})

Analysis of P_{Srv} indicates systemic service-related failures clustered in high-density zones (Figure 7, Table 6). Significant hotspots (95% confidence) at Wonnapha and Wong Amat beaches signify recurring

issues in vendor quality and safety management. In contrast, the Koh Kood group maintained its status as a model zone (95% coldspot), emphasizing quality-over-quantity development. The identification of P_{Srv} hotspots in areas undergoing rapid growth, such as Koh Larn, suggests that service quality control often lags behind mass-transit expansion, necessitating stricter operator regulations.

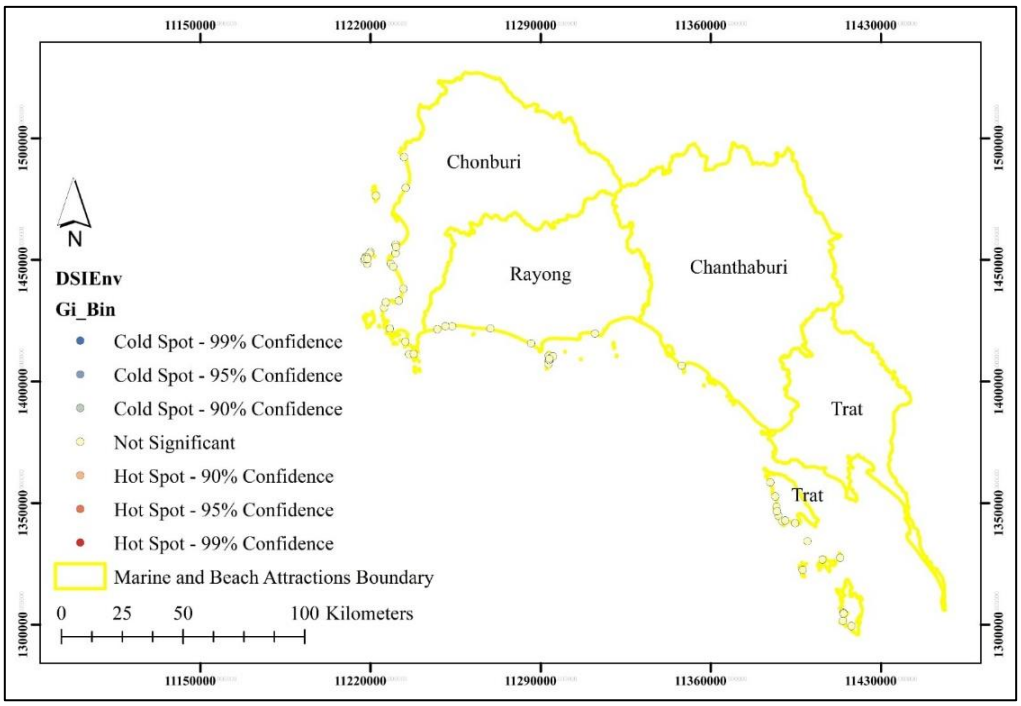


Figure 5. Geospatial hotspot analysis of Environmental sustainability (DSI_{Env})

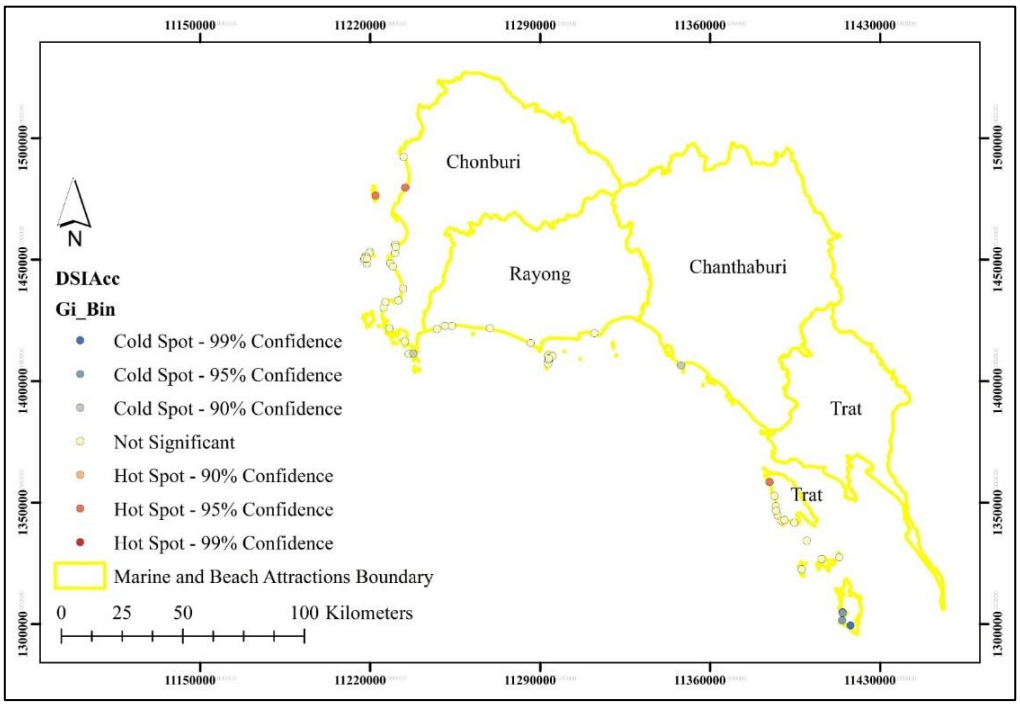


Figure 6. Geospatial hotspot analysis of Congestion/Access sustainability (DSI_{Acc})

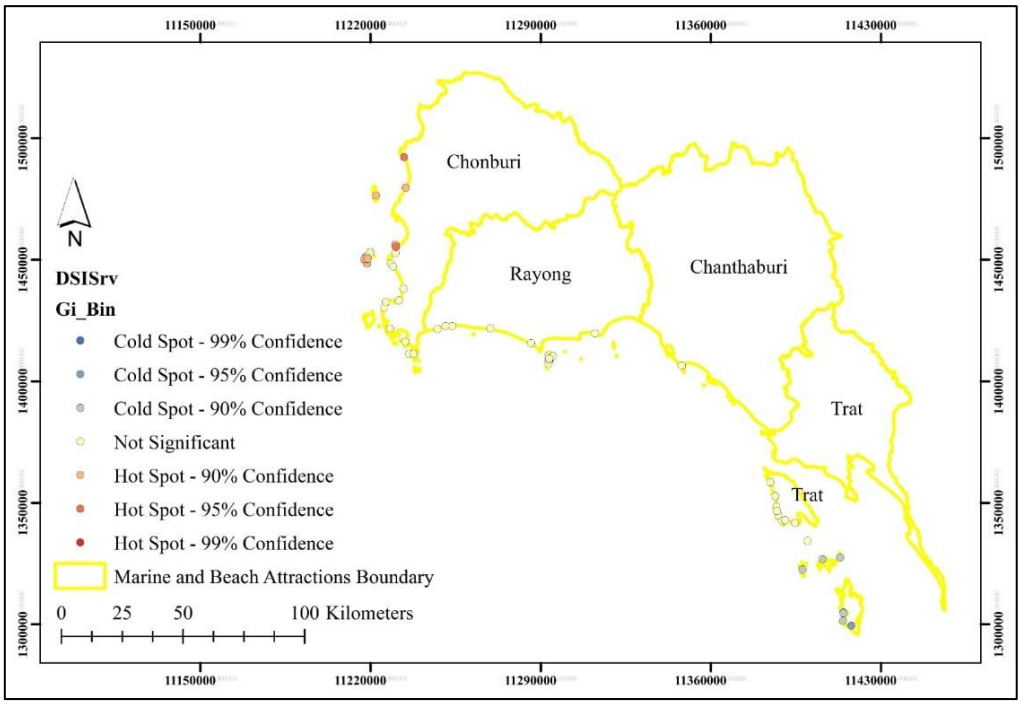


Figure 7. Geospatial hotspot analysis of service/value sustainability (DSI_{Srv})

3.5 Synthesis of geospatial risks and strategic policy implications

Based on the multi-dimensional hotspot analysis, the sustainability profile of Eastern Thailand's marine attractions can be synthesized into three strategic management domains:

(1) Critical intervention zones (priority hotspots): The Chonburi cluster (specifically Pattaya, Koh Si Chang, and Koh Loi) is identified as the highest priority area due to simultaneous Hotspot clustering in DSI_{Acc} and DSI_{Srv} dimensions. This overlap signifies a "complex structural crisis" where rapid, unmanaged growth has outpaced infrastructure capacity and service quality. While Koh Larn demonstrates high-density localized risks in the service dimension, the statistical G_i^* analysis prioritizes the Chonburi mainland and near-shore islands for regional-scale intervention. Urgent policy intervention is required, specifically focusing on strategic infrastructure investment—upgrading piers and waste systems while establishing rigid carrying capacity ceilings and tourism management fees to mitigate congestion.

(2) Model preservation zones (structural strengths): The Koh Kood cluster (Trat Province) consistently exhibits coldspot clustering, serving as the region's best practice management model. Policies for this zone must shift from development to preservation and scaling. By designating these areas as "premium sustainable zones," the government can provide incentives to operators while utilizing their low-density, high-quality management blueprint as a benchmark for other emerging destinations.

(3) Risk-based resource allocation: The Gi_Bin results provide an empirical foundation for optimized budget distribution. Locations categorized as significant hotspots (Gi_Bin≤-2) should be prioritized for structural budget allocation to rectify utility and transport deficits. Conversely, significant coldspots (Gi_Bin≥+2) should receive funding for sustainability maintenance and "quality-focused" marketing. For not significant areas with local issues, decentralized management is recommended to resolve site-specific problems without requiring regional-scale intervention.

4. CONCLUSION

This research successfully established a robust geospatial methodology for identifying "priority hotspots" of unsustainability in Eastern Thailand's marine destinations. By integrating a fine-tuned transformer-based BERT model (Pysentimiento) with the novel Destination Sustainability Index (DSI) and Getis-Ord G_i^* statistics, this study transformed 11,047 tourist reviews into empirical geospatial evidence. The model's high precision (87%) in classifying negative sentiments ensured that the 5% density threshold effectively isolated structural problems from localized

noise, providing a reliable foundation for regional policy formulation.

Key findings: (1) Dimensional vulnerability: N-gram analysis confirmed that environmental degradation (waste management) and congestion are the primary drivers of tourist dissatisfaction. The $DSI_{Overall}$ remains low across both attraction types (Island: 0.47, Beach: 0.40), with environmental quality (DSI_{Env}: 0.58) identified as the sole structural strength of the island group. (2) Spatial significance: The G_i^* analysis verified that sustainability risks are not randomly distributed but spatially clustered. The Chonburi cluster (specifically Koh Si Chang, and Koh Loi) emerged as the highest priority hotspot due to simultaneous failures in accessibility (DSI_{Acc}) and service quality (DSI_{Srv}). Conversely, the Koh Kood cluster (Trat) was consistently identified as a structural coldspot, representing a high-sustainability benchmark for the region.

ACKNOWLEDGEMENTS

The authors would like to thank the TripAdvisor website for the valuable information used in this research. Special thanks to the reviewers for their constructive comments and suggestions, which helped to improve the quality of this manuscript.

AUTHOR CONTRIBUTIONS

Methodology, software, formal analysis, data curation, validation, investigation, resources, visualization, and writing-original draft preparation, T.C.; writing-review and editing, N.P.; conceptualization-AI, A.S.; conceptualization-tourism, P.N. All authors have read and agreed to the published version of the manuscript

DECLARATION OF CONFLICT OF INTEREST

The authors declare no conflict of interest.

REFERENCES

Abirami A. Marine pollution and waste management. Journal of Law and Legal Research Development 2024;1(2):20-4.

Alfred R, Chen Z, Eboy O, Luxuan Z, Renjie L. Analyzing trends in the spatial-temporal visitation patterns of mainland Chinese tourists in Sabah, Malaysia based on Weibo social big data. Heliyon 2023;11(15):e43981.

Baltranaite E, Inácio M, Pinto LV, Bogdziewicz K, Rocha J, Gomes E, et al. Tourism impacts on marine and coastal ecosystem services: A systematic review. Geography and Sustainability 2025;6(2):Article No. 100277.

Bird S, Klein E, Loper E. Natural Language Processing with Python. CA, USA: O'Reilly Media, Inc.; 2009.

Chakriswaran P, Vincent DR, Srinivasan K, Srinivasan K, Sharma V, Chang CY, et al. Emotion AI-driven sentiment analysis: A survey, future research directions, and open issues. Applied Sciences 2019;9(24):Article No. 5462.

Charfaoui K, Mussard S. Sentiment analysis for tourism insights: A machine learning approach. Stats 2024;7(4):1527-39.

Cui Y, He Q. Travel Behavior Analysis with Social Media Data and Smartphone GPS Data. NY, USA: University Transportation Center, University of Buffalo; 2019.

Devlin J, Chang MW, Lee K, Toutanova K. BERT: Pre-training of deep bidirectional transformers for language understanding. Proceedings of the 2019 Conference of the North American Chapter of the Association for Computational Linguistics: Human Language Technologies; 2019; Minneapolis, MN: USA; 2019.

Department of Tourism (DOT). Natural Tourist Attraction Quality Standard Assessment Manual. Office of Tourism Development [Internet]. 2018 [cited 2025 Nov 20]. Available from: https://www.dot.go.th/ebooks/ebooks-view/417.

Gadekar D. A study of tourist satisfaction index (TSI) of heritage tourist place of Ajanta Cave in Chatrapati Sambhaji Nagar District of Maharashtra State in India. Heritage: Journal of Multidisciplinary Studies in Archaeology 2024;11(2):1195-9.

Getis A, Ord K. The analysis of spatial association by use of distance statistics. Geographical Analysis 1992;24(3):189-206.

Jabalameli S, Xu Y, Shetty S. Spatial and sentiment analysis of public opinion toward COVID-19 pandemic using twitter data: At the early stage of vaccination. International Journal of Disaster Risk Reduction 2022;80:Article No. 103204.

Jeacle I, Carter C. In TripAdvisor we trust: Rankings, calculative regimes and abstract systems. Accounting Organizations and Society 2011;36(4):293-309.

Li X, Pan B, Law R, Huang X. Forecasting tourism demand with composite search index. Tourism Management 2017;59: 57-66.

Ministry of Tourism and Sports Thailand (MOTS). National Tourism Development Plan No. 3 (2023-2027) [Internet]. 2023 [cited 2025 Nov 20]. Available from: https://online.anyflip.com/zzfck/rptc/mobile/index.html.

Muthukadan B. Selenium Python Bindings [Internet]. 2024 [cited 2025 Oct 7]. Available from: https://selenium-python. readthedocs.io/.

Ojo O, Gelbukh A, Calvo H, Adebanji OO. Performance study of N-grams in the analysis of sentiments. Journal of the Nigerian Society of Physical Sciences 2021;3(4):477-83.

Office of Natural Resources and Environmental Policy and Planning (ONEP). Environmental Quality Situation Report 2024 [Internet]. 2024 [cited 2025 Oct 7]. Available from: https://www.onep.go.th/book/soe2567/.

Pérez JM, Rajngewerc M, Giudici JC, Furman DA, Luque F, Alemany LA, et al. Pysentimiento: A Python Toolkit for Opinion Mining and Social NLP tasks [Internet]. 2023 [cited 2025 Oct 7]. Available from: https://doi.org/10.21203/rs.3.rs-3570648/v1.

Pleerux N, Boonpook W, Chaiyo A, Nardkulpat A. Trip advisor restaurant customer reviews analysis in Bangkok, Thailand. Proceedings of the International Conference on Cyber Management and Engineering (CyMaEn); 2023 Jan 26-27; Bangkok, Thailand; 2023.

Ramadhani A, Sutoyo E, Widartha VP. LSTM-based deep learning architecture of tourist review in Tripadvisor. Proceedings of the Sixth International Conference on Informatics and Computing (ICIC); 2021 Nov 3-4; Jakarta: Indonesia; 2021.

Sari PI, Lestari YD. Determinants of tourist satisfaction and dissatisfaction on tourism village. Journal Pendidikan Ekonomi Dan Bisnis 2021;9(1):9-24.

Singgalen YA, Wahyuningtyas SY, Widodo YE, Dasra MNA, Setiawan RW. Sentiment analysis for tourism destination reviews using cross-industry standard process for data-minning. Journal of Theoretical and Applied Information Technology 2024;102(17):6364-79.

Tourism Authority of Thailand (TAT). Survey Project for Analysis of International Tourist Behavior 2024 [Internet]. 2024 [cited 2025 Nov 20]. Available from: https://intelligencecenter.tat.or.th/articles/12311#tab-2.

Valdivia A, Luzón M, Herrera F. Sentiment analysis on TripAdvisor: Are there inconsistencies in user reviews? Proceedings of the International Conference on Hybrid Artificial Intelligence Systems (HAIS); June 21-23; La Rioja: Spain; 2017.

Xi Z, Min L, Yadong S. Night tourism satisfaction in the Qinghefang tourism and Leisure block based on an improved Kano Model. Journal of Resources and Ecology 2024; 15(1):55-65.

Yuan X. Evaluation of rural tourism development level using BERT-enhanced deep learning model and BP algorithm. Scientific Reports 2024;14:Article No. 25748.

Yusoh MP, Mapjabil J, Hanafi N, Idris MAM. Tourism carrying capacity and Social Carrying capacity: A literature review. SHS Web of Conferences 2021;124(4):Article No. 02004.

Zhu Y, Newsam S. Spatio-temporal sentiment hotspot detection using geotagged photos. Proceedings of the 24th ACM SIGSPATIAL International Conference on Advances in Geographic Information Systems; 2016 Oct 31-Nov 3; Burlingame, CA: USA; 2016.

Environment and Natural Resources Journal

Volume 24
Issue 6
2026

Scenario-Based Assessment of Greenhouse Gas Mitigation in the Municipal Solid Waste: Cambodia Case Study and Regional Comparison in Asia

Kyoko Take[1] and Thai-Huyen Nguyen[2*]

[1]*Institute for Global Environmental Strategies (IGES), Japan*
[2]*Hanoi Architectural University, Vietnam*

ARTICLE INFO

Received: 5 Jan 2026
Received in revised: 19 Jun 2026
Accepted: 24 Jun 2026
Published online: 3 Sep 2026
DOI: 10.32526/ennrj/24/20260009

Keywords:
Solid waste management/ GHG mitigation/ Policy/ Asia/ Cambodia

*** Corresponding author:**
E-mail: huyen.nt@hau.edu.vn

ABSTRACT

This study estimates future waste generation and evaluates greenhouse gas (GHG) mitigation potential under alternative waste management strategies in Cambodia. Key mitigation measures include waste reduction, improved collection efficiency, recycling, and methane recovery. Recycling is identified as the most effective option, contributing approximately 60% and 77% of total GHG reductions in 2030 and 2050, respectively, while methane recovery provides an additional 28% in 2030 and 22% in 2050. Under the Business-as-Usual (BaU) scenario, waste-sector GHG emissions are projected to increase from 1.6 $MtCO_2eq$ in 2010 to 5.7 $MtCO_2eq$ in 2030 and 15.2 $MtCO_2eq$ in 2050. A regional comparison indicates that Cambodia's waste-related GHG emissions are high relative to its income level and are comparable to those of more developed countries such as Japan, while exceeding those of Singapore, primarily due to limited waste treatment capacity and a high organic fraction in waste. Implementation of countermeasure strategies could reduce emissions by 13% in 2030 and 39% in 2050 compared to the BaU scenario, demonstrating substantial mitigation potential in Cambodia's waste sector. The study employs the Extended Snapshot (ExSS)/Waste model (a bottom-up engineering approach) and provides evidence-based insights to support climate-oriented waste management policy in Cambodia and comparable developing countries in the region.

HIGHLIGHTS

- Cambodia's waste-sector GHG emissions are projected to rise from 1.6 to 15.2 $MtCO_2eq$ by 2050 under BaU.
- Industrial waste dominates future emissions, exceeding 70% of total waste-sector GHG by 2050.
- Countermeasure strategies can reduce emissions by 13% in 2030 and 39% in 2050 vs. BaU.
- Recycling accounts for about 77% and methane recovery for about 22% of total reductions by 2050.
- The ExSS/Waste model provides a transferable framework for GHG mitigation in developing Asia.

1. INTRODUCTION

Inappropriate waste management practices lead to emissions of methane (CH_4), carbon dioxide (CO_2), and nitrous oxide (N_2O), which contribute significantly to climate change. Over a 100-year time horizon, methane has a global warming potential approximately 27.2 without climate-carbon feedbacks and 29.8 with feedbacks relative to CO_2 (IPCC, 2021). Globally, methane emissions from waste disposal sites account for approximately 10-12% of total anthropogenic methane emissions, representing nearly half of emissions attributed to the waste sector (US EPA, 2006; IPCC, 2007).

Although the waste sector contributes only about 3-5% of total global GHG emissions, it is increasingly recognized as a key mitigation sector due to its high reduction potential through alternative treatment technologies and improved management systems (UNFCCC, 2005; Ragossnig and Hilger, 2008; IPCC, 2019). Measures such as waste minimization, recycling, composting, and methane recovery can substantially reduce upstream and downstream GHG emissions.

Citation: Take K, Nguyen T-H. Scenario-based assessment of greenhouse gas mitigation in the municipal solid waste: Cambodia case study and regional comparison in Asia. Environ. Nat. Resour. J. 2026;24(6):701-712. (https://doi.org/10.32526/ennrj/24/20260009)

In Cambodia, municipal waste generation has increased rapidly in recent years, reflecting the country's rapid urbanization, economic growth, and expansion of the tourism sector. Municipal solid waste generation in Cambodia exceeded 3 Mt/year by the late 2010s, driven by rapid urbanization, economic growth, and tourism development (Ministry of Environment, 2025; World Bank, 2021). Per capita municipal solid waste generation in Cambodia has risen to around 0.6-0.7 kg/person/day in recent years, with higher levels in urban areas (World Bank, 2018; Ministry of Environment, 2025). Without effective intervention, inadequate waste management may lead to resource degradation, land scarcity, public health risks, and increased climate impacts.

Various models have been developed to estimate GHG emissions and mitigation potential in the waste sector. Inventory-based models, particularly those following the IPCC Waste methodology, are widely applied for national GHG reporting and mitigation assessment under the UNFCCC framework (IPCC, 2019; IPCC, 2022). Life cycle assessment (LCA)-based models, such as those reviewed in recent global assessments, are commonly used to compare technology-specific emission impacts of waste treatment options, including recycling, composting, and incineration (UNEP, 2024). In contrast, bottom-up scenario-based models, such as the Extended Snapshot (ExSS)/Waste model, are designed for long-term mitigation and policy analysis; recent applications in Vietnam and Malaysia indicate that waste-sector emissions could exceed 60 $MtCO_2eq$ by 2030 under Business-as-Usual conditions, while recycling and methane recovery could reduce emissions by more than 30% (Nguyen and Matsuoka, 2017; Siong et al., 2013).

This study addresses three specific objectives: (1) to project future solid waste and wastewater generation in Cambodia from 2010 to 2050; (2) to quantify GHG emissions under a Business-as-Usual (BaU) scenario; and (3) to evaluate mitigation potential under a Countermeasure (CM) scenario, with regional comparison across selected Asian countries. By assessing these mitigation scenarios, this paper provides evidence-based insights to support policy development and strategic planning for sustainable waste management in Cambodia. To the best of the authors' knowledge, this study represents one of the early national-scale assessments linking municipal waste management strategies and climate change mitigation in the Cambodian context.

2. METHODOLOGY

2.1 General model description

There are some models available to help determine the best options for reducing GHG emissions from waste (IPCC, 2006; US EPA, 2012). Among the models used to identify optimal strategies for reducing GHG emissions, the Extended Snapshot (ExSS)/Waste model, a bottom-up engineering model, is employed for estimation purposes. The model quantifies GHG emissions from three main sources: (1) fossil CO_2 released during incineration of fossil-derived waste; (2) CH_4 generated from the decomposition of organic carbon in disposed solid waste and from wastewater treatment; and (3) N_2O from wastewater treatment.

For solid waste disposal, the model applies the First-Order Decay (FOD) method (IPCC Tier 1) to capture the delayed release of methane following waste burial, with methane correction factor (MCF) and degradable organic carbon (DOC) serving as key parameters. For wastewater, GHG emissions are estimated on a per-person basis using BOD/COD activity data. Because this methodology is applied at the individual level, emissions from commercial wastewater are incorporated into the domestic wastewater category. It should be noted that the model does not account for energy consumption or GHG emissions associated with energy use in waste management operations, nor does it include vehicle operation emissions.

The model encompasses the entire national waste system; however, the scenario analysis and modelling assessment focus specifically on the municipal waste system. Waste generation is categorized into two streams, solid waste and wastewater originating from the residential, commercial, industrial, and construction sectors. Population data and industrial output are provided to the ExSS/Waste model as exogenous inputs. The study covers the time horizon from 2010 to 2050. A detailed description of the model methodology is provided in Nguyen and Matsuoka (2017).

2.2 Scenarios description

The BaU scenario assumes the continuation of current waste generation trends and management practices without major additional interventions. Waste generation is projected based on population growth and economic development pathways consistent with Cambodia's transition toward upper-middle-income status by 2030 and high-income status

by 2050, as outlined in national development and climate policy frameworks (Royal Government of Cambodia, 2013; Ministry of Environment, 2025).

The CM scenario assumes accelerated implementation of waste management measures beyond existing plans, including higher recycling rates, expanded incineration, and enhanced methane recovery from disposal sites and wastewater treatment systems. Based on consultations with domestic experts and alignment with recent national climate commitments, the CM scenario assumes recycling of 40%, incineration of 6%, and methane recovery of 15% relative to the BaU scenario (IPCC, 2019; Ministry of Environment, 2025; IPCC, 2022). Socioeconomic assumptions are held constant across both scenarios to isolate the effects of waste management strategies.

The assumed future socio economic conditions of Cambodia are the same in both cenarios as follow:

Cambodia has maintained robust economic growth over the past decade, and the Government of the Kingdom of Cambodia has reaffirmed its long-term development objectives to attain upper-middle-income status by 2030 and high-income status by 2050, as outlined in national strategic frameworks (Royal Government of Cambodia, 2018). Achieving these targets requires sustained economic growth supported by structural transformation and macroeconomic stability. Population assumptions in this study are based on the United Nations World Population Prospects. Cambodia's population is projected to reach approximately 18.5 million by 2030 and around 22.0 million by 2050 under the medium-variant scenario, which is consistent with national development projections (United Nations, 2022).

2.3 Waste generation projection

2.3.1 Solid waste generation

Waste generation per capita in the residential sector for 2030 and 2050 is assumed to correspond to current upper-income and current high-income levels, respectively ("What a Waste"; Hoornweg and Bhada-Tata, 2012). Intermediate years between 2000 and 2050 are linearly interpolated. Solid waste in commercial, industrial and construction sectors are assumed to maintain the same generation factor as the base year. Since data is limited for Cambodia, and Vietnam is ahead of Cambodia in urbanization and per capita income, generation factors for these sectors are taken from Vietnam (Nguyen and Matsuoka, 2017). The resulting solid waste generation projections are summarized in Table 1.

Table 1. Solid waste generation

Indicator	Base year	Target year		References
	2010	2030	2050	
Population (person)	**13,959,000**	**18,391,000**	**21,964,000**	Statistic yearbook of Cambodia (National Institute of Statistic, 2024); World Population Prospects 2022 (United Nations, 2022)
- Urban	2,741,000	5,434,000	9,835,000	
- Rural	11,218,000	12,957,000	12,129,000	
Output of industry (million USD)	**28,334**	**119,549**	**486,468**	Chan and Oum (2011); Mao (2015); World Bank (2022), Ministry of Economy and Finance (MEF). (2023)
- Commercial sector	6,472	25,845	100,322	
- Industrial sector	10,635	45,480	187,596	
• Agriculture, fishery and forestry	3,136	9,265	30,082	
• Mining	125	558	2,338	
• Manufacturing	7,374	35,657	155,176	
- Construction sector	592	2,743	10,955	
Generation factor				
- Residential sector (kg/person/day)	0.3	0.6	1.3	Sethy (2013); Nguyen and Matsuoka (2017); UNEP (2024), Ministry of Environment (2025)
- Commercial sector (ton/million USD·year)	69.0	69.0	69.0	
- Industrial sector (ton/million USD·year)	64.8	64.8	64.8	
- Construction sector (ton/million USD·year)	431.8	431.8	431.8	
Waste generation (ton/year)	**2,919,392**	**10,074,706**	**34,142,096**	
- Residential sector	1,528,511	4,161,883	10,341,749	Estimated by multiplying waste generation per capita and population in the year

Table 1. Solid waste generation (cont.)

Indicator	Base year	Target year		References
	2010	2030	2050	
- Commercial sector	446,424	1,782,835	6,920,399	Estimated by multiplying waste generation factor in commercial sector and output of commercial sector in monetary units
- Industrial sector	688,802	2,945,617	12,149,988	Estimated by multiplying waste generation factor in industrial sector and output of industrial sector in monetary units
- Construction sector	255,656	1,184,371	4,729,959	Estimated by multiplying waste generation factor in construction sector and output of construction sector in monetary units

2.3.2 Wastewater generation

The activity data is used to calculate emissions from domestic wastewater treatment including population and degradable organic components or biochemical oxygen demand (BOD), while those for industrial wastewater treatment include industrial production and chemical oxygen demand (COD).

For domestic wastewater, GHG emissions are calculated using population and the IPCC default BOD per capita value of 14.6 kg BOD/capita/year (IPCC, 2006, Table 6-5, p. 6.23). The total domestic BOD load (kg/year) is obtained by multiplying this per capita factor by annual population. This BOD load is then used to estimate the maximum methane production capacity (B0), which, combined with the treated fraction and the methane correction factor (MCF) for each treatment system type, yields annual CH_4 emissions following IPCC Tier 1 methodology. The BOD generation factor is held constant from 2000 to 2050, consistent with IPCC default assumptions.

For industrial wastewater, only the main industries that process large volumes of organic wastewater with the largest potential for wastewater emission are considered, the value of COD differs between different industries (Table 2). The eneration factor in every year is assumed to be the same as that in 2010. Industrial wastewater was estimated by multiplying the wastewater generation factor in the industrial sector and the output of the industrial sector in monetary units in every year.

$$\text{Generation factor of 2010} = \frac{\text{Total COD/year}}{\text{Output of industry in 2010}} = \frac{6564.43}{10635.00} = 0.878\left(\frac{\text{ton COD}}{\text{million USD/year}}\right)$$

Table 2. Industrial wastewater generation in 2010

	Industrial production	Wastewater generated	Total wastewater generated	COD	Total organic degradable material in wastewater
Unit	ton/year	m^3/t	m^3/year	kgCOD/m^3	kgCOD/year
Beer and malt	159,285[(1)]	10.00[(3)]	1,592,850	3.50[(3)]	5,574,975
Fish processing	35,000[(1)]	21.50[(3)]	752,500	1.20[(3)]	903,000
Starch production	961[(2)]	9.00[(4)]	8,645	10.00[(3)]	86,455
Total	195,246	12.06	2,353,995		6,564,430

[(1)] FAO (2015), [(2)] Royal Government of Cambodia (2014a,b), [(3)] Nguyen and Matsuoka (2017), [(4)] IPCC (2006)

2.4 Waste composition

The study does not clarify the composition of wastewater; however, the composition of solid waste is defined in different sectors as below:

2.4.1 Residential and commercial solid waste

The composition of residential and commercial solid waste has some common characteristics such as a high rate of organic origin fraction; a high content of soil, sand, and brick and stone fragments; and high moisture content, with low specific heat energy (Nguyen, 2014). Socio-economic conditions that enable an increase in standards of living of the economy will influence the composition of the waste generated. The major types of residential and

commercial solid waste are food waste, paper, textile, plastic, metal, rubber, glass and other. In this study, the composition of solid waste in the two sectors in 2010 was derived from solid waste composition in Phnom Penh in Cambodia (Yim et al., 2023), and in 2030 and 2050 were assumed to be those in current upper income and current high-income sectors as reported by Hoornweg and Bhada-Tata (2012). As can be seen from Table 3, the largest percentage is the organic fraction at 66.3% (2010), and 54% (2030). Due to urbanization, the country will generate a high percentage of paper (14% in 2030 and 31% in 2050).

Table 3. Composition of residential and commercial solid waste

Waste composition (%)	2010[(1)]	2030[(2)]	2050[(2)]
Paper	4.6%	14.0%	31.0%
Textile	0.8%	2.0%	5.0%
Organic	66.3%	54.0%	28.0%
Wood	0.6%	0.6%	0.6%
Garden	0.2%	0.2%	0.2%
Rubber	0.4%	0.4%	0.4%
Plastic	9.8%	11.0%	11.0%
Metal	2.0%	3.0%	6.0%
Glass	3.0%	5.0%	7.0%
Other	12.5%	9.8%	10.9%

[(1)] Yim et al. (2023), [(2)] Hoornweg and Bhada-Tata (2012)

2.4.2 Industrial solid waste

Composition of industrial solid waste is very complicated, depending on the raw materials, technological processes and final products of each production center and its related services. There are various industries in Cambodia but information is lacking, therefore only one type of waste composition, namely "Other", was assumed for the industrial sector in this study. This simplification introduces uncertainty into industrial solid waste emission estimates. However, since industrial solid waste is predominantly non-organic relative to residential waste, the impact on total national GHG estimates is expected to be limited. Future studies should collect Cambodia-specific industrial waste composition data to refine these estimates.

2.4.3 Construction solid waste

Since no Cambodia-specific construction waste composition data is available, this study adopted composition data from Vietnam (Nguyen and Matsuoka, 2017), with one expert-adjusted modification: the wood fraction was reduced from 5% (Vietnam) to 2%, reflecting differences in construction practices.We assumed that waste composition would not change during the period 1990 to 2050. The waste composition waste is separated into metal (0.83%), brick (1.16%), concrete (65.83%), wood (2.00%), soil and sand (26.93%), and other (3.25%).

2.5 Waste management strategy

Cambodia's waste management framework is founded on early regulatory instruments, including the Sub-Decree on Solid Waste Management (Royal Government of Cambodia, 1999a) and the Sub-Decree on Water Pollution Control (Royal Government of Cambodia, 1999b), which continue to provide the legal basis for waste governance. More recently, waste management has been increasingly integrated into national climate policy through the Cambodia Updated Nationally Determined Contribution (NDC 3.0), submitted by the Ministry of Environment in 2025. NDC 3.0 commits Cambodia to an enhanced economy-wide greenhouse gas mitigation target compared to previous submissions and identifies the waste sector as a priority mitigation area, emphasizing waste reduction, recycling, organic waste treatment, and methane mitigation from disposal sites and wastewater systems (Ministry of Environment, 2025). While NDC 3.0 provides clearer mitigation directions and indicative actions for the waste sector, it does not specify technology- or pathway-specific quantitative targets. Therefore, scenario-based modeling is required to translate these policy commitments into explicit treatment shares and mitigation potentials, as implemented in this study.

The BaU scenario treatment shares (Tables 4 and 5) were derived from: (1) current observed practices in Cambodia (limited formal recycling, near-total reliance on open disposal); (2) regional trends in comparable lower-middle-income countries; and (3) national waste management objectives. The CM scenario shares were informed by: (1) realistic implementation bounds given current infrastructure; (2) NDC 3.0 guidance (Ministry of Environment, 2025); and (3) analogous ExSS/Waste model targets for Vietnam and Malaysia (Nguyen and Matsuoka, 2017; Siong et al., 2013). Expert judgment balanced policy ambition against technical feasibility.

Targets of solid waste treatment developed by the model are based on actual and current measures applied in the world including composting, recycling, incineration, and disposal.

Based on targets of waste management in Cambodia and components of waste in different sectors, estimations of specific target for each treatment measures applied in each sector are shown in Table 4 and Table 5.

Table 4. Estimation of composition of solid waste management in BaU and CM

Sector	Waste type	Management	BaU			CM	
			2010	2030	2050	2030	2050
Residential and commercial	Paper, textile, nappies, plastic, etc.	Recycling	0.01	0.10	0.30	0.30	0.70
		Incineration	0.00	0.01	0.04	0.05	0.10
		Composting	0.00	0.00	0.00	0.00	0.00
		Disposal	0.99	0.89	0.66	0.65	0.20
	Food, garden, wood, etc.	Recycling	0.01	0.10	0.30	0.10	0.20
		Incineration	0.00	0.01	0.04	0.05	0.10
		Composting	0.00	0.10	0.40	0.30	0.50
		Disposal	0.99	0.79	0.26	0.55	0.20
	Others (metal, glass, brick, concrete, etc.)	Recycling	0.01	0.10	0.30	0.30	0.70
		Incineration	0.00	0.00	0.00	0.00	0.00
		Composting	0.00	0.00	0.00	0.00	0.00
		Disposal	0.99	0.90	0.70	0.70	0.30
Industrial	Others	Recycling	0.10	0.20	0.50	0.30	0.70
		Incineration	0.00	0.01	0.04	0.05	0.10
		Composting	0.00	0.00	0.00	0.00	0.00
		Disposal	0.90	0.79	0.46	0.65	0.20
Construction	Wood, brick, soil, concrete, etc.	Recycling	0.10	0.20	0.50	0.30	0.70
		Incineration	0.00	0.00	0.00	0.00	0.00
		Composting	0.00	0.00	0.00	0.00	0.00
		Disposal	0.90	0.80	0.50	0.70	0.30

Table 5. Estimation of composition of wastewater management in BaU and CM

Sector	Management option	BaU	CM	
		2010-2050	2030	2050
Residential wastewater	Non-treated	0.80	0.20	0.00
	Treated	0.20	0.80	1.00
Industrial wastewater	Non-treated	0.60	0.25	0.00
	Treated	0.40	0.75	1.00

2.4.4 Methane (CH_4) recovery

At present, there are no targets for collecting CH_4 from waste in Cambodia from disposal sites and wastewater. In the BaU scenario, there is no CH_4 colleting system in 2010, and only 1% and 5% of CH_4 are expected to collect in years 2030 and 2050, respectively. In the CM scenario, we assumed, there will be 5% and 20% collected from disposal sites and 5% and 20% collected from treated wastewater, respectively for the years 2030 and 2050.

3. RESULTS

In BaU scenario, GHG emissions increased from 1.6 $MtCO_2eq$ in 2010 to 5.7 in 2030 and 15.2 $MtCO_2eq$ in 2050. GHG emissions from the industrial sector are expected to continue to increase in importance due to rapid industrial expansion and to contribute the highest level of emissions accounting for more than 70% of the total emissions in the future (see Table 6). GHG emissions increase sharply in 2050 in the BaU scenario accounting for 15.2 $MtCO_2eq$.

Assuming a better waste management strategy and increased methane recovery, GHG emissions can be reduced 13% in 2030 and 39% in 2050.

The rapid BaU emissions increase is driven primarily by industrial output growth (amplifying industrial solid waste and landfill methane) and urbanization. The limited 2030 reduction versus 2050 reflects the FOD time-lag: methane from pre-scenario waste continues emitting for years. By 2050, cumulative recycling and methane capture benefits compound substantially, underscoring the importance of early policy intervention.

Among GHG, methane emission is the biggest emission source accounting for approximately 40% of total emissions from waste (see Figure 1).

From the disposal site, methane emitted from industrial waste accounts for the largest share compared to other waste types, as summarized in Table 7. The industrial methane contribution is projected to reach 3.36 $MtCO_2eq$ (total 4.33 $MtCO_2eq$ in 2030) and 4.54 $MtCO_2eq$ (total 5.95 $MtCO_2eq$ in 2050).

Table 6. GHG emissions by sector in BaU and CM scenarios ($MtCO_2eq$)

		Business-as-usual (BaU)			Countermeasure (CM)	
GHG Source	Sector	2010	2030	2050	2030	2050
CH_4 from disposal site	Residential	0.17	0.56	0.76	0.49	0.46
	Commercial	0.17	0.41	0.64	0.36	0.39
	Industrial	1.11	3.36	4.54	2.92	2.77
	Construction	0.000	0.010	0.010	0.010	0.010
	Sub-total	*1.46*	*4.33*	*5.95*	*3.77*	*3.63*
CH_4 from wastewater	Residential	0.0003	0.0019	0.0029	0.0017	0.0018
	Industrial	0.0001	0.0004	0.0014	0.0003	0.0009
	Sub-total	*0.0004*	*0.0023*	*0.0043*	*0.0020*	*0.0026*
Fossil CO_2 from incineration	Residential and Commercial	0.14	1.37	9.25	1.19	5.64
TOTAL		1.59	5.71	15.20	4.97	9.27

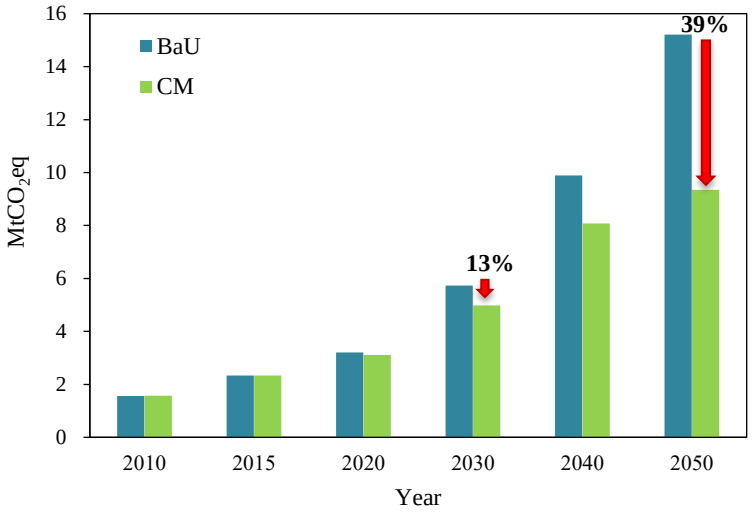


Figure 1. GHG emissions/reductions in BaU and CM scenarios in Cambodia

Table 7. Emission from disposal site in the period of 2010-2050

Methane from disposal site ($MtCO_2eq$)				
	2010	2030	2050	2030 (US EPA, 2012)
Residential	0.17	0.56	0.76	0.5
Commercial	0.17	0.41	0.64	
Industrial	1.11	3.36	4.54	
Construction	0.00	0.01	0.01	
Total	1.46	4.33	5.95	

US EPA (2012) has studied global mitigation of Non-CO_2 GHG in the period from 2010 to 2030 including Cambodia. It estimated methane from disposal sites from the residential sector in Cambodia in 2030 with a value of 0.5 $MtCO_2eq$. This number is quite similar to this study's estimation.

From wastewater treatment process, methane emission from residential wastewater is significantly greater than that from industrial wastewater in Cambodia (see Table 8).

4. DISCUSSION

4.1 Global climate and environmental benefits results from GHG emission reduction in waste sector

Efforts to reduce GHG emissions from the waste sector include reducing the amount of waste generation (recycling, recovery), improving the efficiency of waste collection, expanding methane avoidance (renewable energy replacing fossil fuel energy sources), and carbon bound in soil through compost application etc. These are key components of an integrated waste management strategy that would enable the waste sector to become a global net emissions saver.

Waste recycling receives the highest priority to reduce the amount of waste disposed, representing significant potential for reducing GHG emissions by conserving raw materials and fossil fuels. This is also the most favorable reduction option in Cambodia, accounting for approximately 77% of total reduction amount in 2050.

Waste offers a significant source of renewable energy. Through methane recovery, which accounted for 22% of the total GHG emissions reduction in 2050 in Cambodia, energy generated from methane combustion can displace other fossil fuels, either as a process energy resource or as electricity.

Table 8. Emission from wastewater in the period of 2010-2050

CH_4 from wastewater treatment ($MtCO_2eq$)				
	2010	2030	2050	2030 (US EPA, 2012)
Residential	0.0003	0.0019	0.0029	0.0
Industrial	0.0001	0.0004	0.0014	
Total	0.0004	0.0023	0.0043	

Note: In US EPA (2012), it estimated for residential waste only using Waste model in IPCC (2006), the activity data for population was referred to US Census database for countries that did not provide their own population data.

Through biological treatment, organic wastes (food waste, wood waste and garden waste) can be recovered and transformed into fertilizers. These processes reduce GHG emissions by sequestering carbon in soils and replenishing soil nutrients. Organic waste constitutes a large component of the waste stream, ranging from 30-70% of total residential and commercial waste (66% in Cambodia in 2010). Therefore, separate collection of the organic component of waste can offer a valuable contribution to GHG emission reduction and soil improvement.

There is a need to consider the environmental, economic, and social aspects of different waste management options in order to reduce GHG emissions. The assessment does not concentrate only on the amount of mitigated GHG, but also on regional conditions, such as the implementation feasibility of each option, direct and environmental costs, land availability, and so forth. The selected integrated system of waste management should deliver both economic and environmental sustainability.

The sound and strong policies and regulations of waste management are very important national drivers to reduce GHG emissions, especially in developing countries. Each country's initiatives cannot be exported to another country or region without taking into account local waste characteristics, infrastructure, climate and economic conditions. Governments have a range of policy options to encourage waste management practices that will reduce greenhouse gas emissions.

These findings are consistent with national-level assessments using the ExSS/Waste model in Vietnam and Malaysia, where recycling and methane recovery were also the dominant mitigation measures (Nguyen and Matsuoka, 2017; Siong et al., 2013). Compared to IPCC inventory-based approaches, the scenario-based ExSS/Waste model allows more explicit quantification of technology-specific mitigation pathways, providing actionable insights for national climate planning in developing countries.

4.2 Waste sector and GHG emissions in Cambodia and other Asian countries

Table 9 presents a comparison of municipal solid waste generation and associated GHG emissions across Cambodia and selected Asian countries for the year 2025. Waste generation amounts are estimated based on country-specific per capita generation rates and population data. Generation rates for Cambodia are derived from this study, while those for Vietnam, Malaysia, and Japan are taken from Nguyen and Matsuoka (2017), Siong et al. (2013), and Hoornweg and Bhada-Tata (2012), respectively; rates for the remaining countries are based on Nguyen and Schnitzer (2009).

Japan exhibits the highest per capita waste generation rate, followed by Singapore, Malaysia, and Indonesia, reflecting the higher income levels and consumption patterns. In contrast, Cambodia, the Philippines, Thailand, and Vietnam show relatively similar generation rates, ranging from 0.52 to 0.64 kg/capita/day. However, despite lower generation rates, Cambodia, Vietnam, Indonesia, and Malaysia, have a high organic fraction in municipal solid waste, exceeding 55%.

This high organic content is a key driver of elevated methane emissions from waste disposal, explaining why countries such as Vietnam, Indonesia, and Malaysia exhibit substantial GHG emissions from the waste sector (62.9, 73.3, and 61.0 $MtCO_2eq$, respectively). Although Cambodia remained at a lower level of economic development in 2025, its estimated waste-related GHG emissions are comparable to those of Japan and approximately double those of Singapore, primarily due to limited waste treatment infrastructure and reliance on disposal-based management. These findings highlight the significant mitigation potential in Cambodia's waste sector, and support the effectiveness of countermeasure scenarios that achieve emission reductions of 13% by 2030 and 39% by 2050 relative to the BaU scenario.

The results of this study are consistent with previous national-level assessments that applied the ExSS/Waste model in Southeast Asia. Similar to the findings reported for Vietnam and Malaysia, this study identifies recycling and methane recovery as the dominant mitigation measures, jointly accounting for more than 80% of total emission reductions by 2050 (Nguyen and Matsuoka, 2017; Siong et al., 2013). However, the relative mitigation potential in Cambodia is higher when expressed as a share of baseline emissions, reflecting the current dominance of disposal-based waste management and the high organic fraction of municipal solid waste.

Compared with studies based on the IPCC Waste Model, which primarily focus on inventory-level emission estimates, the ExSS/Waste approach applied in this study allows a more detailed assessment of technology-specific mitigation pathways under long-term scenarios. While IPCC-based estimates for several Asian countries report comparable absolute methane emissions from disposal sites, this study demonstrates that the early implementation of integrated waste management strategies in Cambodia could yield mitigation outcomes comparable to or greater than those observed in more economically advanced economies. These comparisons position Cambodia as a high-impact case for waste-sector mitigation in the region and highlight the contribution of this study as the third national application of the ExSS/Waste model.

4.3 Uncertainty and limitations

Several sources of uncertainty should be acknowledged. First, waste generation projections rely on income-based assumptions (Hoornweg and Bhada-Tata, 2012) that may not fully capture Cambodia-specific drivers. Second, industrial and construction waste composition data, rely on Vietnamese proxy values; given the predominantly inorganic nature of waste in these sectors, the impact on total GHG estimates is expected to be limited. Third, CM scenario treatment shares are based on expert consultation and regional analogies rather than bottom-up engineering feasibility assessments. Fourth, the model excludes GHG emissions from waste collection vehicles. Fifth, FOD parameters rely on IPCC default values that may deviate from actual Cambodian site conditions. Future work should address these limitations through field measurement campaigns and sensitivity analyses.

5. CONCLUSION

This study assessed future waste generation and GHG emissions in Cambodia for the period 2010-2050. The results indicate that total waste generation is projected to increase to approximately 10.1 million tons/year by 2030 and 34.1 million tons/year by 2050, corresponding to 3.5 and 11.7 times the 2010 level, respectively. Under the BaU scenario, total GHG emissions from the waste sector are estimated to rise from 1.6 $MtCO_2eq$ in 2010 to 5.7 $MtCO_2eq$ in 2030 and 15.2 $MtCO_2eq$ in 2050.

Table 9. Waste generation and GHG emissions in Cambodia and other Asian countries in 2025

Country	GDP per capita (USD)		Population		Waste generation rates (kg/cap/day)		Organic fraction in waste[e] (%)	GHG emissions ($MtCO_2eq$)	GHG emission estimation method
	2010[a]	2025[b]	Urban[c] (%)	Total[b] (million)	Generation rates (kg/cap/day)	Waste generation amount (tons/year)			
Cambodia	783	985	48.6	17.2	0.62[g]	3,884,666	55	4.3[g]/0.5[h]	ExSS/Waste Model[d]
Vietnam	1,334	2,010	39.0	93.4	0.61[d]	20,799,963	60	62.9[d]/10.3[h]	ExSS/Waste Model[d]
Philippines	2,136	2,691	74.3	107.7	0.52[c]	20,435,766	41	12.9[h]	IPCC Waste Model[i]
Indonesia	3,137	3,376	60.7	253.6	0.76[c]	70,351,414	62	73.3[h]	IPCC Waste Model[i]
Thailand	4,803	5,617	39.1	67.7	0.64[c]	15,824,064	48	10.6[h]	IPCC Waste Model[i]
Malaysia	8,754	11,204	72.7	30.1	0.81[c]	8,890,196	62	61.0[f]	ExSS/Waste Model[d]
Singapore	46,570	55,135	100.0	5.6	1.10[c]	2,236,355	44	2.1[h]	IPCC Waste Model[i]
Japan	42,909	37,530	100.0	127.1	1.70[e]	78,865,550	26	4.3[h]	IPCC Waste Model[i]

[a] GDP per capita. The World Bank. HP <http://data.worldbank.org/indicator/NY.GDP.PCAP.CD>

[b] List of Countries Forecast 2025. HP<http://www.deagel.com/country/forecast.aspx?pag=4&sort=Alphabetical&ord=DESC>

[c] Nguyen and Schnitzer (2009)

[d] Nguyen and Matsuoka (2017)

[e] Hoornweg and Bhada-Tata (2012)

[f] Siong et al. (2013)

[g] This study

[h] US EPA (2012)

[i] IPCC (2006)

Implementation of CM scenarios could reduce emissions by approximately 13% in 2030 and 39% in 2050 relative to BaU. Recycling is identified as the most effective mitigation option, accounting for about 60% and 77% of total GHG reductions in 2030 and 2050, respectively, while methane recovery represents the second most significant mitigation measure. A comparison with other Asian countries indicates that Cambodia's waste-sector emissions are relatively high in relation to its income level, largely due to the high organic fraction of waste and limited treatment capacity, highlighting substantial mitigation opportunities through improved waste management practices.

Overall, the findings demonstrate that low-carbon waste management strategies can substantially reduce GHG emissions while simultaneously improving waste management performance. The results provide quantitative evidence to support the formulation of sustainable and climate-oriented waste management policies in Cambodia. In practical terms, policymakers should prioritize investments in: separate collection infrastructure for recyclables; expansion of organic waste composting in urban centers; and installation of landfill gas capture systems at major disposal sites. Early action is critical, as delayed implementation locks in disposal-dominated emission trajectories. Future research should: (1) derive Cambodia-specific waste decay parameters through field measurement campaigns; (2) conduct cost-benefit analyses of CM scenario interventions; and (3) extend scenario analysis to additional mitigation pathways such as waste-to-energy and extended producer responsibility schemes.

ACKNOWLEDGEMENTS

The authors acknowledge the support received during the preparation of this manuscript. No external funding was received for this study.

AUTHOR CONTRIBUTIONS

Conceptualization, Thai-Huyen Nguyen and Kyoko Take; Data curation, Thai-Huyen Nguyen; Investigation, Thai-Huyen Nguyen; Resources, Thai-Huyen Nguyen; Writing and original draft, Thai-Huyen Nguyen; Methodology, Kyoko Take; Software, Kyoko Take; Formal analysis, Kyoko Take; Visualization, Kyoko Take; Validation, Thai-Huyen Nguyen and Kyoko Take; Writing-review and editing, Thai-Huyen Nguyen and Kyoko Take; Funding acquisition, not applicable.

DECLARATION OF CONFLICT OF INTEREST

The authors declare that they have no known competing financial interests or personal relationships that could have appeared to influence the work reported in this paper.

REFERENCES

Chan S, Oum S. Impact of Garment and Textile Trade Preferences on Livelihoods in Cambodia. Boston: Oxfam America; 2011.

Food and Agriculture Organization of the United Nations (FAO). FAOSTAT Database [Internet]. 2015 [cited 2024]. Available from: http://www.fao.org/faostat.

Hoornweg D, Bhada-Tata P. What a Waste: A Global Review of Solid Waste Management. Washington DC: World Bank; 2012.

Intergovernmental Panel on Climate Change (IPCC). 2006 IPCC Guidelines for National Greenhouse Gas Inventories, Volume 5: Waste. Hayama: Institute for Global Environmental Strategies; 2006.

Intergovernmental Panel on Climate Change (IPCC). Climate Change 2007: The Physical Science Basis. Cambridge: Cambridge University Press; 2007.

Intergovernmental Panel on Climate Change (IPCC). 2019 Refinement to the 2006 IPCC Guidelines for National Greenhouse Gas Inventories. Hayama: Institute for Global Environmental Strategies; 2019.

Intergovernmental Panel on Climate Change (IPCC). Climate Change 2021: The Physical Science Basis. Cambridge: Cambridge University Press; 2021.

Intergovernmental Panel on Climate Change (IPCC). Climate Change 2022: Mitigation of Climate Change. Contribution of Working Group III to the Sixth Assessment Report. Cambridge: Cambridge University Press; 2022.

Mao H. A design of Low-carbon Development Action Towards 2050 in Cambodia [dissertation]. Kyoto: Kyoto University; 2015.

Ministry of Economy and Finance (MEF). Macroeconomic Framework and Public Financial Management Reform Program. Phnom Penh: MEF; 2023.

Ministry of Environment. Cambodia's Third Nationally Determined Contribution (NDC 3.0). Phnom Penh: Ministry of Environment; 2025.

National Institute of Statistics (NIS). Statistical Year Book of Cambodia 2024. Phnom Penh: Ministry of Planning; 2024.

Nguyen NU, Schnitzer H. Sustainable solutions for solid waste management in Southeast Asian countries. Waste Management 2009;29(6):1982-95.

Nguyen TKT. Municipal solid waste management in Vietnam: challenges and solutions. In: Pariatamby A, Tanaka M, editors. Municipal Solid Waste Management in Asia and the Pacific Islands. Singapore: Springer; 2014. p. 355-77.

Nguyen TH, Matsuoka Y. Analysis of greenhouse gas emissions and mitigation in the waste sector of Vietnam. Mitigation and Adaptation Strategies for Global Change 2017;22(3): 427-46.

Ragossnig A, Hilger H. Waste management: Stepping up to the climate change challenge. Waste Management and Research: The Journal for a Sustainable Circular Economy 2008; 26(1):3-4.

Royal Government of Cambodia. Sub-Decree on Solid Waste Management. Phnom Penh: Royal Government of Cambodia; 1999a.

Royal Government of Cambodia. Sub-Decree on Water Pollution Control. Phnom Penh: Royal Government of Cambodia; 1999b.

Royal Government of Cambodia. Rectangular Strategy Phase III (2013-2018). Phnom Penh: Royal Government of Cambodia; 2013.

Royal Government of Cambodia. National Strategic Development Plan 2014-2018. Phnom Penh: Royal Government of Cambodia; 2014a.

Royal Government of Cambodia. Cambodia Trade Integration Strategy 2014-2018. Phnom Penh: Royal Government of Cambodia; 2014b.

Royal Government of Cambodia. Rectangular Strategy Phase IV. Phnom Penh: Royal Government of Cambodia; 2018.

Sethy S. Solid Waste Management in Cambodia. Paper presented at: FY2012 Final Meeting of the Partnership Project; Okayama, Japan; 2013.

Siong HC, Wai CL, Matsuoka Y, Gomi K, Simon J, Osawa R, et al. Low-Carbon Society Scenarios Malaysia 2030. Tsukuba: National Institute for Environmental Studies (NIES); 2013.

United Nations, Department of Economic and Social Affairs (DESA), Population Division. World Population Prospects 2022. New York: United Nations; 2022.

United Nations Environment Programme (UNEP). Global Waste Management Outlook 2024. Nairobi: UNEP; 2024.

United Nations Framework Convention on Climate Change (UNFCCC). Key GHG Data. Bonn: UNFCCC; 2005.

United States Environmental Protection Agency (US EPA). Solid Waste Management and Greenhouse Gases: A Life-Cycle Assessment of Emissions and Sinks. 3rd ed. Washington DC: US EPA; 2006.

United States Environmental Protection Agency (US EPA). Global Anthropogenic Non-CO_2 Greenhouse Gas Emissions: 1990-2030. Washington DC: US EPA; 2012.

World Bank. What a Waste 2.0: A Global Snapshot of Solid Waste Management to 2050. Washington DC: World Bank; 2018.

World Bank. Cambodia Country Environmental Analysis. Washington DC: World Bank; 2021.

World Bank. Cambodia Economic Update. Washington DC: World Bank; 2022.

Yim M, Lim S, Hoy SR, Pasicolan TJA, Pasicolan PN. Current situation of municipal solid waste management in the urban and peri-urban of Phnom Penh, Cambodia. Annals of Civil and Environmental Engineering 2023;7(1):67-72.

Environment and Natural Resources Journal

Volume 24
Issue 6
2026

Effects of Climate Change on Streamflow of Upper Lam Nam Chi and Lam Saphung Subwatershed Using SWAT Model

Chawakon Sakkaew, Supattra Thueksathit*, and Patchares Chacuttrikul

Department of Conservation, Faculty of Forestry, Kasetsart University, Bangkok, Thailand

ARTICLE INFO

Received: 11 Nov 2025
Received in revised: 11 May 2026
Accepted: 30 Jun 2026
Published online: 8 Sep 2026
DOI: 10.32526/ennrj/24/20250322

Keywords:
Streamflow/ SWAT model/ Climate change

*** Corresponding author:**
E-mail: fforstt@ku.ac.th

ABSTRACT

The upper Lam Nam Chi and Lam Saphung subwatershed in Thailand is an area at risk of drought and water scarcity, with climate change having the potential to increase the severity of these problems. Therefore, this study evaluated streamflow and investigated the impact of climate change on streamflow in the research area, applying the Soil and Water Assessment Tool model under climate change scenarios RCP4.5 and RCP8.5. Streamflow data were used from two stations of the Royal Irrigation Department during 2012-2022 for model calibration, with model accuracy being analyzed using the Nash-Sutcliffe efficiency and PBIAS. The findings showed that the average annual streamflow of the upper Lam Nam Chi and Lam Saphung Subwatershed during 2012-2022 was 856.40 million cubic meters. The highest discharge occurred in September and the lowest in January. There was a considerable increase in the predicted annual streamflow under the climate change scenarios RCP4.5 and RCP8.5 in the near-term (2041-2060), medium-term (2061-2080), and long-term (2081-2100). The highest streamflow occurred in July and August and the lowest in April and May. In particular, the estimated annual streamflow under the long-term scenario without adopting any measures or policies for GHG emission control (RCP8.5) was notably different, being more than 4 times higher than the current streamflow. In conclusion, climate change influenced the streamflow in this watershed, which could lead to severe flooding and water scarcity in this watershed in the future.

HIGHLIGHTS

This research examined the impact of climate change on streamflow using the Soil and Water Assessment Tool model. The model was calibrated by adjusting the parameters related to streamflow. The Nash-Sutcliffe efficiency and percent bias (PBIAS) were used to analyze the accuracy of the model. The results showed that the average annual streamflow from RCP4.5 and RCP8.5 greatly increased from the current situation.

1. INTRODUCTION

Water resources are a cornerstone of socio-economic stability, particularly in agrarian-based economies like Thailand, where water availability directly influences agricultural productivity and national development (Ingrao, 2023). The hydrological process, specifically the conversion of rainfall into streamflow, is a complex interaction governed by topography, soil infiltration, and evapotranspiration (Chacuttrikul and Thueksathit, 2023). Understanding these dynamics is essential for effective water management and for securing the livelihood of local communities.

Globally, climate change has disrupted the traditional water cycle, leading to intensified natural disasters and seasonal shifts (Kiguchi et al., 2021). While previous studies have examined climate impacts on major systems like the Chao Phraya and Mun River Basins, the approaches and focus areas vary. For instance, Li and Fang (2021) utilized the SWAT model to evaluate streamflow changes in the Mun River, while Budhathoki et al. (2022) and Panneerselvam et al. (2024) focused on bias correction and sediment supply under shifting climates in the Chao Phraya River Basin. Despite these contributions, a critical knowledge gap remains regarding long-term

Citation: Sakkaew C, Thueksathit S, Chacuttrikul P. Effects of climate change on streamflow of upper Lam Nam Chi and Lam Saphung Subwatershed using SWAT Model. Environ. Nat. Resour. J. 2026;24(6):713-722. (https://doi.org/10.32526/ennrj/24/20250322)

streamflow projections in smaller, highly vulnerable subwatersheds. Specifically, the inherent uncertainties in climate trajectories through the end of the 21st century necessitate more localized, high-resolution modeling. Such detailed assessments are crucial for developing robust adaptation plans, particularly in regions where seasonal water scarcity is already a primary concern, like the upper reaches of the Chi River Basin.

The Chi River Basin is a vital hydrological system in Northeastern Thailand, with the Chi River stretching approximately 765 kilometers and draining a basin area of 49,480 square kilometers. According to the drought risk assessment by the National Water Resources Office (2021), the Upper Lam Nam Chi and Lam Saphung subwatersheds have been identified as high-priority areas, facing water shortages and drought risks more severe than other regions within the basin. Consequently, evaluating the long-term impacts of climate change on these specific subwatersheds is essential. This study utilizes the Soil and Water Assessment Tool (SWAT), a robust model capable of simulating complex hydrological processes (Neitsch et al., 2002) by integrating key variables such as soil characteristics and land use (Neitsch et al., 2011), As a public domain model widely recognized in both domestic and international research (Thueksathit et al., 2023), SWAT was employed to forecast streamflow under the RCP4.5 and RCP8.5 climate scenarios for the period 2041-2100. These scenarios from CMIP5 represent two distinct climate pathways: RCP4.5 assumes a future with effective greenhouse gas mitigation, while RCP8.5 serves as the worst-case, high-emission scenario (Furphy, 2013; Hausfather, 2019; Lee et al., 2021). The findings of this study are expected to support the development of efficient water management guidelines and inform disaster mitigation efforts, enabling proactive planning to address the increasing threats of floods and droughts in the Upper Lam Nam Chi and Lam Saphung subwatersheds.

2. METHODOLOGY

This study was divided into five steps: 1) site selection, 2) data preparation, 3) estimation of streamflow using the SWAT model, 4) calibration of the SWAT model and 5) estimation of streamflow under climate change scenarios. The details of the steps are as follows:

2.1 Site selection

The upper Lam Nam Chi and Lam Saphung Subwatershed is fed by tributaries of the Lam Chi Basin, covering most of Chaiyaphum Province and some areas of Phetchabun Province, Thailand. The upper Lam Nam Chi and Lam Saphung Subwatershed has a total area of 3,222.14 square kilometers, of which 3,157.32 square kilometers are in Chaiyaphum Province and 64.82 square kilometers in Phetchabun Province. The water in the basin flows from the highlands on the western side, which consist of densely forested mountain ridges, to the east. The average height above mean sea level is in the range 196.01-1,319.84 meters (Institute of Water and Agricultural Resources Information (Public Organization), 2012). The topography of the study area consists of forest-covered mountains, while the flat areas are used as agricultural land, urban areas and buildings, and water sources.

2.2 Model data preparation

Data preparation for the factors affecting water quantity and the details and data formats specified by the model (weather data, spatial data, and runoff data) are discussed below:

2.2.1 Weather data

Data were collected in the range 1993-2022 (30 years), containing precipitation data and air temperature data (highest and lowest), on a daily basis format from 5 precipitation measuring stations and 3 weather measuring stations of the Meteorological Department, Thailand (The Meteorological Department, 2024).

2.2.2 Spatial data

Spatial data consisted of a digital elevation model, land use data in 2018, soil group data in 2005 (Land Development Department, 2019), and watershed and stream data in 2021 as geographic information data (Department of Water Resources, 2024). All spatial data were processed at a spatial resolution (cell size) of 30×30 meters. This study focuses on climate change impacts while assuming static land use, which may not reflect future changes in urbanization or policy.

2.2.3 Monthly streamflow data

The data were obtained from measurements at 2 hydrological stations of the Royal Irrigation Department from April 2012 to December 2022 (Royal Irrigation Department, 2018). These data were compared to the SWAT model in the calibration process.

2.3 Streamflow estimation using SWAT model before calibration

The SWAT model is a type of hydrological model that can adjust the parameter values according to the physical data of the real area. It divides the watershed area into subwatersheds according to the characteristics of land use, soil groups, and slopes of the area (Hydrological Response Units; HRUs). The assessment of streamflow using the SWAT model consisted of 5 steps (Royal Forest Department, 2021):

Step 1 The watershed delineation was performed using the Digital Elevation Model (DEM) to define the subwatershed in the upper Lam Nam Chi and Lam Saphung watersheds. This process automatically divided the study area into 29 subwatersheds (Figure 1).

Step 2 The Hydrologic Response Units (HRUs) were defined by overlaying three spatial datasets: land use, soil type, and slope.

Step 3 Input of climatic data (Write SWAT input tables)

Step 4 Evaluation of the runoff volume (Run SWAT)

Step 5 Displaying the results (Read SWAT output)

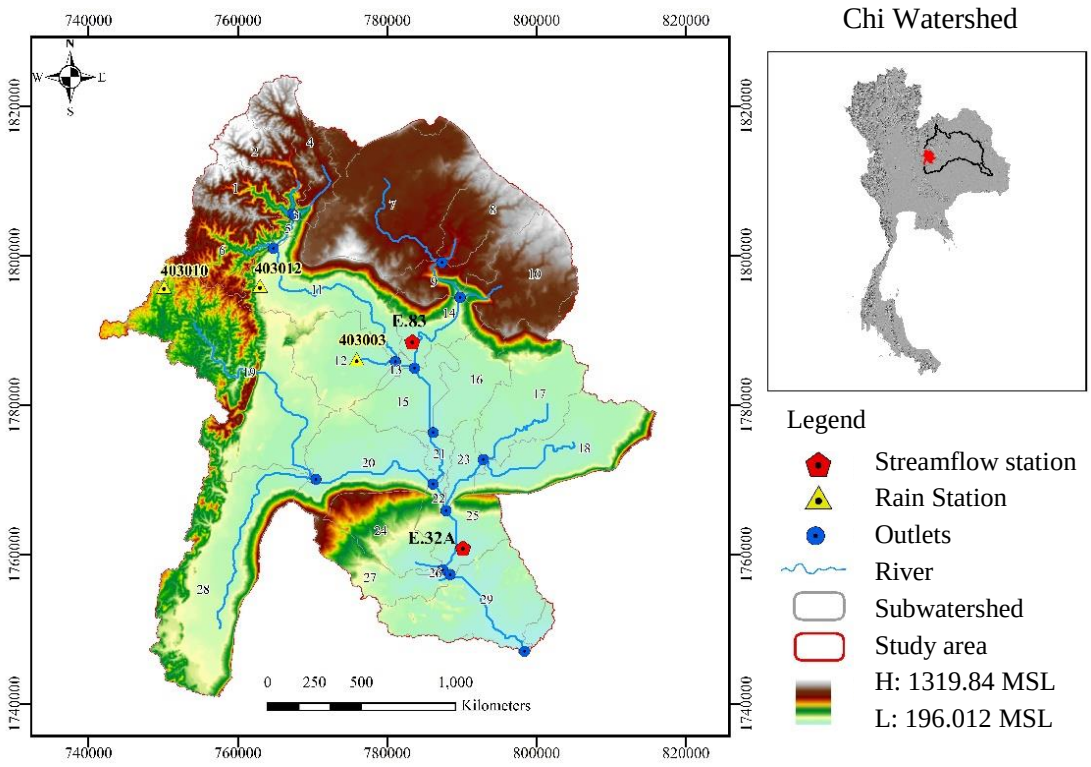


Figure 1. Boundary of upper Lam Nam Chi and Lam Saphung Subwatershed and 29 subwatershed from SWAT model

2.4 SWAT model calibration

The model was calibrated by adjusting the parameters related to streamflow and comparing the results with actual measurements from stations E.83 (Ban Na Charoen) and E.32A (Ban Nong O) of the Royal Irrigation Department. The calibration period was limited to April 2012 through December 2022, based on the availability of consistent hydrological data at these stations. The Nash-Sutcliffe efficiency (NSE) and the percent bias (PBIAS) were used to evaluate the model's accuracy. The NSE value explains the correlation between the measured and simulated results, while the PBIAS value evaluates the overall water balance performance of the SWAT model, indicating the extent to which it over- or underestimates the total streamflow. The NSE value greater than 0.5 and a PBIAS within ±25% indicate that the model performance is satisfactory (Moriasi et al., 2007; Moriasi et al., 2015; Makumbura et al., 2022). The NSE equation is shown in equation 1 (Nash and Sutcliffe, 1970):

$$NSE = 1 - \frac{\sum_{i=1}^{n}(Y_i^{obs} - Y_i^{sim})^2}{\sum_{i=1}^{n}(Y_i^{obs} - Y^{ave})^2} \quad (1)$$

The PBIAS equation is shown in equation 2 (Moriasi et al., 2007):

$$PBIAS = \frac{\sum_{i=1}^{n}(Y_i^{obs} - Y_i^{sim}) \times 100}{\sum_{i=1}^{n}(Y_i^{obs})} \quad (2)$$

Where; Y_i^{obs}=the observed value at time step i, where n is the total number of observations; Y_i^{sim}=the simulated value from the model at time step I; Y^{ave}=the average of Y_{obs}.

2.5 Streamflow assessment for climate change scenarios

The assessment of streamflow under climate change scenarios was conducted using future climate projections from the MRI-CGCM3 model. This model was selected for its high spatial resolution, low bias, and consistency with observed historical data in Thailand (Supharatid, 2015; Ruangrassamee et al., 2015; Wetchayont and Chotpantarat, 2015). These projections are part of the Coupled Model Intercomparison Project Phase 5 (CMIP5), specifically utilizing the RCP4.5 and RCP8.5 scenarios. The values 4.5 and 8.5 represent the projected increase in radiative forcing by the year 2100 (Lee et al., 2021).

2.5.1 RCP4.5

RCP4.5 is an intermediate stabilization scenario that assumes the implementation of climate policies and mitigation measures to limit greenhouse gas emissions. Under this scenario, atmospheric CO_2 concentrations are projected to reach approximately 520 parts per million (ppm) within the next few decades, representing a significant increase compared to 2000 levels. (Furphy, 2013; Hausfather, 2019).

2.5.2 RCP8.5

RCP8.5 is a simulation of the worst-case scenario of greenhouse gas emissions without measures to control greenhouse gas reduction. It predicts that greenhouse gas emissions will increase rapidly. The concentration of carbon dioxide in the atmosphere is expected to exceed 900 parts per million by 2100. This is almost 4 times the 8 gigatons of carbon dioxide emissions per year in 2000 (Riahi et al., 2011; Furphy, 2013; Hausfather, 2019).

2.6 Statistical testing

The current and future projected annual streamflow were compared using Welch's t-test to assess the statistical significance of changes in streamflow patterns under climate change scenarios.

3. RESULTS AND DISCUSSION

The effects of climate change on the streamflow in the upper Lam Nam Chi and Lam Saphung subwatershed can be explained by applying the SWAT model as follows:

3.1 SWAT model calibration

There were 7 parameters that were related and sensitive to the amount of streamflow in the upper Lam Nam Chi and Lam Saphung subwatershed. The parameter having the most impact on the amount of streamflow was the curve number, CN2 that was related to the surface runoff coefficient, describing the relationship between the soil's permeability and the antecedent soil water conditions, including the land use of the study area. The next parameters were related to groundwater, namely GWQMN and GW_DELAY, followed by the parameter related to the hydrological response unit, namely ESCO, while the soil parameters were SOIL_AWC, SOIL_K, and SOIL_Z. The details of these parameters are shown in Table 1.

Table 1. Sensitive parameters, their descriptions, and calibrated values for streamflow simulation

Parameters	Description	File type	Value
CN2	surface runoff coefficient	.mgt	88-97
GWQMN	Threshold depth of water in the shallow aquifer required for return flow	.gw	0-300
GW_DELAY	Groundwater delay time	.gw	1-20
ESCO	Soil evaporation	.hru	0.65
SOIL_AWC	Available water capacity of the soil layer	.sol	0.4-0.9
SOIL_K	Depth from soil surface to bottom of layer (mm)	.sol	1-300
SOIL_Z	Saturated hydraulic conductivity	.sol	80-120

After adjusting the sensitive parameters, the accuracy and compatibility of the monthly flow rates were evaluated by comparing the SWAT model outputs with the observed streamflow data from the Royal Irrigation Department for the upper Lam Nam Chi and Lam Saphung subwatersheds. For station E.32A, the NSE and PBIAS values were 0.5 and -10.67%, respectively. These results indicate that the

model performance is satisfactory, although the negative PBIAS suggests a slight overestimation. In contrast, for station E.83, the model showed a higher performance with an NSE of 0.62, while the PBIAS of -0.75% was categorized as very good according to the guidelines of Moriasi et al. (2007). This exceptionally low PBIAS suggests that the model achieved an excellent water balance and total volume estimation, which is a critical requirement for a reliable hydrological assessment. Based on this analysis, the model's performance in simulating streamflow was satisfactory for this study area. This was consistent with Prasancham et al. (2022), who studied the efficiency of the SWAT model in simulating the streamflow of the Mun River Basin, with their analysis indicating that the model was effective in simulating the streamflow at a reliable level, especially in the watershed area without water storage projects. In addition, based on the results from the current study, the model calibration with time series plots produced a streamflow curve from the model assessment whose fluctuations were similar to the observed streamflow. However, the peak flow was lower than the values obtained from both monitoring stations, especially during 2020-2022. The results as shown in Figure 2.

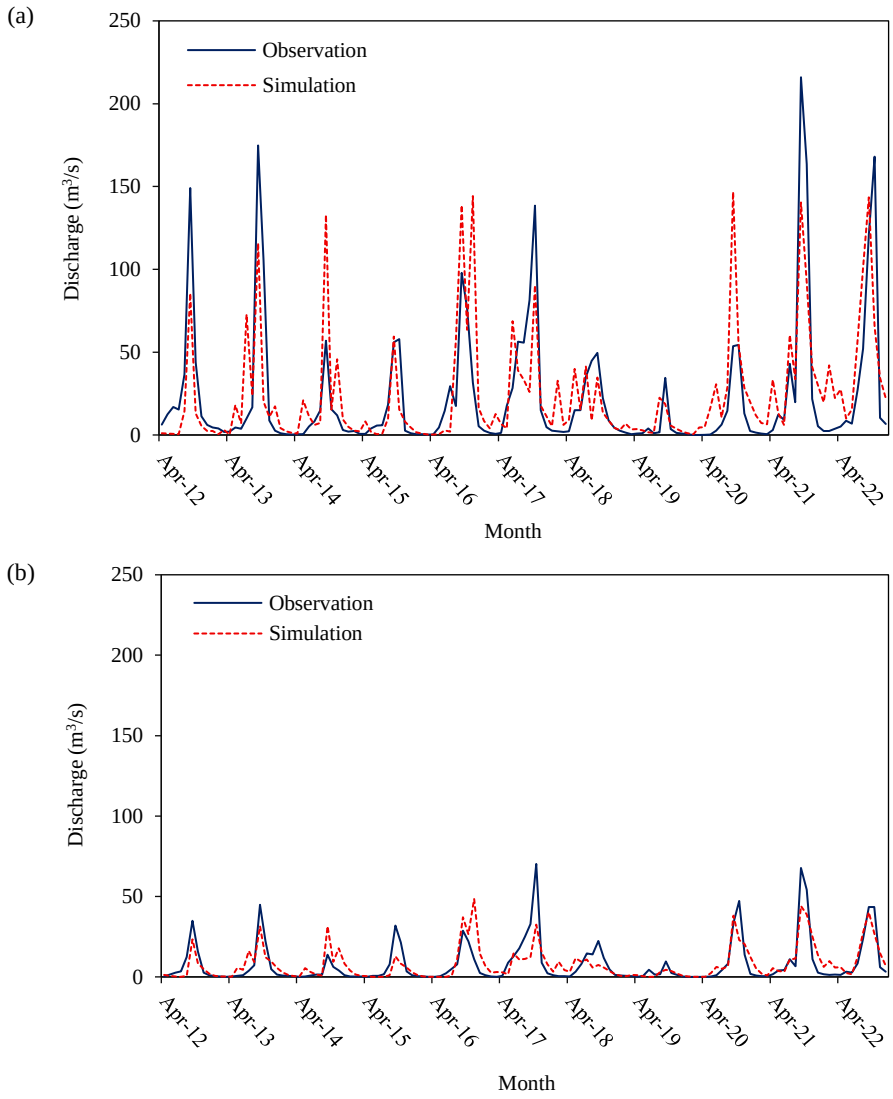


Figure 2. Calibration results for SWAT Model: (a) Station E.32A; (b) Station E.83, where NSE=Nash-Sutcliffe efficiency and PBIAS=Percent bias

3.2 Streamflow estimation for current situation using SWAT model

After calibration of the SWAT model, the streamflow was estimated for the current situation (using climatic data for 2012-2022). Based on these results, the average annual streamflow for 2012-2022 (11 years) in the upper Lam Nam Chi and Lam Saphung subwatershed was 856.40 million cubic

meters per year (MCM; 75.03 percent of annual rainfall). The highest average streamflow was in 2022 (1,650.13 MCM) and the lowest was in 2019 (221.39 MCM). The highest average monthly streamflow was in September (275.04 MCM) and the lowest was in January (16.27 MCM). In addition, during the wet period (May-October), the average streamflow was 645.66 MCM or 75.39 percent of the average annual streamflow while during the dry period (November-April), the average discharge was 210.75 MCM or 24.61 percent of the average annual streamflow. The results are shown in Table 2.

Table 2. Streamflow simulated by the SWAT model at upper Lam Nam Chi and Lam Saphung Subwatershed during 2012 to 2022

Month / Year	Streamflow (MCM)												
	Jan	Feb	Mar	Apr	May	Jun	Jul	Aug	Sep	Oct	Nov	Dec	Total
2012	0.19	0.00	38.95	2.18	2.21	2.11	1.90	46.07	247.35	36.60	14.42	6.61	398.59
2013	7.16	0.91	9.27	0.40	53.81	19.09	220.77	69.50	335.78	57.58	28.51	52.28	855.07
2014	11.20	5.37	3.08	1.99	62.10	33.45	18.09	22.43	387.36	43.30	130.38	25.17	743.93
2015	13.02	6.19	6.15	23.11	5.23	1.24	2.69	31.29	174.14	44.04	21.51	12.84	341.45
2016	4.56	1.82	0.47	0.58	1.37	8.92	5.81	174.61	401.96	186.41	414.19	43.74	1,244.43
2017	22.88	9.83	7.66	8.60	11.24	201.56	116.76	99.52	73.32	267.17	46.38	31.79	936.71
2018	14.67	88.16	16.87	24.52	119.16	42.58	125.34	25.00	103.25	40.12	25.15	13.35	638.16
2019	9.17	19.54	9.67	9.94	7.87	4.73	3.60	71.16	53.81	15.94	10.36	5.60	221.39
2020	3.06	1.17	13.65	13.26	50.89	90.36	30.33	86.77	427.00	160.19	76.81	56.63	1,010.11
2021	34.20	19.39	19.33	96.09	38.83	16.52	185.20	99.77	403.74	268.82	111.80	86.82	1,380.50
2022	58.88	114.65	66.40	79.64	29.84	46.42	174.42	303.14	417.71	192.94	99.41	66.68	1,650.13
Average	16.27	24.27	20.14	24.57	34.78	42.45	80.45	93.57	275.04	119.37	88.99	36.50	856.40

3.3 Streamflow estimation for climate change scenarios

Assessment of streamflow was carried out in the upper Lam Nam Chi and Lam Saphung subwatershed under climate change scenarios, RCP4.5 and RCP8.5, during 2041-2100 (60 years) by dividing the analysis into 3 periods: near-term (2041-2060), medium-term, (2061-2080), and long-term (2081-2100). The results of the study are discussed as follows:

3.3.1 Using climate data from RCP4.5

In the near-term, the average annual streamflow was 2,176.21 MCM, with the highest streamflow in 2060 (3,850.98 MCM) and the lowest in 2042 (903.31 MCM). In the medium-term, the average annual streamflow was 2,729.75 MCM, with the highest streamflow being 6,101.67 MCM in 2069 and the lowest was 1,014.80 MCM in 2064. In the long-term, the average annual streamflow was 2,742.36 MCM, with the highest and lowest streamflow being 5,215.77 and 1,176.41 MCM in 2092 and 2081, respectively.

The average annual streamflow during the wet period (May-October) for the near-term was 1,837.80 MCM or 84.45 percent of the average annual streamflow, while during the dry period (November-April) it was 338.41 MCM or 15.55 percent of the average annual streamflow. In the medium-term, the average annual streamflow in wet and dry periods were 2,307.95 and 421.80 MCM, which were 84.55 and 15.45 percent of the average annual streamflow, respectively. Finally, the average annual streamflow during the wet and dry periods in the long-term were 2,406.75 and 335.61 MCM, which corresponded to 87.76 and 12.24 percent of the average annual streamflow, respectively.

The highest average monthly streamflow during all 3 periods were in August (639.54, 838.94, and 779.51 MCM in near-term, medium-term, and long-term, respectively). However, although the lowest values for the medium-term and long-term were in April (27.88 and 3.45 MCM, respectively), for the near-term, the lowest value was in May (18.03 MCM), as shown in Table 3.

3.3.2 Using climate data from RCP8.5

In the near-term, medium-term, and long-term, the average annual streamflow was 2,644.63, 2,842.99, and 3,858.43 MCM, respectively. The near-term had the highest volume in 2056 (5,155.52 MCM) and the lowest volume in 2045 (771.81 MCM). The average annual streamflow was 2,248.03 MCM in the wet period (85.00 percent of the average annual streamflow) and 396.60 MCM in the dry period (15.00 percent of the average annual streamflow). The medium-term had the highest streamflow in 2064 (4,645.66 MCM and the lowest in 2069 (1,292.96 MCM). During the wet and dry periods, the average annual streamflow was 2,395.25 and 447.75 MCM,

respectively, or 84.25 and 15.75 percent of the average annual streamflow, respectively. Furthermore, the highest streamflow in the long-term was 7,268.79 MCM in 2092 and the lowest was 898.05 MCM in 2082. The average annual streamflow was 3,302.27 MCM in the wet period and 556.16 MCM in the dry period, or 85.59 and 14.41 percent of the average annual streamflow, respectively.

The average monthly streamflow was the highest in the near-term and long-term in August, while it was July in the medium-term (825.18, 1,108.85, and 748.49 MCM, respectively). In addition, the lowest volumes in the near-term and medium-term were 26.14 and 30.40 MCM, respectively, in April, whereas in the long-term it was in May (30.14 MCM). The results are summarized in Table 3 and Figure 3.

Comparing the streamflow for the different climate change scenarios, the average annual streamflow from RCP8.5 was higher than that from RCP4.5. However, compared to the streamflow in the current scenario, the streamflow from RCP4.5 and RCP8.5 in the near-term increased from the current situation by 1,319.81 and 1,788.23 MCM, respectively. In the medium-term, the streamflow of both scenarios were slightly different, with RCP8.5 being 113.24 MCM higher than RCP4.5. Furthermore, the streamflow in RCP4.5 and RCP8.5 tended to be greater than in the current situation, namely to 1,873.35 and 1,986.59 MCM, respectively. In the long-term, the greatest difference was between the streamflow of RCP4.5 and RCP8.5, equaling 1,116.07 MCM. Compared to the current situation, the streamflow from RCP4.5 and RCP8.5 increased substantially by 1,885.96 and 3,002.03 MCM, respectively, or 320.21 and 450.54 percent, respectively. This result was due to the rainfall in the future scenario being greater than currently, especially in the long-term for RCP8.5. The results are shown in Table 3 and Figure 3.

Table 3. Streamflow prediction based on SWAT modeling by climate change scenario

Month	Streamflow (MCM)						
	2012-2022	2041-2060		2061-2080		2081-2100	
	Present	RCP4.5	RCP8.5	RCP4.5	RCP8.5	RCP4.5	RCP8.5
January	16.27	55.85	68.36	71.84	76.89	43.68	93.88
February	24.27	36.58	44.08	47.04	51.39	15.23	63.68
March	20.14	30.09	35.40	37.80	41.43	6.85	50.42
April	24.57	21.33	26.14	27.88	30.40	3.45	36.60
May	34.78	18.03	27.23	45.31	41.36	31.24	30.14
June	42.45	175.77	133.14	226.36	161.56	216.54	240.35
July	80.45	463.99	685.91	600.64	748.49	638.97	979.54
August	93.57	639.54	825.18	838.94	695.89	779.51	1108.85
September	275.04	386.00	411.59	384.54	533.01	462.53	706.90
October	119.37	154.47	164.98	212.16	214.94	277.97	236.49
November	88.99	111.03	122.53	134.93	137.87	167.12	181.73
December	36.50	83.54	100.09	102.31	109.78	99.29	129.85
Total	856.40	2,176.21	2,644.63	2,729.75	2,842.99	2,742.36	3,858.43
Difference from current situation (%)	-	254.11	308.81	318.75	331.97	320.21	450.54

3.4 Effects of climate change on streamflow in upper Lam Nam Chi and Lam Saphung subwatershed

Based on the results, climate change under the RCP4.5 and RCP8.5 scenarios would increase the annual streamflow of the upper Lam Nam Chi and Lam Saphung subwatershed. Specifically, the streamflow under the RCP8.5 scenario in the long term (2081-2100) is projected to be more than 4 times higher than the current situation, contingent upon Thailand facing the worst-case conditions represented by the RCP8.5 scenario. This projection assumes a trajectory where greenhouse gas emissions continue to rise unabated without any mitigation measures through the end of the century. Under this pathway, greenhouse gas emissions are expected to increase rapidly, with atmospheric carbon dioxide concentrations exceeding 900 parts per million by 2100 nearly four times the 8 gigatons of carbon dioxide emitted per year in 2000 (Riahi et al., 2011;

Furphy, 2013; Hausfather, 2019). These findings underscore the potential hydrological risks Thailand may encounter if global climate actions fail to deviate from the RCP8.5 pathway. Furthermore, these results are consistent with Vo et al. (2018), who found that streamflow in Vietnam significantly increases under the RCP8.5 scenario. Similarly, Gao et al. (2021) estimated the impact of climate change in China and found that streamflow under RCP8.5 increases significantly from 2080 onwards.

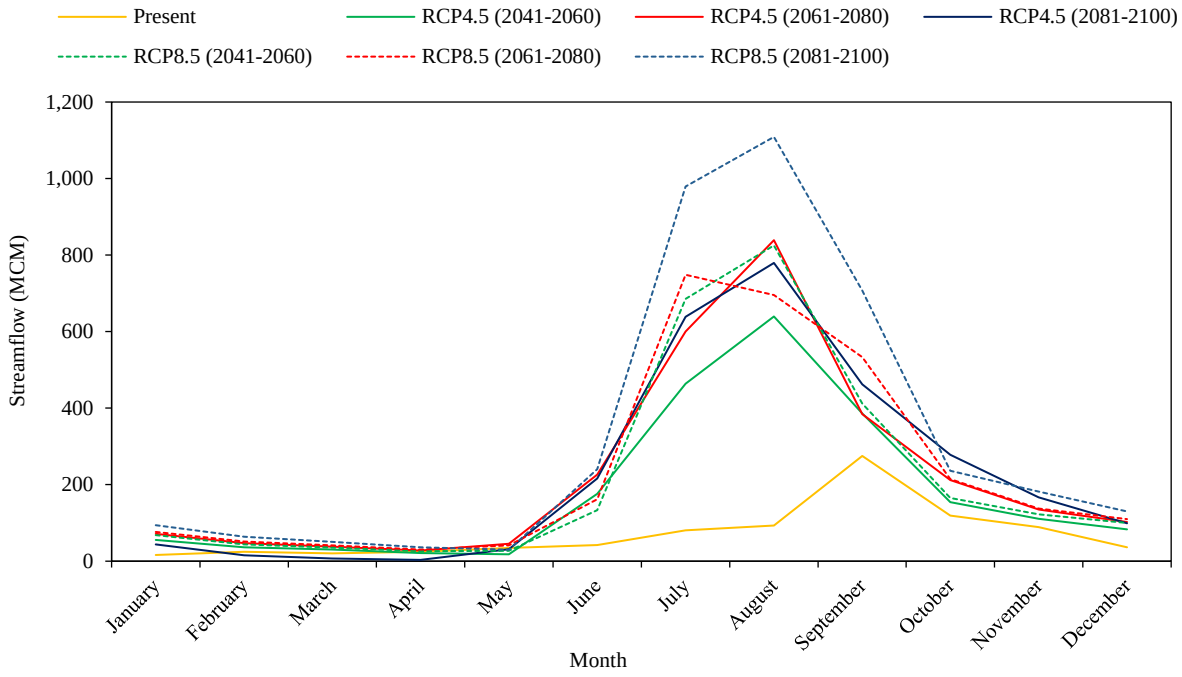


Figure 3. Streamflow in upper Lam Nam Chi and Lam Saphung Subwatershed under RCP4.5 and RCP8.5 scenarios compared to current situation

In the current scenario, the wet period's highest streamflow occurred in September. However, under climate change scenarios, the peak streamflow shifted to July and August. This shift resulted from the peak precipitation projected by the CMIP5 models, which may exhibit uncertainties associated with future greenhouse gas emission scenarios. Similarly, the dry period's lowest streamflow, originally in January, moved to April and May. Consequently, the timing of the wet and dry periods within the upper Lam Nam Chi and Lam Saphung Subwatershed would alter compared to present conditions. This could be attributed to a projected increase in rainfall under the RCP4.5 and RCP8.5 scenarios. In particular, in the long-term (2081-2100) under RCP8.5, the average annual rainfall greatly increased, and the peak rainfall month shifted to July and August. These findings were consistent with Vechpanich (2015), who studied the effects of climate change on streamflow in the upper Chao Phraya River Basin using the MRI-AGCM3.2 (AR5) model. That study reported that the rainfall in future rainy seasons would be quite volatile and much higher than in the past, resulting in a higher streamflow in the rainy season than in the past. Furthermore, this was consistent with Chacuttrikul et al. (2018) who studied the impacts of climate and land use changes on streamflow in northeast Thailand and found that climate change had a greater effect on streamflow, with the main factor being the amount of rain. To determine the significance of the projected changes, a Welch's t-test was performed to compare the current scenario and future projections. The results indicated that the increases in annual streamflow under both the RCP4.5 and RCP8.5 scenarios are statistically significant ($p<0.01$).

Finally, the average monthly streamflow under the RCP4.5 and RCP8.5 scenarios was projected to exceed that of the current scenario, particularly during the wet season. This intensified streamflow is likely to result in more severe flooding within the subwatershed during future wet periods. While streamflow in dry periods is also projected to be slightly higher, the risk of drought persists in certain years.

4. CONCLUSION

The SWAT model was effective in estimating streamflow in the upper Lam Nam Chi and Lam Saphung Subwatersheds. Based on the calibration results, the NSE and PBIAS values indicated that the model's performance was satisfactory. Streamflow estimated using the SWAT model under the RCP4.5 and RCP8.5 climate change scenarios for the near-term (2041-2060), medium-term (2061-2080), and long-term (2081-2100) indicated a major increasing trend compared to the current situation. Furthermore, shifts were observed in the months of maximum and minimum streamflow. The estimated monthly streamflow increased notably during the wet period, especially in the scenario without measures and policy for GHG emission control (RCP8.5). Therefore, this may result in severe flooding problems in the upper Lam Nam Chi and Lam Saphung subwatershed, particularly during the wet period, while drought problems may still persist. Ultimately, these findings provide a vital scientific basis for policymakers to formulate proactive disaster mitigation plans and optimize hydraulic infrastructure to better withstand future climatic extremes.

ACKNOWLEDGEMENTS

The Thai Meteorological Department, the Royal Irrigation Department, and Department of Land Development, Thailand provided meteorological data, hydrological data, and land use data, respectively.

AUTHOR CONTRIBUTIONS

Conceptualization, S.T. and P.C.; Methodology, S.T., C.S. and P.C.; Data Curation, S.T., C.S. and P.C.; Writing-Original Draft Preparation, S.T. and P.C.; Writing-Review and Editing, S.T. and P.C.; Supervision, S.T.; Project Administration, S.T.

DECLARATION OF CONFLICT OF INTEREST

The authors declare that there are no conflicts of interest.

REFERENCES

Budhathoki A, Tanaka T, Tachikawa Y. Correcting streamflow bias considering its spatial structure for impact assessment of climate change on floods using d4PDF in the Chao Phraya River Basin, Thailand. Journal of Hydrology: Regional Studies 2022;42:Article No. 101150.

Chacuttrikul P, Kiguchi M, Oki T. Impacts of climate and land use changes on river discharge in a small watershed: A case study of the Lam Chi Subwatershed, Northeast Thailand. Hydrological Research Letters 2018;12(2):7-13.

Chacuttrikul P, Thueksathit S. Estimating land use change effects on groundwater recharge in Nadi and Kabinburi, Thailand. Environment and Natural Resources Journal 2023;21(5):471-8.

Department of Water Resources. Natural water routes according to FGDS standards [Internet]. 2024 [cited 2025 May 22]. Available from: https://gis.dwr.go.th/portal/home/webmap/viewer.html?webmap=27baac5c7a9f40a9aec56576af69a072&extent=85.409,4.3301,117.7308,21.642.

Furphy D. What on Earth is an RCP? [Internet]. 2013 [cited 2025 May 22]. Available from: https://medium.com/@davidfurphy/what-on-earth-is-an-rcp-bbb206ddee26.

Gao D, Chen T, Yang K, Zhou J, Ao T. Projecting the impacts of climate change on streamflow in the upper reaches of the Yangtze River Basin. Journal of Water and Climate Change 2021;12(5):1724-43.

Hausfather Z. Explainer: The high-emissions 'RCP8.5' global warming scenario [Internet]. 2019 [cited 2025 May 22]. Available from: https://www.carbonbrief.org/explainer-the-high-emissions-rcp8-5-global-warming-scenario.

Ingrao C, Strippoli R, Lagioia G, Huisingh D. Water scarcity in agriculture: An overview of causes, impacts and approaches for reducing the risks. Heliyon 2023;9(8):1-16.

Institute of Water and Agricultural Resources Information (Public Organization). Data Collection and Analysis for the Development of Data Warehousing System for 25 Watersheds and Flood and Drought Models Project [Internet]. 2012 [cited 2025 May 22]. Available from: https://tiwrm.hii.or.th.

Kiguchi M, Takata K, Hanasaki N, Archevarahuprok B, Champathong A, Ikoma E, et al. A review of climate-change impact and adaptation studies for the water sector in Thailand. Environmental Research Letters 2021;16(2):Article No. 023004.

Land Development Department. Summary of Land Use Types, Thailand 2019 [Internet]. 2019 [cited 2025 May 22]. Available from: https://dinonline.ldd.go.th.

Lee J-Y, Marotzke J, Bala G, Cao L, Corti S, Dunne JP, et al. Future Global Climate: Scenario-Based Projections and Near-Term Information. In: Climate Change 2021: The Physical Science Basis. Contribution of Working Group I to the Sixth Assessment Report of the Intergovernmental Panel on Climate Change (IPCC). United Kingdom and USA: Cambridge University Press; 2021. p. 553-672.

Li C, Fang H. Assessment of climate change impacts on the streamflow for the Mun River in the Mekong Basin, Southeast Asia: Using SWAT model. Catena 2021;201:Article No. 105199.

Makumbura R, Gunathilake M, Samarasinghe J, Confesor R, Muttil N, Rathnayake U. Comparison of calibration approaches of the Soil and Water Assessment Tool (SWAT) Model in a tropical watershed. Hydrology 2022;9(10):1-21.

Moriasi D, Arnold J, Van Liew M, Bingner R, Harmel R, Veith T. Model evaluation guidelines for systematic quantification of accuracy in watershed simulations. American Society of Agricultural and Biological Engineers 2007;50(3):885-900.

Moriasi D, Gitau M, Pai N, Daggupati P. Hydrologic and water quality models: Performance measures and evaluation criteria. American Society of Agricultural and Biological Engineers 2015;58(6):1763-85.

National Water Resources Office. Chi River Basin Information [Internet]. 2021 [cited 2025 May 22]. Available from: http://rbmd.onwr.go.th.

Nash JE, Sutcliffe JV. River flow forecasting trough conceptual models, Part1: A discussion of principles. Journal of Hydrology 1970;10(3):282-90.

Neitsch SL, Arnold JG, Kiniry JR, Srinivasan R, Williams JR. Soil and Water Assessment Tool User's Manual Version 2000. Texas, United states: Water Resources Institute; 2002.

Neitsch SL, Arnold JG, Kiniry JR, Williams JR. Soil and Water Assessment Tool Theoretical Documentation Version 2009. Texas, United states: Water Resources Institute; 2011.

Panneerselvam B, Charoenlerkthawin W, Ekkawatpanit C, Namsai M, Bidorn B, Saravanan S, et al. Climate change influences on the streamflow and sediment supply to the Chao Phraya River Basin, Thailand. Environmental Research 2024;251:Article No. 118638.

Prasancham H, Chaovivat W, Muangthong S, Sarinnapakorn K, Boonyarunnet S. Evaluation of SWAT hydrological model performance for runoff simulation using multi-site calibration and validation techniques in Mun River Basin. Proceedings of the 27th National Convention on Civil Engineering; 2022 August 24-26; The Heritage Chiang Rai, Chiang Rai: Thailand; 2022.

Ruangrassamee P, Khamkong A, Chuenchum P. Assessment of precipitation simulations from CMIP5 climate models in Thailand. Proceedings of the 3rd EIT International Conference on Water Resources Engineering (ICWRE3); 2015 August 5-7; Centara Hotel and Convention Centre, Udon Thani: Thailand; 2015.

Riahi K, Rao S, Krey V, Cho C, Chirkov V, Fischer G, et al. RCP 8.5—A scenario of comparatively high greenhouse gas emissions. Climate Change 2011;109:33-57.

Royal Forest Department. SWAT User Manual [Internet]. 2021 [cited 2025 May 22]. Available from: https://pubhtml5.com/perl/zuze/basic.

Royal Irrigation Department. Work Manual: A Study of the Relationship between Average Annual Streamflow and Catchment Area in 25 Major River Basins of Thailand. Thailand: Royal Irrigation Department, Bangkok; 2018.

Supharatid S. Assessment of CMIP3-CMIP5 climate models precipitation projection and implication of flood vulnerability of Bangkok. American Journal of Climate Change 2015;4:140-62.

The Meteorological Department. Meteorological Measurement and statistics service [Internet]. 2024 [cited 2025 May 22]. Available from: https://data-service.tmd.go.th.

Thueksathit S, Tuankrua V, Prasanai K, Chacuttrikul P. Application of SWAT model for estimate the effect of Land Use to Streamflow at Mae Thang subwatershed, Phrae Province. Thai Forest Ecological Research Journal 2023; 7(1):79-92 (in Thai).

Vechpanich E. Climate and Land Use Change Impact Assessment on Rainfall-Runoff Simulations Using SiBUC Model: A Case Study in The Upper Chao Phraya River Basin [dissertation]. Chulalongkorn University; 2015.

Vo ND, Nguyen QB, Vu HC, Gourbesville P, Nguyen TH. Effects of climate change on streamflow in Kon-Ha Thanh River Watershed, Vietnam. Proceedings of 13th International Conference on Hydroinformatics, HIC 2018; 2018 July 1-6; Palermo: Italy; 2018.

Wetchayont P, Chotpantarat S. Evaluation of precipitation over Northern Thailand in CMIP5 MRI-CGCM3 Simulations. Proceedings of THA 2015 International Conference on "Climate Change and Water and Environmental Management in Monsoon Asia"; 2015 January 28-30; Bangkok: Thailand; 2015.

Environment and Natural Resources Journal

Volume 24
Issue 6
2026

Changes in Carbon Stocks and the Economic Value of Forest Carbon in a Secondary Forest of Mt. Nacolod, Silago, Southern Leyte, Philippines

Christian Albert L. Martinez[1*], Renezita S. Come[1*], Dennis P. Peque[1], Moises Neil V. Seriño[2], and Melvin Lippe[3]

[1]Faculty of Forestry and Environmental Science, Visayas State University, Baybay City, Philippines
[2]Faculty of Management and Economics, Visayas State University, Baybay City, Philippines
[3]Johann Heinrich von Thünen Institute, Institute of Forestry, Hamburg, Germany

ARTICLE INFO

Received: 18 Nov 2025
Received in revised: 17 Jun 2026
Accepted: 30 Jun 2026
Published online: 26 Aug 2026
DOI: 10.32526/ennrj/24/20250329

Keywords:
Carbon sequestration/ Forest carbon/ Economic valuation/ Tropical secondary forest/ Permanent plots

*** Corresponding author:**
E-mail:
christian.martinez@vsu.edu.ph

ABSTRACT

Tropical forests play a critical role in climate mitigation, yet long-term data on their carbon dynamics remain scarce, particularly in the Philippines. This study examines forest structure and carbon sequestration in a 1-hectare permanent plot established in a secondary forest on Mt. Nacolod, Southern Leyte, Philippines using 2012, 2016, and 2024 tree inventory data. The study aimed to (1) assess biomass and carbon storage trends, and (2) estimate the economic value of carbon. The secondary forest stored 202.4 Mg C/ha, comparable to reported values of old-growth forests in the Philippines. Its sequestration rate of 2.53 Mg C/ha/year is approximately nine times faster than old-growth forests and exceeds regional dipterocarp regrowth rates. Although sequestration slowed post-2016, the site remained a robust carbon sink. The estimated economic value of the stand's carbon stock increased from USD 4,798 in 2012 to USD 7,220 in 2024, while carbon sequestered over the 12 years was valued at USD 1,076 under prevailing carbon credit prices. Key findings underscore the dominance of Dipterocarpaceae and the site's high carbon sequestration capacity, emphasizing its critical role in regional climate mitigation strategies. Continuous monitoring reinforces its value as a long-term carbon sink, providing a benchmark for conservation and climate policy for tropical forests in the region.

HIGHLIGHTS

The permanent plot stored 202.4 Mg C/ha which is comparable to reported old-growth forest carbon stock-values. Its sequestration rate was approximately nine times higher than reported old-growth uptake. Dipterocarp stands maintained strong carbon stocks after 2016. Stored carbon represents substantial climate-mitigation and economic value. The site serves as a vital carbon sink and model for tropical forest management.

1. INTRODUCTION

Climate change has led to significant negative consequences, affecting environmental, social, political, and economic systems (Abbass et al., 2022; IPCC, 2023). Forests are essential for climate regulation, carbon sequestration, and biodiversity, playing a central role in climate change mitigation strategies (Bonan, 2008; Kaarakka et al., 2021; Millar and Stephenson, 2015; Mori et al., 2021; Pan et al., 2011; Whitehead, 2011). However, forests face threats from anthropogenic and natural disturbances (Elkin et al., 2013; Kurz et al., 2008; Reyer et al., 2014; Reyer et al., 2017). While natural disturbances are common, increased frequency and intensity may exceed the forests' adaptive capacity, degrading ecosystem services crucial for climate mitigation (Dale et al., 2000; Marcos-Martinez et al., 2019; Trumbore et al., 2015).

Climate change will substantially influence forests and may alter their composition and structure (Dale and Rauscher, 1994). Recent studies show that climate change will exacerbate forest disturbance impacts, with potentially far-reaching ecological and socioeconomic consequences (Huo et al., 2019; Seidl et al., 2017). Tropical forests have already exhibited such changes (Condit, 1998; Phillips et al., 2004;

Citation: Martinez CAL, Come RS, Peque DP, Seriño MNV, Lippe M. Changes in carbon stocks and the economic value of forest carbon in a secondary Forest of Mt. Nacolod, Silago, Southern Leyte, Philippines. Environ. Nat. Resour. J. 2026;24(6):723-736. (https://doi.org/10.32526/ennrj/24/20250329)

Phillips and Gentry, 1994). Under certain climate scenarios, existing carbon stocks in tropical forests may become significant carbon sources, even without further deforestation (Cox et al., 2000; Cramer et al., 2001). Furthermore, remnant forests face degradation and fragmentation from climate change and other pressures, with extinction risk for species unable to rapidly adapt (Deb et al., 2016).

Long-term forest dynamics, crucial for conservation and management, can be studied through permanent plots (Baithalu et al., 2013; Brearley et al., 2019). These plots enable the study of long-term changes in tree communities under human pressure and climate change (Chazdon et al., 2005; Murthy et al., 2016). Research on tropical forest biomass and carbon stocks is crucial for assessing atmospheric CO_2 removal, estimating net carbon gains, and improving conservation and management strategies (Heriansyah et al., 2007; Siregar and Heriyanto, 2010; Subiandono et al., 2013). Biomass data also provide insights into ecosystem productivity (Nelson et al., 1999).

Beyond ecological roles, forests provide measurable economic value through carbon markets and climate finance. Carbon credits, representing one metric ton of CO_2 equivalent sequestered or avoided, have become central to global climate policy under frameworks such as REDD+ (Fuss et al., 2021; UN-REDD Programme, 2023). Protecting and enhancing tropical forest carbon stocks can generate billions in potential cost savings for climate stabilization (Scheinkman, 2024). In the Philippines, legislative initiatives aim to establish a domestic carbon crediting system aligned with the Paris Agreement, highlighting the growing relevance of forest carbon valuation (Enviliance ASIA, 2023).

Permanent plots are particularly valuable as they provide long-term, verifiable data on biomass and carbon dynamics, essential for credible carbon accounting and valuation (PennState Extension, 2023; Phillips, 2023). By linking ecological monitoring with economic valuation, permanent plots serve as reference sites demonstrating the potential of secondary forests to contribute to biodiversity conservation and climate finance opportunities. This is especially relevant for Eastern Visayas, Philippines, where extensive upland and mangrove forests store substantial carbon stocks, highlighting both ecological resilience and potential for carbon markets (Asilo and Yap-Dejeto, 2025; Meniano, 2024).

Given climate change's global impact, long-term forest monitoring is crucial for understanding forest structure, dynamics, and ecosystem functions. This study investigated current carbon storage and sequestration changes within a one-ha permanent plot measured in 2012, 2016 and 2024 in a Long-Term Ecological Research (LTER) site established in Barangay Catmon, Silago, Southern Leyte in 2012. Specifically, it aimed to: (1) assess current biomass, carbon storage and sequestration trends over time; and (2) estimate the economic value of stored and sequestered carbon.

2. METHODOLOGY

2.1 Site description

The study was conducted in a one-hectare subplot within the 50-hectare permanent ecological research plot in Mt. Nacolod, Barangay Catmon, Silago, Southern Leyte (10°5'45"N, 125°09'30"E) (Figure 1). This area, known as Silago Biodiversity Research Station or SilBioRS, was established for long-term ecological research on forest structure, dynamics, and processes (Philippine Tropical Forest Conservation Foundation, 2013).

The province of Southern Leyte is characterized by a type IV climate featuring evenly distributed rainfall throughout the year, averaging 2,565.4 mm annually. Based on the Köppen-Geiger climate classification at 1-km resolution (Beck et al., 2018), the province falls under the Af (tropical rainforest) category, characterized by consistently high rainfall and absence of a pronounced dry season. Elevation in the study area ranges from 577-582 meters above sea level (Jarvis et al., 2008). Southern Leyte's mountainous areas consist primarily of Ultisols (Barrera et al., 1954), characterized by their acidic nature, clayey texture, and low nutrient levels (Piamonte et al., 2014).

Approximately two-thirds of Silago's forests lie within the Mt. Nacolod Forest Reserve (14,000 ha), recognized as a Key Biodiversity Area (Mallari et al., 2014; NewCAPP, 2014). In October 2012, following the stakeholder presentation of assessment results, the Provincial Board of Southern Leyte approved Ordinance No. 2012-43, designating Mt. Nacolod as a Forest Conservation Area (NewCAPP, 2014).

Mt. Nacolod features diverse vegetation, including tropical lowland forests, secondary forests, and mossy forests (Cabras et al., 2023). The study site was formerly dominated by lowland dipterocarp forests; however commercial logging from the 1950s until 1989, altered the site into a regenerating logged forest or secondary forest (Carandang et al., 2013;

Fernando et al., 2008; Langenberger and Belonias, 2011; Veridiano et al., 2020). At present, the site is under conservation management, although stand dynamics may still be influenced by natural mortality, recruitment, tree competition, and localized human disturbances such as access trails or nearby land-use activities.

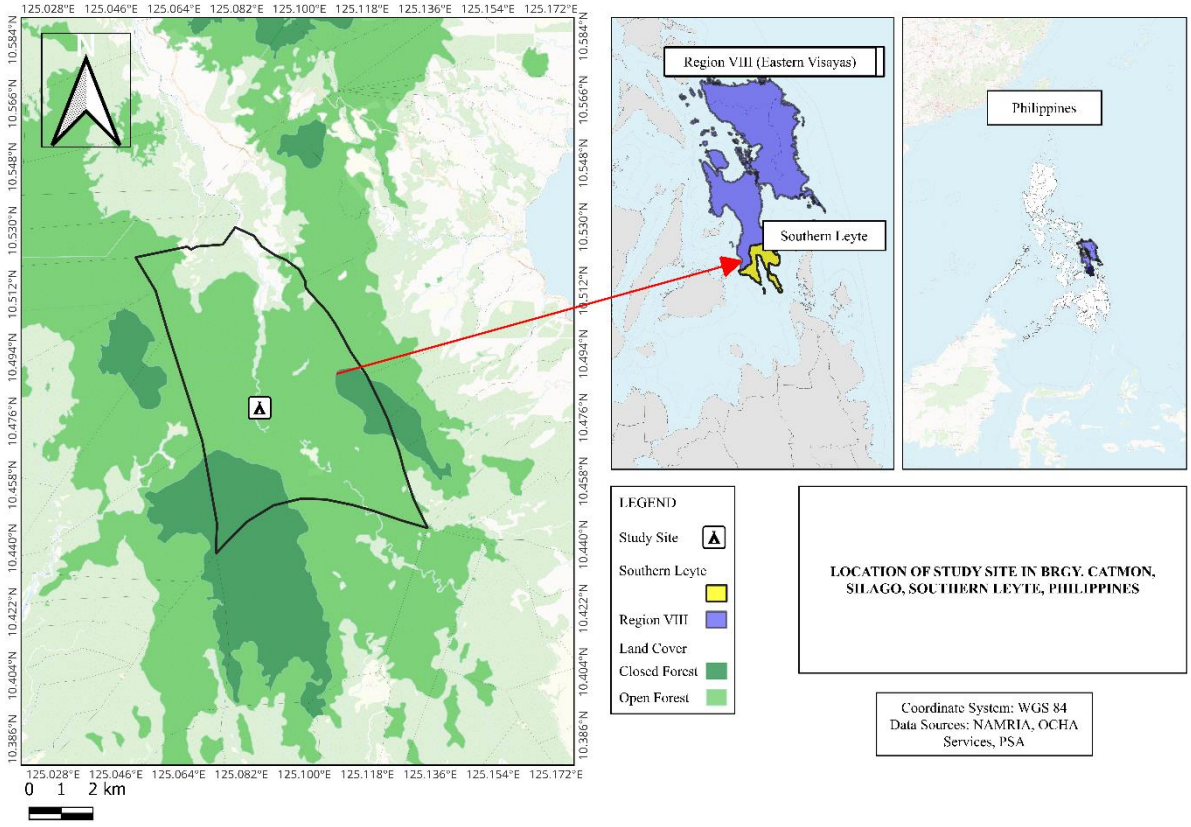


Figure 1. Location map of the study site

2.2 Research design

2.2.1 Plot establishment

This study used secondary data from tree inventories conducted in the one-hectare plot in 2012 and 2016. All calculations and analyses, including 2024 measurements, used the same formulas for biomass and carbon content estimation. The one-hectare plot was used because it forms part of the long-term ecological monitoring design of the Silago Biodiversity Research Station and contains tagged trees with repeated measurements from 2012, 2016, and 2024. The plot location was selected during the original establishment of the permanent ecological research site to represent the regenerating lowland dipterocarp-secondary forest condition of Mt. Nacolod and to allow repeated measurement of the same individuals through time. The analysis is based on a single one-hectare subplot, therefore the results should be interpreted as plot-level evidence of forest recovery and carbon accumulation rather than as a direct estimate for the entire 50-ha research plot or the whole Mt. Nacolod landscape.

The initial 2012 inventory established twenty-five 20 m × 20 m subplots, identified and tagged trees with a diameter at breast height (DBH) ≥10 cm for future remeasurement (Philippine Tropical Forest Conservation Foundation, 2013). In 2016, Veridiano et al. remeasured tagged trees and recorded new recruits that met the DBH criterion (Veridiano et al., 2020). Trees recorded in earlier censuses but no longer alive during remeasurement were treated as mortality and were excluded from live aboveground biomass estimates for the corresponding census year. Newly recruited individuals that reached the ≥10 cm DBH threshold were included in the census year in which they first met the measurement criterion. Thus, net biomass change reflects the combined effects of survivor growth, mortality losses, and recruitment gains. Remeasurement was conducted in 2024 for this study.

2.2.2 Aboveground biomass and carbon content

Height and diameter of trees ≥10 cm DBH were measured and recorded. Aboveground biomass was calculated using the allometric equation (1) developed by Chave et al. (2014) for tropical trees:

$$Y = 0.0673 \times (\rho D^2 H_t)^{0.976} \quad (1)$$

Where; Y=aboveground biomass (kg); ρ=wood density (g/cm^3); D=DBH (cm); H_t=total height (m).

Veridiano et al. (2020) used Chave et al.'s (2014) pantropical allometric equation because country-specific allometric equations for Philippine secondary-growth dipterocarp forests remain limited (Lasco and Pulhin, 2009). The present study applied the same equation to maintain comparability with the 2012 and 2016 secondary data. While the equation is suitable for broad tropical forest applications—incorporating DBH, tree height, and wood density—it may introduce uncertainty when applied to this specific Philippine secondary forest due to local variation in tree architecture, wood density, disturbance history, and stand structure. Tree carbon content was computed as 50% of aboveground biomass, a default value used in studies (Brown and Lugo, 1992; Malhi et al., 2004; Roy et al., 2001). This study focused only on live aboveground tree biomass and therefore provides a conservative estimate of total forest carbon stock. Other major forest carbon pools, including belowground biomass, deadwood, litter, and soil organic carbon, were not included because comparable measurements were unavailable across the census periods. Forest carbon pools include living aboveground and belowground biomass, dead organic matter, and soil organic matter, therefore the actual total carbon stock and potential economic value of the site are likely higher than reported here.

2.2.3 Carbon accounting

This study used the inventory approach to estimate carbon-stock change and sequestration between inventory periods (2012, 2016, and 2024). The formula, Equation (2), adapted from UNDP Forest Carbon Accounting: Overview & Principles (UNDP, 2015) is:

$$\Delta C = \sum \frac{(C_{t2} - C_{t1})}{(T_2 - T_1)} \quad (2)$$

Where; ΔC=carbon stock change (Mg C/year); C_{t1}=carbon stock (Mg C) at time t_1; C_{t2}=carbon stock (Mg C) at time t_2.

2.2.4 Economic value of carbon

Several studies have used international or national carbon market price averages to estimate the economic value of forest carbon storage (Danardono et al., 2019; Hussainzad and Mohd Yusof, 2020; Pache et al., 2020; Raihan et al., 2021; Rumahorbo et al., 2019). This study used the average forest carbon credit price for each inventory year, from reports published by Forest Trends' Ecosystem Marketplace (Hamrick and Gallant, 2017; Peters-Stanley et al., 2013; Procton, 2024). Recorded prices were used to estimate the economic value of forest carbon storage within the one-hectare plot during inventory years.

This study also compared the site's economic value of aboveground carbon across 2012, 2016, and 2024. To ensure a fair comparison, estimated economic values of carbon stock in 2012 and 2016 were converted to equivalent 2024 U.S. dollar values using the Consumer Price Index (CPI). This adjustment accounts for inflation, allowing a more accurate representation of the economic value of carbon stock. The CPI-based adjustment follows the formula shown in Equation (3):

$$\text{Adjusted Value}_{2024} = \text{Value}_t \times \frac{\text{CPI}_{2024}}{\text{CPI}_t} \quad (3)$$

Where; t represents the year of interest (2012 or 2016). This approach ensures that all values are expressed consistently, reflecting their real economic significance in 2024.

The monetary value of carbon sequestration was determined using established CO_2e pricing as outlined by Gallant et al. (2020). Furthermore, carbon credits are generally issued based on net carbon gains within a project area rather than gross gains from only the highest-performing sections; therefore, the valuation of sequestration should account for the net change in carbon stock across the monitoring period (American Forest Foundation, 2025).

To estimate the economic value of carbon sequestration from 2012 to 2024, this study multiplied net carbon sequestered by the 2023 average carbon credit price of USD 9.72/tCO_2 in forestry and land use. The United Nations Environment Programme (UNEP), through the UN-REDD Programme, indicates that high-quality forest carbon emission reductions are cost-effective but not cheap, with the average cost of forest carbon estimated at approximately USD 30-50/tCO_2. These values should not be interpreted as the market price of the carbon stored in the one-hectare plot alone. Rather, they

reflect the estimated cost of generating high-integrity forest carbon emission reductions, including REDD+ implementation, monitoring, accounting, and opportunity costs. Thus, the present valuation remains conservative because it covers only aboveground carbon sequestration and excludes broader ecosystem services, biodiversity, watershed protection, cultural values, and non-use values (UN-REDD, 2023).

3. RESULTS AND DISCUSSION

3.1 Stand dynamics and aboveground biomass

Across the three census periods, the plot contained 721, 853, and 832 trees with DBH ≥10 cm in 2012, 2016, and 2024, respectively. These recorded trees represented 26 families in 2012 and 2016, and 24 families in 2024, and identified species richness remained stable at 48 species. In 2024, the five most dominant species based on Importance Value Index were *Shorea palosapis* (IVI=39.28), *Pinanga* spp. (IVI=35.52), *Shorea negrosensis* (IVI=34.37), *Shorea almon* (IVI=27.43), and *Lithocarpus celebicus* (IVI=20.34). These results indicate that the stand was structurally dominated by dipterocarps, with increasing ecological importance of palms and declining contribution of Fagaceae. In 2024, the plot was dominated by medium-sized trees, with 673 individuals or 80.9% of all trees falling within the 10-30 cm DBH class. Large trees with DBH >30 cm represented 159 individuals or 19.1% of the stand. Tree height ranged from 2.3 to 62.0 m, with most individuals measuring between 10.1 and 20.0 m tall. This structure indicates that although medium-sized trees were more abundant, larger trees remained important contributors to aboveground biomass and carbon storage.

Total aboveground biomass (AGB) in the one-hectare plot increased steadily across all inventory periods, reflecting ongoing forest growth and carbon accumulation (Table 1). AGB increased from 344.07 Mg/ha in 2012 to 372.82 Mg/ha in 2016, then 404.79 Mg/ha by 2024. Growth slowed over time, with annual gains averaging 7.19 Mg/ha between 2012-2016 and 3.99 Mg/ha from 2016-2024.

Table 1. Aboveground biomass in the site

Year	Biomass (Mg/ha)	Total increment (Mg/ha)	Annual increment (Mg/ha)
2012	344.07	-	-
2016	372.82	28.75	7.19
2024	404.79	31.97	3.99

Dipterocarpaceae consistently represented the largest share of aboveground biomass across all inventory years (Figure 2). In 2012, the family accounted for 195.46 Mg/ha, equivalent to 56.81% of total biomass. This increased to 215.41 Mg/ha, or 57.78%, in 2016 and further to 252.78 Mg/ha or 62.44% in 2024. This sustained increase indicates that biomass accumulation in the plot was largely driven by dipterocarp species, particularly large and mature individuals that persisted across the monitoring period. In 2024, the leading species contributors were *Shorea palosapis* (63.35 Mg/ha), *S. falciferoides* (55.01 Mg/ha), *S. polysperma* (44.86 Mg/ha), *S. almon* (37.19 Mg/ha), *S. negrosensis* (26.58 Mg/ha), and *S. astylosa* (17.75 Mg/ha). Together, these Dipterocarpaceae species confirm the family's central role in maintaining forest structure, biomass retention, and aboveground carbon storage in the secondary forest.

The dominance of Dipterocarpaceae in aboveground biomass reflects the stand structure, where large trees contribute disproportionately despite being fewer than medium-sized trees. Large trees with DBH >30 cm accounted for most of the biomass, contributing 77.81%, 76.29%, and 81.69% of total biomass in 2012, 2016, and 2024, respectively. Although the total number of Dipterocarpaceae individuals slightly declined from 306 in 2016 to 285 in 2024, their relative biomass share increased, highlighting the growth advantage and persistence of surviving large dipterocarps. In contrast, Fagaceae declined from 51.13 Mg/ha (14.86%) in 2012 to 38.13 Mg/ha (9.93%) in 2024, accompanied by a reduction in individual numbers from 96 to 55 and mortality events during the study period. These patterns suggest structural and successional shifts in this regenerating secondary forest, where biomass and carbon storage are increasingly concentrated in large, carbon-dense dipterocarp trees. This interpretation is consistent with recent studies showing that biomass accumulation during secondary succession is influenced by stand maturation, demographic shifts, mortality, and recruitment dynamics (Tian et al., 2023; Ordoñez et

al., 2024). The observed trend may therefore reflect density-dependent competition, shade-driven suppression of smaller stems, and the differential survival and growth of large remnant trees, rather than an increase in overall species diversity.

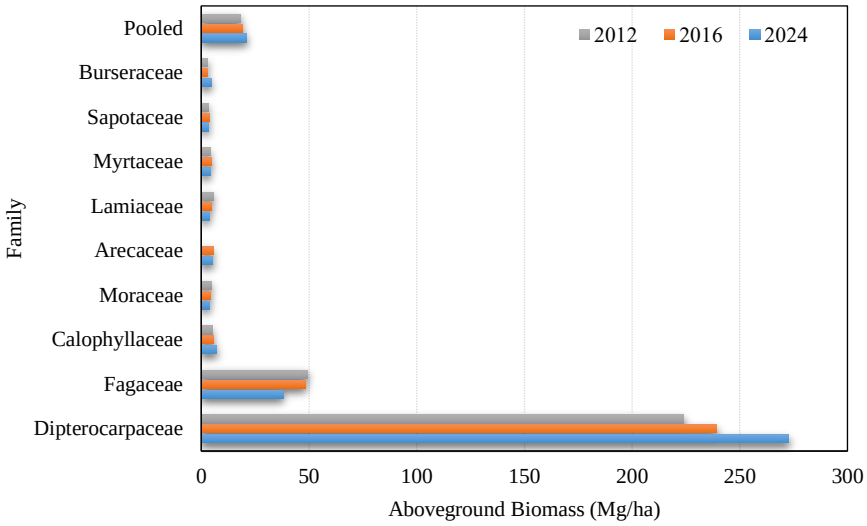


Figure 2. Total aboveground biomass of trees according to family (Note: Pooled refers to the aggregate biomass of the remaining minor tree families at the site)

3.1.2 Comparison of aboveground biomass

Aboveground biomass at the site aligns with published values for various forest types, particularly dipterocarp forests (Table 2). However, as a secondary forest, the site exhibits relatively lower biomass compared to a secondary forest in Mt. Makiling, Philippines.

Araza et al. (2022) compiled a global reference dataset from National Forest Inventories and research networks, encompassing more than 100,000 plots across all major biomes. These plots (0.02 to 25 ha) provided standardized AGB estimates (Mg/ha) for global carbon stock assessments. The study site's AGB is relatively higher than reported average AGB values for tropical forest plots in the global dataset. Within the Asian tropical forest plots compiled by Araza et al. (2022), where AGB values averaged 139.3 Mg/ha and ranged from 25.9 to 703.3 Mg/ha, the study site's AGB falls in the upper portion of this distribution.

Table 2. Aboveground biomass of various sites and forests using various allometric equations

Forest type and location	Aboveground biomass (Mg/ha)	Source
Secondary forest (Mt. Nacolod) (2024)	404.79	This study
Tropical forest plots AGB		
Africa	234.1	Araza et al. (2022)
Asia	139.3	Araza et al. (2022)
Australia	70.4	Araza et al. (2022)
C. America	125.8	Araza et al. (2022)
S. America	326.5	Araza et al. (2022)
Sri Lanka		
Old-growth mixed dipterocarp forest	430.11	Ediriweera et al. (2024)
Philippines		
Secondary forest (Mt. Makiling)	538.05	Lasco et al. (2004)
Selectively logged dipterocarp forest (Surigao del Sur)	399.00	Lasco et al. (2004)
Natural forest (Aurora Province)	131.30	Raga-as (2004)
Plantation forest (Aurora Province)	72.20	Raga-as (2004)
Samar	401.07	Abino et al. (2014)

Differences in AGB among Mt. Nacolod, Mt. Makiling, Samar Island, and other secondary forests may reflect variation in stand age, disturbance history, species composition, soil conditions, rainfall, and the abundance of large trees (Becknell and Powers, 2014; Poorter et al., 2016; Oberleitner et al., 2021). In Mt. Nacolod, the relatively high AGB appears to be associated with the continued dominance of large Dipterocarpaceae individuals.

3.1.3 Aboveground biomass according to DBH classes

The distribution of aboveground biomass (AGB) across tree size classes offers valuable insight into the forest's structural composition and successional stage. Following Li et al.'s (2023) classification, trees were grouped into two main DBH classes: Medium (10-30 cm), representing growing individuals, and Large (>30 cm), representing mature trees. AGB distribution reveals a clear structural pattern: while smaller trees are more numerous, biomass is disproportionately concentrated in larger individuals (Figure 3). In 2012, large trees held most of the biomass, accounting for 77.81% of the total biomass (267.73 Mg/ha), while more abundant medium-sized trees contributed 22.19% (76.33 Mg/ha). This pattern persisted in 2016 and 2024, with large trees maintaining dominance at 76.29% and 81.69% of total biomass, respectively (Table 3).

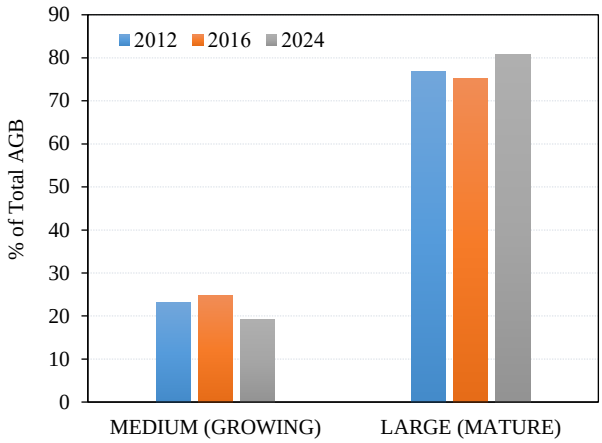


Figure 3. Percentage of total aboveground biomass by DBH class of trees within the one-hectare permanent plot

Table 3. Aboveground biomass growth by DBH class of trees

DBH classification	2016 Biomass (Mg/ha)	2024 Biomass (Mg/ha)	Biomass growth (Mg/ha)
Medium (10-30 cm)	87.02	72.78	-14.24
Large (>30 cm)	266.28	328.89	46.18

Stephenson et al. (2014) challenged the assumption that tree growth slows as size increases. Their findings show that across most species, large, old trees continue to actively sequester substantial amounts of carbon—often at rates exceeding those of smaller trees. In extreme cases, a single large tree can fix as much carbon in a year as an entire mid-sized tree contains in its biomass. The results of our study show the same pattern—large trees contribute disproportionately to biomass growth within the stand. Applying Li et al.'s DBH classification and excluding new recruits confirms that large trees account for the most substantial biomass increase.

3.2 Carbon accounting

3.2.1 Carbon stocks

The 1-hectare permanent plot consistently accumulated aboveground carbon stocks over the 12-year period, reinforcing its role as a sustained carbon sink (Table 4). Carbon stocks increased from 172.03 Mg C/ha in 2012 to 202.40 Mg C/ha in 2024, reflecting a net gain of 30.37 Mg C/ha. While the mean annual increment of carbon stocks slowed from 3.40 Mg C/ha (2012-2016) to 2.00 Mg C/ha (2016-2024), the overall trend confirms continued sequestration. The decline in mean annual carbon increment may be associated with stand maturation and structural change. As the stand accumulated biomass, the proportional rate of biomass gains likely slowed because larger trees increasingly dominated total carbon stock, while mortality, recruitment limitation, and competition may have reduced net gains during the longer 2016-2024 interval. The longer second measurement period may also smooth short-term growth pulses, making the annualized increment appear lower. Similar patterns have been observed in tropical secondary forests, where AGB accumulation rates can decline as biomass increases during succession, and where mortality and recruitment are important determinants of forest structural processes and biomass turnover (Tian et al., 2023; Ordoñez et al., 2024).

Table 4. Aboveground carbon stock across inventory periods

Year	Carbon (Mg C/ha)	Increase from previous inventory
2012	172.03	-
2016	186.41	14.38 Mg C/ha (6.51%)
2024	202.40	15.99 Mg C/ha (8.58%)

According to Pan et al. (2024), a carbon sink is a system where carbon gains from growth and recruitment exceed losses from mortality or disturbance. The observed net increase observed in the plot aligns with this definition and places the site within broader discussions on the contribution of tropical forests to global carbon uptake.

The study site, a secondary forest, exhibits a carbon stock of 202.4 Mg C/ha, placing it within the range reported for old-growth forests in the Philippines (Table 5). Lasco and Pulhin (2009) documented that old-growth forests in the country typically store around 201 Mg C/ha, indicating the carbon storage capacity is comparable to these mature forests. Furthermore, the site's carbon stock exceeds other natural forest types in the Philippines, including mossy (189 Mg C/ha), mangrove (184 Mg C/ha), and pine (191 Mg C/ha).

The carbon stock can be further evaluated against the findings of Peters et al. (2023), who examined aboveground carbon across various Philippine Forest types under different disturbance levels, interpreted through the forest transition theory. This model explains that regions move through stages: an initial stage with largely intact forests and low deforestation, an intermediate stage with accelerated forest loss, and a later stage where forest cover stabilizes and may increase. Peters et al. (2023), described several forest categories under different disturbance histories, including reference forests (least disturbed), logged forests (previously subjected to timber extraction), and plantation forests (planted stands, often monocultures). Against this backdrop, the Silago secondary-growth forest (202.4 Mg C/ha) stored less carbon than Eastern Visayas reference forests (260.27±80.31 Mg C/ha) but more than logged (99.6±52.09 Mg C/ha) and plantation forests (59.85±29.43 Mg C/ha) in the same region. It also exceeded both reference (131.68±80.31 Mg C/ha) and logged forests (56.51±30.38 Mg C/ha) in Cagayan Valley, Philippines, which Peters et al. (2023) considered to be in the initial transition stage.

Table 5. Comparison of carbon stocks in forests from published studies

Forest type and location	Carbon stock (Mg C/ha)		Source
	Average	Range	
Study site	202.4		This study
Natural Forests in the Philippines			
- Old-growth	201		Lasco and Pulhin (2009)
- Mossy	189		Lasco and Pulhin (2009)
- Mangrove	184		Lasco and Pulhin (2009)
- Pine	191		Lasco and Pulhin (2009)
Forests in Eastern Visayas, Philippines (Intermediate disturbance)			
- Reference	260.27	123-397	Peters et al. (2023)
- Logged	99.6	48-152	Peters et al. (2023)
- Plantations	59.85	30-89	Peters et al. (2023)
Forests in Cagayan Valley, Philippines (Low disturbance)			
- Reference	131.68	51-212	Peters et al. (2023)
- Logged	56.51	26-86	Peters et al. (2023)
Dipterocarp forests			
- Philippines		93-193	Lasco and Pulhin (2009)
- Philippines (Plantation)	221		Lasco and Pulhin (2009)
- Malaysia (Moderate to Superior)		190-260	Lasco and Pulhin (2009)
Regenerating secondary forest stands in Panama (40-120 years old)			
- 40	61.35		Jones et al. (2019)
- 60	75.11		Jones et al. (2019)

Table 5. Comparison of carbon stocks in forests from published studies (cont.)

Forest type and location	Carbon stock (Mg C/ha)		Source
	Average	Range	
- 90	96.25		Jones et al. (2019)
- 120	96.86		Jones et al. (2019)
Bukit Timah Nature Reserve in Singapore			
- Primary Forest	167.5		Ngo et al. (2013)
- Secondary Forest	104.5		Ngo et al. (2013)

When compared with dipterocarp forests in Malaysia, the study site's carbon stock falls between the moderate condition (190 Mg C/ha) and superior condition categories (220 Mg C/ha) suggesting it is in a relatively advanced recovery state and functioning effectively as a carbon-storage system. Furthermore, the carbon stock in the study site was comparably higher than secondary forests in Panama and Singapore (Table 5). These carbon-stock patterns provide the basis for evaluating the site's annual carbon sequestration rate across the monitoring period.

3.2.2 Carbon sequestration

The study site exhibited a carbon sequestration rate of 2.53 Mg C/ha/year from 2012 to 2024. This rate declined over time, averaging 3.60 Mg C/ha/year from 2012 to 2016 and 2.00 Mg C/ha/year from 2016 to 2024 (Table 6).

Table 6. Overall sequestration rate (2012-2024)

Carbon stock (Mg/ha)	Total increment	Sequestration rate	Year
202.40	30.37 Mg/ha	2.53	2012-2024

When compared with similar forests, this rate falls within expected ranges for dipterocarp ecosystems and secondary tropical forests (see Table 7). Relative to dipterocarp forests, the study site's sequestration rate exceeds those reported for Philippine dipterocarps (1.33 Mg C/ha/year; 54) and Malaysian dipterocarps (1.2 Mg C/ha/year) (Kayode, 2024); but slightly lower than the rate reported for Java dipterocarp forests (2.89 Mg C/ha/year) (Hairiah and Sitompul, 2000).

Compared to secondary tropical forests, the study site's sequestration rate is slightly below the 3.05 Mg C/ha/year recorded by Poorter et al. (2016), who noted that this rate was 11 times faster than carbon uptake of old-growth forests. In comparison, the study site's sequestration rate of 2.53 Mg C/ha/year was approximately 9.13 times higher than old-growth uptake, indicating substantial carbon accumulation in the regenerating stand. Compared to fast-growing species, the study site's sequestration rate was moderate. While reforestation projects in Leyte and Nueva Ecija recorded higher rates (Table 7), the site's steady carbon accumulation highlights the value of long-term storage in naturally regenerating secondary forests.

Table 7. Carbon sequestration rates of different forest types

Forest type and location	Carbon sequestration (Mg C/ha/year)	Source
Study Site	2.53	This study
Dipterocarps		
Java	2.89	Hairiah and Sitompul (2000)
Philippines	1.33	Lasco and Pulhin (2009)
Malaysia	1.2	Kayode (2024)
Mt. Makiling (Reforestation)		
Mahogany and Dipterocarp	2.8	Racelis et al. (2019)
Fast-growing species (Reforestation)		
Nueva Ecija	0.30-3.73	Racelis et al. (2019)

Table 7. Carbon sequestration rates of different forest types (cont.)

Forest type and location	Carbon sequestration (Mg C/ha/year)	Source
Leyte	0.7-9.0	Racelis et al. (2019)
Natural forests (Philippines)	>1	Lasco and Pulhin (2003)
Secondary Tropical Forests	3.05	Poorter et al. (2016)

However, because this study is based on a single one-hectare subplot within a larger 50-ha research area, its estimates should not be directly extrapolated to the entire Mt. Nacolod landscape without additional spatial replication. The plot provides valuable long-term evidence of carbon accumulation under a specific secondary-forest condition, but broader estimates of regional carbon mitigation potential and economic value require additional plots across different disturbance histories, elevations, soil conditions, and stand structures.

3.3 Economic value of carbon

3.3.1 Carbon stock

The economic value of the stand's carbon stock increased between 2012 and 2024, primarily due to two factors: (1) carbon stock accumulation and (2) carbon credit price appreciation. Without adjusting for inflation, total economic value rose by 51.97%, increasing from USD 4,798.34 in 2012 to USD 7,219.94 in 2024—an average annual increase of approximately USD 200 (Table 8).

Table 8. Economic valuation of carbon stock

Year	Carbon stock (tons)	CO_2e (tons)	Price per tCO_2e (USD)	Economic value (USD)	Inflation adjusted value (USD)
2012	172.03	631.36	7.60	4,798.35	6,553.53
2016	186.41	684.13	5.10	3,489.04	4,563.12
2024	202.40	742.79	9.72	7,219.94	-

Note: Carbon credit prices were sourced from annual reports by Forest Trends' Ecosystem Marketplace

3.3.2 Carbon sequestration

If the total carbon sequestered at the site over 12 years were converted into carbon credits in 2024, the CO_2 equivalent of 110.70 tons would be valued at USD 1,076.00, or an average of USD 89.67 per year (see Table 9). Under the same assumptions, stakeholders in the Philippines engaged in carbon trading would need to monitor approximately 18-19 hectares of the same forest stand to generate USD 20,000 in revenue over 12 years.

Table 9. Value generated from carbon sequestration (2012-2024)

Carbon sequestered (ton)	CO_2 equivalent (ton)	Value generated (USD)	Annual increment (USD)
30.37	110.70	1,076.00	89.67

However, these figures capture only one component of the forest's total economic value: the carbon sequestered in a single hectare. For instance, the total economic valuation of ecosystem services (Direct Use Value, Indirect Use Value, and Non-use Value) of Malaysian tropical forests was estimated at USD 3 billion, (Emerton and Aung, 2014).

As mentioned previously, the United Nations Environment Programme recommends increasing carbon credit prices in Forestry and Land-use to USD 20-50 per ton of CO_2 to align with Paris Agreement targets and USD 30-50 per ton to incentivize meaningful climate action. However, with USD 9.72 as the baseline price, the disparity between current carbon credit values and levels necessary to effectively combat climate change is evident (see Table 10). Bridging this gap is crucial for ensuring carbon markets provide sufficient financial incentives for climate mitigation. For example, at UNEP's recommended carbon credit prices of USD 20, USD 30, and USD 50 per ton of CO_2, stakeholders would only need approximately nine, six, or three hectares, respectively, to generate USD 20,000 in revenue, compared to 18 to 19 hectares at the baseline price (Table 10).

Table 10. Value of carbon sequestration using UNEP recommended prices

Price of carbon credit	Value generated per ha (USD)	Value Ggenerated per ha (Philippine Peso)
USD 9.72*	1,076.00	59,578.34
USD 20	2,124.00	122,589.20
USD 30	3,321.00	183,883.80
USD 50	5,535.00	306,473.00

4. CONCLUSION

Over decades of regeneration, Mt. Nacolod's secondary forest has emerged as a significant carbon sink, with aboveground biomass and carbon stocks now rivaling those of old-growth forests. This recovery—driven by sustained biomass accumulation and enduring dominance of carbon-rich Dipterocarpaceae—demonstrates the critical role of regenerating tropical forests in climate mitigation. Long-term monitoring proved indispensable, revealing gradual but ecologically meaningful trends that short-term studies might overlook.

Economically, growing carbon stocks in Mt. Nacolod reflect an underutilized opportunity. While the financial value of stored carbon has increased over time, current market prices for credits remain far below the thresholds needed to incentivize large-scale conservation. This gap between ecological potential and economic recognition underscores the urgency of policy reforms and market mechanisms that properly value tropical forests as climate assets.

By bridging ecological data with economic analysis, this study reinforces the dual potential of secondary forests: as robust carbon sinks and as strategic investments in climate resilience. Protecting these forests demands not only scientific validation but also financial frameworks that translate carbon storage into tangible returns, including stronger carbon pricing, payments for ecosystem services, blended public-private finance, and local conservation incentives that reward communities and managers for maintaining regenerating secondary forests.

ACKNOWLEDGEMENTS

We are grateful to VELUX STIFTUNG for funding the project CITIZEN-SDSS and to the Local Government Unit of Silago, Southern Leyte, especially to Barangay Catmon. We extend our sincere appreciation to Samuel O. Bernaldez and Martin Jan Mercurio for their leadership in the study, and to Jayson Espregante for his valuable assistance during data collection. Their contributions were instrumental to the success of this research.

AUTHOR CONTRIBUTIONS

Conceptualization, Come R, Martinez CA; Methodology, Come R, Martinez CA, Peque D, Seriño MN; Formal Analysis, Martinez CA; Investigation, Come R, Martinez CA; Data Curation, Come R and Martinez CA; Writing-Original Draft Preparation, Martinez CA; Writing-Review and Editing, Martinez CA, Come R, Peque D, Lippe M, Seriño MN; Visualization, Martinez CA; Validation, Come R, Peque D, Lippe M, Seriño MN; Supervision, Come R, Lippe M; Project Administration, Come R, Lippe M; Funding Acquisition, Come R, Lippe M.

DECLARATION OF CONFLICT OF INTEREST

The authors declare no conflict of interest.

REFERENCES

Abbass K, Qasim MZ, Song H, Murshed M, Mahmood H, Younis I. A review of the global climate change impacts, adaptation, and sustainable mitigation measures. Environmental Science and Pollution Research 2022;29(28):42539-59.

Abino AC, Castillo JAA, Lee YJ. Assessment of species diversity, biomass, and carbon sequestration potential of a natural mangrove stand in Samar, the Philippines. Forest Science and Technology 2014;10(1):2-8.

American Forest Foundation. A Trust for Permanence. Washington, DC: American Forest Foundation; 2025.

Araza A, De Bruin S, Herold M, Quegan S, Labriere N, Rodriguez-Veiga P, et al. A comprehensive framework for assessing the accuracy and uncertainty of global above-ground biomass maps. Remote Sensing of Environment 2022;272:Article No. 112917.

Asilo HAM, Yap-Dejeto LG. Understanding blue carbon management strategies: Quantitative assessment of blue carbon stock among three mangrove stands in Eastern Visayas, Philippines, W. Pacific Border. Carbon Research 2025;4(1):Article No. 63.

Baithalu S, Anbarashan M, Parthasarathy N. Two-decadal changes in forest structure and tree diversity in a tropical dry evergreen forest on the Coromandel Coast of India. Tropical Ecology 2013;54(3):397-403.

Barrera A, Aristirenas I, Tingzon J. Soil Survey of Leyte Province Philippines. Manila, Philippines: Bureau of Printing; 1954.

Beck HE, Zimmermann NE, McVicar TR, Vergopolan N, Berg A, Wood EF. Present and future Köppen-Geiger climate classification maps at 1-km resolution. Scientific Data 2018;5(1):Article No. 180214.

Becknell JM, Powers JS. Stand age and soils as drivers of plant functional traits and aboveground biomass in secondary tropical dry forest. Canadian Journal of Forest Research 2014;44(6):604-13.

Bonan GB. Forests and climate change: Forcings, feedbacks, and the climate benefits of forests. Science 2008;320(5882): 1444-9.

Brearley FQ, Adinugroho WC, Cámara-Leret R, Krisnawati H, Ledo A, Qie L, et al. Opportunities and challenges for an Indonesian forest monitoring network. Annals of Forest Science 2019;76(2):Article No. 54.

Brown S, Lugo AE. Aboveground biomass estimates for tropical moist forests of the Brazilian Amazon. Interciencia 1992;17(1):8-18.

Cabras AA, Senarillos TLP, Ibañez JC. Two new species of *Metapocyrtus heller*, 1912 (Curculionidae: Entiminae: Pachyrhynchini) from Leyte Island, Philippines. Ecologica Montenegrina 2023;67:66-76.

Carandang A, Bugayong L, Dolom P, Garcia L, Villanueva M, Espiritu N. Forestry Development Center, University of the Philippines Los Banos. Analysis of key drivers of deforestation and forest degradation in the Philippines. Germany: Deutsche Gesellschaft für Internationale Zusammenarbeit (GIZ) GmbH; 2013.

Chave J, Réjou-Méchain M, Búrquez A, Chidumayo E, Colgan MS, Delitti WBC, et al. Improved allometric models to estimate the aboveground biomass of tropical trees. Global Change Biology 2014;20(10):3177-90.

Chazdon RL, Redondo Brenes A, Vilchez Alvarado B. Effects of climate and stand age on annual tree dynamics in tropical second-growth rain forests. Ecology 2005;86(7):1808-15.

Condit R. Ecological implications of changes in drought patterns: Shifts in forest composition in Panama. Climatic Change 1998;39(2/3):413-27.

Cox PM, Betts RA, Jones CD, Spall SA, Totterdell IJ. Acceleration of global warming due to carbon-cycle feedbacks in a coupled climate model. Nature 2000;408(6809):184-7.

Cramer W, Bondeau A, Woodward FI, Prentice IC, Betts RA, Brovkin V, et al. Global response of terrestrial ecosystem structure and function to CO_2 and climate change: Results from six dynamic global vegetation models. Global Change Biology 2001;7(4):357-73.

Dale VH, Joyce LA, McNulty S, Neilson RP. The interplay between climate change, forests, and disturbances. Science of the Total Environment 2000;262(3):201-4.

Dale VH, Rauscher HM. Assessing impacts of climate change on forests: The state of biological modeling. Climatic Change 1994;28:65-90.

Danardono, Haryono E, Widyastuti M. Potential of carbon stocks and its economic values in tropical karst landscape (case study in Biduk-Biduk Karst, East Kalimantan, Indonesia). Journal of Physics: Conference Series 2019;1373(1):Article No. 012030.

Deb JC, Rahman HMT, Roy A. Freshwater swamp forest trees of Bangladesh face extinction risk from climate change. Wetlands 2016;36(2):323-34.

Ediriweera S, Bandara C, Lakkana T, Jayasinghe S, Woodbury D, Dayanandan A, et al. Old-growth mixed dipterocarp forests show variable losses and gains in aboveground biomass and standing carbon over forty years. Forest Ecosystems 2024;11(1):Article No. 100163.

Elkin C, Gutiérrez AG, Leuzinger S, Manusch C, Temperli C, Rasche L, et al. A 2°C warmer world is not safe for ecosystem services in the European Alps. Global Change Biology 2013;19(6):1827-40.

Emerton L, Aung Y. Assessing, Demonstrating and Capturing the Economic Value of Marine and Coastal Ecosystem Services in the Bay of Bengal Large Marine Ecosystem. Phuket, Thailand: FAO Bay of Bengal Large Marine Ecosystem (BOBLME) Project; 2014.

Enviliance ASIA. The Philippines' Legislative Initiatives on Carbon Crediting Systems. Enviliance ASIA [Internet]. 2023 [cited 2025 Apr 5]. Available from: https://enviliance.com/regions/southeast-asia/ph/ph-carbon-credit.

Fernando E, Suh MH, Lee J, Lee DK. Forest Formations of the Philippines. Seoul, Korea: ASEAN-Korea environmental cooperation unit (AKECU); 2008.

Fuss S, Golub A, Lubowski R. The economic value of tropical forests in meeting global climate stabilization goals. Global Sustainability 2021;4:e1.

Gallant K, Withey P, Risk D, van Kooten GC, Spafford L. Measurement and economic valuation of carbon sequestration in Nova Scotian Wetlands. Ecological Economics 2020; 171:Article No. 106619.

Hairiah K, Sitompul S. Assessment and Simulation of Aboveground and Belowground C Stocks and Dynamics. Bogor, Indonesia: CDM IC-SEA, BIOTROP; 2000.

Hamrick K, Gallant M. Unlocking Potential: State of the Voluntary Carbon Markets 2017. Washington, DC: Forest Trends' Ecosystem Marketplace; 2017.

Heriansyah I, Miyakuni K, Kato T, Kiyono Y, Kanazawa Y. Growth characteristics and biomass accumulations of Acacia mangium under different management practices in Indonesia. Journal of Tropical Forest Science 2007;19(3):226-35.

Huo LZ, Boschetti L, Sparks AM. Object-based classification of forest disturbance types in the conterminous United States. Remote Sensing 2019;11(5):Article No. 477.

Hussainzad EA, Mohd Yusof MJ. Assessing the economic value of carbon sequestration in Taman Negara Pahang. IOP Conference Series: Earth and Environmental Science 2020;540(1):Article No. 012058.

Intergovernmental Panel on Climate Change (IPCC). Summary for Policymakers. In: Climate Change 2022—Mitigation of Climate Change. Cambridge, UK: Cambridge University Press; 2023. p. 3-48.

Jarvis A, Reuter HI, Nelson A, Guevara E. Hole-filled SRTM for the Globe Version 4 [Internet]. 2008 [cited 2025 Apr 5]. Available from: https://srtm.csi.cgiar.org.

Jones IL, DeWalt SJ, Lopez OR, Bunnefeld L, Pattison Z, Dent DH. Above- and belowground carbon stocks are decoupled in secondary tropical forests and are positively related to forest age and soil nutrients respectively. Science of the Total Environment 2019;697:Article No. 133987.

Kaarakka L, Cornett M, Domke G, Ontl T, Dee LE. Improved forest management as a natural climate solution: A review. Ecological Solutions and Evidence 2021;2(3):e12090.

Kayode JO. Improved Logging in Tropical Rainforest for Carbon Sequestration: A Case Study in Borneo, Malaysia [dissertation]. Umeå: Swedish University of Agricultural Sciences; 2024.

Kurz WA, Stinson G, Rampley GJ, Dymond CC, Neilson ET. Risk of natural disturbances makes future contribution of Canada's forests to the global carbon cycle highly uncertain. Proceedings of the National Academy of Sciences 2008;105(5):1551-5.

Langenberger G, Belonias B. The status of floristic analysis of Mt. Pangasugan, Leyte, Philippines – a conservation priority area classified as "Extremely High Critical." Annals of Tropical Research 2011;33(2):1-21.

Lasco RD, Guillermo IQ, Cruz RVO, Bantayan NC, Pulhin FB. Carbon stocks assessment of a secondary forest in Mount Makiling Forest Reserve, Philippines. Journal of Tropical Forest Science 2004;16(1):35-45.

Lasco RD, Pulhin F. Carbon budgets of forest ecosystem in the Philippines. Journal of Environmental Science and Management 2009;12(1):1-13.

Lasco RD, Pulhin FB. Philippine forest ecosystems and climate change: Carbon stocks, rate of sequestration and the Kyoto Protocol. Annals of Tropical Research 2003;25(2):37-51.

Li Y, Nyongesah MJ, Deng L, Haider FU, Liu S, Mwangi BN, et al. Clustered tree size analysis of bio-productivity of Dinghushan National Nature Reserve in China. Frontiers in Ecology and Evolution 2023;11:Article No. 1118175.

Malhi Y, Baker TR, Phillips OL, Almeida S, Alvarez E, Arroyo L, et al. The above-ground coarse wood productivity of 104 Neotropical forest plots. Global Change Biology 2004;10(5):563-91.

Mallari NAD, Rico ELB, de Alban JD, Diesmos AC, Altamirano R, Puna N, et al. Biodiversity Baseline Assessment in the REDD-Plus Pilot and Key Biodiversity Area in Mt. Nacolod, Southern Leyte. Manila, Philippines: Deutsche Gesellschaft für Internationale Zusammenarbeit GmbH; 2014.

Marcos-Martinez R, Bryan BA, Schwabe KA, Connor JD, Law EA, Nolan M, et al. Projected social costs of CO_2 emissions from forest losses far exceed the sequestration benefits of forest gains under global change. Ecosystem Services 2019;37:Article No. 100935.

Meniano S. DENR reactivates task force to protect E. Visayas Forest [Internet]. 2024 [cited 2025 Apr 5]. Available from: https://www.pna.gov.ph/articles/1231147.

Millar CI, Stephenson NL. Temperate forest health in an era of emerging megadisturbance. Science 2015;349(6250):823-6.

Mori AS, Dee LE, Gonzalez A, Ohashi H, Cowles J, Wright AJ, et al. Biodiversity-productivity relationships are key to nature-based climate solutions. Nature Climate Change 2021; 11(6):543-50.

Murthy IK, Bhat S, Sathyanarayan V, Patgar S, Beerappa M, Bhat PR, et al. Vegetation structure and composition of tropical evergreen and deciduous forests in Uttara Kannada District, Western Ghats under different disturbance regimes. Tropical Ecology 2016;57(1):77-88.

Nelson BW, Mesquita R, Pereira JLG, de Souza SGA, Batista GT, Couto LB. Allometric regressions for improved estimate of secondary forest biomass in the central Amazon. Forest Ecology and Management 1999;117(1):149-67.

NewCAPP. Managing the Mt. Nacolod landscape: A shared conservation challenge. Quezon City, Philippines: New Conservation Areas in the Philippines Project; 2014.

Ngo KM, Turner BL, Muller-Landau HC, Davies SJ, Larjavaara M, Nik Hassan NFB, et al. Carbon stocks in primary and secondary tropical forests in Singapore. Forest Ecology and Management 2013;296:81-9.

Oberleitner F, Egger C, Oberdorfer S, Dullinger S, Wanek W, Hietz P. Recovery of aboveground biomass, species richness and composition in tropical secondary forests in SW Costa Rica. Forest Ecology and Management 2021;479:Article No. 118580.

Ordoñez JC, Pinto E, Bernardi A, Cuesta F. Tree mortality and recruitment in secondary Andean tropical mountain forests along a 3,000 m elevation gradient. PLoS One 2024;19(3):e0300114.

Pache R-G, Abrudan IV, Niță M-D. Economic valuation of carbon storage and sequestration in Retezat National Park, Romania. Forests 2020;12(1):Article No. 43.

Pan Y, Birdsey RA, Fang J, Houghton R, Kauppi PE, Kurz WA, et al. A large and persistent carbon sink in the world's forests. Science 2011;333(6045):988-93.

Pan Y, Birdsey RA, Phillips OL, Houghton RA, Fang J, Kauppi PE, et al. The enduring world forest carbon sink. Nature 2024;631(8021):563-9.

PennState Extension. Methods for estimating carbon within forests [Internet]. 2023 [cited 2025 Apr 5]. Available from: https://extension.psu.edu/methods-for-estimating-carbon-within-forests.

Peters F, Lippe M, Eguiguren P, Günter S. Forest ecosystem services at landscape level - why forest transition matters? Forest Ecology and Management 2023;534:Article No. 120782.

Peters-Stanley M, Gonzalez G, Yin D. Covering New Ground: State of the Forest Carbon Markets 2013. Washington, DC: Forest Trends' Ecosystem Marketplace; 2013.

Philippine Tropical Forest Conservation Foundation. Terminal Report. Community-Based Forest Restoration and Biodiversity Protection and Management of Lowland Dipterocarp Forests in Silago, Southern Leyte. Philippines: Philippine Tropical Forest Conservation Foundation; 2013.

Phillips OL. Sensing forests directly: The power of permanent plots. Plants 2023;12(21):Article No. 3710.

Phillips OL, Baker TR, Arroyo L, Higuchi N, Killeen TJ, Laurance WF, et al. Pattern and process in Amazon tree turnover, 1976-2001. Philosophical Transactions of the Royal Society of London Series B: Biological Sciences 2004;359(1443): 381-407.

Phillips OL, Gentry AH. Increasing turnover through time in tropical forests. Science 1994;263(5149):954-8.

Piamonte MK, Asio V, Lina S. Morpho-physical and chemical characteristics of strongly weathered soils in Silago, Southern Leyte, Philippines. Annals of Tropical Research 2014; 36(2):115-47

Poorter L, Bongers F, Aide TM, Almeyda Zambrano AM, Balvanera P, Becknell JM, et al. Biomass resilience of Neotropical secondary forests. Nature 2016;530(7589):211-4.

Procton A. On the Path to Maturity: State of the Voluntary Carbon Markets 2024. Washington (DC): Forest Trends Association; 2024.

Racelis E, Racelis D, Luna A. Carbon sequestration by large leaf mahogany (Swietenia macrophylla King.) plantation in Mount Makiling forest reserve, Philippines: A decade after. Journal of Environmental Science and Management 2019;22(1): Article No. 1.

Raga-as M. Comparison of Carbon Benefits between Natural and Plantation Forests in Aurora Province, Philippines [dissertation]. Los Baños, Philippines: University of the Philippines Los Baños; 2004.

Raihan A, Begum R, Nizam M. A meta-analysis of the economic value of forest carbon stock. Malaysian Journal of Society and Space 2021;17(4):Article No. 22.

Reyer C, Lasch-Born P, Suckow F, Gutsch M, Murawski A, Pilz T. Projections of regional changes in forest net primary productivity for different tree species in Europe driven by climate change and carbon dioxide. Annals of Forest Science 2014;71(2):211-25.

Reyer CPO, Bathgate S, Blennow K, Borges JG, Bugmann H, Delzon S, et al. Are forest disturbances amplifying or canceling out climate change-induced productivity changes in European forests? Environmental Research Letters 2017;12(3):Article No. 034027.

Roy J, Saugier B, Mooney HA. Terrestrial Global Productivity. San Diego, CA: Academic Press; 2001.

Rumahorbo BT, Keiluhu HJ, Hamuna B. The economic valuation of mangrove ecosystem in Youtefa Bay, Jayapura, Indonesia. Ecological Questions 2019;30(1):47-54.

Scheinkman JA. Carbon prices and reforestation in tropical forest [Internet]. 2024 [cited 2025 Apr 5]. Available from: https://www.bis.org/publ/work1223.htm.

Seidl R, Thom D, Kautz M, Martin-Benito D, Peltoniemi M, Vacchiano G, et al. Forest disturbances under climate change. Nature Climate Change 2017;7(6):395-402.

Siregar CA, Heriyanto NM. Accumulation of carbon biomass under secondary forest scenario in Maribaya, Bogor, West Java. Jurnal Penelitian Hutan dan Konservasi Alam 2010;7(2):215-26.

Stephenson NL, Das AJ, Condit R, Russo SE, Baker PJ, Beckman NG, et al. Rate of tree carbon accumulation increases continuously with tree size. Nature 2014;507(7490):90-3.

Subiandono E, Bismark M, Heriyanto N. The ability of *Avicennia marina* (Forsk.) Vierh. and *Rhizophora apiculata* Bl. in absorbing heavy metal pollutants. Jurnal Penelitian Hutan Dan Konservasi Alam 2013;10(1):93-102 (in Indonesian).

Tian L, Tong Y, Cheng Y, Li M, Letcher SG, Zang R, et al. Drought diminishes aboveground biomass accumulation rate during secondary succession in a tropical forest on Hainan Island, China. Forest Ecology and Management 2023; 544:Article No. 121222.

Trumbore S, Brando P, Hartmann H. Forest health and global change. Science 2015;349(6250):814-8.

United Nations Development Programme. Forest Carbon Accounting: Overview and Principles. New York, NY: UNDP; 2015.

UN-REDD Programme. Pricing Forest Carbon: Implications of the Average Cost of REDD+ Emission Reductions. Nairobi, Kenya: United Nations Environment Programme; 2023.

Veridiano RK, Schröder JM, Come R, Baldos A, Günter S. Towards forest landscape restoration programs in the Philippines: Evidence from logged forests and mixed-species plantations. Environments 2020;7(3):Article No. 3.

Whitehead D. Forests as carbon sinks—benefits and consequences. Tree Physiology 2011;31(9):893-902.

Environment and Natural Resources Journal

Volume 24
Issue 6
2026

Integrating Phytoremediation and Socio-Economic Potential of Water Hyacinth for Sustainable Post-Mining Void Management

Priyaji Agung Pambudi[1,2*], Suyud Warno Utomo[3], and Roni Setyo Handoko[4]

[1]*Graduate School of Environmental Science, Universitas Gadjah Mada, Yogyakarta, Indonesia*
[2]*Faculty of Geography, Universitas Gadjah Mada, Yogyakarta, Indonesia*
[3]*Graduate School of Sustainable Development, Universitas Indonesia, Jakarta, Indonesia*
[4]*Department of Civil Engineering, Faculty of Engineering, State University of Malang, Malang, Indonesia*

ARTICLE INFO

Received: 14 Nov 2025
Received in revised: 3 Jul 2026
Accepted: 16 Jul 2026
Published online: 29 Sep 2026
DOI: 10.32526/ennrj/24/20250324

Keywords:
Ecological restoration/ Post-mining management/ Phytoremediation/ Sustainable development/ Water hyacinth

*** Corresponding author:**
E-mail:
priyajiagungpambudi@ugm.ac.id

ABSTRACT

Post-mining void represents critical environmental challenges due to water contamination, unstable slopes, and limited ecological recovery. These problems persist in many coal mining areas in Indonesia, threatening surrounding ecosystems and communities. Addressing these challenges requires an integrated reclamation approach that combines ecological and socio-economic functions. Therefore, this study aimed to develop an integrated reclamation model using *Eichhornia crassipes* (water hyacinth) as a phytoremediation agent for sustainable post-mining void management. A qualitative literature synthesis was conducted using Scopus, Web of Science (WoS), and Garuda databases, focusing on peer-reviewed articles published between 2017 and 2025. References were screened based on publication type, language, ecological relevance, and applicability to tropical environments. The selected studies were analyzed through content analysis, tabulation, and conceptual design synthesis to identify phytoremediation mechanism and formulate a reclamation model. The results showed that *E. crassipes* effectively removed heavy metals, nutrients, and organic pollutants across diverse wastewater conditions, while the harvested biomass offered opportunities for value-added utilization. This multifunctional approach connects ecological restoration with community participation and circular biomass management. However, pilot-scale validation and economic feasibility assessments remain necessary before broader implementation in post-mining landscapes.

HIGHLIGHTS

- A nature-based reclamation model using *E. crassipes* in the proposed model.
- The design integrates phytoremediation and local livelihoods.
- *E. crassipes* improves water quality in post-mining void.
- Biomass utilization creates added socio-economic value.
- The model supports sustainable post-mining management.

1. INTRODUCTION

Coal mining activities have generated extensive post-mining void that pose persistent environmental challenges worldwide, particularly in major coal-producing countries (Pambudi et al., 2025). In Indonesia, hundreds of mining voids remain after extraction activities, many of which contain stagnant water characterized by low pH, elevated concentrations of dissolved metals, and poor ecological productivity (Pagoray and Ghitarina, 2020; Pambudi et al., 2023). These abandoned voids not only threaten surrounding aquatic ecosystems but also increase the risk of slope instability, accidental drowning, and long-term environmental degradation (Martyushev et al., 2025).

Acid mine drainage (AMD) is one of the most critical issues associated with post-mining void (Moyo et al., 2024). Oxidation of sulfide minerals, particularly pyrite, produces acidic conditions that mobilize toxic metals such as Fe, Mn, Pb, Cd, and Cu

Citation: Pambudi PA, Utomo SW, Handoko RS. Integrating phytoremediation and socio-economic potential of water hyacinth for sustainable post-mining void management. Environ. Nat. Resour. J. 2026;24(6):737-750. (https://doi.org/10.32526/ennrj/24/20250324)

into water column (Mahanta et al., 2024; Shi et al., 2025). Previous studies have reported pH values below 4 and heavy metal concentrations exceeding environmental thresholds in several tropical coal mining voids, thereby limiting natural recovery processes and constraining post-mining land utilization (Srivastava et al., 2017; Woodbury et al., 2020). Consequently, reclamation strategies are required to comply with regulatory obligations, restore ecological functions, and reduce risks to nearby communities (Pambudi et al., 2025; Yuan et al., 2024).

Conventional remediation approaches for mining voids commonly rely on physical and chemical treatments, including liming, coagulation, and an active neutralization system (Edo et al., 2024; Noor et al., 2024). Despite being effective in improving water quality, these methods are often expensive, energy-intensive, and require continuous maintenance, thereby limiting long-term applicability, particularly in developing countries (Mothetha et al., 2023; Pambudi et al., 2025; Sekhohola-dlamini et al., 2022). This limitation has stimulated growing interest in nature-based solutions that are environmentally compatible and economically feasible.

Bioremediation can be further classified into phytoremediation (plants) (Sharma et al., 2023), mycoremediation (fungi) (Shruthi and Hemavathy, 2024), phycoremediation (algae) (Ordóñez et al., 2023), microbioremediation (Abo-Alkasem et al., 2023), and zoobioremediation (animals) (Reich et al., 2023). Each group plays a specific remedial role depending on the contaminated medium and pollutant characteristics (Chen and Ding, 2023). Among these methods, phytoremediation is the most widely used and well-known approach (Sharma et al., 2023), employing plants to reduce or even eliminate environmental pollutants, specifically in water and soil (Buslima et al., 2025; Sachin and Sonal, 2023). Common plants used in phytoremediation include *Eichhornia crassipes* (water hyacinth) (González-Tavares et al., 2023; Serafini et al., 2024), *Helianthus annus* (Waseem et al., 2024), *Azolla pinnata* (Soliman et al., 2025), *Pistia stratiotes* (Khambali et al., 2024), and *Salvinia molesta*. Among these species, *E. crassipes* has attracted considerable attention because of its rapid growth, extensive root system, high adaptability, as well as remarkable capacity to accumulate heavy metals and excess nutrients from contaminated water (Pagoray and Ghitarina, 2020; Ullah and Rahman, 2024).

The majority of existing studies on *E. crassipes* have focused on domestic wastewater (Buslima et al., 2025), industrial effluents, rivers, lakes, or artificial ponds (Panneerselvam and Priya, 2023; Tumembouw et al., 2024). Studies investigating its application in coal mining remain scarce and predominantly evaluate only pollutant removal efficiency (Hasani et al., 2021; Pagoray and Ghitarina, 2020). Furthermore, previous studies rarely extend the discussion beyond technical remediation outcomes, overlooking how harvested *E. crassipes* biomass could generate socio-economic benefits that support the sustainability of reclamation programs.

Although phytoremediation capacity of *E. crassipes* has been extensively documented, limited attention has been given to integrating ecological restoration functions with biomass-based livelihood opportunities in post-mining landscapes. This integration is important because the harvested biomass has demonstrated potential as a feedstock for compost production (Gezahegn et al., 2024), handicrafts (Ifa et al., 2023), animal feed supplements (Guchhait et al., 2025), and bioenergy products (Nandiyanto et al., 2023), thereby creating incentives for community participation in reclamation activities.

The novelty of this study lies in proposing an integrated conceptual model that combines phytoremediation function of *E. crassipes* with socio-economic utilization to support sustainable post-mining void reclamation. In contrast to previous investigations primarily assessing pollutant removal performance, this study develops a reclamation design that simultaneously addresses water quality improvement, ecological recovery, biomass valorization, and local community empowerment. Therefore, this study aimed to investigate the potential of *E. crassipes* as a phytoremediation agent for coal mining void reclamation and to formulate an integrated reclamation model based on ecological and socio-economic considerations. By connecting environmental restoration with community-based biomass utilization, the results contribute a nature-based and socially inclusive approach that may enhance the effectiveness and long-term sustainability of post-mining management.

2. METHODOLOGY

This study employed a qualitative approach aimed at understanding the potential of *E. crassipes* as a phytoremediation agent. The process started with determining the study topic, followed by selecting the

databases that would be used for literature exploration. To improve transparency and reproducibility, the literature synthesis followed the Preferred Reporting Items for Systematic Reviews and Meta-Analyses (PRISMA) model as a guiding procedure for identification, screening, eligibility assessment, and inclusion of relevant studies (Page et al., 2021). Although this study did not aim to conduct a quantitative meta-analysis, the PRISMA approach was adopted to minimize selection bias as well as ensure a systematic and traceable review process. The number of records identified, screened, excluded, and retained at each stage was documented and summarized using PRISMA flow diagram (Figure 1). Three databases were selected to ensure comprehensive and credible sources, namely Scopus and Web of Science (WoS) as an international database and Garuda (Garba Rujukan Digital), a trusted national database. The selection of Scopus, WoS, and Garuda databases was based on complementary considerations. Scopus and WoS were selected because both represent two of the largest international abstract and citation databases, covering high-quality peer-reviewed journals across environmental science, ecological restoration, and mining disciplines. Meanwhile, Garuda was included to capture nationally relevant studies and Indonesian experiences related to post-mining reclamation and the use of *E. crassipes* that may not be indexed internationally. The combination of both databases enabled broader coverage of global scientific evidence while maintaining contextual relevance to tropical and Indonesian post-mining conditions.

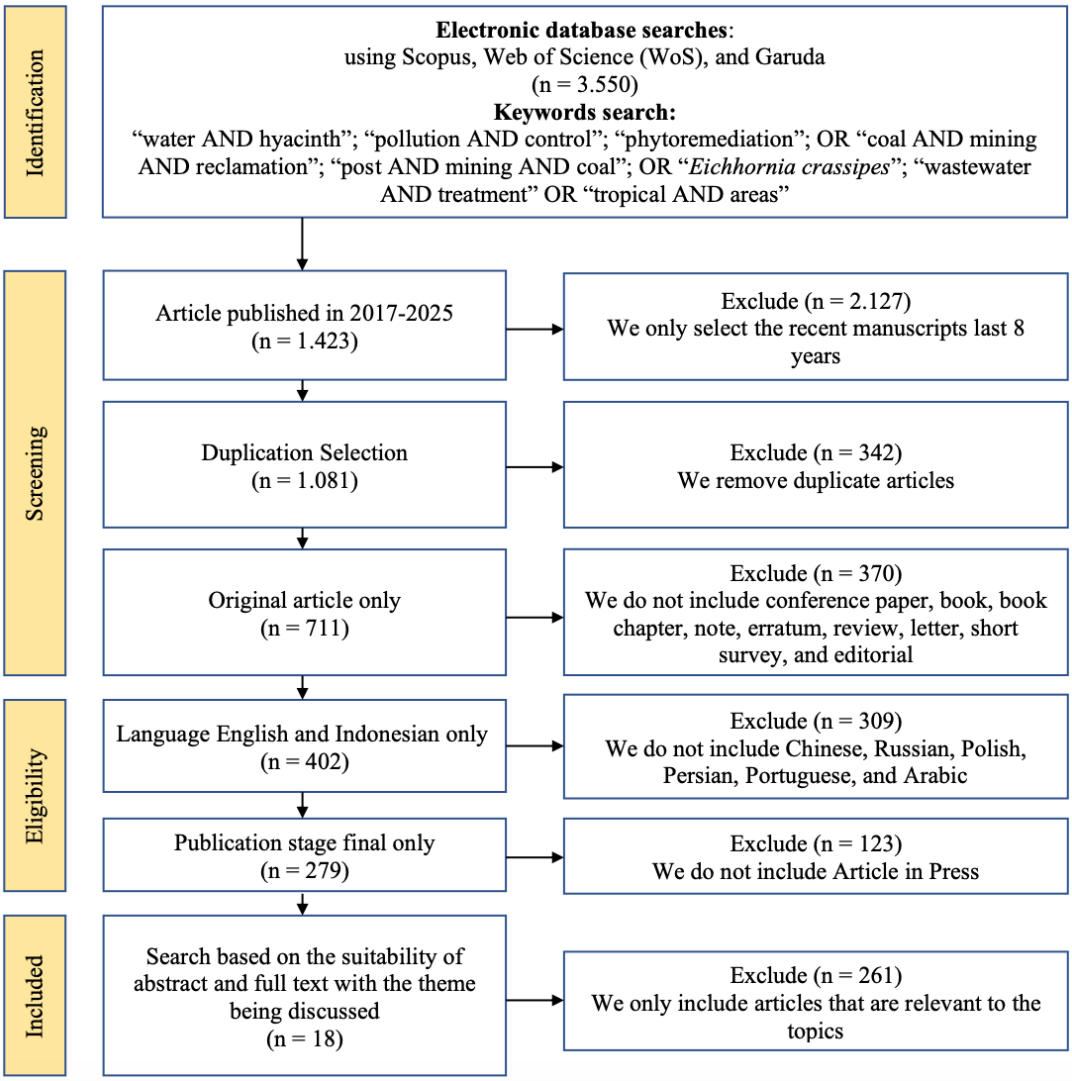


Figure 1. PRISMA workflow

In both databases, a set of specific keywords was applied to guide and refine the search process. These keywords included waste management, pollution control, bioremediation, phytoremediation,

water hyacinth, and *E. crassipes*. Using the same keyword sets across databases ensured consistency in identifying relevant and comparable studies.

The next step involved the selection of references based on several criteria:

(1) The source must be an article-type publication,

(2) Published between 2017 and 2025,

(3) Written in English and Indonesian, and

(4) Focused on tropical areas, where *E. crassipes* commonly grows and is widely utilized.

The publication period of 2017-2025 was intentionally selected to capture the most recent developments in phytoremediation studies and post-mining reclamation practices. During this period, there has been a growing emphasis on nature-based solution circular economic considerations in environmental restoration initiatives. Restricting the review to studies published in the last decade ensured that the synthesized evidence reflected current technological advancements and evolving perspectives on sustainable mine reclamation. Moreover, the selected timeframe coincides with the increasing recognition of *E. crassipes* not only as a phytoremediation agent but also a potential biomass resource, thereby aligning the reviewed literature with the integrated ecological and socio-economic focus of this study. The criteria ensured that the reviewed literature was current, relevant, and aligned with ecological context of the study. After the references were screened and selected, data processing was carried out in three stages:

1. Content analysis to extract core findings related to phytoremediation ability of *E. crassipes*,

2. Tabulation analysis to organize data systematically into tables, matrices, and comparable categories, and

3. Illustrations, where visual summaries and diagrams were developed to enhance clarity and understanding.

The processed information was then used in the data analysis stage, employing exploratory descriptive analysis to interpret patterns, mechanisms, and applications of *E. crassipes* in pollutant removal. Since this study proposed a conceptual reclamation design, a validity assessment was conducted through triangulation of evidence derived from the reviewed literature. The proposed model was developed only from design components that consistently emerged across multiple studies concerning phytoremediation performance, post-mining rehabilitation requirements, and biomass utilization pathways. The conceptual design was subsequently evaluated using four criteria adapted from design-based environmental studies, including environmentally sustainable, economically profitable, socially acceptable, and technologically manageable. This process strengthened the credibility of the proposed model and ensured that it was supported by convergent evidence rather than isolated results.

3. RESULTS AND DISCUSSION

3.1 Ecosystem services of water hyacinth (*E. crassipes*)

E. crassipes is an aquatic plant that offers diverse benefits across multiple dimensions. Environmentally, it is highly effective as phytoremediation agent due to the remarkable ability to absorb heavy metals and pollutants, thereby contributing to the rehabilitation of aquatic ecosystems (Nooryaneti et al., 2022). Economically, the plant can be processed into handicrafts, compost, animal feed, and even biogas feedstock, all of which have the potential to enhance community income (Guchhait et al., 2025; Ifa et al., 2023; Maulidyna et al., 2021). From a social perspective, the utilization creates new employment opportunities and fosters local community empowerment (Goel and Kalamdhad, 2018; Islam et al., 2021). Figure 2 shows the various potential benefits of *E. crassipes* across social, economic, and environmental aspects.

E. crassipes offers substantial potential benefits across social, economic, and environmental dimensions. From a social standpoint, it can be used as a raw material for creative industries and small and medium enterprises (Ifa et al., 2023). Furthermore, women farming groups or community organizations, such as the family welfare and empowerment organization (PKK), may process *E. crassipes* into handicraft products such as bags, mats, and other woven goods with high market value (Agustin et al., 2023). This plant has also been used in the production of traditional medicine due to the bioactive compounds. Gebrehiwot et al. (2022) identified several properties in *E. crassipes*, including anti-inflammatory, antioxidant, antifungal, anti-aging, anticancer, hepatoprotective, and antibacterial activities. Considering these bioactive properties, the plant holds strong potential to enhance community productivity through community-based economic empowerment initiatives.

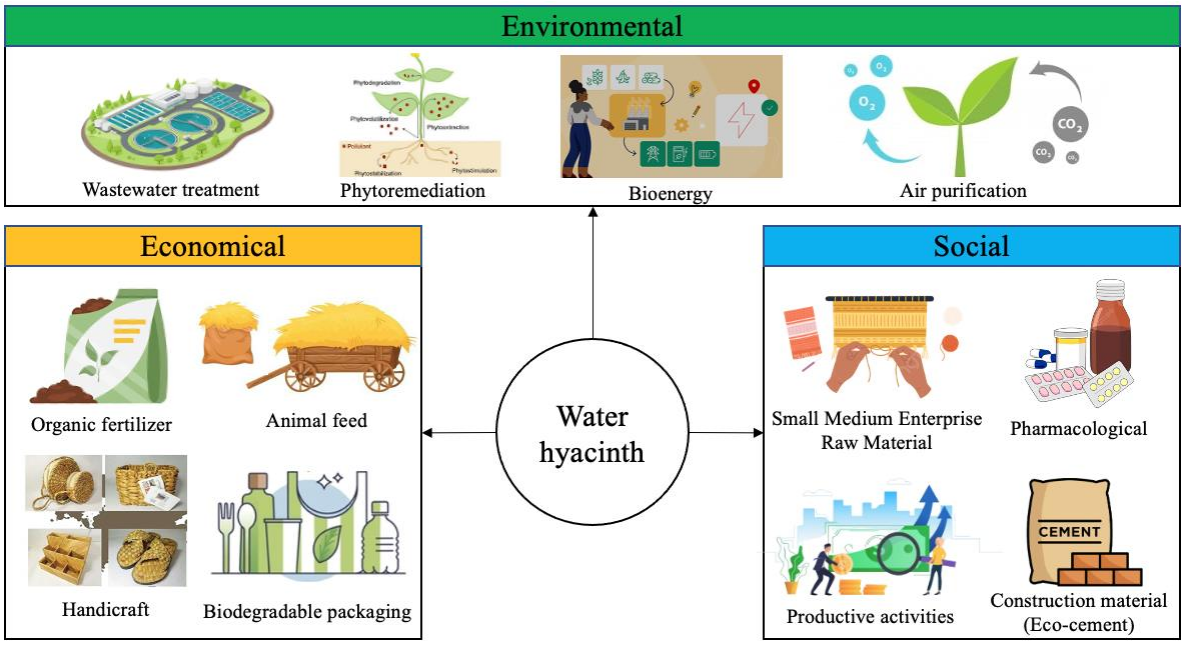


Figure 2. Potential benefits of *E. crassipes* from social, economic, and environmental perspectives. Source: Authors illustration

From an economic perspective, *E. crassipes* offers considerable potential for value addition. The plant can be processed into high-quality organic fertilizer. Sofyan et al. (2023) reported that compost made from *E. crassipes* combined with N, P, K, and S fertilizers significantly improved shallot yields, as evidenced by greater fresh and dry weights and a higher number of bulbs. These results indicate that compost can enhance agricultural productivity while reducing dependence on chemical fertilizers. Furthermore, Fanta et al. (2024) found that the plant could replace up to 37.5% of commercial concentrate used for the growth and fattening of sheep and goats. This implies that the plant serves as a functional feed alternative and lowers livestock production costs. In addition, *E. crassipes* also serve as a raw material for handicrafts, including bags and other accessories. According to Ifa et al. (2023), handicraft products, such as baskets, are sold for 55,000-65,000 IDR, while placemat baskets are priced at 24,000-30,000 IDR, marketed both offline and online through platforms including Instagram, TikTok, websites, Shopee, Tokopedia, and Facebook marketplaces. Albushairi and Huda (2021) further demonstrated that *E. crassipes*-based handicrafts possess high market appeal, particularly when promoted as eco-friendly products aligned with the principles of green products and behaviour. Moreover, Duruin et al. (2022) showed that eco-friendly packaging, particularly bioplastics made from *E. crassipes*, is increasingly in demand as a sustainable alternative to single-use plastics.

From an environmental perspective, ecological value is closely related to the ability to support pollutant removal and ecosystem restoration, which are discussed in detail in the following section (Panneerselvam and Priya, 2023). Studies have shown that *E. crassipes* can reduce levels of biochemical oxygen demand (BOD), total dissolved solids (TDS), and heavy metals such as lead in domestic wastewater (Huynh et al., 2021). Moreover, the plant holds great potential as a source of bioenergy, particularly biogas and biofuel, due to the high cellulose and hemicellulose content (Nandiyanto et al., 2023; Archibong and Ekanim, 2023). *E. crassipes* also contributes to air purification by absorbing airborne pollutants and enhancing oxygen levels in the surrounding environment (Iqbal et al., 2025).

3.2 Application of water hyacinth (*E. crassipes*) as a phytoremediation agent

E. crassipes is highly effective as a phytoremediation agent, capable of absorbing pollutants including nitrates, phosphates, and heavy metals from aquatic environments (Singh and Balomajumder, 2021). The plant shows rapid growth and strong adaptability to polluted water conditions (Iqbal et al., 2025). According to these characteristics, *E. crassipes* has significant potential to improve water quality and support the restoration of aquatic ecosystems, including those found in mining areas, particularly in void ecosystems. Table 1 shows data on the use of *E. crassipes* as a phytoremediation agent.

Table 1. Application of *E. crassipes* as a phytoremediation agent

No	Type of Waste	Contaminant	Country	Results	References
1	Domestic wastewater	COD, NH3-N, & PO_4^{3-}	Malaysia	Reduce COD by 86.7-100%, NH_3-N by 79-99.6%, and PO_4^{3-} by up to 80%.	Buslima et al. (2025)
2	Organochlorine pollutants	POPs	Indonesia	POPs absorbed in roots up to 1.12 ppm, stems 0.88 ppm, and leaves 0.53 ppm on average.	Tumembouw et al. (2024)
3	Industrial wastewater	Cu, Al, Pb, Hg, Cd, Ar, PO_4^{3-}, & N	Colombia	Reduces concentrations of Cu, Al, Pb, Hg, Cd, and Ar up to 70% and PO_4^{3-}, and N compounds by 50%.	Monroy-Licht et al. (2024)
4	Industrial wastewater	Ni & Cu	Mexico	At 30°C, absorbed Ni at 349 mg/g and Cu at 294.1 mg/g.	González-Tavares et al. (2023)
5	Industrial wastewater	Pb	Indonesia	After 12 days of treatment, biomass reached 75.46 g for 4 ppm Pb and 79.00 g for 2 ppm Pb.	Fahruddin et al. (2023)
6	Textile industry wastewater	pH, COD, TS, TSS, Cl, & SO_4	India	Increased pH by 25.62%, reduced COD by 69%, TS by 25.71%, TDS by 34.61%, Sulphate and Chloride by 45%.	Sachin and Sonal (2023)
7	Textile industry wastewater	TSS	Indonesia	Reduced TSS by 54 mg/L, equivalent to 71.12%.	Nooryaneti et al. (2022)
8	Petroleum effluent	COD & BOD	Indonesia	At 20% effluent concentration after 2 months, COD and BOD decreased by 3.73 mg/L and 9.14 mg/L, respectively at 30% concentration, COD and BOD decreased by 3.73 mg/L and 1.22 mg/L.	Hardestyariki and Fitria (2022)
9	Reclaimed coal mining in South Kalimantan, Indonesia	Fe	Indonesia	The application of organic material (OM) in *E. crassipes* media increased Q_{max} values from 2,077 to 2,348-3,259 mg/kg.	Saidy et al. (2021)
10	Lake Tana, Ethiopia	DO, SRP, TP, NO_3-N, & TN	Ethiopia	Increased DO from 3.3 to 4. Mg/L, SRP from 0.012 to 0.023 mg/L, TP from 0.24 to 0.28 mg/L, NO_3-N from 0.074 to 0.097 mg/L, and TN from 2.1 to 3.2 mg/L.	Endgaw (2021)
11	Wastewater	Phenol & CN-	India	Reduced phenol by 96.42% (300 mg/L) and cyanide by 92.66% (30 mg/L).	Singh and Balomajumder (2021)
12	Domestic wastewater	COD, BOD, & pH	Indonesia	Reduced pH from 9 to 7, maintained COD at 296.45 mg/L, and increased BOD from 14.813 mg/L to 80.850 mg/L.	Rahmawati and Warsito (2020)
13	Industrial wastewater	Cr^{6+}	Indonesia	At 120 ppm for 14 days, remediated Cr^{6+} by 62-68%.	Taufikurahman et al. (2020)
14	Laboratory-based small-scale experiment	Cr & Cu	Pakistan	Cr accumulation in root was 90 mg, in leaves 53 mg and Cu accumulation in root was 86 mg, in leaves 50 mg. The heavy metal significantly decreased from day 1 to day 30.	Tabinda et al. (2020)
15	Ramsar Wetland, Central Mexico	Co, Zn, As, Ni, Cu, Pb, Ti, Cr, Ba, Mo, & V	Mexico	*E. crassipes* absorb potential toxic metals from the water in the total plant was (all values in mg/kg of dry weight), is Co 21±9, Zn 408±300, As 12±6, Ni 93±21, Cu 93±69, Pb 53±29, Ti 1,067±643, Cr 78±55, Ba 362±39, Mo 14±0.6, and V 96±35.	Tabla-Hernandez et al. (2019)
16	Batujai Reservoir Pollution	Pb	Indonesia	Average Pb accumulation in roots reached 33.83 bioconcentration factor (BAF), ranging from 19.74 70 42.11 BAF.	Rahim and Soeprobowati (2018)

Notes: BOD (Biological Oxygen Demand), Cd (Cadmium), Cl (Chloride), CN- (Cyanide), COD (Chemical Oxygen Demand), Cu (Copper), Cr (Chromium), Cr^{6+} (Hexavalent Chromium), DO (Dissolved Oxygen), Pb (Lead), POPs (Persistent Organic Pollutants), SRP (Soluble Reactive Phosphorus), TP (Total Phosphorus), TN (Total Nitrogen), TSS (Total Suspended Solids)

Table 1 shows that *E. crassipes* has broad phytoremediation capabilities across diverse wastewater types, ranging from domestic and industrial effluents to petroleum, textile, and reservoir pollution. A consistent trend arising from these studies is the species ability to improve key water quality parameters, including reductions in COD, BOD, TSS, nutrients, and selected toxic compounds, while simultaneously accumulating heavy metals, namely Pb, Cu, Cr, Ni, Hg, and Cd. However, remediation performance was not uniform among contaminants. Organic pollutants and nutrients generally showed relatively high removal efficiencies, as reflected by COD reductions reaching 86.7-100% and ammonia removal up to 99.6% (Buslima et al., 2025), while heavy metal uptake varied considerably depending on the metal species, exposure duration, wastewater characteristics, and environmental conditions. These variations suggest that the effectiveness of *E. crassipes* is highly context-dependent and influenced by factors such as pH, pollutant concentration, hydraulic retention time, and plant physiological responses.

Despite these promising results, several limitations remain evident in the existing literature. Most studies were conducted under controlled experimental conditions or focused on conventional wastewater systems, while evidence from more complex environments such as post-mining void remains scarce. Mining void waters are typically characterized by acidic conditions (Woodbury et al., 2020), elevated dissolved metal concentrations (Gupta et al., 2025), fluctuating hydrological regimes (Martyushev et al., 2025), and low ecological productivity (Sukarman and Gani, 2020), which may affect phytoremediation performance differently from municipal or industrial wastewater systems. In addition, previous studies have predominantly emphasized short-term pollutant removal efficiency while paying limited attention to post-harvest biomass management, long-term maintenance requirements, and socio-economic feasibility. These gaps underscore the need for future studies to evaluate *E. crassipes* under actual post-mining conditions and to adopt integrated approaches that combine remediation effectiveness with sustainable biomass utilization and community participation to support long-term reclamation outcomes.

3.3 Opportunities and challenges of water hyacinth (*E. crassipes*) as a phytoremediation agent

E. crassipes has great potential for utilization as a phytoremediation agent. However, several challenges must be addressed to ensure the effective and sustainable application. To provide a more comprehensive understanding, Table 2 presents a summary matrix of the key opportunities and challenges associated with the use of *E. crassipes* in environmental remediation. This matrix aims to help readers gain an integrated overview and make informed decisions regarding the appropriate strategies for remediating environmental pollution.

Table 2. Opportunities and challenges of *E. crassipes* as a phytoremediation agent

Aspect	Opportunities	Challenges
Availability	Widely distributed, abundant, and easily obtained.	Potentially invasive, may dominate aquatic environments, and disrupt ecosystem stability.
Remediation capacity	Effective in stabilizing pH, reducing COD, TSS, and BOD, and absorbing heavy metals and excess nutrients.	Effectiveness varies depending on environmental conditions.
Cost	Low-cost due to easy accessibility and simple processing.	Requires post-mining handling for optimization and further treatment.
Socio-Economic	Potential to enhance community income through the production of handicrafts, compost fertilizer, and biogas.	Requires training and capacity building to produce value-added products.
Ecological	Contributes to improving and restoring water quality (aquatic habitats) affected by mining activities.	Risk of invasiveness leading to eutrophication and massive surface coverage.
Technological	Opportunities for integration with ecological engineering and technology to optimize remediation performance.	Limited research and development in certain regions and a need for stronger financial support.

Based on Table 2 and considering both the opportunities and challenges, *E. crassipes* demonstrates strong potential to serve as a phytoremediation agent in mining void due to the high adaptability and rapid colonization capability. According to Singh and Balomajumder (2021),

E. crassipes possesses a fibrous root system that extends deeply into the water column, enabling it to trap a wide range of pollutants. Hardestyariki and Fitria (2022) also reported that the plant hollow stems and broad leaves allow for pollutant accumulation in both tissue structures.

The opportunities and challenges associated with *E. crassipes* underscore a common trade-off in nature-based remediation strategies. The same biological characteristics that contribute to the remediation efficiency, including rapid growth and extensive biomass production, also underline the invasive potential (Correa-Mejía and Garcés-Gómez, 2025). Consequently, successful implementation depends not only on pollutant removal capacity but also on adaptive management strategies such as periodic harvesting, biomass monitoring, and stakeholder involvement. Without these supporting mechanisms, *E. crassipes*-based remediation may inadvertently generate new ecological problems despite its environmental benefits.

Socio-economic utilization should not be viewed only as an additional benefit but a mechanism to enhance the sustainability of reclamation programs. By converting harvested biomass into compost, handicrafts, or bioenergy products, operational costs associated with biomass disposal can be reduced while simultaneously creating incentives for community participation. This circular approach transforms waste management into value creation and may improve the long-term viability of phytoremediation initiatives in post-mining regions.

The variability in remediation performance observed across the studies presented in Table 1 suggests the effectiveness of *E. crassipes* is governed not only by external environmental conditions but also a series of physiological and biochemical adaptations that enable the plant to tolerate and process contaminants. Understanding this mechanism is important for interpreting why this species consistently performs well across different wastewater matrices while showing differences in removal efficiency among pollutant types. Figure 3 shows the principal pathways involved in metal uptake, translocation, detoxification, and sequestration in *E. crassipes*, providing a mechanistic explanation for the trends identified in the reviewed studies.

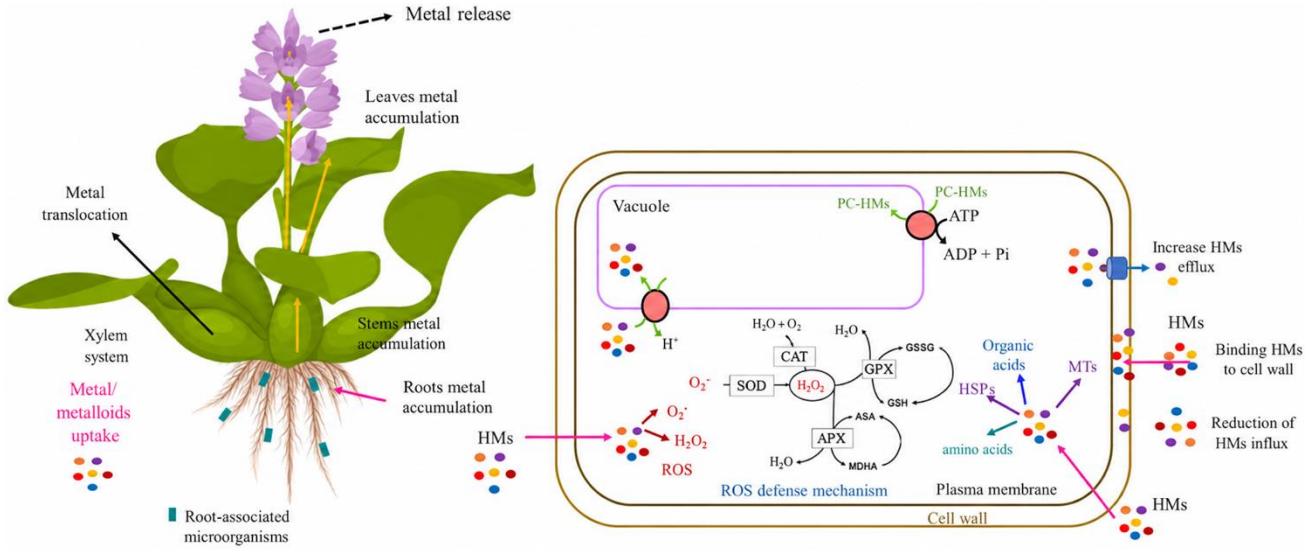


Figure 3. Mechanism of heavy metal elimination/accumulation at the cellular level. Notes: (CAT: Catalase, GPx: Glutathione peroxidase, GSH: Glutathione, GTS: Glutathione S-transferase, HMs: Heavy metals, PC: Phytochelatins, SOD: Superoxide dismutase). Source: Processed from Monroy-Licht et al. (2024)

As shown in Figure 2, phytoremediation by *E. crassipes* involves a coordinated process starting with the absorption of contaminants through the root system, followed by translocation through xylem tissues and subsequent accumulation in roots, stems, or leaves. Once inside plant cells, excess metals can trigger the formation of reactive oxygen species (ROS), which are counteracted by antioxidant enzymes such as superoxide dismutase (SOD), catalase (CAT), glutathione peroxidase (GPX), and ascorbate peroxidase (APX). In parallel, detoxification mechanisms involving phytochelatins,

metallothioneins, organic acids, and vacuolar sequestration reduce metal toxicity and allow the plant to survive under contaminated conditions (Monroy-Licht et al., 2024). These mechanisms help explain the broad contaminant spectrum reported in Table 1 and suggest that the adaptability of *E. crassipes* may be advantageous for the reclamation of mining void waters characterized by multiple stressors. However, the efficiency of these physiological responses may decline under extreme acidity or excessive metal loads commonly found in acid mine drainage environments, indicating that field-scale validation under actual post-mining conditions remains necessary (Pagoray and Ghitarina, 2020).

3.4 Integrated reclamation model for sustainable post-mining void management

Mining void or post-mining pond is an ecological legacy of extraction activities that pose serious environmental challenges (Christian et al., 2023), particularly concerning poor water quality (Mugova and Wolkersdorfer, 2025), elevated concentrations of dissolved heavy metals (Gupta et al., 2025), unstable slopes, and declining ecological functions (Du et al., 2023). Within this context, *E. crassipes* can serve as a nature-based solution due to the high phytoremediation capacity, ecological adaptability, and potential socio-economic benefits (Pagoray and Ghitarina, 2020). However, contrary to previous investigations that primarily focus on pollutant removal efficiency, this study proposes an integrated reclamation model combining ecological restoration with biomass valorization and community participation. The proposed model shifts reclamation practice from a remediation-oriented approach toward a multifunctional system capable of generating environmental, economic, and social benefits simultaneously (Ifa et al., 2023). A simplified schematic design of the proposed reclamation model is shown in Figure 4.



Figure 4. Simple Design of Void Management Based on *E. crassipes*. Source: Authors illustration

The system consists of five interconnected components, including floating *E. crassipes* rafts, vegetative buffer zones, controlled inlet-outlet channels, water quality monitoring points, and biomass utilization areas. Floating rafts act as the primary phytoremediation units, facilitating the uptake of heavy metals and excess nutrients from void waters through an extensive root system (Buslima et al.,

2025). Buffer vegetation established around void perimeter contributes to slope stabilization, runoff filtration, and erosion prevention, particularly important given that mining void slopes may range from 3° to 47° and are highly susceptible to degradation processes (Pambudi et al., 2023). Controlled hydraulic structures regulate circulation patterns and hydraulic retention time to optimize purification efficiency, while monitoring points located at the inlet and outlet sections enable adaptive management through periodic assessment of pH, dissolved oxygen, TSS, and heavy metal concentration (Gupta et al., 2025; Ma et al., 2021). The technical characteristics of each component are summarized in Table 3.

Beyond the technical functions, the proposed model emphasizes the integration of ecological and socio-economic objectives as a prerequisite for long-term sustainability. Periodic harvesting of *E. crassipes* biomass not only prevents uncontrolled proliferation of this invasive species but also creates opportunities for producing compost, handicrafts, animal feed, bioplastics, and bioenergy products. This circular approach transforms harvested biomass from a potential environmental liability into an economic resource that can strengthen local livelihoods and foster community participation (Agustin et al., 2023). The multifunctionality of each system component, as summarized in Table 4, shows that successful mining void reclamation should extend beyond pollution control to ecosystem recovery, economic empowerment, and local stewardship.

Table 3. Design elements of void reclamation system

Component	Function	Technical description	Reference
Floating *E. crassipes* zone	Phytoremediation of water contaminated with heavy metals, nitrates, and phosphates	Constructed using bamboo or recycled plastic rafts	Nash et al. (2019)
Edge buffer vegetation	Absorbs surface runoff and stabilizes void edges/slopes	Planted with vetiver, elephant grass, or *Acacia* sp.	Abba and Sabarinath (2025)
Inlet-outlet flow channels	Regulates circulation and extends hydraulic retention time	Inlet flow from surface runoff or rainfall	Iqbal et al. (2025)
Water quality monitoring points	Measures phytoremediation performance periodically	Fixed side points for pH, heavy metals, DO, TSS, and TDS	Correa-Mejía and Garcés-Gómez (2025)
Biomass utilization area	Harvesting zone for *E. crassipes* to produce handicrafts, fertilizers, bioplastics, and bioenergy	Scheduled based on optimal growth cycle	Nandiyanto et al. (2023)

Table 4. Ecological and socio-economic function matrix of the system design

Component	Function	Technical description	Reference
E. crassipes	Absorbs heavy metal	Used for handicrafts, animal feed, fertilizers, and bioenergy	Gezahegn et al. (2024), Guchhait et al. (2025), Ifa et al. (2023), Nandiyanto et al. (2023)
Artificial floating raft	Supports phytoremediator habitat	Community engagement in raft construction	Agustin et al. (2023), Iqbal et al. (2025)
Buffer vegetation	Prevents erosion and improves landscape	Provides fodder plants and supports soil conservation	Krishnani et al. (2025), Prasetyo et al. (2022)
Water monitoring zone	Evaluates system effectiveness continuously	Generates scientific data and provides community training	Datta et al. (2021), Dechassa (2020), Pambudi et al. (2026)
Biomass harvesting area	Regulates plant life cycle	Alternative source of local income	Degaga (2019), Maulidyna et al. (2021)

The proposed model reflects a transition from conventional post-mining rehabilitation practices toward integrated landscape restoration. This study positions phytoremediation in a broader sustainability perspective in which ecological resilience, circular biomass utilization, and community engagement are mutually reinforcing. However, because the model was developed through literature synthesis, its operational effectiveness under field conditions should be validated via pilot-scale implementation in actual mining void environments. Future studies should evaluate system performance under varying

hydrological and geochemical conditions while assessing economic feasibility and social acceptance among surrounding communities.

Despite the potential advantages, the practical implementation of this model requires careful consideration of operational feasibility and scale-related constraints. The use of floating phytoremediation systems based on locally available materials such as bamboo and recycled plastics may reduce initial investment costs compared to conventional chemical treatments or large-scale engineered remediation technologies (Malik et al., 2025). However, the effectiveness of the proposed system is possibly to vary according to void size, hydrological characteristics, contaminant loads, and maintenance capacity. A larger mining void may require phased implementation strategies and periodic harvesting programs to maintain treatment efficiency and prevent excessive proliferation of *E. crassipes.* Although nature-based solutions are generally considered cost-effective over the long term due to lower energy requirements and the possibility of biomass valorization (Gezahegn et al., 2024), detailed cost-benefit analysis and pilot-scale studies are still needed to determine economic viability under specific site conditions. Therefore, field-based experimentation involving local stakeholders should be prioritized to validate system performance, identify operational limitations, and refine the proposed model before wider adoption in post-mining reclamation practices.

4. CONCLUSION

In conclusion, the reclamation system designed for post-mining void using *E. crassipes* demonstrates a promising, eco-socio-technical approach to sustainable land and water restoration. The integration of floating phytoremediation zones, vegetative buffer strips, controlled inlet-outlet channels, water quality monitoring points, and biomass utilization areas effectively enhances water purification, stabilizes void slopes, and supports local livelihoods. The results confirm that *E. crassipes* efficiently absorbs heavy metals and nutrients, while supporting ecosystem resilience and socio-economic empowerment through biomass valorization. The system is consistent with sustainable reclamation principles, bridging ecological restoration and community-based resource management. Future studies should focus on quantifying long-term remediation efficiency, optimizing plant-microbe interactions, and developing scalable models adaptable to diverse post-mining landscapes. Strengthening policy integration and community participation will be crucial to mainstream this nature-based solution into broader sustainable development and post-mining management models.

AUTHOR CONTRIBUTIONS

Conceptualization; literature search; literature review; writing manuscript: Pambudi PA. Concept-ualization; reviewing manuscript: Utomo SW. Literature search; literature review; illustrating: Handoko RS.

DECLARATION OF CONFLICT OF INTEREST

The authors declare no conflict of interest.

REFERENCES

Abba A, Sabarinath S. Sustainable management of water hyacinth (*Eichhornia crassipes*): Community-Led strategies for livelihood enhancement in rural India. Results in Engineering 2025;26:Article No. 105033.

Abo-Alkasem MI, Hassan NH, Abo Elsoud MM. Microbial bioremediation as a tool for the removal of heavy metals. Bulletin of the National Research Center 2023;47(1):Article No. 31.

Agustin D, Anggriani N, Dewi AS, I FOC. Training on the utilization of water hyacinth waste into handicraft products for PKK women in Tambak Oso Village, Sidoarjo. Proceedings of the 7th International Seminar of Research; 2022 June 12-13; UPN Jatim, Surabaya: Indonesia 2023.

Albushairi SA, Huda N. Analysis of performance and competitiveness of water hyacinth crafts based on product differentiation, creativity, and green entrepreneurial. Proceedings of the International Conference on Management, Business, and Technology (ICOMBEST 2021), 2021 October 12, University of Jember; Indonesia; 2021. p. 127-32.

Archibong E, Ekanim M. Production of biogas using water waste products (water hyacinth and cow dung). Biomedical Science and Clinical Resesearch 2023;2(1):128-43.

Buslima FA, Abu Hasan H, Alias J, Jaganathan JS, Buhari J, Subramanian SV, et al. Performance of integrated biofilm-phytoremediation process in reclaiming water from domestic wastewater. Water (Switzerland) 2025;17(2):1-14.

Chen S, Ding Y. Tackling heavy metal pollution: Evaluating governance models and frameworks. Sustainability 2023;15(22):1-12.

Christian Y, Afandi A, Prabowo B, Rikardi N. The feasibility of converting ex-coal mining void into aquaculture in North Kalimantan. Journal of Degraded and Mining Lands Management 2023;10(2):4143-53.

Correa-Mejía LF, Garcés-Gómez YA. Water hyacinth invasion and management in a tropical hydroelectric reservoir: Insights from random forest and SVM classification. Ecologies 2025;6(8):1-15.

Datta A, Maharaj S, Prabhu GN, Bhowmik D, Marino A, Akbari V, et al. Monitoring the spread of water hyacinth (*Pontederia crassipes*): Challenges and future developments. Frontiers Ecology and Evolution 2021;9:Article No. 631338.

Dechassa N. Origin, Distribution, impact and management of water hyacinth (*Eichhornia crassipes* (Martius) Solm): A review. Journal of Environment and Earth Science 2020;10(10):13-18.

Degaga AH. Water hyacinth (*Eichhornia crassipes*) biology and its impacts on ecosystem, biodiversity, economy and human well-being. Journal of Life Science and Biomedicine 2019;8(6):94-100.

Du Z, Feng L, Wang H, Dong Y, Luo D, Zhang X, et al. Identification of ground deformation patterns in coal mining areas via rapid topographical analysis. Land 2023;12(6): Article No. 221.

Duruin AA, Lalantacon XF, Leysa JG, Lucero R, Obena RA, Sapal A, et al. Potential production of bioplastic from water hyacinth (*Eichornia crassipes*). ASEAN Journal of Science and Engineering 2022;2(2):139-42.

Edo GI, Itoje-akpokiniovo LO, Obasohan P, Ikpekoro VO, Samuel PO, Jikah AN, et al. Impact of environmental pollution from human activities on water, air quality and climate change. Ecological Frontiers 2024;44(5):874-89.

Endgaw F. Socio-ecological impacts of water hyacinth, Eichhornia crassipes (MART.) in Lake Tana, Gulf of Gorgora, Ethiopia. Journal of Applied Sciences and Environmental Management 2021;24(12):2017-25.

Fahruddin, Borrong DT, Tanjung RE, Abdullah A, Tuwo M. Morphological changes of water hyacinth (*Eichhornia crassipes*) during heavy metal phytoremediation. Jurnal Ilmu Alam dan Lingkungan 2023;14(1):65-71.

Fanta Y, Kechero Y, Yemane N. Effects of feeding water hyacinth (*Eichhornia crassipes*) fodder with or without commercial concentrate on zoo-technical performance and. bioRxiv 2024;12:1-27.

Gebrehiwot H, Dekebo A, Endale M. Chemical composition, pharmacological activities, and biofuel production of *Eichhornia crassipes* (Water Hyacinth): A review. Journal of the Turkish Chemical Society 2022;9(3):849-66.

Gezahegn A, Selassie YG, Agegnehu G, Addisu S, Mihretie FA, Kohira Y, et al. Sustainable weed management and soil enrichment with water hyacinth composting and mineral fertilizer integration. Environmental Challenges 2024;16:Article No. 101007.

Goel G, Kalamdhad AS. A practical proposal for utilisation of water hyacinth: Recycling in fired bricks. Journal of Cleaner Production 2018;190:261-71.

González-Tavares C, Salazar-Hernández M, Talavera-López A, Salgado-Román JM, Hernández-Soto R, Hernández JA. Removal of Ni(II) and Cu(II) in aqueous solutions using treated water hyacinth (*Eichhornia crassipes*) as bioadsorbent. Separations 2023;10(5):1-24.

Guchhait S, Paria DS, Shrestha R, Pradhan P, Roy A. Potentiality of *Eichhornia crassipes* as partial bovine feed: A step towards managing its invasiveness. Asian Journal of Agriculture 2025;9(1):60-7.

Gupta SK, Gupta R, Nage S, Kumar N, Kumari R, Gupta A, et al. Heavy metal accumulation and biomarker responses of Nile tilapia from a coal void reservoir cage aquaculture system. Journal of Hazardous Materials Advances 2025;18:Article No. 100631.

Hardestyariki D, Fitria S. Effectiveness and adaptability of water hyacinth (*Eichornia Crassipes*) mart. solm in its role in reducing COD and BOD levels in petroleum liquid waste. Journal of Ecological Engineering 2022;23(5):26-9.

Hasani Q, Pratiwi NTM, Wardiatno Y, Effendi H, Martin AN, Efendi E, et al. Phytoremediation of iron in ex-sand mining waters by water hyacinth (*Eichhornia crassipes*). Biodiversitas 2021;22(2):838-45.

Huynh AT, Chen YC, Tran BNT. A small-scale study on removal of heavy metals from contaminated water using water hyacinth. Processes 2021;9(10):Article No. 1802.

Ifa K, Meilan R, Yulianti A. Commercialization of handicraft products from water hyacinth in Aren Handicrafts. Empowerment Society 2023;6(2):59-65.

Iqbal U, Wahab A, Rafiq S, Noreen S, Abid S, Sharif M, et al. Structural traits driving water hyacinth (*Eichhornia crassipes*) aggressive spread and ecosystem disruption. Water, Air, Soil and Pollution 2025;236(7):Article No. 413.

Islam MN, Rahman F, Papri SA, Faruk MO, Das AK, Adhikary N, et al. Water hyacinth (*Eichhornia crassipes* (Mart.) Solms.) as an alternative raw material for the production of bio-compost and handmade paper. Journal of Environmental Management 2021;294:Article No. 113036.

Khambali, Anwar T, Wardoyo S. Innovation in utilisation of Apu-Apu (*Pistia stratiotes*) for phytoremediation of heavy metal contaminants in industrial wastewater - A case study on Local bodiversity. Journal of Ecological Engineering 2024; 25(12):333-9.

Krishnani KK, Boddu VM, Nagendrasai K, Arambam K, Jacob J, Chakraborty P, et al. The invasive aquatic macrophyte weed - Eichhornia: Its management, bioremediation potential, and valorisation. Journal of Environmental Chemical Engineering 2025;13:Article No. 119462.

Ma T, Luo H, Huang K, Pan Y, Tang T, Tao X, et al. Integrated ecological risk assessment of heavy metals in an oil shale mining area after restoration. Journal of Environmental Management. 2021;300:Article No. 113797.

Mahanta A, Sarmah D, Bhuyan N, Saikia M, Phukan S, Subramanyam KSV, et al. Geochemical and petrological studies of high sulfur coal and overburden from Makum coalfield (Northeast India) towards understanding and mitigation of acid mine drainage. International Journal of Coal Science and Technology 2024;11(7):Article No. 7.

Malik K, Iftikhar A, Maqsood Q, Tariq MR, Ali SW. Cleaner horizons: Exploring advanced technologies for pollution remediation. Biotechnology Reports 2025;46:e00890.

Martyushev DA, Ponomareva IN, Davoodi S, Kazemzadeh Y, Kadkhodaie A, Tao Z. Deformation of the void space of pores and fractures of carbonates: Comprehensive analysis of core and field data. Energy Geoscience 2025;6:Article No. 100364.

Maulidyna A, Alicia F, Agustin HN, Dewi IR, Nurhidayah I, Dewangga A, et al. Review: Economic impacts of the invasive species water hyacinth (*Eichhornia crassipes*): Case study of Rawapening Lake, Central Java, Indonesia. International Journal of Bonorowo Wetlands 2021;11(1):18-31.

Monroy-Licht A, Carranza-Lopez L, De la Parra-Guerra AC, Acevedo-Barrios R. Unlocking the potential of *Eichhornia crassipes* for wastewater treatment: phytoremediation of aquatic pollutants, a strategy for advancing Sustainable Development Goal-06 clean water. Environmental Science and Pollution Research 2024;31(31):43561-82.

Mothetha M, Kebede K, Masindi V, Msagati TAM. Effective treatment of real acid mine drainage using MgO-metakaolinite nanocomposite. Journal of Water Process Engineering 2023;51:Article No. 103370.

Moyo A, Do Amaral Filho JR, Harrison STL, Broadhurst JL. Acid mine drainage and metal(loid) risk potential of South African coal processing wastes. Mineral Engineering 2024;215:Article No. 108825.

Mugova E, Wolkersdorfer C. Understanding the influence of stratification for mine water management: A comparative study. Scientific Reports 2025;15(1):Article No. 2757.

Nandiyanto ABD, Ragadhita R, Hofifah SN, Al Husaeni DF, Al Husaeni DN, Fiandini M, et al. Progress in the Utilization of Water Hyacinth as Effective Biomass Material. Vol. 26, Environment, Development and Sustainability. Netherlands: Springer; 2023. p. 24521-68.

Nash DAH, Abdullah SRS, Hasan HA, Idris M, Muhammad NF, Al-Baldawi IA, et al. Phytoremediation of nutrients and organic carbon from sago mill effluent using water hyacinth (*Eichhornia crassipes*). Journal of Engineering and Technological Sciences 2019;51(4):573-84.

Noor I, Arifin YF, Priatmadi BJ, Saidy AR, Triantoro A. Integrated acid mine drainage treatment with post-mining reclamation via Swampy Forest System. Mining, Metallurgy and Exploration 2024;41(6):3409-17.

Nooryaneti M, Tuhuloula A, Irawan C. Phytoremediation processes of sasirangan textile industrial wastewater treatment using water hyacinth. Jurnal Kimia Valensi 2022;8(2):232-9.

Ordóñez JI, Cortés S, Maluenda P, Soto I. Biosorption of heavy metals with algae: Critical review of its application in real effluents. Sustainability 2023;15(6):Article No. 5521.

Page MJ, McKenzie JE, Bossuyt PM, Boutron I, Hoffmann TC, Mulrow CD, et al. The PRISMA 2020 statement: An updated guideline for reporting systematic reviews. British Medical Journal 2021;372:Article No. 71.

Pagoray H, Ghitarina G. The use of aquatic plants as organic absorbent in coal mining void used for aquaculture. AACL Bioflux 2020;13(2):857-64.

Pambudi PA, Utomo SW, Handoko RS. Assessment of toxic metal contamination and water source usage in mining-affected communities. Journal of Water and Land Development 2026;69:149-65.

Pambudi PA, Utomo SW, Handoko RS. Coal mining reclamation: Lessons learned from tropical and subtropical countries. Journal of Environmental Science and Sustainable Development 2025;8(1):148-84.

Pambudi PA, Utomo SW, Soelarno SW, Takarina ND. Coal mining reclamation as an environmental recovery effort: A review. Journal of Degraded and Mining Lands Management 2023;10(4):1001-11.

Panneerselvam B, Priya KS. Phytoremediation potential of water hyacinth in heavy metal removal in chromium and lead contaminated water. International Journal of Environmental Analytical Chemistry 2023;103(13):3081-96.

Prasetyo S, Anggoro S, Soeprobowati TR. Water hyacinth *Eichhornia crassipes* (Mart) solms management in Rawapening Lake, Central Java. AACL Bioflux 2022;15(1):532-43.

Rahim A, Soeprobowati TR. Bioaccumulation of lead (Pb) by the common water hyacinth *Eichhornia crassipes* (Mart.) solms in Batujai reservoir, central Lombok regency, Indonesia. AACL Bioflux 2018;11(5):1435-44.

Rahmawati A, Warsito. Domestic wastewater treatment using water hyacinth to produce clean water. Rekayasa Hijau: Jurnal Teknologi Ramah Lingkungan 2020;4(1):1-8.

Reich MS, Kindra M, Dargent F, Hu L, Flockhart DTT, Norris DR, et al. Metals and metal isotopes incorporation in insect wings: Implications for geolocation and pollution exposure. Frontiers in Ecology and Evollution 2023;11:e1085903.

Tabinda AB, Irfan R, Yasar A, Iqbal A, Mahmood A. Phytoremediation potential of *Pistia stratiotes* and *Eichhornia crassipes* to remove chromium and copper. Environmental Technology 2020;41(12):1514-9.

Tabla-Hernandez J, Rodriguez-Espinosa PF, Mendoza-Pérez JA, Sánchez-Ortíz E, Martinez-Tavera E, Hernandez-Ramirez AG. Assessment of potential toxic metals in a ramsar wetland, Central Mexico and its self-depuration through *Eichhornia crassipes*. Water (Switzerland) 2019;11(6):Article No. 1248.

Taufikurahman T, Rahmawati A, Ardiansyah MA, Ilhamsyah DPA, Rosanti S. Physiological strategies of *Eichhornia crassipes* (Mart.) Solms to tolerate Cr^{6+} accumulation, compared to a sensitive species *Pistia stratiotes* L. Jurnal Ilmu Lingkungan 2020;18(1):82-8.

Sachin CG, Sonal CG. Phytoremediation process of textile industry effluent by *Eichhornia crassipes* and *Pistia stratiotes*. International Journal for Multidisciplinary Research 2023; 5(6):1-9.

Saidy AR, Priatmadi BJ, Septiana M. Influence of type and amount of organic matters on the iron sorption of acid mine drainage onto reclaimed-mining soils. Journal of Degraded and Mining Lands Management 2021;8(4):2985-94.

Serafini LF, Arrobas M, Rodrigues MÂ, Feliciano M, Miguens F, Oliveira V, et al. The composting of water hyacinth: A life cycle assessment perspective. Waste and Biomass Valorization 2024;16:507-23.

Sekhohola-dlamini LM, Keshinro OM, Masudi WL, Cowan AK. Elaboration of a phytoremediation strategy for successful and sustainable rehabilitation of disturbed and degraded land. Minerals 2022;12(2):Article No. 111.

Sharma JK, Kumar N, Singh NP, Santal AR. Phytoremediation technologies and their mechanism for removal of heavy metal from contaminated soil: An approach for a sustainable environment. Frontiers Plant Science 2023;(14):e1076876.

Shi Y, Feng Y, Wang J, Bai Z, Feng X, Chen B. Optimal allocation of technical reclamation and ecological restoration for a cost-effective solution in Pingshuo Opencast Coal Mine area of China. Journal of Environmental Management 2025;373: Article No. 123951.

Shruthi S, Hemavathy RV. Myco-remediation of chromium heavy metal from industrial wastewater: A review. Toxicology Reports 2024;(13):Article No. 101740.

Singh N, Balomajumder C. Phytoremediation potential of water hyacinth (*Eichhornia crassipes*) for phenol and cyanide elimination from synthetic/simulated wastewater. Applied Water Science 2021;11:Article No. 144.

Sofyan ET, Gumelar FA, Yuniarti A, Joy B, Wicaksono FY. Effectiveness of water hyacinth compost and N, P, K, S fertilizer on S-available, S uptake, protein content, and yield of shallot in Inceptisols from Jatinangor. Kultivasi 2023;22(1):16-25.

Soliman ERS, Moustafa K, Khamis M, Shedeed ZA. Chromium "(VI)" phytoremediation using *Azolla pinnata*: Effects on Vicia faba growth, physiology, cytogenetics, and gene expression profiling. BMC Plant Biology 2025;25(1):Article No. 160.

Srivastava V, Sarkar A, Singh S, Singh P, de Araujo ASF, Singh RP. Agroecological responses of heavy metal pollution with special emphasis on soil health and plant performances. Frontiers Environmental Science 2017;5:Article No. 64.

Sukarman, Gani RA. Ex-coal mine lands and their land suitability for agricultural commodities in South Kalimantan. Journal of Degraded and Mining Lands Management 2020;7(3):2171-83.

Tumembouw SS, Pangkey H, Kusen DJ. Water hyacinth (*Eichhornia crassipes*) as a phytoremediator for organochlorine pollutants in Lake Tondano. AACL Bioflux 2024;17(4):1388-95.

Ullah MH, Rahman MJ. Adsorptive removal of toxic heavy metals from wastewater using water hyacinth and its biochar: A review. Heliyon 2024;10(17):e36869.

Waseem M, Khilji SA, Tariq S, Jamal A, Alomrani SO, Javed T. Phytoremediation of heavy metals from industrially contaminated soil using sunflower (*Helianthus annus* L.) by inoculation of two indigenous bacteria. Plant Stress 2024;11:Article No. 100297.

Woodbury DJ, Yassir I, Arbainsyah, Doroski DA, Queenborough SA, Ashton MS. Filling a void: Analysis of early tropical soil and vegetative recovery under leguminous, post-coal mine reforestation plantations in East Kalimantan, Indonesia. Land Degraddation and Development 2020;31(4):473-87.

Yuan Y, Cao C, Feng Y, Miao Y, Zhou Z, Zhang S. Influence of long-term ecological reclamation on carbon and nitrogen cycling in soil aggregates: The role of bacterial community structure and function. Science of the Total Enviroment 2024;954:Article No. 176729.

Environment and Natural Resources Journal

Volume 24
Issue 6
2026

Performance of Microbial Fuel Cells Integrated with a Photo-Bioreactor: Effects of Light Regimes and Microalgae (*Chlorella* vs. *Scenedesmus*)

Hoang Phuong Tuan Nguyen[1,2], Nguyen Xuan Que Vo[1,2], Thanh Son Dao[1,2], and Hoang Dung Nguyen[1,2*]

[1]*Ho Chi Minh City University of Technology (HCMUT), 268 Ly Thuong Kiet Street, Dien Hong Ward, Ho Chi Minh City, Vietnam*
[2]*Vietnam National University Ho Chi Minh City, Tan Lap Quarter, Dong Hoa Ward, Ho Chi Minh City, Vietnam*

ARTICLE INFO

Received: 29 Dec 2025
Received in revised: 5 Jun 2026
Accepted: 10 Jun 2026
Published online: 25 Aug 2026
DOI: 10.32526/ennrj/24/20250392

Keywords:
Microbial fuel cells/ Photo-bioreactor/ Energy recovery/ Wastewater treatment/ Microalgae

*** Corresponding author:**
E-mail:
dungnguyen@hcmut.edu.vn

ABSTRACT

Microbial fuel cells (MFCs) represent a promising technology for wastewater treatment and energy recovery, because of their ability to simultaneously convert organic matter into electricity via electroactive bacteria in anode chambers. This technology can significantly decrease the high energy costs typically associated with conventional wastewater treatment. The incorporation of green microalgae to self-supply oxygen may further enhance the environmental sustainability of the MFC system. This study evaluates the feasibility of integrating a double-chamber MFC with a photo-bioreactor (PBR) using specific microalgae under different light conditions. The experimental results indicated that chemical oxygen demand (COD) removal efficiencies using *Chlorella vulgaris* and *Scenedesmus protuberans* were 76.28% and 86.71%, respectively. A notable variation in cell voltage was observed when shifting from continuous illumination to a 12-hour light/12-hour dark (12/12) cycle. Under the 12/12 light/dark regime, *Chlorella* and *Scenedesmus* produced voltages of 350 mV and 340 mV, respectively, while continuous light resulted in higher voltages of 390 mV and 400 mV. Power densities achieved under continuous and 12/12 lighting were 1,140 mW/m^3 and 975 mW/m^3 for *Chlorella*, and 1,350 mW/m^3 and 1160 mW/m^3 for *Scenedesmus*, respectively. Overall, the system's performance could be substantially improved by stabilizing influent concentration and flow rate. The integration of PBR into MFCs proved effective for simultaneous wastewater treatment and bioenergy recovery, with *Scenedesmus* and continuous illumination yielding superior performance.

HIGHLIGHTS

- MFC-PBR integration treats wastewater and recovers energy.
- Microalgae supply oxygen to boost energy recovery in MFCs.
- The photo-bioreactor optimizes microbial fuel cell power.
- Light regimes significantly impact wastewater treatment.

1. INTRODUCTION

Water pollution and energy scarcity are major global challenges, while urban wastewater remains a significant pollution source, with only about 12.5% treated before discharge. Conventional treatment is also energy-intensive due to aeration, highlighting the need for more energy-efficient technologies. Microbial Fuel Cell (MFC) technology is a promising bioenergy approach that has attracted significant attention in recent years due to its ability to simultaneously generate electricity and treat wastewater (Elangovan et al., 2023; Zhang et al., 2011). First reported over a century ago (Potter, 1911), MFCs convert organic matter in wastewater into electricity via bacterial oxidation in the anode, with electrons transferred to the cathode where oxygen acts as the electron acceptor. Although more efficient than conventional anaerobic systems, MFCs are still

Citation: Nguyen HPT, Vo NXQ, Dao TS, Nguyen HD. Performance of microbial fuel cells integrated with a photo-bioreactor: Effects of light regimes and microalgae (*Chlorella* vs. *Scenedesmus*). Environ. Nat. Resour. J. 2026;24(6):751-763. (https://doi.org/10.32526/ennrj/24/20250392)

limited by low power output and aeration energy demand. Microalgae are fast-growing photosynthetic microorganisms with applications in biofuel production, biomass generation, and environmental remediation. Species such as *Chlorella vulgaris* and *Scenedesmus protuberans* are widely studied for their high photosynthetic efficiency, CO fixation, oxygen production or ability to remove pollutants (Abdelfattah et al., 2023; Li et al., 2023). The application of algae in wastewater treatment has also become widespread, particularly when combining wastewater-grown microalgae with activated sludge (Su et al., 2011). Consequently, integrating green microalgae into MFC systems presents a promising approach to enhancing wastewater treatment efficiency, generating electricity, and conserving energy. Incorporating an algal photobioreactor (PBR) into the MFC cathode chamber may further improve cathodic reactions and supply an oxygen-enriched electrolyte to the cathode.

In MFC systems, coupling microalgae with a photobioreactor (PBR) at the cathode can enhance oxygen supplies, improve cathodic reactions, and reduce external aeration requirements. In addition, microalgae contribute to CO_2 sequestration, pH stabilization, biofilm interactions, and nutrient removal, thereby improving both treatment efficiency and energy recovery.

This study evaluates an integrated MFC-PBR system using real wastewater, different light regimes, and two microalgae. Unlike previous work using synthetic wastewater, this study focuses on realistic conditions with varying organic loads. *Chlorella* and *Scenedesmus* were selected due to their distinct physiological traits and reported effectiveness. The novelty lies in the combined evaluation of real wastewater, light regimes, and microalgae in a single system, providing more practical insights for real-world applications.

2. METHODOLOGY

2.1 MFCs reactor configuration

The MFC system was designed with two chambers: an anode chamber (5.5×5.5×8.0 cm) and a cathode chamber (5.5×5.5×4.5 cm). The two reaction chambers were separated by gaskets and a cation exchange membrane (CEM) (CMI-7000S, size: 100 mm × 100 mm; Membrane International, USA).

The electrodes consisted of carbon cloth fibers wrapped around a platinum wire core (1 mm in diameter). The electrodes were connected via cooper wires to an external resistor, forming a closed circuit. Wastewater and microalgae were recirculated from storage tanks into the corresponding electrode chambers by a peristaltic pump (77200-50, Masterflex, USA).

An acrylic tubular photobioreactor (PBR) (d=0.14 m, h=0.37 m) equipped with white LED lamps (1×0.7×4 cm) providing a light intensity of 1285 lux (Model HLN3S, IST, Korea) was utilized to cultivate and supply oxygen-rich microalgae suspension to the cathode chamber. The oxygen-rich suspension from the microalgae reactor was filtered using a 0.01 μm UF filter (IONPIA, Korea) before being pumped into the cathode chamber to prevent algae from entering the electrochemical system. A timer was additionally installed to control the on/off mode of the LED light source, supporting the photosynthetic activity of microalgae in the photobioreactor (Figure 1).

2.2 Inoculation and medium

The system was acclimated with mixed wastewater in two steps. In step 1, synthetic wastewater (2.2 g $Na_2HPO_4 \cdot 12H_2O$; 0.53 g KH_2PO_4; 0.5 g NaCl; 0.03 g $MgSO_4 \cdot 7H_2O$; 0.02 g $CaCl_2 \cdot 7H_2O$; 2.92 g CH_3COONa for 1 L) containing acetate substrate (COD=2,000 mg/L; COD: Total Kjeldahl Nitrogen (TKN)=50:1; Q=1.0 mL/min) was used to acclimate and enrich the electroactive microbial community in the anode chamber. Anaerobic sludge was supplemented 2-3 times / (10 mL each time with MLSS=3,000 mg/L) into the anolyte solution during the first week of acclimation to improve the electrode-attached microbial community. In step 2, the system continued to be acclimated with mixed wastewater WW1 (COD=800 mg/L COD: TKN=3:1, Q=1.0 mL/min) for 14 days and WW2 (COD=1,500 mg/L; COD: TKN=5:1, Q=1.0 mL/min) for the following 14 days, until the cell potential became stable. Data for evaluating experimental performance was collected thereafter.

During the acclimation phase, WW1 and WW2 were prepared by mixing livestock wastewater collected from a cattle farm in Vinh Loc B Commune, Binh Chanh District (Ho Chi Minh City) and domestic wastewater collected from the drainage outlet behind Building B1 (of Ho Chi Minh City University of Technology) at a ratio of 1:10.

The microalgae culture solution was prepared with distilled water containing nutrient components including $MgSO_4$ (2.86 mg/L), $NaNO_3$ (93.4 mg/L),

$Ca(NO_3)_2$ (8.2 mg/L), $K_2HPO_4 \cdot 3H_2O$ (6.26 mg/L), Na_2CO_3 (4.2 mg/L), $FeCl_3$ (1.68 mg/L), EDTA (triplex) (3.705 mg/L), and 1 mL of trace element medium (Graffron solution) with microalgae cultivated in modified Z8 medium. The prepared solution had a COD=3 mg/L, PO_4^{3-}-P (Ortho-phosphate-P)=3 mg/L, and TKN=0.5 mg/L.

Biomass (both anode and cathode) was stored separately and pumped into the system at 1.0 mL/min during acclimation and 1.5 mL/min during operation. No mixing was applied in either chamber. The anode was fed with synthetic and real wastewater, while the cathode received the microalgae culture solution.

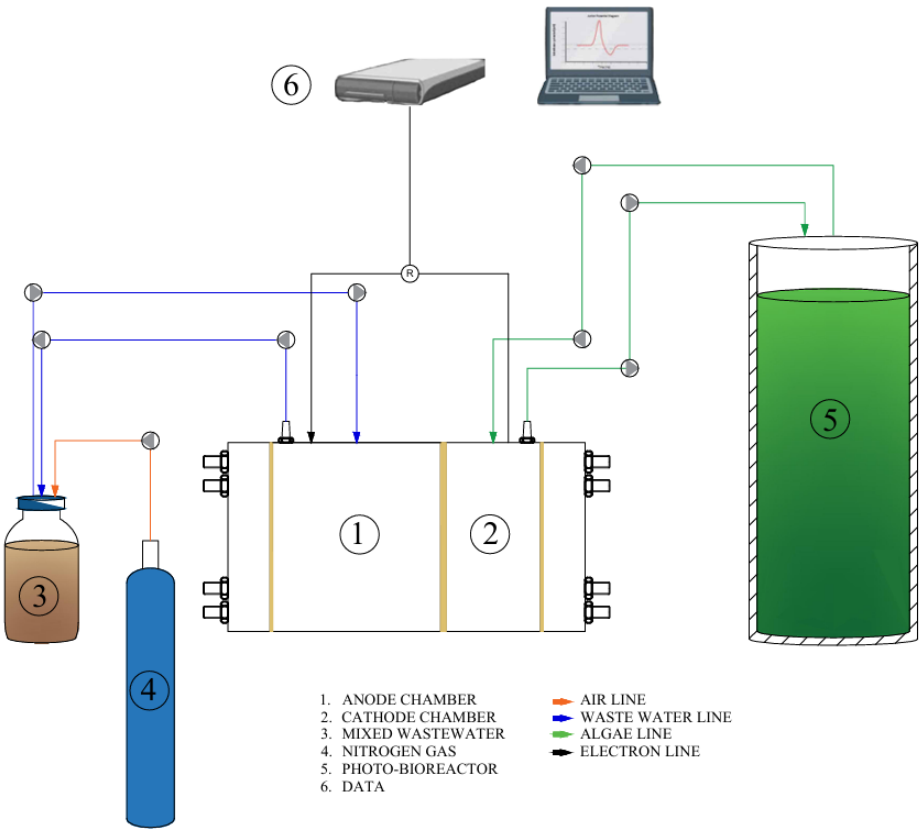


Figure 1. MFC with a PBR reactor setup

2.3 Start-up and operation

After the second acclimation phase, the MFC system entered the experimental stage using real wastewater. In MFC studies, varying external resistance is generally used to determine the open-circuit voltage and maximum power point, thereby balancing electricity generation, microbial growth, and overall system performance. Here, the optimal performance was evaluated using polarization curves. External resistance (Rext) was gradually decreased from 9,000 Ω to 0 Ω in steps of 100 Ω. Cell voltage and current were continuously recorded using a data logger (ADC-20, PicoTech, UK) every 30 min.

Current density normalized to anode volume was calculated as:

$$I = \frac{U}{R_{ext} \times V_{Chamber\ Anode}} \quad (1)$$

Where; I is current density (A/m³), U is voltage (V), Rext is external resistance (Ω), and Vanode is anode volume (m³).

Power density was calculated as:

$$P = U \times I \quad (2)$$

Where; P is power density (W/m³), U is voltage (V), and I is current density (A/m³).

U-I and P-I curves were constructed from measured and calculated data. Internal resistance was determined using a previously reported method (Zhang et al., 2015). Polarization curves were analyzed prior to operation.

The MFC-PBR system was evaluated using wastewater WW3 (COD=3,000 mg/L; COD:TKN= 10:1; Q=1.5 mL/min) with two microalgae under different light conditions (24/0 and 12/12) in the PBR.

The system was operated in batch mode with a flow rate of 1.5 mL/min, corresponding to HRTs of 90 min (anode) and 50 min (cathode). Wastewater was stored in an external reservoir and pumped into the reactor via a bottom inlet, creating an upflow regime. Effluent exited from the top outlet and was recirculated to the reservoir. Each batch lasted three days before being replaced with fresh wastewater.

Chlorella vulgaris and *Scenedesmus protuberans*, provided by the Ecotoxicology Laboratory, Ho Chi Minh City University of Technology, were cultured in sterile nutrient medium under aeration and continuous light. To evaluate illumination effects, the light regime was controlled at 12/12 (6:00 AM-6:00 PM) to support microalgae photosynthesis in the PBR. The microalgae medium and biomass were replaced at regular intervals.

2.4 Analysis and calculations

Parameters such as COD, PO_4^{3-}-P, and TKN were analyzed according to Standard Methods. COD was determined using the kali dichromate method, PO_4^{3-} was analyzed using the ascorbic acid method, and TKN was measured using the Kjeldahl method. Prior to analysis, samples were filtered through a 0.45 µm paper filter. This study focused on dissolved substrates as they represent the readily bioavailable fraction for microbial activity. The potential contribution of particulate matter, which may undergo hydrolysis and subsequent degradation, was not explicitly considered and should be addressed in future studies.

The organic matter consumption rate (kgCOD/m^3/day) was calculated based on the decrease in COD concentration over a given period and the volume of the anode chamber.

Coulombic efficiency (CE) was calculated based on the amount of COD removed using the following formula:

$$CE\ (\%) = \frac{M \times I}{F \times q \times n \times \Delta COD} \quad (3)$$

Where; M, I, F, q, n, and ΔCOD are respectively the molecular weight of O_2 (32 g/mol), current (A), Faraday's constant (96,485 C/mol), anolyte flow rate (L/s), the number of electrons exchanged per mole of O_2 (4 mol e^-/mol), and the difference in COD concentration between the influent and effluent of the anode chamber (g/L).

The volumetric power density (P_v, mW/m^3) of the MFC system was calculated using the effective volume of the anode chamber:

$$P_v(mW/m^3) = \frac{U \times I \times 10^{-3}}{v} \quad (4)$$

Where; U is the output voltage (V), v is the anode chamber volume (m^3), and I is the current (µA).

COD removal efficiency (%) was calculated as:

$$H\,(\%) = \frac{\Delta COD}{COD_{t0}} \times 100 \quad (5)$$

Where; ΔCOD is the difference in COD concentration between the start and end of the batch (3 days) (mg/L), and COD_{t0} is the influent COD concentration (mg/L).

The TKN removal efficiency (%) was calculated according to the following equation:

$$H\,(\%) = \frac{\Delta TKN}{TKN_{t0}} \times 100 \quad (6)$$

Where; ΔTKN is the difference in TKN concentration between the start and end of the batch (3 days) (mg/L), and TKN_{t0} is the influent TKN concentration (mg/L).

The TKN removal rate (mg/L/day) was calculated as:

$$H\,(mg/L/day) = \frac{\Delta TKN}{t} \quad (7)$$

Where; ΔTKN is the difference in TKN concentration between the start and end of the batch (3 days) (mg/L), and t is the hydraulic retention time or cycle duration (days).

3. RESULTS AND DISCUSSION

3.1 Voltage

Polarization analysis was conducted before operation to evaluate electrochemical performance. The maximum power output within the tested range was observed at around 1,000 Ω (Figure 2), which was therefore selected as the fixed external resistance for all experiments.

Data corresponding to each of the both microalgae (*Scenedesmus* and *Chlorella*) are clearly distinguished throughout the figures and text using consistent labeling and color coding.

3.1.1 Adaptation stage with acetate and mixed wastewater

Before operating with real wastewater, the system was acclimated using acetate (COD=2,000 mg/L) to ensure microbial adaptation. During this stage, COD reduction led to noticeable voltage fluctuations of 150-200 mV (Figure 3). Voltage increased sharply after fresh medium replacement but then decreased again within the following two days, reflecting substrate-dependent system behavior (from 211.96±12.72 mV down to 150.47±16.88 mV).

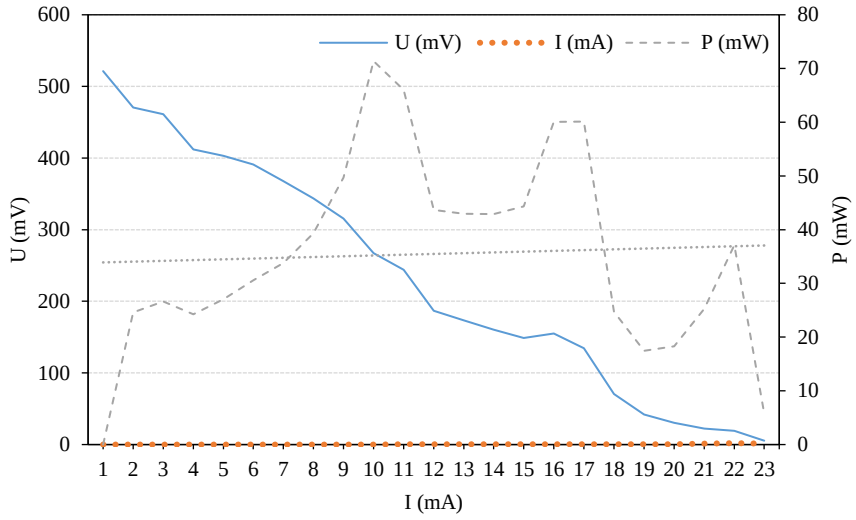


Figure 2. Polarization test

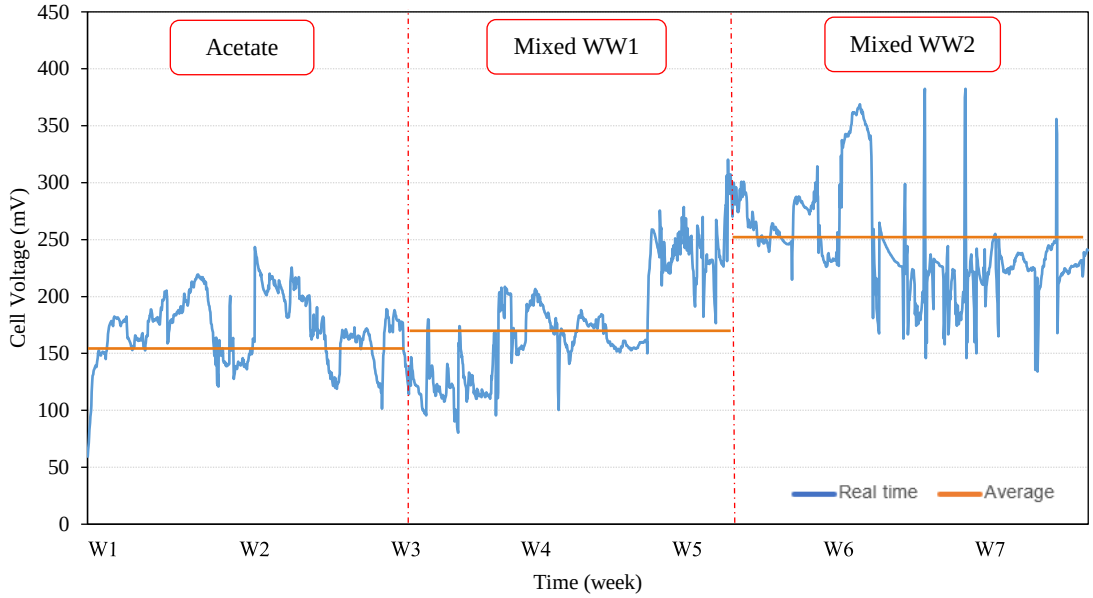


Figure 3. Cell voltage during the adaptation stage

After the adaptation stage with acetate as the substrate, the system was switched to adaptation with mixed wastewater WW1 (COD=800 mg/L; COD:TKN=3:1) for the following two weeks, and then to WW2 (COD=1,500 mg/L; COD:TKN=5:1) for four weeks (Figure 3). Previous studies on MFC systems have shown that low substrate concentrations significantly limit electricity generation. When COD levels decrease below a critical threshold, electron donor availability becomes insufficient, leading to reduced cell voltage and even system instability or shutdown (Logan et al., 2019; Zhang et al., 2015).

For WW1, cell voltage remained relatively high (>150 mV) and stable during the first week, then decreased and stabilized at 130-170 mV. This decline may be due to competing anaerobic processes such as

fermentation and methanogenesis, which consume substrates and reduce electron transfer. The higher COD threshold required for stable operation with real wastewater compared to simple substrates (e.g., acetate) reflects its complex and less biodegradable nature, limiting electroactive microbial activity (Zarabadi et al., 2019).

For WW2, voltage fluctuated between 175-300 mV (244.46±62.78 mV). Sharp drops occurred when COD fell below 140 mg/L, due to insufficient substrates, but recovery was observed after supplementation. Fluctuations compared to acetate-fed operation were attributed to shock loading and incomplete biofilm acclimation. Instability may also be related to microalgae inhibition under continuous illumination and biomass aging or decay (Montoya-Vallejo et al., 2025). Voltage spikes up to ~400 mV likely resulted from accumulation of dead algae, reducing photosynthetic efficiency, and indicating the need for periodic culture replacement.

It was observed that during the second week of the WW2 stage, the system sometimes spiked from about 150 mV up to nearly 400 mV. These spikes are likely attributed to the dynamic response of the anodic biofilm to the shock loading from the increased COD concentration. Specifically, the rapid hydrolysis and consumption of readily degradable organic fractions temporarily boosted electron transfer rates, leading to short-term voltage increases. After these easily degradable substrates were depleted, the voltage dropped again, reflecting that the microbial community had not yet fully stabilized and adapted. The dead microalgae cells settled, aggregated, and hindered the photosynthetic activity of the remaining healthy cells. Therefore, it should be noted that replacing the microalgae culture solution after each experimental run is necessary for system stability.

3.1.2 Operation stage with mixed wastewater

For the cathode chamber, the influent was supplied from the PBR under the conditions of two light/dark cycles: illumination conditions of 24/00 and 12 hours/day (12/12), in combination with *Chlorella*. Over the course of three weeks, the system was operated under 12/12 illumination in the PBR. At this time, the obtained cell voltage was 353.81±39.18 mV, fluctuating between 300-375 mV during the first two weeks, then increasing to 360-420 mV in the final week. The system was then switched to the WW3 (COD=3,000 mg/L; COD:TKN=10:1; Q=1.5 mL/min) *Chlorella* experiment with 24/00 illumination in the PBR. Cell voltage was then maintained at 391.72±47.62 mV and stabilized within 350-450 mV, with the highest value reaching 461.5 mV (Figure 4). At the beginning of each phase, voltage fluctuated due to system adaptation, and changing illumination conditions. After about one week, performance became more stable as both the anodic microbial community and PBR microalgae acclimated, improving overall system operation. Under the 12/12 light/dark regime, clear day-night voltage fluctuations were observed, whereas continuous illumination (24/0) resulted in higher and more stable voltage outputs. Compared to the acclimation phase, overall voltage performance was also higher during operation.

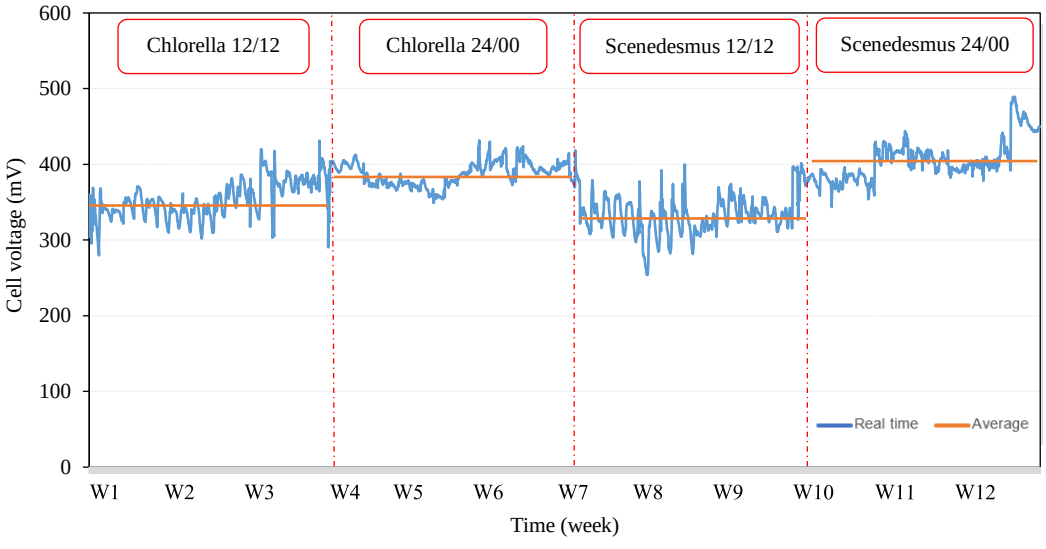


Figure 4. Cell voltage during operation stage with *Chlorella* and *Scenedesmus* microalgae

After the two WW3 experiments using *Chlorella*, the system process was performed with *Scenedesmus* under different illumination regimes of 24/00 and 12/12. During the first three weeks under the 12/12 light/dark cycle, the voltage was 339.47±19.28 mV, fluctuating between 300 and 360 mV. Continuous illumination (24/00) followed, and the cell voltage fluctuated around 400 mV, with an average of 393.96±32.97 mV and peak of 490 mV reached in the final week. Similar to the *Chlorella* experiments, the 12/12 regime showed clear voltage differences between light and dark phases, while continuous illumination (24/00) resulted in higher and more stable voltage due to improved system adaptation. Under 12/12, voltage drops (~250 mV) were linked to substrate depletion but rapidly recovered (>350 mV) after replenishment, indicating strong dependence on organic matter availability.

The superior performance of *Scenedesmus* should be interpreted cautiously, as previous studies have reported higher voltages for *Chlorella*, indicating strong dependence on operating conditions. The improved performance of *Scenedesmus* may be due to its ability to form stable cathodic biofilms, enhancing oxygen transfer and reducing internal resistance, while *Chlorella* may show different oxygen production behavior (Zhang et al., 2024; Argiz et al., 2022). Microalgae-microbial interactions may also influence electroactive communities and redox mediator production, making performance system-dependent.

Comparison of WW3 between the two microalgae species showed that under continuous illumination (24/00), *Scenedesmus* generated higher average and maximum voltages than *Chlorella*, although with greater fluctuations. Under the 12/12 light-dark regime, *Scenedesmus* produced lower voltages than *Chlorella* (Mathimani et al., 2021). In both microalgae systems, continuous illumination maintained higher and more stable voltages, with decreases observed only when COD dropped below 500 mg/L. Voltage rapidly recovered after wastewater replacement, indicating stable activity of acclimated electroactive microorganisms in the anode, consistent with previous studies (Zhang et al., 2024; Argiz et al., 2022). In contrast, intermittent illumination caused clear voltage fluctuations (approximately 50-75 mV), likely due to periodic changes in oxygen availability for cathodic reduction.

These differences can be explained by the influence of light on photosynthetic oxygen production in the cathode chamber. Continuous illumination supports stable cathodic reactions, whereas light/dark cycles may increase internal resistance and reduce system stability. Performance variations between *Chlorella* and *Scenedesmus* may also be related to their distinct physiological characteristics. *Scenedesmus* can form aggregates that potentially improve light utilization and interactions with cathodic biofilms, thereby enhancing oxygen transfer and electron transfer processes.

Compared with conventional MFCs, which rely on passive diffusion or aeration, an integrated PBR enables in situ oxygen production through photosynthesis, in turn reducing energy demands and improving cathodic performance (Logan, 2006; Argiz et al., 2022). However, microalgae-assisted systems also introduce more complex biological interactions and greater sensitivity to environmental conditions such as light regimes and nutrient availability.

3.2 Substrate removal

COD removal mainly depends on microbial activity and wastewater composition. Sequential biodegradation of complex organics also plays a key role (Edmundson and Huesemann, 2015; Sforza et al., 2012). In this study, higher influent COD led to better performance, with the highest efficiency (>85%) at 3,000 mg/L COD and a COD:TKN ratio of 10:1. Synthetic wastewater showed higher removal than real wastewater due to simpler substrates, consistent with typical MFC performance (~80%) (Zhang et al., 2011; Zhang et al., 2015). In the dual-chamber MFC system, osmotic pressure differences between the anolyte and catholyte may induce water transport across the membrane, potentially leading to partial dilution of the anolyte and an overstatement of the biological COD removal efficiency (Ge and He, 2012). However, no noticeable volume changes were observed during the experimental period, suggesting that this effect was limited. Therefore, although osmotic dilution may have contributed to a minor extent, COD removal was mainly attributed to biological degradation and electrochemical activity within the MFC system.

The organic loading rate (OLR) was defined as the mass of COD applied per unit reactor volume per unit time (kgCOD/m³/day). At a WW3 with *Chlorella vulgaris*, the system under continuous illumination (24/00 cycle) showed 0.86±0.05 kgCOD/m^3/day with a removal efficiency of 89.82±1.2%, which was superior to the 12/12 light/dark cycle 0.68±0.03 kgCOD/m³/day and 76.28±4.11%. This improvement can be attributed to the abundant substrate, which

promoted both biomass growth and electron flow. For *Scenedesmus protuberans* under the same condition, both the 24/00 and 12/12 cycles achieved showed slightly higher removal efficiency compared to *Chlorella* with 0.81±0.01 kgCOD/m³/day; 86.71± 2.3% in 12/12 and 0.91±0.08 kgCOD/m³/day; 89.95±1.6% in 24/00 (Figure 5).

Thus, it can be seen that COD removal efficiency is influenced by the illumination conditions in the PBR. Continuous lighting accelerates the COD removal rate, thereby enhancing the overall performance of the system. Compared with other studies which also used domestic wastewater and reported a COD removal efficiency of approximately 86% (Valladares Linares et al., 2019), our study achieved higher removal efficiencies for both microalgae species under continuous illumination (24/00). Only in the case of *Chlorella* under the 12/12 light-dark cycle was the COD removal efficiency slightly lower than that reported in previous studies. Meanwhile, the illumination conditions in the PBR influenced the stability of the cathodic oxygen supply-thereby supporting the overall electrochemical balance. Under continuous illumination (24/00), the system produced higher and more stable voltages, likely due to continuous oxygen supply supporting cathodic reactions and lowering internal resistance. In contrast, the 12/12 regime caused voltage fluctuations from periodic oxygen limitation and system adaptation. Overall, performance is governed by the balance between COD-driven electron supplies and DO-driven cathodic reactions. However, these conclusions remain preliminary due to limited microbial and controlled experimental data.

The relationship between COD removal and voltage was not strictly proportional. Although higher voltages were observed under continuous illumination (~393.96±32.97 mV vs. ~339.47±19.28 mV), the increase in COD removal was moderate. With DO consistently above 8 mg/L, oxygen limitation was unlikely, suggesting that performance differences are more related to system stability and biological interactions. Therefore, the results are interpreted cautiously, emphasizing trends rather than definitive causality.

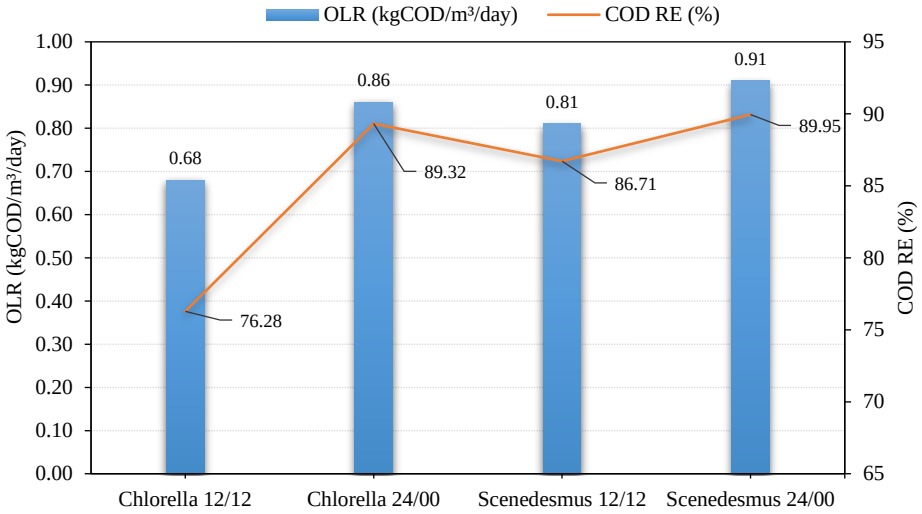


Figure 5. Organic loading rate and COD removal efficiency in operation stage

Coulombic efficiency (CE) reflects the proportion of electrons recovered from organics via electrochemical activity of biofilms dominated by *Geobacter sulfurreducens* (Ewusi-Mensah et al., 2021), and it fluctuates throughout MFC operation depending on the influent substrate. The results from this study show that CE under continuous illumination was higher than under the 12/12 light-dark cycle in both microalgae. Among them, *Scenedesmus protuberans* produced the highest result with 0.57±0.02%, under continuous illumination. Meanwhile, under the 12/12 light-dark condition, both microalgae gave almost similar results (Figure 6). However, compared with previous studies reporting a coulombic efficiency (CE) in the range of 1-10% (Valladares Linares et al., 2019), the energy conversion efficiency in this study was lower, even though the COD removal efficiency was comparable or higher.

The differences in performance between *Chlorella* and *Scenedesmus* should be interpreted cautiously within the specific conditions of this study. Although *Scenedesmus* showed higher voltage outputs (e.g., ~393.96±32.97 mV under 24/00 vs. ~339.47±19.28 mV under 12/12), this trend likely results from the combined effects of biological and operational factors rather than a single mechanism. One possible explanation relates to species-specific characteristics. *Scenedesmus* can form aggregates, which may enhance light utilization and interactions with cathodic biofilms, potentially improving oxygen transfer and system stability.

Overall, the superior performance of *Scenedesmus* in this study appears to be condition-dependent. Variations in factors such as OLR, reactor configuration, and microbial community may also contribute, and therefore the results should be interpreted as indicative trends rather than definitive conclusions.This superior performance is likely due to the higher photosynthetic efficiency of *Scenedesmus protuberans*, which ensured a more abundant oxygen supply for the cathodic reduction reaction, largely because its clustered chain-like cellular morphology enables more efficient light absorption (Min and Logan., 2004).

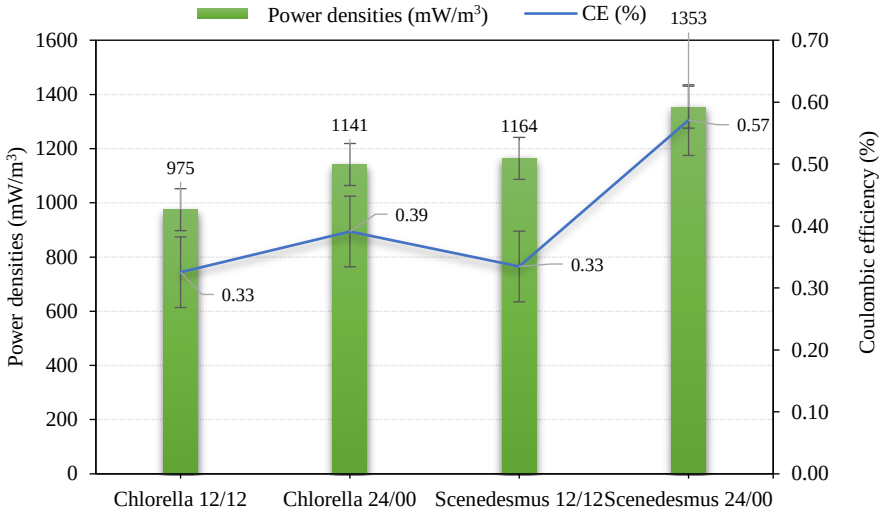


Figure 6. Power densities and coulombic efficiency in operation stage

3.3 Changes in the indicators PO_4^{3-}- P, TKN in the anode chamber

Phosphorus in this study was recorded in the form of PO_4^{3-}- P. In *Chlorella Vulgaris*, the PO_4^{3-}- P level on the first day in anode was 34.12±1.4 mg/L, then decreased to 26.37±2.3 mg/L under 12/12 light/dark condition. Under 24/00 illumination, initial PO_4^{3-}-P concentrations exceeded 43 mg/L. Overall, *Scenedesmus* showed higher phosphate removal efficiency than *Chlorella*, particularly under the 12/12 condition (Figure 7). Higher substrate loading in the anode corresponded to increased PO_4^{3-}-P levels, while differences between 24/00 and 12/12 suggest that PBR illumination may influence phosphorus dynamics in the anode. However, in the *Scenedesmus* system, similar influent phosphate levels led to comparable effluent concentrations, indicating that phosphate removal was more strongly governed by loading conditions than light regime alone. Phosphate removal depends on biological uptake and intracellular storage, which are limited by nutrient availability and biomass activity. Therefore, the effect of light should be interpreted cautiously when influent conditions are not strictly controlled, and further controlled studies are needed.

TKN was only recorded in the influent and the final sample of each wastewater batch due to experimental operating constraints. Based on the research results, the TKN of all experiments on the final day was lower when compared to the first day. In *Chlorella vulgaris*, the TKN level on the first day in anode was 316.83±11.2 mg/L, then decreased to 233.89±7.43 mg/L under 12/12 light/dark condition and 332.45±10.1 mg/L, then decreased to 272.43±8.6 mg/L with 24/00 illumination condition. In *Scenedesmus protuberans*, the TKN level on the first day was 331.74±6.2 mg/L, then decreased to 291.08±5.45 mg/L under 12/12 light/dark condition and 336.40±6.6 mg/L, then decreased to 289.58±9.5 mg/L with 24/00 illumination condition (Figure 8).

Chlorella showed higher TKN removal than *Scenedesmus*, especially under the 12/12 regime, likely due to differences in influent conditions affecting system activity. The decrease in TKN in wastewater was partly due to the conversion of ammonium into nitrite and nitrate during the nitrification process. First, ammonium, a primary component of TKN, migrates across the CEM to the cathode chamber to maintain electroneutrality during current generation (Nguyen and Babel, 2024). Once transported to the oxygen-rich environment of the PBR-cathode chamber, ammonium can undergo aerobic nitrification. Second, a portion of the nitrogen is assimilated into cellular biomass by the anodic electroactive biofilm for growth and metabolism. This suggests that nitrogen removal cannot be attributed to a single pathway. The TKN concentrations under the 12/12 and 24/00 illumination conditions for *Scenedesmus* were highly comparable. Therefore, no statistically significant difference in TKN removal was observed between these two lighting regimes for this specific microalgae.

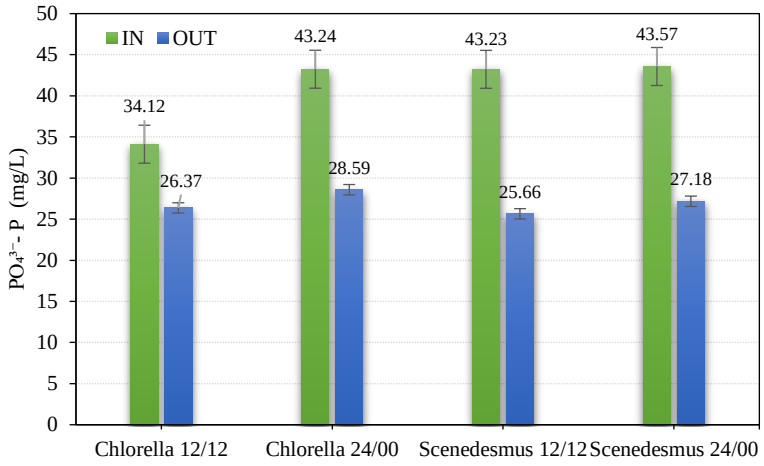


Figure 7. PO_4^{3-}- P in operation stage

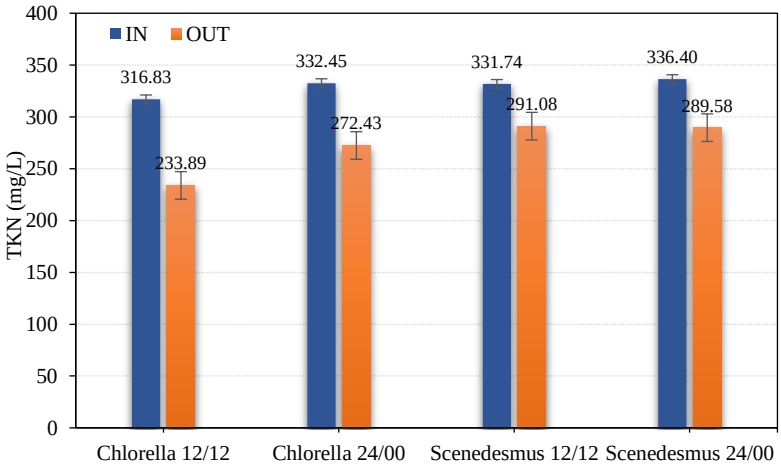


Figure 8. TKN in operation stage

3.4 Effect of light/dark regimes in the photobioreactor on MFC performance

In the photobioreactor, continuous microalgae growth is essential for electricity generation, requiring suitable conditions such as light/dark cycles, carbon sources, aeration, pH, and temperature (Zarabadi et al., 2019). Microalgae metabolism occurs in both light and dark phases, while respiration in the dark phase is important for biomass growth (Edmundson and Huesemann, 2015). Photosynthetic efficiency decreases under non-optimal conditions (Sforza et al., 2012). Therefore, the system was operated under two light regimes (24/00 and 12/12) to evaluate DO and pH using WW3 with *Chlorella* and *Scenedesmus*.

For WW3-*Chlorella*, DO under 12/12 started at 8.26 mg/L, increased above 8.0 mg/L, and then remained stable. Under 24/00, DO started at 8.4 mg/L and stabilized at 8-9 mg/L for two weeks. For WW3-

Scenedesmus, DO under 12/12 started at 9.09 mg/L and stabilized above 9.2 mg/L, while under 24/00 it increased from 6.86 mg/L to 9-10 mg/L. Overall, *Scenedesmus* produced about 1 mg/L higher DO than *Chlorella*, with more stable voltage generation (Figure 9). Although the DO difference (8 vs. 9 mg/L) may not strongly affect cathodic oxygen availability, it could influence microbial community structure and redox mediator production, thereby indirectly affecting electricity generation.

With the same initial conditions in both experiments (200 mL algae in 5 L medium), it was shown that dissolved oxygen fluctuated more under 12/12 (8.26±0.52 mg/L in *Chlorella* and 9.09±0.35 mg/L in *Scenedesmus*) than under 24/00 (8.4±0.26 mg/L in *Chlorella* and 9.3±0.44 mg/L in *Scenedesmus*). This was reasonable since during 12h of darkness, algae undergo respiration, leading to fluctuations in dissolved oxygen. Compared to previous studies (Zhang et al., 2011; Zhang et al., 2015), dissolved oxygen concentrations in this study were lower across all experiments. Despite fluctuations between the two regimes, dissolved oxygen consistently remained above 8 mg/L throughout the experiments.

MFC performance was also influenced by pH in the photobioreactor. Under 24/00, pH started at 8.0 and stabilized at ~8.4, while under 12/12 it remained around 8.6. Overall, pH showed no significant variation between the beginning and end of each batch and was lowest when DO decreased (8.0, DO=6.8 mg/L). Thus, light conditions had little effect on pH, and values in both regimes remained suitable for microalgae growth (Zarabadi et al., 2019) (Figure 10).

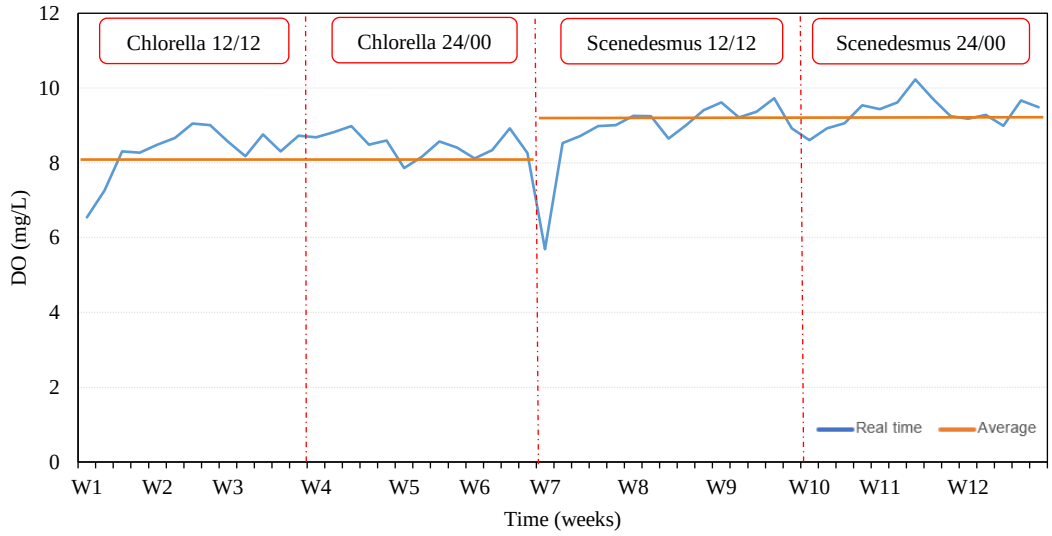


Figure 9. Dissolved oxygen in PBR during operation stage

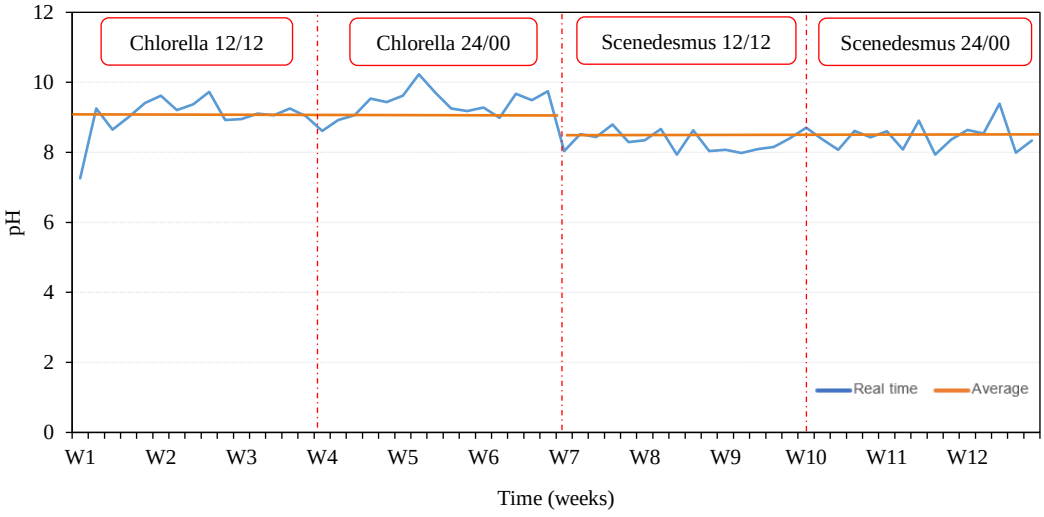


Figure 10. pH in PBR during operation stage

4. CHALLENGES AND FUTURE PERSPECTIVES

From the research results, it is evident that the MFC-PBR system holds great potential for wastewater treatment combined with energy recovery. *Chlorella vulgaris* demonstrated stable performance in both COD removal and energy recovery across two experimental runs under different light conditions. *Scenedesmus protuberans* achieved slightly higher efficiency. The system exhibited more consistent power output over time under the 24/00 condition, suggesting a potential improvement in operational stability. Moreover, the results also indicated that the system is capable of effectively treating wastewater with high concentrations, suggesting the possibility of applying it to various types of wastewater with different characteristics. In addition, testing multiple light regimes could help identify optimal illumination conditions for system development.

5. CONCLUSION

The results confirmed the feasibility of the MFC-PBR system under different light regimes, COD loadings, and microalgae. *Scenedesmus* consistently produced higher voltages than *Chlorella*, and continuous illumination (24/00) led to more stable and higher performance than the 12/12 cycle. For WW3-Scenedesmus, voltages were 339.47±19.28 mV (12/12) and 393.96±32.97 mV (24/00), with fluctuations observed under light/dark conditions. COD removal was higher under continuous light (89.64%) than under 12/12 cycles (81.5%), though differences may also be influenced by loading and dilution effects. DO remained >8 mg/L in both cases, suggesting that microbial interactions and redox mediators may also affect performance. Overall, light regime influences system behavior but cannot be considered independent of other factors. Continuous light improves stability due to sustained oxygen production, while light/dark cycles cause transient limitations. Differences between microalgae species indicate the role of physiological traits and biofilm interactions in system performance.

ACKNOWLEDGEMENTS

This research is funded by Vietnam National University HoChiMinh City (VNU-HCM) under grant number: C2025-20-14.

AUTHOR CONTRIBUTIONS

Hoang Phuong Tuan Nguyen: Conduct the research, prepare the draft paper and revise the paper based on the comments. Hoang Dung Nguyen: Supervision of research, correction of the submitted and revised manuscript, corresponding author. Nguyen Xuan Que Vo, Thanh Son Dao: revise and finalize the manuscript.

DECLARATION OF CONFLICT OF INTEREST

The authors declare that they have no known competing financial interests or personal relationships that could have appeared to influence the work reported in this paper.

REFERENCES

Abdelfattah A, Ali SS, Ramadan H, El-Aswar EI, Eltawab R, Ho S-H, et al. Microalgae-based wastewater treatment: Mechanisms, challenges, recent advances, and future prospects. Environmental Science and Ecotechnology 2023;13:Article No. 100205.

Argiz L, Correa-Galeote D, Del Río ÁV, Mosquera-Corral A, González-Cabaleiro R. Valorization of lipid-rich wastewaters: A theoretical analysis to tackle the competition between polyhydroxyalkanoate and triacylglyceride-storing populations. Science of the Total Environment 2022; 807:Article No. 150761.

Edmundson SJ, Huesemann MH. The dark side of algae cultivation: Characterizing night biomass loss in three photosynthetic algae, *Chlorella sorokiniana*, *Nannochloropsis salina*, and *Picochlorum* sp. Algal Research 2015;12:470-6.

Elangovan K, Saravanan P, Campos CH, Sanhueza-Gómez F, Khan MMR, Chin SY, et al. Outline of microbial fuel cells technology and their significant developments, challenges, and prospects of oxygen reduction electrocatalysts. Frontiers in Chemical Engineering 2023;5:Article No. 1228510.

Ewusi-Mensah D, Huang J, Chaparro LK, Rodenas P, Ramírez-Moreno M, Ortiz JM, et al. Algae-assisted microbial desalination cell: Analysis of cathode performance and desalination efficiency assessment. Processes 2021;9(11): Article No. 2011.

Ge Z, He Z. Effects of draw solutions and membrane conditions on electricity generation and water flux in osmotic microbial fuel cells. Bioresource Technology 2012;109:70-6.

Li L, Gao K, Yang M, Zheng Q, Zhang M, Deng X. Challenges and potential solutions of microalgae-based systems for wastewater treatment and resource recovery. Frontiers in Bioengineering and Biotechnology 2023;11:Article No. 1210228.

Logan BE, Rossi R, Ragab A, Saikaly PE. Electroactive microorganisms in bioelectrochemical systems. Nature Reviews Microbiology 2019;17(5):307-19.

Logan BE. Energy diversity brings stability. Environmental Science and Technology 2006;40(17):Article No. 5161.

Mathimani T, Sekar M, Shanmugam S, Sabir JSM, Chi NTL, Pugazhendhi A. Relative abundance of lipid types among *Chlorella* sp. and *Scenedesmus* sp. and ameliorating homogeneous acid catalytic conditions using central composite design (CCD) for maximizing fatty acid methyl ester yield. Science of the Total Environment 2021;771:Article No. 144700.

Min B, Logan BE. Continuous electricity generation from domestic wastewater and organic substrates in a flat plate microbial fuel cell. Environmental Science and Technology 2004;38(21):5809-14.

Montoya-Vallejo C, Quintero Díaz JC, Yepes YA, Fernández-Morales FJ. Microalgal microbial fuel cells: A comprehensive review of mechanisms and electrochemical performance. Applied Sciences 2025;15(6):Article No. 3335.

Nguyen HD, Babel S. Bioelectricity recovery through isolation and removal of nitrogen from wastewater by shortcut nitrification-denitrification in a coupled microbial fuel cell system. Fuel 2024;359:Article No. 130497.

Potter MC. Electrical effects accompanying the decomposition of organic compounds. Proceedings of the Royal Society of London. Series B, Containing Papers of a Biological Character 1911;84(571):260-76.

Sforza E, Simionato D, Giacometti GM, Bertucco A, Morosinotto T. Adjusted light and dark cycles can optimize photosynthetic efficiency in algae growing in photobioreactors. PLoS One 2012;7(6):e38975.

Su Y, Mennerich A, Urban B. Municipal wastewater treatment and biomass accumulation with a wastewater-born and settleable algal-bacterial culture. Water Research 2011;45(11): 3351-8.

Valladares Linares R, Domínguez-Maldonado J, Rodríguez-Leal E, Patrón G, Castillo-Hernández A, Miranda A, et al. Scale up of microbial fuel cell stack system for residential wastewater treatment in continuous mode operation. Water 2019;11(2): Article No. 217.

Zarabadi MP, Charette SJ, Greener J. Toggling Geobacter sulfurreducens metabolic state reveals hidden behaviour and expanded applicability to sustainable energy applications. Sustainable Energy and Fuels 2019;3(9):22110-7.

Zhang X, He W, Ren L, Stager J, Evans PJ, Logan BE. COD removal characteristics in air-cathode microbial fuel cells. Bioresource Technology 2015;176:23-31.

Zhang Y, Cheng K, Mei H, Qin W. A novel algal-algal microbial fuel cell for enhanced chemical oxygen demand removal. Water 2024;16(19):Article No. 2798.

Zhang Y, Min B, Huang L, Angelidaki I. Electricity generation and microbial community response to substrate changes in microbial fuel cell. Bioresource Technology 2011;102(2): 1166-73.

Environment and Natural Resources Journal

Volume 24
Issue 6
2026

A Preliminary Physical Property Characterization of *Artocarpus blancoi* (Antipolo) from Maguindanao Province of Mindanao

Ben G. Dres[1], Rafael T. Acob[1], Jayric F. Villareal[1*], Cindy E. Poclis[1], Rowena C. Benavides[1], and Oliver S. Marasigan[2]

[1]College of Forestry and Environmental Studies, Mindanao State University-Maguindanao, Dalican, Datu Odin Sinsuat, 9601, Maguindanao del Norte, Bangsamoro Autonomous Region in Muslim Mindanao (BARMM), Philippines
[2]Forest Products Research and Development Institute (FPRDI), Department of Science and Technology (DOST), College, Laguna, 4031 Philippines

ARTICLE INFO

Received: 8 Apr 2026
Received in revised: 20 Jul 2026
Accepted: 27 Jul 2026
Published online: 22 Sep 2026
DOI: 10.32526/ennrj/24/20260141

Keywords:
Basic density/ Height levels/ Moisture content/ Philippine endemic species/ Volumetric shrinkage

*** Corresponding author:**
E-mail:
jfvillareal@msumaguindanao.edu.ph

ABSTRACT

This study examined the physical properties of *Artocarpus blancoi* wood, focusing on moisture content (MC), basic density (BD), and directional and volumetric shrinkage across tree samples and height levels. Three trees aged approximately 5 to 10 years, were sampled from Maguindanao del Norte in the Bangsamoro Autonomous Region in Muslim Mindanao (BARMM), Philippines. Testing procedures based on ASTM D143 standards were employed. Results showed that tree 1 recorded the lowest MC (98.58%) and the highest BD (384.28 kg/m³). Along height levels, the top portion exhibited the lowest MC (110.51%), while the bottom portion recorded the highest BD (398.62 kg/m³). For shrinkage properties, tree 2 consistently showed the lowest values for tangential shrinkage (TS) (4.59%), radial shrinkage (RS) (2.44%), and longitudinal shrinkage (0.17%), and the lowest volumetric shrinkage (VS) (6.93%). Relative to height levels, the top portion exhibited the lowest TS (4.34%) and VS (7.14%), whereas RS and LS did not differ significantly among height levels. Statistical analyses revealed significant differences in MC and BD among both individual trees and height levels. The RS, LS, and VS varied significantly among individual trees, while TS and VS differed across height levels. Based on the classification systems for density and volumetric shrinkage established by the Forest Products Research and Development Institute (FPRDI), *A. blancoi* falls under low density and falls within the low to moderately low shrinkage classes. These findings suggest that *A. blancoi* has potential as a resource for value-added wood products from high end to standard grade furniture and other non-structural applications, light weight and dimensional stability are of great advantageous. However, it is vital to note that this study was limited to physical property assessment, and did not encompass anatomical and mechanical characterization, durability and/or processing tests, which are valuable for a more comprehensive evaluation of this species.

HIGHLIGHTS

This study employed a systematic sampling approach that examined physical properties of *A. blancoi* wood, including moisture content, basic density, and directional and volumetric shrinkage across tree samples and height levels (bottom, middle, and top), with statistical comparisons performed through analysis of variance. Results revealed significant difference in all measured properties among tree samples, except for tangential shrinkage. Moreover, moisture content, basic density, and tangential and volumetric shrinkages decreased significantly from bottom to top portions. Classification according to FPRDI standards positions *A. blancoi* in low density and within low to moderately low volumetric shrinkage groups, indicating preliminary suitability for non-structural applications pending further mechanical and durability assessment.

1. INTRODUCTION

Wood is one of the most used renewable raw materials and the main source of livelihood of the people belonging to the forest products sector. As a structural material, wood can be used in many forms of construction, but it is fundamental to know the properties and its relationship. In the Philippines, the demand for wood and other timber products has

Citation: Dres BG, Acob RT, Villareal JF, Poclis CE, Benavides RC, Marasigan OS. A preliminary physical property characterization of *Artocarpus blancoi* (Antipolo) from Maguindanao Province of Mindanao. Environ. Nat. Resour. J. 2026;24(6):764-774. (https://doi.org/10.32526/ennrj/24/20260141)

increased over the years (Mendoza et al., 2019). The country possesses significant potential for a thriving wood industry due to its rich biodiversity of over 3,600 native tree species, of which 65% are endemic (Fernando et al., 2008), which could also serve as sustainable raw material sources. However, this potential resource remains largely unexploited due to inadequate evaluation of lesser-known species, persistent research gaps, habitat loss, and socioeconomic and other human-caused pressures, which collectively result in inefficient utilization and missed economic opportunities (DENR-FMB, 2020). Moreover, the Philippine government, in pursuant to Executive Order 23 Series 2011, declares a moratorium on the cutting and harvesting of timber in the entire country's natural and residual forests (Government of the Philippines, 2011).

Artocarpus blancoi, commonly known as 'Antipolo', a fast-growing and endemic species to the Philippines, exemplifies this challenge. It naturally thrives from low to mid-elevation forests in various provinces, from Luzon to Mindanao islands (EDC, 2020). Considering its significant contribution culturally and traditionally for furniture and carving, its potential remains constrained by critical knowledge gaps in wood science, particularly in understudied regions like Maguindanao. It is locally known as 'Tegep', characterized as a medium to large tree reaching a height of 30 m and a diameter up to 60 cm valued for its durable wood, and classified as moderately low strength (Alipon et al., 2022). *A. blancoi* also serves as a substitute for *Artocarpus heterophyllus* (Jackfruit) in construction purposes, furniture, cabinets, and musical instruments. Its bark possesses antimicrobial properties, its leaves are consumed by the Aeta people in Porac, Pampanga, and burned as a mosquito repellent, and its seeds are edible when boiled (Malabrigo and Umali, 2022).

Basically, *A. blancoi* faces dual threats like ecological vulnerability and technical neglect. Under the Philippine Native Plants Conservation Society, *A. blancoi* is classified as Vulnerable (Stuart, 2020). Its populations are declining due to habitat loss from urbanization, mining operations, small-scale and large-scale logging operations, and other unsustainable farming practices (DENR-FMB, 2020). Despite these threats, *A. blancoi* was globally assessed as Least Concern, considering its widespread distribution all throughout the country (EDC, 2020). Simultaneously, the absence of comprehensive wood property data hampers sustainable industrial use. Current knowledge of *A. blancoi* in the Philippines is predominantly limited to basic botanical descriptions, anatomical features, and silvicultural assessments (FPRDI, 1986; EDC, 2020; Malabrigo and Umali, 2022). A recent characterization of its physical and mechanical properties, along with other fruit-bearing and underutilized tree species, was conducted on samples collected from Caraga region, Batangas city, and Quezon province (Alipon et al., 2022). The study classified *A. blancoi* wood under moderately low density, comparable to *Artocarpus heterophyllus* and *Sandoricum koetjape*, and falls under moderately low volumetric shrinkage, similar to *Litsea perrottetti*.

However, wood properties typically vary with site conditions, and the existing findings cannot reliably extrapolate across geographic locations. Notably, no comprehensive study has been conducted of *A. blancoi* growing specifically in the Maguindanao region, leaving a critical gap in region-specific physical and mechanical property data. This leads to a consequence that *A. blancoi* species remains largely underutilized as firewood or low-value timber, frequently misapplied in structural uses without proper engineering data, and harvested unsustainably because of undefined growth-yield relationships (Alipon and Bondad, 2008). Nevertheless, previous reports have acknowledged the potential of *A. blancoi*'s trunks as a good source of timber for suitable medium weight construction applications such as posts and boats, among others (EDC, 2020), a prospect that needs urgent region-specific evaluation, particularly for Maguindanao region.

Being part of the biodiversity-rich island of Mindanao and the neighboring area of the largest freshwater wetlands in the island (the Ligawasan Marsh), the Maguindanao region presents unique edaphoclimatic conditions that may influence *A. blancoi'*s wood properties (Tanalgo et al., 2024; PhilAtlas, 2026). Despite being common in the region, studies documenting the material characteristics of *A. blancoi* at the local level remain limited, contributing to its underutilization and a major constraint for effective conservation (EDC, 2020, Alipon et al., 2022). In consideration also to the historical armed conflict in the area, research efforts are still very scarce (Tanalgo et al., 2024), like ecosystem assessment and comprehensive characterization of native and underutilized tree species, including *A. blancoi* tree. By situating *A.*

blancoi within regional forestry and industrial contexts, this research aims to support evidence-based conservation strategies and promote sustainable utilization of Philippine native tree species. Therefore, this study aims to characterize the key physical properties *A. blancoi* including moisture content, basic density, and both directional and volumetric shrinkage, across inter-tree and height level variations in Maguindanao. The findings provide essential data for scientifically assessing the potential of *A. blancoi* wood for value-added applications such as crafts, furniture, interior construction, veneer, and ceiling panels. Moreover, by establishing region-specific physical properties, this research would address the current improper utilization of the species due to limited characterization data, and facilitates evidence-based species grading.

2. METHODOLOGY

2.1 Plant materials and wood samples collection

Three (3) mature *A. blancoi* trees, approximately 5 to 10 years old, were sampled from Barangay Ambolodto, Datu Odin Sinsuat (DOS), Maguindanao del Norte, in the Bangsamoro Autonomous Region in Muslim Mindanao (BARMM), Philippines. Considering that all tree samples were sourced from a naturally regenerated stand, the tree age range was estimated based on the local landowner knowledge with morphological indicators like diameter at breast height (DBH, 1.3 m from the ground level) and bark surface rugosity, with DBH values of 27 cm, 30 cm and 26 cm recorded for trees 1, 2, and 3, respectively. The geographic coordinates and elevation for each tree were recorded as follows: tree 1 (7° 3' 40" N, 124° 19' 45" E; 90 m a.s.l.), tree 2 (7° 3' 48" N, 124° 19' 28" E; 110 m a.s.l.), and tree 3 (7° 3' 41" N, 124° 19' 45" E; 85 m a.s.l.), with a pairwise distance of 580.24 m between trees 1 and 2, 30.19 m between trees 1 and 3, and 565.32 m between trees 2 and 3 (Figure 1). Both trees 1 and 3 grown in a swampy area and sparse forest canopy, where trees are widely spaced with low canopy cover, and the ground layer was dominated with shrubs and grasses, while tree 2 thrives in a semi-dry area and moderately closed canopy with coconut trees where canopy cover is significant but gaps are still present. The site was experiencing a tropical monsoon climate (Köppen classification: Am), with a mean annual temperature of 35.41°C and an average monthly rainfall of 91.02 mm. Wood samples were collected from the selected trees for subsequent analysis.

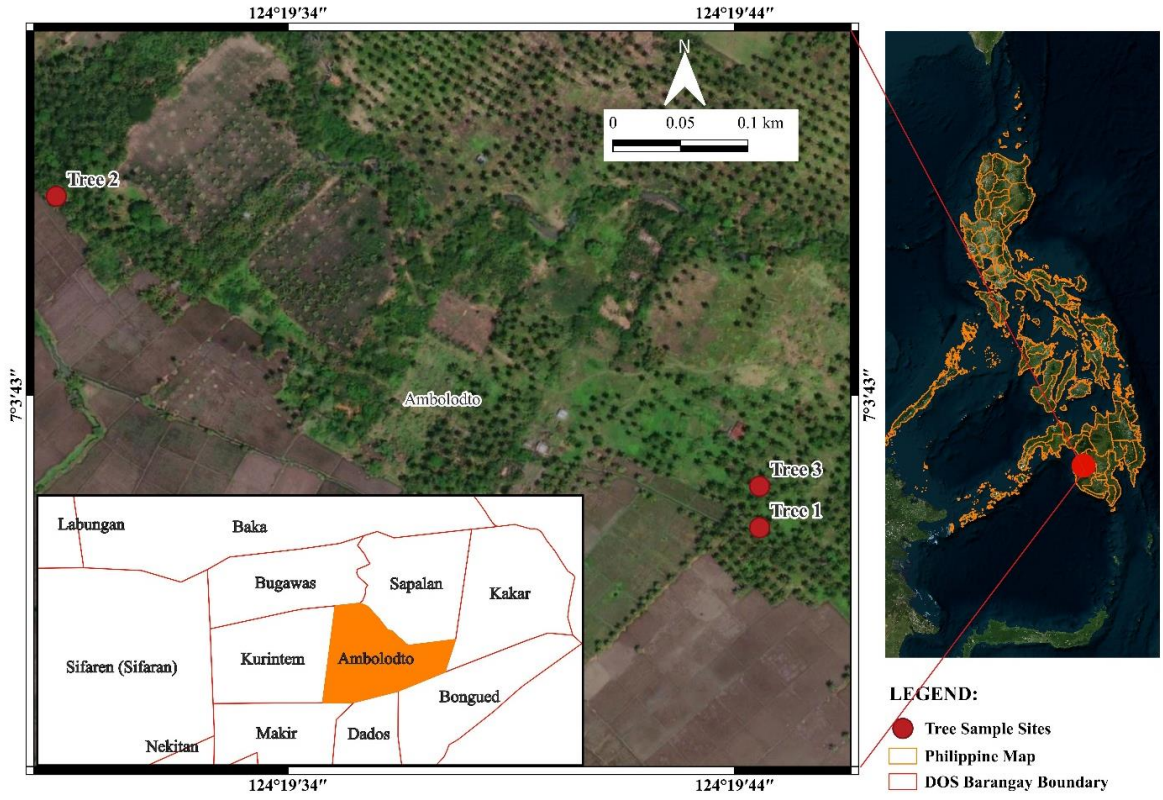


Figure 1. Location map of the *A. blancoi* tree samples in Maguindanao del Norte, Philippines (*Source:* Geoportal.gov.ph for administrative boundary & Google Earth for satellite image)

2.2 Sampling and sample preparation

Each trunk was divided into three height levels from the DBH level (1.3 m from the ground level): the bottom, middle, and top portions, each measuring 2.4 m length. From these portions, a total of nine disks (152 mm thick) were obtained and designated for the determination of physical properties (Figure 2). Sample preparation followed the ASTM standard for small clear specimens of timber (ASTM, 2019). Wood samples were collected across the cross-section of the stem to capture radial variability in properties. For moisture content (MC, %) and basic density (BD, kg/m^3), wood sample cubes (25 mm × 25 mm × 25 mm) were cut from each disk. While for shrinkage properties, rectangular samples (25 mm × 25 mm × 100 mm) were cut. Each height level within each tree constituted an experimental unit, represented by multiple replicate specimens for each test. Right after preparation, samples were soaked in a container of water at ambient temperature to prevent moisture loss until testing commenced.

The green moisture content (MC), basic density (BD), and shrinkage properties were determined following the ASTM D143 (2019). For MC and BD, the fresh weight of each specimen was determined using a analytical balance, and its volume was obtained by water displacement. Subsequently, the samples were oven dried at 103±2 °C until constant mass was achieved. A total number of 54 samples (18 per tree) were evaluated for MC and BD and the values were obtained using Equations 1 and 2.

$$\text{MC}\ (\%) = \frac{\text{Green weight} - \text{Oven dried weight (kg)}}{\text{Oven dried weight } (m^3)} \times 100 \quad (1)$$

$$\text{BD}\ \left(\frac{\text{kg}}{\text{m}^3}\right) = \frac{\text{Oven dried of wood (kg)}}{\text{Green volume of wood (m}^3\text{)}} \quad (2)$$

The directional and volumetric shrinkage, the radial (R), tangential (T), and longitudinal (L) were identified, and the dimensional changes were measured using a digital caliper. For each tree, 18 samples were prepared and tested, for a total of 54 samples. The shrinkage percentage was calculated using Equation 3:

$$\text{Shrinkage}\ (\%) = \frac{\text{Green volume} - \text{Oven dried volume}}{\text{Green volume}} \times 100 \quad (3)$$

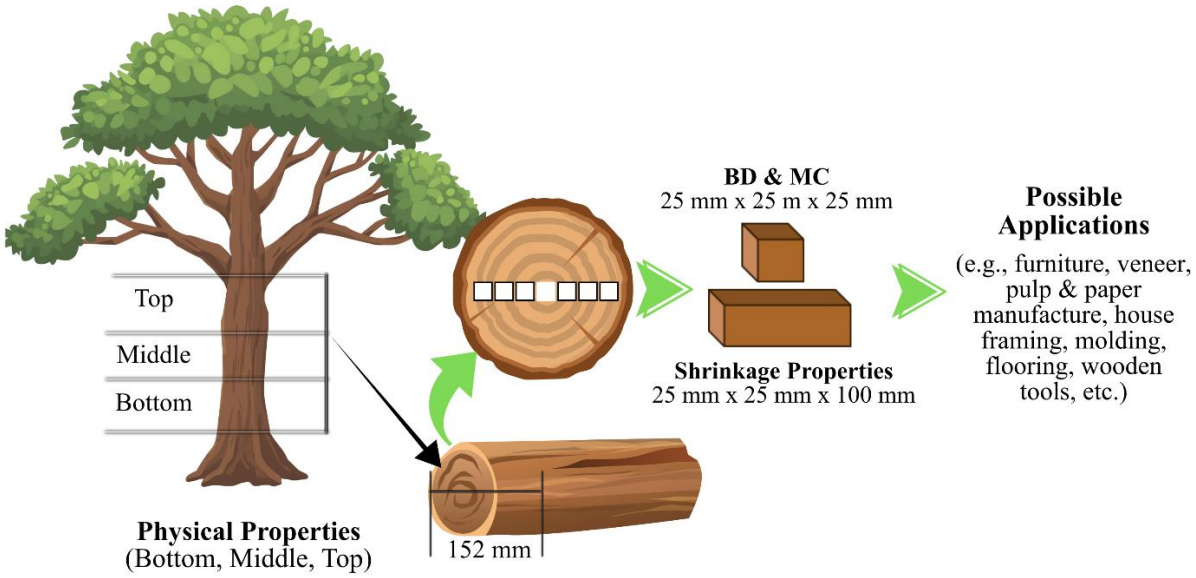


Figure 2. The schematic sampling followed in the study

2.3 Data analysis

Two-way analysis of variance (ANOVA) was used to compare the physical properties (moisture content, basic density, and shrinkages) of *A. blancoi*, across tree samples and height levels (bottom, middle, and top portions). Before the analysis of variance (ANOVA), the Kolmogorov-Smirnov normality test showed no significant results ($p>0.05$), confirming that the data were normally distributed. Tukey's Honestly Significant Difference (HSD) post hoc test was subsequently used to identify specific significant differences among group means. Moreover, the statistical analyses were performed using Jamovi version 2.3 (Jamovi Project, 2022).

Table 1. The moisture content and basic density of *A. blancoi* wood samples across tree samples and height levels

Parameters	Moisture content (%)	Basic density (kg/m^3)
Tree No.		
1	98.58b (21.52)	384.28a (61.10)
2	185.85a (68.31)	287.92c (56.26)
3	105.24b (10.64)	344.90b (65.68)
p-value	<0.0001*	<0.0001*
Height Levels		
Bottom	139.05a (42.48)	398.62a (51.62)
Middle	140.11a (82.48)	321.04b (68.82)
Top	110.51b (30.14)	297.44b (54.86)
p-value	<0.0001*	<0.0001*

Means in the same column followed by common letters are not significantly different 5% by Tukey's post hoc test; *significant; values in parentheses denote standard deviation.

3. RESULTS AND DISCUSSION

The physical properties of *A. blancoi* wood were presented in Tables 1 and 2. In evaluating the sources of variability, a two-way analysis of variance (ANOVA) was performed (α=0.05), revealing significant variations in wood properties both among sample trees and across height levels.

3.1 Moisture content (MC, %)

MC strongly influences most physical and mechanical properties of wood. Hence, accurate determination of MC is essential prior to conducting any tests (Shmulsky and Jones, 2019; Forest Products Laboratory, 2021). In this study, tree 2 exhibited exceptionally high MC of 185.85%, which was significantly greater than tree 1 with 98.58% and tree 3 with 105.24%. The statistical result confirms that the difference of results is highly significant between tree 2 and both tree 1 and tree 3, displaying a p-value of less than 0.0001 (Table 1). The present MC was likely influenced by site-specific differences and canopy cover, as tree 2 grown in a moderately closed canopy, while trees 1 and 3 grown in sparse forest canopy, which aligns with the previous reports by Zobel and van Buijtenen (1989), Alipon et al. (2022) and Tian et al. (2025). Relative to tree height levels, the MC values decreased towards the top portion, wherein the bottom portion (139.05%) and middle portion (140.11%) were statistically comparable, signifying no meaningful variation of MC between these two height portions. However, a significant decreased of MC was observed at the top portion, where the value drops at 110.51% having a p-value of less than 0.0001, signifying a high degree of difference between the top portion and both the bottom and middle portions. This result demonstrates that MC remains relatively stable at the bottom and middle portions of the tree height but markedly decreased towards top portion.

The present result value differs from the 152.68% reported for Philippine-grown *A. blancoi* (Alipon et al., 2022), suggesting possible site-specific environmental effects or genetic variation. Moreover, the observed axial variation in MC aligns with the typical moisture gradients documented in hardwoods (Kollmann and Côté, 1968), and with established findings on MC distribution in wood components, recognizing spatial heterogeneity in MC as a critical determinant of material behavior (Tian et al., 2025). The decreasing trend of MC towards the top portion observed in this present study is consistent with the findings of Van Duong et al. (2019) and Marasigan and Mundin (2024) on *Melia azedarach* grown in the Vietnam and the Philippines, respectively. This MC variation along the height level was also attributed to density differences and relatively affected by various anatomical properties such as cell wall thickness and fiber length, among others (Shmulsky and Jones, 2019; Forest Products Laboratory, 2021; Van Duong et al., 2021). Also, the sapwood to heartwood transition or ratio was reported as a source of MC variation between and within species, wherein the amount of MC decreases accompanied by the deposition of extractives as wood in a tree change from sapwood to heartwood (Shmulsky and Jones, 2019). MC greater than 150% implies extended kiln-drying requirements, increased susceptibility to fungal degradation, and dimensional instability during processing, affecting the performance and serviceability (Dietsch et al., 2015; Forest Products Laboratory, 2021). It was also reported that elevated MC significantly influences moisture-induced stresses and shrinkage cracking during drying while serving as

a critical factor in fungal decay resistance (Shmulsky and Jones, 2019; Li et al., 2025). However, proper drying could address this higher MC issue of *A. blancoi* wood, ensuring favorable overall performance and serviceability.

3.2 Basic density (BD, kg/m^3)

BD is widely considered as a key indicator of wood quality and suitability of wood for multi-applications (Shmulsky and Jones, 2019; Forest Products Laboratory, 2021). In this study, the BD of *A. blancoi* revealed distinct differences among tree samples examined. Particularly, tree 1 demonstrated the highest BD value, followed by tree 3 and tree 2, respectively. Statistical analysis confirmed that the observed differences in *A. blancoi*'s BD values among tree samples were significantly different, displaying a p-value of less than 0.0001 (Table 1). In consideration to the established role of BD in influencing wood mechanical properties and other processing behavior, tree 1 reflects greater mass per unit volume among tree samples examined. This inter-tree variation, suggests the influence of inherent variability like cambial age, and localized micro-environmental factors like site fertility, spatial distribution, canopy cover, temperature, precipitation, and elevation (Zobel and van Buijtenen, 1989; Fajardo et al., 2022; Stöd et al., 2025; Fischer et al., 2026).

Furthermore, the mean BD values across the height levels exhibited a decreasing trend of values from bottom (398.62 kg/m^3) to top (297.44 kg/m^3) portions demonstrating a clear axial gradient along the stem. The analysis of variance revealed a significant difference, displaying a p-value of less than 0.0001 (Table 1), particularly the bottom portion relative to the two upper portions. This axial decrease in wood BD towards the top portion is consistent with the findings in tropical hardwoods, where such patterns are attributed to physiological gradients, cambial age, and mechanical loading requirements along the height position (Zobel and van Buijtenen, 1989; Fajardo et al., 2022; Dimou et al., 2025). Also, axial variation of density can directly reflects cellular compositions/ types like a greater proportion of mature cells with thicker cell walls and narrower empty spaces or vessel diameter will give densier wood and improve mechanical properties, making wood more resistant and durable (Tanabe et al., 2016; Mendoza et al., 2019; Shmulsky and Jones, 2019; Hamdan et al., 2020; Forest Products Laboratory, 2021; Eloy et al., 2024; de Oliveira Monteiro et al., 2026). Between the density and mechanical properties, a correlation was also recorded by Izekor et al. (2010), Machado et al. (2014), and Fanny et al. (2018). Additionally, wood density exhibited a positive relationship with strength properties (Alipon et al., 2005). This report was corroborated by Hamdan et al. (2020), who indicated that wood density serves as a strong predictor for modulus of rupture, modulus of elasticity, compression parallel to grain, and shear parallel to grain, showing positive correlations that ranged from weak-to-strong. Given the BD result (low density, Table 1) of *A. blancoi*, the mechanical performance and potential applications of this species might be projected, associated with the observed MC and shrinkage performance. Although this present study only explores *A. blancoi*'s physical properties and does not extend to an investigation of physical-anatomical-mechanical relationships. This comparison of the present findings with previously reported properties may nonetheless offer valuable insights to predict the technological behavior and potential uses of the species and provide further information for future research and comprehensive wood characterization.

Based on the classification system established by the Forest Products Research and Development Institute (FPRDI) (Alipon et al., 2005), *A. blancoi* BD result falls under low density (≤360 kg/m^3). This BD result positions *A. blancoi* in the same class with *Falcataria falcata*, but was lighter compared to *Gmelina arborea* (moderately low density, 370-440 kg/m^3), and *Swietenia macrophylla* (medium density, 450-530 kg/m^3), the most common industrial tree plantation species in the Philippines (Marasigan et al., 2025). Moreover, Alipon et al. (2022) reported a relatively higher density of *A. blancoi* with 470 kg/m^3, along with other fruit-bearing and underutilized tree species such as *Sandoricum koetjape*, *Artocarpus heterophyllus*, *Alstonia macrophylla*. While *Durio zibethinus* and *Litsea perrottetti* fall under the same class of the present result. Furthermore, thirteen senile fruit-bearing trees in the country were studied by Marasigan et al. (2024). As compared to the present result, *A. blancoi* exhibited lighter density to *Mangifera indica*, *Mangifera altissima*, *Persea americana*, *Lansium domesticum*, *Sandoricum koetijape*, *Artocarpus heterophyllus*, *Syzygium cumini*, *Antidesma bunius*, *Citrus maxima*, and *Manikara zapota*, while falls in same density class with *Artocarpus odoratissimus*, *Annona muricata*, and *Annona squamosa* (Marasigan et al., 2024).

Compared with other *Artocarpus* species documented internationally, the present BD of *A. blancoi* exhibited lighter BD than of *Artocarpus heterophyllus* (500 kg/m^3) from Tanzania (Hamza et al., 2001), *Artocarpus altilis* from southwestern Nigeria (581 kg/m^3) (Areo et al., 2020) and Gambari Forest Reserve, Oyo State, Nigeria (~571-603 kg/m^3) (Areo, 2021), and four among the six *Artocarpus* species from Central Kalimantan, Indonesia, namely, *A. dadah* (490 kg/m^3), *A. nitidus* (475 kg/m^3), *A. anisophyllus* (740 kg/m^3), and *A. odoratissimus* (548 kg/m^3) (Takeuchi et al., 2019). The remaining two Indonesian species, *A. elasticus* (210 kg/m^3) and *A. tamaran* (345 kg/m^3) exhibited BD values comparable to the present range.

Overall, the placement of *A. blancoi* BD as low density carries some implications for potential material use as non-structural applications such as carving, veneer, furniture webbing, though may require reinforcement for any load-bearing purposes, and eco-friendly preservative treatments for favorable exterior use against termites and fungal decay.

3.3 Shrinkage properties (%)

Wood is an anisotropic material, naturally displaying directionally dependent (shrinkage or swelling) along tangential, radial, and longitudinal sections (Shmulsky and Jones, 2019; Forest Products Laboratory, 2021). In this study, the shrinkage properties of *A. blancoi* across tree samples and height levels were examined, as shown in Table 2.

3.3.1 Tangential shrinkage (TS)

Although tangential shrinkage (TS) numerically varied among *A. blancoi* tree samples (Table 2), the differences were not statistically significant (p=0.234), indicating comparable tangential dimensional behavior across sampled trees. Compared with previous reports, the TS values obtained in this study (4.59-5.12%) were slightly higher than those reported for *A. blancoi* (3.64%) (Alipon et al., 2022), and for related species, including *A. odoratissimus* (4.56%) and *A. heterophyllus* (4.54%) (Marasigan et al., 2024). Such differences may reflect intraspecific variability associated not only with genetic factors but also with site-specific edaphoclimatic conditions that influence wood formation processes (Zobel and van Buijtenen, 1989; Almeida et al., 2026). Variations in soil nutrient availability, moisture regime, and local precipitation patterns can affect cambial activity, cell wall deposition, and anatomical development, thereby contributing to differences in shrinkage behavior and dimensional stability among trees growing under different environmental conditions (Fajardo et al., 2022; Pumijumnong et al., 2023). Nevertheless, because environmental variables were not directly measured in this study, these mechanisms should be interpreted cautiously and warrant further investigation.

Table 2. The shrinkage of properties of *A. blancoi* wood across tree samples and height levels

Parameters	Shrinkage properties (%)			
	Tangential	Radial	Longitudinal	VS
Tree No.				
1	5.12a (1.33)	3.14a (0.90)	0.46a (0.73)	8.11a (1.26)
2	4.59a (1.15)	2.44b (1.64)	0.17b (0.12)	6.93b (1.19)
3	5.03a (0.88)	2.64ab (1.58)	0.23b (0.13)	7.55a (1.28)
p-value	0.234^{ns}	0.031*	0.010*	0.001*
Height levels				
Bottom	5.44a (1.50)	2.74a (1.49)	0.32a (0.73)	8.04a (1.69)
Middle	4.96ab (1.10)	2.57a (1.58)	0.32a (0.23)	7.41b (1.27)
Top	4.34b (0.77)	2.92a (0.88)	0.23a (0.16)	7.14b (0.65)
p-value	0.004*	0.444 ^{ns}	0.617 ^{ns}	0.010*

Means in the same column followed by common letters are not significantly different 5% by Tukey's post hoc test; *significant; ns-not significant; VS-volumetric shrinkage

TS showed a significant axial decrease along tree height (p=0.004; Table 2), indicating improved dimensional stability toward the upper portions of the stem. This pattern is consistent with previous observations in hardwood and softwood species, where variation in shrinkage behavior along the stem has been associated with cambial age (Shmulsky and Jones, 2019; Forest Products Laboratory, 2021; Stöd et al., 2025). Also, the direct interplay between wood density and shrinkage towards the top is an important

influencing factor, where higher TS generally associates to higher density (Forest Products Laboratory, 2021; Stöd et al., 2025), corroborating the findings of the present result. Moreover, wood generally exhibits greater dimensional change in the tangential direction than in the radial and longitudinal directions due to its anisotropic nature, particularly affected by some anatomical traits difference like the presence of ray tissue, pits, and amount of cell wall material variability (Shmulsky and Jones 2019; Forest Products Laboratory 2021).

3.3.2 Radial shrinkage (RS)

Relative to RS, result revealed that tree 1 was significantly higher shrinkage value than the other tree samples, displaying a p-value of 0.031 (Table 2). When compared to previously reported findings, the present RS results (ranging from 2.44% to 3.14%) were notably lower than 5.68% reported for *A. blancoi* species by Alipon et al. (2022), while relatively comparable for *A. odoratissimus* (2.13%) and *A. heterophyllus* (2.91%) (Marasigan et al., 2024). This observed differences of findings suggest that age differences, and/or genetic factors may play a pivotal role in the shrinkage characteristics of the samples (Stöd et al., 2025; de Oliveira Monteiro et al., 2026), accompanied by some properties like MC and cell wall microfibril angle variation, which also significant factors affecting both strength and directional shrinkage properties of wood (Shmulsky and Jones, 2019).

With respect to height levels, RS did not differ significantly among the bottom, middle, and top portions (p=0.444; Table 2), indicating relatively uniform radial dimensional behavior of *A. blancoi* along the stem. This result suggests that height levels had limited influence on RS within the sampled trees.

3.3.3 Longitudinal shrinkage (LS)

Longitudinal shrinkage (LS) differed significantly among tree samples (p=0.010; Table 2), indicating variation in longitudinal dimensional behavior within *A. blancoi*. The LS values obtained in this study were generally comparable with previous reports for *A. blancoi* (Alipon et al., 2022) and related *Artocarpus* species reported by Marasigan et al. (2024). Minor differences among studies may reflect variation in provenance, local growth conditions, and tree age, which can influence wood formation and dimensional behavior. Given that the sampled trees in this study were relatively young (5-10 years old), differences in growth environment and site conditions may have contributed to the observed variation. Similar influences of growth conditions and site-related factors on variation in wood properties have been documented in previous studies (Stöd et al., 2025; Fajardo et al., 2022). Nevertheless, these factors were not directly evaluated in the present study and should therefore be interpreted cautiously.

Relative to height levels, LS did not vary significantly along the height levels (p=0.617; Table 2). In general, LS remains minimal compared with TS and RS and is often considered negligible for most practical applications (Shmulsky and Jones, 2019; Forest Products Laboratory, 2021).

Overall, the directional shrinkage values observed in this study clearly demonstrate the anisotropic behavior of wood. Consistent with typical wood behavior, TS exceeded RS, while both transverse directions exhibited greater dimensional change than LS, reflecting differences in wood structure across anatomical directions. This anisotropic behavior and dimensional stability are influenced by the combined effects of wood anatomical heterogeneity, including variation in cell type proportions, cell dimensions, and wood maturity, rather than by isolated structural factors alone (Stöd et al., 2025; de Oliveira Monteiro et al., 2026).

3.3.4 Volumetric shrinkage (VS)

Volumetric shrinkage (VS) varied significantly among tree samples (p=0.001; Table 2). This variation may reflect the combined influence of environmental conditions, wood anatomical adjustments, and potential genetic variability (Butterfield, 2003; Pandey, 2021; Fajardo et al., 2022; Haryjanto et al., 2024; Stöd et al., 2025; de Oliveira Monteiro et al., 2026). Wood properties are recognized as phenotypic responses shaped by genotype × environment interactions, and differences observed among sampled trees may partly reflect localized growing conditions in Maguindanao alongside inherent biological variability (Butterfield, 2003; Shmulsky and Jones, 2019; Fajardo et al., 2022; Stöd et al., 2025). However, these factors were not directly evaluated in the present study.

Along height levels, the VS result showed a significant decrease towards the top portion, displaying a p-value of less than 0.010 (Table 2). The VS results indicate that the top portion of *A. blancoi* is more dimensionally stable, which relates to its lighter density. Moreover, this corroborates to the previous reports of Bello (1997) and Alipon et al. (2022), where they highlighted the strong linear correlation of VS and BD, and also emphasized the significant

contribution of BD to the VS performance of wood. Furthermore, the typical trends of cambial age along the tree height, relatively affect dimensional stability (Shmulsky and Jones, 2019; Forest Products Laboratory, 2021; Stöd et al., 2025). Anatomical properties also influenced wood shrinkage behavior, where a greater number of narrow vessels, a higher proportion of fibers, and taller and wider rays exhibited greater shrinkage values (de Oliveira Monteiro et al., 2026). The present findings demonstrated that *A. blancoi* exhibits a consistent alignment between density and shrinkage behavior. This supports the principle that denser wood generally undergoes greater dimensional change from the green to oven-dried condition (Schulgasser and Witztum, 2015).

The present VS of *A. blancoi* (ranging from 6.93% to 8.11%) was relatively comparable to the findings of Marasigan et al. (2024) for *A. odoratissimus* (6.59%) and *A. heterophyllus* (7.32%), while it was slightly lower than the result obtained by Alipon et al. (2022) for the same *A. blancoi* species (9.07%). Under the FPRDI wood shrinkage classification system (Alipon et al., 2020), the VS values of *A. blancoi* in this study fall within the range of low shrinkage (Group 5; ≤7.8%) to moderately low shrinkage (Group 4; 7.910.5%). This classification indicates that the wood is favorable for wide range of application from high end to standard grade furniture production, as well as other applications such as rotary cut veneer for plywood, house framing, moldings, parquet, flooring, ceiling and even musical instruments, tool handles, and sporting goods, among others (Bowyer et al., 2007; Alipon et al., 2020).

Overall, the combined attributes of light density and low to moderate shrinkage performance of *A. blancoi* suggested its viability for various value-added wood products from high end to standard grade furniture and other non-structural applications, where light weight and dimensional stability are of great advantageous.

4. CONCLUSION

Based on the Forest Products Research and Development Institute (FPRDI) classification system, *A. blancoi* is classified as a low density wood with low to moderately low volumetric shrinkage. These properties indicate its potential for value-added products, particularly furniture and other non-structural applications. The findings provide baseline information to support the sustainable utilization and conservation of *A. blancoi* in the BARMM region while promoting its responsible use as a native timber resource. Further studies on its anatomical, mechanical, durability, and processing properties are recommended for a more comprehensive evaluation.

ACKNOWLEDGEMENTS

The authors are thankful to the faculty and staff of the Mindanao State University-Maguindanao, particularly to the College of Forestry and Environmental Studies, and to the personnel of the Physical and Mechanical Division of the Forest Products Research and Development Institute - Department of Science and Technology for their valuable technical assistance.

AUTHOR CONTRIBUTIONS

BGD, RTA, JFV, CEP, RCB, and OSM conceptualized and finalized the methodology of the study; BGD, RTA, and JFV collected the data and wrote the first draft; BGD, RTA, JFV, and OSM analyzed and validated the data, edited the manuscript, and finalized.

DECLARATION OF CONFLICT OF INTEREST

The authors declare no conflict of interests.

REFERENCES

Alipon MA, Bondad EO. Strength Grouping of Philippine Timbers for Various Uses: FPRDI Trade Bulletin Series No. 4. Laguna, Philippines: Department of Science and Technology - Forest Products Research and Development Institute; 2008. p. 51.

Alipon MA, Bondad EO, Guiang MM. Philippine Wood Properties and Uses. Laguna, Philippines: Department of Science and Technology - Forest Products Research and Development Institute; 2020.

Alipon MA, Bondad EO, Cayabyab PC. Relative Density of Philippine Woods. College, Laguna, Philippines: Forest Products Research and Development Institute; 2005.

Alipon MA, Bondad EO, Sapin GN, Marasigan OS. Physical and mechanical properties of selected fruit-bearing and underutilized tree species in the Philippines. Philippine Journal of Science 2022;151(1):341-56.

Almeida MNF de, Louzada JL, Pezzopane JEM, Rocha SM, Câmara AP, Santos VB dos, et al. Influence of clone-site interaction on basic wood density of *Eucalyptus* clones in brazilian tropical zones. CERNE 2026;32(1):e103566.

American Society for Testing and Materials (ASTM). Methods of Testing Small Clear Specimens of Timber: ASTM D143-52. Philadelphia, USA: American Society for Testing and Materials International; 2019. p. 1-30.

Areo OS. Wood Properties and Natural Durability of *Artocarpus altilis* (Parkinson ex F.A. Zorn) Fosberg [dissertation]. Postgraduate College, University of Ibadan; 2021.

Areo OS, Omole OA, Adejoba AL. Evaluation of selected physical properties of breadfruit wood (*Artocarpus altilis*, Parkinson ex. F.A. Zorn) fosberg grown in the South-Western, Nigeria. Trends in Applied Sciences Research 2020;15(3):226-34.

Bello ED. Specific gravity-volumetric shrinkage relationship of some Philippine wood species. FPRDI Journal 1997;23:15-30.

Bowyer JL, Shmulsky R, Haygreen JG. Forest Products and Wood Science: An Introduction. 5th ed. Malden, MA: Blackwell Publishing; 2007.

Butterfield BG. Wood anatomy in relation to wood quality. In: Barnett JR, Jeronimidis G, editors. Wood Quality and Its Biological Basis. Oxford: Blackwell; 2003. p. 30-49.

de Oliveira Monteiro R, Dória LC, Ribeiro ES, Gonçalez JC, Sonsin-Oliveira J. Wood anatomy and its effects on physical properties in nineteen commercial species. Brazilian Journal of Botany 2026;49:Article No. 13.

Department of Environment and Natural Resources - Forest Management Bureau (DENR-FMB). Philippine Forestry Statistics. Quezon City, Philippines: Department of Environment and Natural Resources; 2020.

Dietsch P, Franke S, Franke B, Gamper A, Winter S. Methods to determine wood moisture content and their applicability in monitoring concepts. Journal of Civil Structural Health Monitoring 2015;5(2):115-27.

Dimou V, Boufidou E, Kitikidou K. Variation in basic density of *Paulownia tomentosa* along axial and radial direction in nurseries in Greece. International Wood Products Journal 2025;16(2):148-56.

Energy Development Corporation (EDC). *Artocarpus blancoi* [Internet]. 2020 [cited 2025 Aug 12]. Available from: https://dx.doi.org/10.2305/IUCN.UK.2020-3.RLTS. T33195A61524790.en.

Eloy E, Mangini TS, Nardini C, Caron BO, Trevisan R, dos Santos AD. Correlation of anatomy with physical properties of wood species from an agroforestry system. Revista Árvore 2024;48(1):1-11.

Fajardo A, Piper FI, García-Cervigón AI. The intraspecific relationship between wood density, vessel diameter and other traits across environmental gradients. Functional Ecology 2022;36:1585-98.

Fanny H, Ramadhani AP, Harry P, Sri S. Effect of growth rate on physical and mechanical properties of 4 year old *Acacia mangium* wood from Wonogiri, Central Java. Journal of Forest Science 2018;12(2):248-58.

Fernando ES, Co LL, Lagunzad DA, Gruezo WSM, Barcelona JF, Madulid DA, et al. Threatened plants of the Philippines: A preliminary assessment. Asia Life Sciences 2008;3:1-52.

Fischer FJ, Chave J, Zanne A, Jucker T, Fajardo A, Fayolle A, et al. Beyond species means: The intraspecific contribution to global wood density variation. New Phytologist 2026; 249(6):2630-51.

Forest Products Research and Development Institute (FPRDI). Anatomical Atlas of Philippine Timber. Laguna, Philippines: Department of Science and Technology - Forest Products Research and Development Institute; 1986.

Forest Products Laboratory. Wood Handbook - Wood as an Engineering Material: General Technical Report FPL-GTR-282. Madison, WI: Department of Agriculture, Forest Service, Forest Products Laboratory; 2021.

Government of the Philippines. Executive Order No. 23, s. 2011 [Internet]. 2011 [cited 2025 Aug 12]. Available from: https://lawphil.net/executive/execord/eo2011/eo_23_2011.html.

Hamdan H, Nordahlia AS, Anwar UMK, Mohd Iskandar M, Mohamad Omar MK, Tumirah K. Anatomical, physical, and mechanical properties of four pioneer species in Malaysia. Journal of Wood Science 2020;66(1):Article No. 59.

Hamza KFS, Makonda FBS, Ishengoma RC, Manumbu E. Determination of basic density of *Artocarpus heterophyllus* (Lam) grown in agroforestry systems in Maramba, Tanzania. Morogoro, Tanzania. Sokoine University of Agriculture, Faculty of Forestry and Nature Conservation; 2001.

Haryjanto L, Indrioko S, Nirsatmanto A, Hidayati F. Genetic variation in growth characteristics and wood properties of *Ficus variegata* blume first generation progeny trials in Indonesia. Journal of the Korean Wood Science and Technology 2024;52(5):473-87.

Izekor DN, Fuwape JA, Oluyege AO. Effects of density on variations in the mechanical properties of plantation grown *Tectona grandis* wood. Applied Science Research 2010; 2(6):113-20.

Jamovi Project. Jamovi (version 2.3) [Internet]. 2022 [cited 2025 Nov 20]. Available from: https://www.jamovi.org.

Kollmann FFP, Côté WA. Principles of Wood Science and Technology: Volume 1. Berlin, Germany: Springer-Verlag; 1968.

Li W, Chen M, Dai Y, Ke L-L. Analysis on moisture-induced stresses in wood cell wall considering periodically graded *microstructures*. International Journal of Solids and Structures 2025;312:Article No. 113277.

Machado JS, Louzada JL, Santos AJA, Nunes L, Anjos O, Rodrigues J, et al. Variation of wood density and mechanical properties of blackwood (*Acacia melanoxylon* R.Br.). Materials and Design 2014;56:975-80.

Malabrigo PL, Umali AGA. Alay: Philippine Native Trees at the Victor O. Ramos Arboretum. Quezon City, Philippines: Philippine Native Tree Enthusiasts; 2022. p. 1-322.

Marasigan OS, Mundin MAM. Physico-mechanical properties and potential utilization of *Melia azedarach* L. grown in Quezon Province, the Philippines. Philippine Journal of Science 2024;153(4):1429-41.

Marasigan OS, Alipon MA, Bondad EO, Hopia KA, Mundin MAM. Physical and mechanical properties of thirteen senile fruit-bearing trees in the Philippines and their potential uses. Journal of Tropical Forest Science 2024;36(1):91-104.

Marasigan OS, Daguinod SA, Villareal JF. Physico-Mechanical properties of two native tree species in the Philippines and their potential as alternatives to exotic industrial tree plantation species. Environment and Natural Resources Journal 2025;23(4):343-56.

Mendoza RC, Daracan VC, Manalo RD, Batallones CHR, Jaurigue KG, Romano AD, et al. Anatomical and physico-mechanical characterization of Narra (*Pterocarpus indicus* Willd.) branchwood collected in Mount Makiling Forest Reserve, Laguna, Philippines. Philippine Journal of Science 2019;148(4):705-13.

Pandey S. Climatic influence on tree wood anatomy: A review. Journal of Wood Science 2021;67(1):Article No. 24.

PhilAtlas. Maguindanao [Internet]. 2026 [cited 2026 Jun 12]. Available from: https://www.philatlas.com/mindanao/barmm/maguindanao.html.

Pumijumnong N, Muangsong C, Buajan S, Songtrirat P, Chatwatthana R, Chareonwong U. Factors affecting cambial growth periodicity and wood formation in tropical forest trees: A review. Forests 2023;14(5):Article No. 1025.

Schulgasser K, Witztum A. How the relationship between density and shrinkage of wood depends on its microstructure. Wood Science and Technology 2015;49:389-401.

Shmulsky R, Jones PD. Forest Products and Wood Science: An Introduction. 7th ed. Hoboken, USA: Wiley-Blackwell; 2019.

Stöd R, Marttila J, Haapala A, Tomppo L, Verkasalo E. Basic density and shrinkage of Scots pine (*Pinus sylvestris* L.) thinning wood. European Journal of Wood and Wood Products 2025;83(6):Article No. 192.

Stuart GU. Antipolo/*Artocarpus blancoi*/Tipolo: Philippine medicinal herbs/Philippine alternative medicine [Internet]. 2020 [cited 2024 Aug 12]. Available from: https://www.stuartxchange.org/Antipolo.html.

Takeuchi R, Wahyudi I, Aiso H, Ishiguri F, Istikowati WT, Ohkubo T, et al. Anatomical characteristics and wood properties of unutilized *Artocarpus* species found in secondary forests regenerated after shifting cultivation in Central Kalimantan, Indonesia. Agroforestry Systems 2019;93:745-53.

Tanabe J, Ishiguri F, Nakayama M, Ohshima J, Iizuka K, Yokota S. Properties of juvenile and mature wood and their effects on the bending properties of lumber in *Pinus taeda* growing in Tochigi, Japan. Forest Products Journal 2016;66(7):428-32.

Tanalgo KC, Manampan-Rubio M, Alvaro-Ele RJ, Hilario-Husain BA, Murray SA, Delos Reyes JL, et al. Ecological indicators of water quality and Marshland Impact Area (MARia) Index of Ligawasan Marsh: A critically important wetland in the Southern Mindanao, Philippines. Discover Environment 2024;2(113):2503-25.

Tian P, Zhang H, Han J, Zhao Y, Han X. Moisture content distribution in cross-section of cylindrical wood components. Polymers 2025;17(22):Article No. 2994.

Van Duong D, Hesagawa M, Matsumura J. The relation of fiber length, wood density, and compressive strength to ultrasonic wave velocity within stem of *Melia azedarach*. Journal of the Indian Academy of Wood Science 2019;16(1):1-8.

Van Duong D, Schimleck L, Tai Tien D, Chu Van T. Radial variation in cell morphology of *Melia azedarach* planted in Northern Vietnam. Maderas Ciencia y Tecnología 2021; 23(7):1-10.

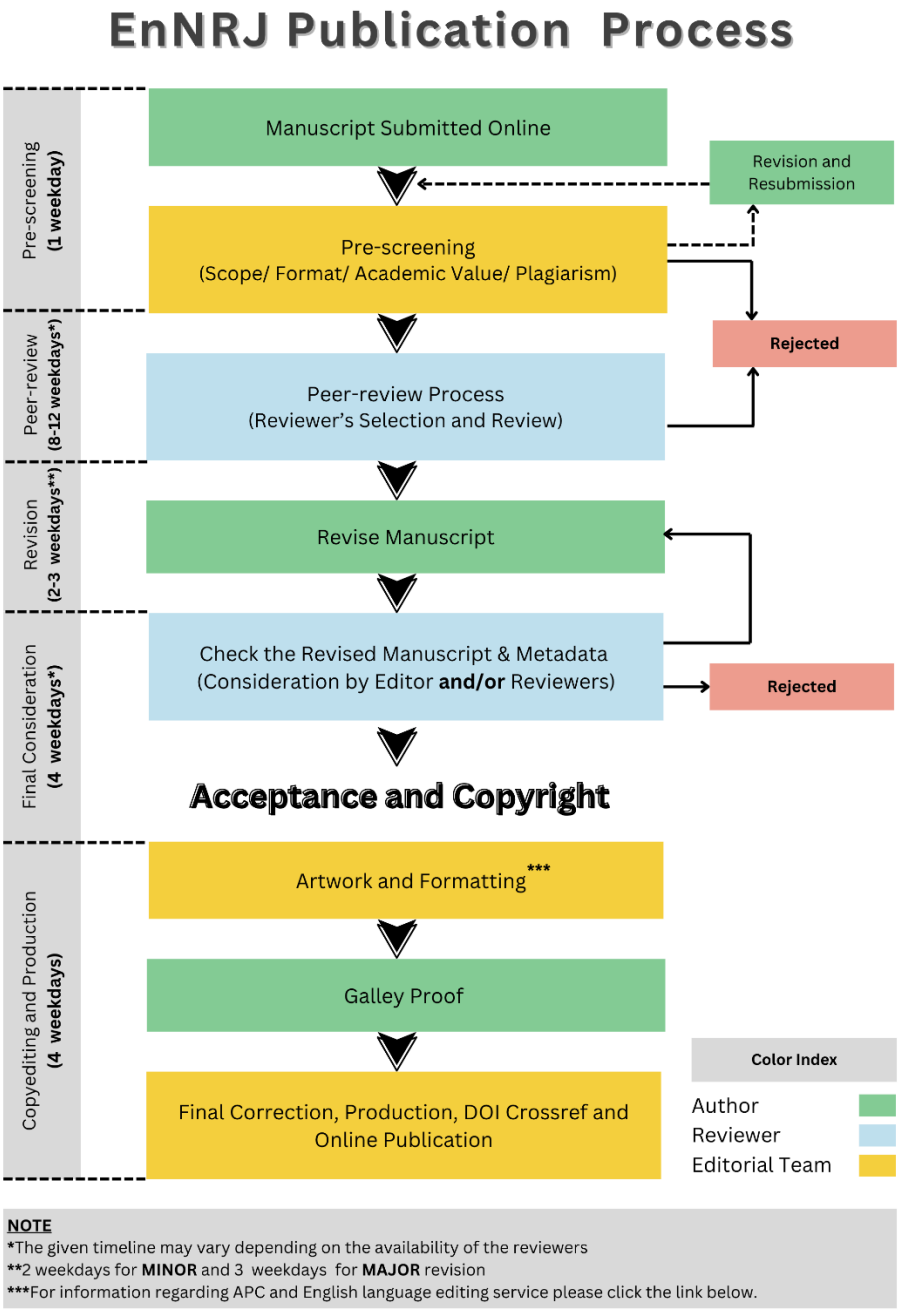
Zobel BJ, Van Buijtenen JP. Wood Variation: Its Causes and Control. Heidelberg, Germany: Springer-Verlag; 1989.

INSTRUCTION FOR AUTHORS

Publication and Peer-reviewing processes of Environment and Natural Resources Journal

Environment and Natural Resources Journal is a peer reviewed and open access journal that is published in six issues per year. Manuscripts should be submitted online at https://ph02.tci-thaijo.org/index.php/ennrj/about/submissions by registering and logging into this website. Submitted manuscripts should not have been published previously, nor be under consideration for publication elsewhere (except conference proceedings papers). A guide for authors and relevant information for the submission of manuscripts are provided in this section and also online at: https://ph02.tci-thaijo.org/index.php/ennrj/author. All manuscripts are refereed through a **single-blind peer-review** process.

Submitted manuscripts are reviewed by outside experts or editorial board members of **Environment and Natural Resources Journal**. This journal uses double-blind review, which means that both the reviewer and author identities are concealed from the reviewers, and vice versa, throughout the review process. Steps in the process are as follows:



The Environment and Natural Resources Journal (EnNRJ) considers and accepts two types of articles for publication as follows:

- *Original Research Article*: This is the most common type of article. It showcases new, innovative or unique findings surrounding a focused research question. Manuscripts should not exceed 4,000 words (excluding references) - see more details in the Preparation of Manuscript section below.
- *Review Article (by invitation)*: This type of article focuses on the in-depth critical review of a special aspect of an environmental-related research question, issue, or topic. It provides a synthesis and critical evaluation of the state of the knowledge of the subject. Manuscripts should not exceed 6,000 words (excluding references).

Submission of Manuscript

The items that the author needs to upload for the submission are as follows:

Manuscript: The manuscript must be submitted as a Microsoft Word file (.doc or .docx). Refer to the **Preparation of Manuscript** section below for detailed formatting instructions.

Cover Letter: The letter should address the Editor and include the following: a statement declaring that the author's paper has not been previously published and is not currently under consideration by another journal.

- a brief description of the research the author reports in the paper, including why the findings are important and why the journal readers should be interested
- contact information of the author and any co-authors
- a confirmation that the author has no competing interests to disclose

Graphical Abstract (Optional): The author is encouraged to submit a graphical abstract with the manuscript. The graphical abstract depicts the research and findings with visuals. It attracts more potential readers as it lets them understand the overall picture of the article within a few glances. Note that the graphical abstract must be original and unpublished artwork. It should be a high-quality illustration or diagram in any of the following formats: TIFF, PDF, JPEG, or PNG. The minimum required size is 750 × 750 pixels (height × width). The size should be of high quality (600 dpi or larger) in order to reproduce well.

Reviewers Suggestion (mandatory): Please provide the names of three potential reviewers, with information about their affiliations as well as their email addresses. The recommended reviewers should not have any conflict of interest with the authors. Each reviewer must represent a different affiliation and not have the same nationality as the author. Please note that the editorial board retains the sole right to decide whether or not the recommended reviewers will be selected.

Declaration of Competing Interest: The author must include a declaration of competing interest form during submission. If there is no conflict of interest, please state, "The authors declare no conflict of interest." Otherwise, authors should declare all interests to avoid inappropriate influence or bias in their published work. Examples of potential conflicts of interest in research projects include but are not limited to financial interests (such as employment, consultancies, grants, and other funding) and non-financial interests (such as personal or professional relationships, affiliations, and personal beliefs).

CrediT (Contributor Roles Taxonomy) Author Statement or Author Contributions: For research articles with several authors, we require corresponding authors to provide co-author contributions to the manuscript using the relevant CRediT roles. CRediT is a taxonomy that shows the contributions of the author and co-author(s), reduces possible authorship disputes, and facilitates collaboration among research team members. The CRediT taxonomy includes 14 different roles describing each contributor's specific contribution to the scholarly output.

The roles are: Conceptualization; Data curation; Formal analysis; Funding acquisition; Investigation; Methodology; Project administration; Resources; Software; Supervision; Validation; Visualization; Roles/Writing – original draft; and Writing – review & editing.

Note that authors may have contributed through multiple roles, and those who contributed to the research work but do not qualify for authorship should be listed in the acknowledgments.

An example of a CRediT author statement is given below:
"Conceptualization, X.X. and Y.Y.; Methodology, X.X.; Software, X.X.; Validation, X.X., Y.Y. and Z.Z.; Formal Analysis, X.X.; Investigation, X.X.; Resources, X.X.; Data Curation, X.X.; Writing – Original Draft Preparation, X.X.; Writing – Review & Editing, X.X.; Visualization, X.X.; Supervision, X.X.; Project Administration, X.X.; Funding Acquisition, Y.Y."

Artwork for the Journal Cover: The author may provide and propose a piece of artwork (with a description) for the journal issue cover. This is an excellent opportunity for the author to promote their article, if accepted, on the cover of a published issue. Alternatively, the editorial team may invite the author to submit a piece of artwork for the cover after their manuscript has been accepted for publication. The final cover artwork selection will be made by the editorial team.

Final Author Checks: In addition to the basic requirements, the author should review this checklist before submitting their manuscript. Following it ensures the manuscript is complete and in accordance with all standards.

Preparation of Manuscript

Format and Style

The manuscript should be prepared strictly as per the guidelines given below. Any manuscript with an incorrect format will be returned, and the corresponding author may have to resubmit a new manuscript with the correct format.

Overall Format

The manuscript must be submitted as a Microsoft Word file (.doc or .docx). The formatting should be as follows:

- File format - .doc or .docx
- Page size - A4
- Page orientation - portrait (some landscape pages are accepted if necessary)
- Page margin - 2.54 cm (left and the right margin) and 1.9 cm (bottom and the top margin)
- Page number (bottom of the page)
- Line number
- Line spacing - 1.5
- Font - 12 point, Times New Roman (unless stated otherwise)

Unit - The use of abbreviation must follow the International System of Units (SI Unit) format.

- The unit separator is a virgule (/) and not a negative coefficient: 10 mg/L not 10 mgL^{-1}
- Liter always has a capital letter: mg/L

Equations

- Insert equations using the dedicated tool in Microsoft Word. Do not use pictures or text boxes.
- Equations that are referenced in the text should be identified by parenthetical numbers, such as (1), and should be referred to in the manuscript as “Equation 1”.

Inclusive Language: The language used in the manuscript acknowledges diversity, promotes equal opportunity, respects all people, and is sensitive to all aspects of differences. The manuscript content should not make assumptions about the beliefs or commitments of any individual. It should not imply superiority regarding age, race, ethnicity, culture, gender, sexual orientation, disability, or health conditions. Moreover, the manuscript must be free from bias, stereotypes, slang, and derogatory terms.

Reference Style: Vancouver style should be used for the reference list and in-text citations throughout the manuscript. Please follow the format of the sample references and citations, as shown in the Body Text Sections portion below.

Front Page

Title: The title of the manuscript should be concise and not longer than necessary. The title should be bold, 12-point size, and Times New Roman. The first letter of major words should be capitalized (as in standard title case).

Author(s) Name: The first and last names of all authors must be given, in bold, Times New Roman, and 12-point font.

Affiliation of All Author(s): Affiliation(s) must be in italics, Times New Roman, and 11-point font. Specify the Department/School/Faculty, University, City/Province/or State, and Country of each affiliation. Do not include positions or fellowships, or postal zip codes.
Each affiliation should be indicated with superscript Arabic numerals. The Arabic numeral(s) should appear immediately after the author’s name, and represent the respective affiliation(s).

Corresponding Author: One author should be responsible for correspondence, and their name must be identified in the author list using an asterisk (*).

- All correspondence with the journal, including article submission and status updates, must be handled by the corresponding author.

- The online submission and all associated processes should be operated by the corresponding author.

*Corresponding author: followed by the corresponding author's email address.

Example:

Papitchaya Chookaew[1], Apiradee Sukmilin[2], and Chalor Jarusutthirak[1*]
[1]Department of Environmental Technology and Management, Faculty of Environment, Kasetsart University, Bangkok, Thailand
[2]Environmental Science and Technology Program, Faculty of Science and Technology, Phranakhon Rajabhat University, Bangkok, Thailand
**Corresponding author: abcxx@xx.ac.th*

Abstract Page

Abstract: The abstract should include the significant findings paired with relevant data. A good abstract is presented in one paragraph and is limited to 250 words. Do not include a table, figure, or references.
Keywords - Up to six keywords are allowed, and they should adequately index the subject matter.

Highlights: Please include 3-5 concise sentences describing innovative methods and the findings of the study. Each sentence should contain at most 85 characters (not words).

Body Text Sections
The main body text of the manuscript normally includes the following sections: 1. Introduction 2. Methodology 3. Results and Discussion 4. Conclusions 5. Acknowledgments 6. Author Contributions 7. Declaration of Competing Interests 8. References

Introduction should include the aims of the study. It should be as concise as possible, with no subheadings. The significance of the problem and the essential background should also be given.

Methodology is sufficiently detailed so that the experiments can be reproduced. The techniques and methods adopted should be supported with standard references.
There should be no more than three levels of headings in the **Methodology and Results and Discussion** sections. Main headings are in bold letters, second-level headings are in bold and italic letters, and third-level headings are in normal letters.

Here is an example:

2. Methodology
2.1 Sub-heading
2.1.1 Sub-sub-heading

Results presents the key findings in figures and tables with descriptive explanations in the text.

Tables
- Tables - look best if all the cells are not bordered; place horizontal borders only under the legend, the column headings, and the bottom.

Figures
- Figures - should be submitted in color. The author must ensure that the figures are clear and understandable. Regardless of the application used to create them, when electronic artworks are finalized, please 'save as' or convert the images to TIFF or JPG and send them separately to EnNRJ. Images require a resolution of at least 600 dpi (dots per inch) for publication. The labels of the figures and tables must be Times New Roman, and their size should be adjusted to fit the figures without borderlines.
- Graph - The font style in all graphs must be Times New Roman, 9-10 size, and black color. Please avoid bold formatting, and set the border width of the graphs to 0.75 pt.

- Graph from MS Excel: Please attach an editable graph from MS Excel within your manuscript. Then please also submit the full MS Excel file used to prepare the graph as a separate document. This helps us customize our layout for aesthetic beauty.
- Graph from another program: Feel free to use whichever program best suits your needs. But as noted above, when your artwork is finalized, please convert the image to TIFF or JPG and send them separately Again, images should be at least 600 dpi. Do not directly cut and paste.

***All figures and tables should be embedded in the text, and also mentioned in the text.**

Discussion shows the interpretation of findings with supporting theory and comparisons to other studies. The Results and Discussion sections can be either separated, or combined. If combined, the section should be named Results and Discussion. **Conclusions** should include a summary of the key findings and take-home messages. This should not be too long, or repetitive but this section is absolutely necessary so that the argument of the manuscript is not uncertain or left unfinished.

Acknowledgments should include the names of those who contributed substantially to the work, but do not fulfill the requirements for authorship. It should also include any sponsor or funding agency that supported the work.

Author Contributions: For research articles with several authors, we require corresponding author contributions listed using the relevant CRediT roles. This should be done by the author responsible for correspondence.

Declaration of Competing Interest: The author must include a declaration of competing interest form during submission. If there is no conflict of interest, please state, "The authors declare no conflict of interest." Otherwise, authors should declare all interests to avoid inappropriate influence or bias in their published work.

References should be cited in the text by the surname of the author(s) and the year. This journal uses the author-date method of citation. The author's last name and date of publication are inserted in the text in the appropriate place. If there are more than two authors, “et al.” must be added after the first author’s name. Examples: (Frits, 1976; Pandey and Shukla, 2003; Kungsuwas et al., 1996). If the author’s name is part of the sentence, only the date is placed in parentheses: “Frits (1976) argued that . . .”

Please ensure that every reference cited in the text is also in the reference list (and vice versa).

In the list at the end of the manuscript, complete references must be arranged alphabetically by the surnames of the first author in each citation. Examples are given below.

Book

Tyree MT, Zimmermann MH. Xylem Structure and the Ascent of Sap. Heidelberg, Germany: Springer; 2002.

Chapter in a book

Kungsuwan A, Ittipong B, Chandrkrachang S. Preservative effect of chitosan on fish products. In: Steven WF, Rao MS, Chandrkachang S, editors. Chitin and Chitosan: Environmental and Friendly and Versatile Biomaterials. Bangkok: Asian Institute of Technology; 1996. p. 193-9.

Journal article

Muenmee S, Chiemchaisri W, Chiemchaisri C. Microbial consortium involving biological methane oxidation in relation to the biodegradation of waste plastics in a solid waste disposal open dump site. International Biodeterioration and Biodegradation 2015;102(3):172-81.

Journal article with Article Number

Sah D. Concentration, source apportionment and human health risk assessment of elements in $PM_{2.5}$ at Agra, India. Urban Climate 2023;49:Article No. 101477.

Non-English articles

Suebsuk P, Pongnumkul A, Leartsudkanung D, Sareewiwatthana P. Predicting factors of lung function among motorcycle taxi drivers in the Bangkok metropolitan area. Journal of Public Health 2014;44(1):79-92 (in Thai).

Article in press

Dhiman V, Kumar A. Biomass and carbon stock estimation through remote sensing and field methods of subtropical Himalayan Forest under threat due to developmental activities. Environment and Natural Resources Journal 2024. DOI: 10.32526/ennrj/22/20240018.

Published in conference proceedings

Wiwattanakantang P, To-im J. Tourist satisfaction on sustainable tourism development, Amphawa floating market Samut Songkhram, Thailand. Proceedings of the 1st Environment and Natural Resources International Conference; 2014 Nov 6-7; The Sukosol hotel, Bangkok: Thailand; 2014.

Ph.D./Master thesis

Shrestha MK. Relative Ungulate Abundance in a Fragmented Landscape: Implications for Tiger Conservation [dissertation]. Saint Paul, University of Minnesota; 2004.

Website

Orzel C. Wind and temperature: why doesn't windy equal hot? [Internet]. 2010 [cited 2016 Jun 20]. Available from: http://scienceblogs.com/principles/2010/08/17/wind-and-temperature-why-doesn/.

Report organization

Intergovernmental Panel on Climate Change (IPCC). IPCC Guidelines for National Greenhouse Gas Inventories: Volume 1-5. Hayama, Japan: Institute for Global Environmental Strategies; 2006.

Royal Gazette

Royal Gazette. Promotion of Marine and Coastal Resources Management Act 2059. Volume 132, Part 21, Dated 26 Mar B.E. 2558. Bangkok, Thailand: Office of the Council of State; 2015a. (in Thai).

Remark

** Please be note that manuscripts should usually contain at least 15 references and some of them must be up-to-date research articles.*

** Please strictly check all references cited in text, they should be added in the list of references. Our Journal does not publish papers with incomplete citations.*

Changes to Authorship

This policy of journal concerns the addition, removal, or rearrangement of author names in the authorship of accepted manuscripts:

Before the accepted manuscript

For all submissions, that request of authorship change during review process should be made to the form below and sent to the Editorial Office of EnNRJ. Approval of the change during revision is at the discretion of the Editor-in-Chief. The form that the corresponding author must fill out includes: (a) the reason for the change in author list and (b) written confirmation from all authors who have been added, removed, or reordered need to confirm that they agree to the change by signing the form. Requests form submitted must be consented by corresponding author only.

After the accepted manuscript

The journal does not accept the change request in all of the addition, removal, or rearrangement of author names in the authorship. Only in exceptional circumstances will the Editor consider the addition, deletion or rearrangement of authors after the manuscript has been accepted.

Copyright transfer

The copyright to the published article is transferred to Environment and Natural Resources Journal (EnNRJ) which is organized by Faculty of Environment and Resource Studies, Mahidol University. The accepted article cannot be published until the Journal Editorial Officer has received the appropriate signed copyright transfer.

Online First Articles

The article will be published online after receipt of the corrected proofs. This is the official first publication citable with the Digital Object Identifier (DOI). After release of the printed version, the paper can also be cited by issue and page numbers. DOI may be used to cite and link to electronic documents. The DOI consists of a unique alpha-numeric character string which is assigned to a document by the publisher upon the initial electronic publication. The assigned DOI never changes.

Environment and Natural Resources Journal (EnNRJ) is licensed under a Attribution-NonCommercial 4.0 International (CC BY-NC 4.0)





Mahidol University

Wisdom of the Land

Faculty of Environment and Resource Studies, Mahidol University, Thailand
999 Phutthamonthon Sai 4 Rd, Salaya, Phutthamonthon District, Nakhon Pathom 73170
E-mail: ennrjournal@gmail.com